

Copyright

by

Samantha Sheller-Miller

2018

**The Dissertation Committee for Samantha Sheller-Miller Certifies that this is the  
approved version of the following dissertation:**

**Feto-Maternal Exosome Characterization, Trafficking and Function  
During Pregnancy and Parturition**

**Committee:**

---

Mariano Garcia-Blanco, MD, PhD, Chair

---

Ramkumar Menon, MS, PhD

---

John Papaconstantinou, PhD

---

Richard Pyles, PhD

---

Janice Endsley, PhD

---

Sam Mesiano, PhD

---

Dean, Graduate School

**Feto-Maternal Exosome Characterization, Trafficking and Function  
During Pregnancy and Parturition**

**by**

**Samantha Sheller-Miller, BS**

**Dissertation**

Presented to the Faculty of the Graduate School of

The University of Texas Medical Branch

in Partial Fulfillment

of the Requirements

for the Degree of

**Doctor of Philosophy**

**The University of Texas Medical Branch**

**May 2018**

## **Dedication**

-To my husband, Michael Miller, without whom I would not be where I am today

-To my parents, Tom and Karen Sheller, for their love and support

-To my siblings, Michael and Matthew Sheller, my work mother, Liz Powell, my lab manager Talar Kechichian, my lab mates and all my friends, both near and far, for being there for me while I powered through this crazy little thing called graduate school.

## **Acknowledgements**

First and foremost, I would like to thank my mentor, Dr. Ramkumar Menon for his patience and dedication to my continuing education in the fields of exosome and perinatal research. I will forever be grateful for the time and commitment put forth to best prepare me for my future in the scientific community. I would like to also thank Dr. George Saade, who made my first two years in the Menon/Saade lab possible. A great deal of thanks to all the researchers in the Menon/Saade lab who taught me everything I needed to know, especially my lab manager, Talar. I am also grateful to have been awarded a T32 grant that provided the financial support to fund a portion of my graduate studies.

I would also like to thank my co-mentor, Dr. John Papaconstantinou, for his support and advice from project ideas to my future in the sciences. Thank you to my committee members who sat through hours of committee meetings and pushed me to a higher standard of science.

Thank you to all our collaborators and members of the UTMB core facilities who were always ready and able to assist me in any way they could.

Last but certainly not least, my loving husband, Michael Miller. He was the greatest support I had and kept me going even during the hardest of times. He was by my side before, during and after graduate school. He supported me emotionally and I will forever be appreciative.

# **Feto-Maternal Exosome Characterization, Trafficking and Function During Pregnancy and Parturition**

Publication No. \_\_\_\_\_

Samantha Sheller-Miller, PhD

The University of Texas Medical Branch, 2018

Supervisor: Ramkumar Menon, MS, PhD

Endocrine factors and signals of fetal organ maturation are well-reported determinants of the timing of birth and have been studied extensively in both humans and animal models. However, decades of research have not yielded answers to the timing of labor. It is evident that endocrine factors alone are not sufficient to fully address timing or mechanisms of labor, which is reflected in the increasing rates of preterm births and other pregnancy complications in most countries. Differences in the endocrine factors between humans and animals have hampered advances in this field. As an alternative to endocrine factors, the studies presented here report paracrine signals are similar between humans and animal models and are attributed by senescence-associated feto-maternal signaling via exosomes. Oxidative stress in utero, most likely due to increased metabolic activity of the fetus, induces cellular senescence of the fetal membranes. We have reproduced this model in vitro to show human amnion epithelial cells can produce exosomes and when cultured under oxidative stress conditions, exosomes cargo signals of cellular damage and inflammation. Amnion cell-derived exosomes can traffic to the maternal tissues and produce labor-associated changes in maternal cells. Additionally, in murine models of pregnancy, exosomes in maternal plasma increase in number prior to delivery and their cargo also increases in pro-inflammatory mediators as term approaches. Independent of endocrine or systemic inflammation, late gestation exosomes cause preterm labor and labor-associated changes in maternal and fetal tissues. Although a fetal-specific marker in humans allows for the study of fetal exosomes in maternal circulation, to study fetal vs maternal exosome contribution to the initiation of labor in mice, we developed a model which utilizes a dual color fluorescent transgenic Cre reporter mouse. Using this model, we show feto-maternal crosstalk via exosomes occurs during pregnancy and can produce functional changes on both sides of the placenta. Further research into the mechanism of feto-maternal signaling via exosomes at term can contribute to the identification of new biomarkers or interventions to combat preterm labor.

# TABLE OF CONTENTS

List of Tables .....	xiv
List of Figures .....	xv
List of Abbreviations .....	xix
<b>CHAPTER 1: GENERAL INTRODUCTION.....</b>	<b>21</b>
Preterm Birth Is a Significant Problem .....	21
Initiators and Effectors of Labor.....	21
Fetal Signals of Organ Maturity .....	22
Fetal-Derived Endocrine Signals .....	22
Maternal-Derived Endocrine Signals.....	23
Immune Cell Activation.....	23
Changes in Maternal Physiology .....	24
Parturition Is an Inflammatory Process.....	24
Fetal Membrane Senescence Leads to Parturition .....	25
Exosomes are Unique Messengers for Intercellular Communication.....	27
Exosomes as Channels of Fetal-Maternal Communication .....	28
Objectives of The Dissertation.....	29
<b>CHAPTER 2: AMNION-EPITHELIAL-CELL-DERIVED EXOSOMES DEMONSTRATE     PHYSIOLOGIC STATE OF CELL UNDER OXIDATIVE STRESS .....</b>	<b>31</b>
Introduction.....	31
Materials and Methods.....	34
Isolation and Culture of Human Amnion Epithelial Cells (AECs).....	34
Stimulation of AECs with Cigarette Smoke Extract (CSE).....	35
Activation of p38 MAPK in AECs Using Flow Cytometry .....	36
Senescence-Associated B-Galactosidase (SA-B-Gal) Activity .....	36
Isolation of Exosomes from Control and CSE-Treated Amnion Cell .....	37
Transmission Electron Microscopy (TEM) Of Whole Mounted Exosomes .....	37
Nanoparticle Tracking Analysis .....	38

Western Blot Analysis .....	38
Flow Cytometry Analysis for Exosome Markers .....	39
Immunofluorescence Staining and Microscopy.....	39
Exosomal localization of cffTF using fluorescent in situ hybridization (FISH) .....	40
Image Processing and Analysis .....	41
Proteomic Analysis of AEC-Derived Exosomes by Mass Spectrometry	42
NGS to Determine Exosomal cffTF and Other Cell-Free Amnion Cell DNA Specificity .....	43
Statistical Analysis.....	44
Results.....	44
Primary AEC Cultures Are Positive for Cytokeratin.....	44
CSE Activates p38 MAPK and Induces Cellular Senescence in Primary AECs .....	44
Characterization of Exosomes from Control and CSE-Treated AECs ....	45
Characterization of Exosomal Cargo from Control and CSE Treated AECs .....	47
Proteomic Analysis of AEC-Derived Exosomes by Mass Spectrometry	51
Discussion .....	56
<b>CHAPTER 3: PARACRINE MEDIATORS OF PARTURITION: EXOSOMES DERIVED FROM AMNION EPITHELIAL CELLS .....</b>	<b>60</b>
Introduction.....	60
Materials and Methods.....	62
Human amnion epithelial cell isolation and culture .....	63
Primary amnion epithelial cells under normal (control) and oxidative stress cell culture conditions .....	63
Exosome isolation.....	63
Transmission electron microscopy .....	63
Nanoparticle tracking analysis with ZetaView .....	63
Myometrial cell culture.....	64
Decidual cell culture .....	64
BeWo cell culture .....	65



Immunofluorescence staining of exosomes and confocal microscopy to localize exosomes in recipient cells .....	65
Exosome treatments of cells .....	66
Exosome blocking experiments .....	67
Enzyme Linked Immunosorbent Assay for determining inflammatory marker response .....	68
Western Blot .....	68
Immunohistochemical analysis of amnion exosomes in maternal gestational tissues .....	68
Statistical analysis .....	69
Results .....	70
Exosome Quantification and Characterization .....	70
Exosomes were localized in recipient cells .....	71
AEC exosomes induce a pro-inflammatory response in myometrial and decidual cells.....	72
74	
Positive control experiments show exosome-mediated effect .....	75
Determination of exosome mediated cytokine response .....	76
Exosomes increase NF- $\kappa$ B activation in myometrial and decidual cells.	76
Increased localization of NANOG in myometrial and decidual tissues at term labor .....	78
Discussion .....	79
Principal findings of the study .....	79
Fetal exosomes, irrespective of the physiologic status of cell of origin, cause inflammatory activation in maternal cells.....	80
Placental cells are refractory to immune response by amnion exosomes	82
Determining fidelity of exosomal functions .....	82
Oxidative stress of amnion epithelial cells leads to production of exosomes with pronounced effect on target cells .....	83

<b>CHAPTER 4: FETO-MATERNAL TRAFFICKING OF EXOSOMES IN MURINE PREGNANCY MODELS .....</b>	<b>85</b>
Introduction.....	85
Materials and Methods.....	86
Patient exclusion criteria.....	86
Isolation and Culture of human Amnion Epithelial Cells (AECs) .....	87
Exosome isolation.....	87
Labeling of Exosomes with DiR.....	87
Exosome Characterization Using Transmission Electron Microscopy (TEM) And Western Blot .....	88
Animals .....	88
Maternal Plasma Exosome Isolation to Localize Trafficking of Exosomes .....	90
Results.....	90
Amnion Epithelial Cell-Derived Exosome Characterization.....	90
Exosome Trafficking in Pregnant Mice .....	90
Exosomes Traffic to The Maternal Serum.....	94
Discussion .....	95
<b>CHAPTER 5: EXOSOMES CAUSE PRETERM BIRTH IN MICE: EVIDENCE FOR PARACRINE SIGNALING IN PREGNANCY .....</b>	<b>97</b>
Introduction.....	97
Materials and Methods.....	99
Animal care.....	99
Maternal plasma collection .....	100
Maternal plasma exosome isolation.....	101
Determination of exosome shape using cryo-electron microscopy .....	102
Determination of exosome size and quantification.....	102
Flow cytometry analysis for exosome markers .....	103
Proteomic analysis of maternal plasma exosomes by mass spectrometry .....	103

Exosome protein clean-up and digestion .....	103
LC-MS/MS analysis of plasma exosomes .....	104
Ingenuity pathway analysis (IPA) of identified proteins .....	105
Injection of E9 and E18 exosomes to determine trafficking and labor-associated functional changes .....	105
Fluorescent labeling of exosomes for determining in vivo trafficking and localization.....	106
Immunofluorescent imaging for exosome trafficking .....	106
Enzyme-linked immunosorbent assay (ELISA) for progesterone levels in maternal plasma .....	107
Immunohistochemistry for macrophage infiltration and activation.....	107
Western blot analysis .....	107
Western blot analysis for exosome markers .....	107
Western blot analysis of fetal and maternal tissues .....	108
Luminex assay to determine inflammatory markers in tissue and plasma .....	108
Statistical analysis.....	108
Results.....	109
Plasma exosomes exhibit classic exosome characteristics .....	109
Exosome concentration increases throughout gestation .....	111
Proteomic analysis of maternal plasma exosomes throughout gestation.....	111
Intraperitoneal injections of E18 exosomes induce preterm birth independent of systemic progesterone withdrawal or inflammation .....	118
Exosome trafficking to intrauterine tissues to cause labor-associated changes.....	121
CFSE-labeled exosomes localize in maternal and fetal tissues .....	121
E18 exosomes promote proinflammatory processes to prepare the cervix and uterus for parturition .....	123
E18 exosomes promote prepartum proinflammatory processes in fetal membranes but not in the placenta .....	125

Discussion .....	129
<b>CHAPTER 6: CRE-REPORTER MOUSE MODEL TO DETERMINE MATERNAL-FETAL EXOSOME COMMUNICATION AND FUNCTIONAL EFFECTS .....</b>	<b>134</b>
Introduction .....	134
Materials and Methods .....	136
Animal care .....	136
Injection of Cre-enriched exosomes to determine maternal to fetal exosome trafficking .....	137
Immunofluorescent imaging for exosome trafficking .....	139
Maternal plasma collection .....	140
Maternal plasma exosome isolation .....	140
Exosome Immunoprecipitation (IP) and flow cytometry analysis .....	140
Determination of exosome size and concentration .....	141
Results .....	141
Validation of the tdTomato exosome mouse model .....	141
Expression of mT in fetal tissues .....	141
Maternal plasma exosomes express mT .....	142
mT expression in WT maternal uterus and cervix .....	143
Cre-enriched exosomes injected on the maternal side traffic to the fetal tissues and induce a functional change .....	145
Fetal exosomes in maternal plasma express mG .....	146
Fetal-derived exosomes traffic to maternal reproductive tissues .....	147
Discussion .....	148
<b>CHAPTER 7: SUMMARY AND CONCLUSIONS .....</b>	<b>152</b>
Exosomes carry signals of sterile inflammation to maternal tissues .....	153
Exosomes as paracrine signalers in pregnancy and parturition .....	154
Transgenic mouse model to determine exosome trafficking and function during pregnancy .....	155
Concluding Remarks .....	155

Supplemental Table 2.1. Proteomics analysis of exosomal cargo identified 30 unique markers in exosomes derived from amnion epithelial cells grown in normal culture conditions. ....	158
Supplemental Table 2.2. Proteomics analysis of exosomal cargo identified 48 unique markers in exosomes derived from amnion epithelial cells grown under oxidative stress conditions.....	160
Appendix B: Supplemental Materials for Chapter 3.....	164
Supplemental Figure 3.1: IL-6 concentration in media from various control experiments performed to confirm exosome specific activation of inflammatory mediators.....	164
Supplemental Figure 3.2. 3D reconstructions of confocal images of each target cell studied.....	165
Supplemental Table 3.1A: Cytokine and PGE2 concentrations in myometrial cells treated with control exosomes.....	166
Supplemental Table 3.1B: Cytokine and PGE2 concentrations in myometrial cells treated with exosomes derived from AEC exposed to cigarette smoke extract (Oxidative stress (OS) exosomes).....	167
Supplemental Table 3.2A: Cytokine and PGE2 concentrations in myometrial cells treated with exosomes derived from AEC exposed to cigarette smoke extract (Oxidative stress (OS) exosomes).....	168
Supplemental Table 3.2B: Cytokine and PGE2 concentrations in decidual cells treated with exosomes derived from AEC exposed to cigarette smoke extract (Oxidative stress (OS) exosomes).....	169
Supplemental Table 3.3A: Cytokine and PGE2 concentrations in BeWo cells treated with control exosomes .....	170
Supplemental Table 3.3B: Cytokine and PGE2 concentrations in BeWo cells treated with exosomes derived from AEC exposed to cigarette smoke extract (Oxidative stress (OS) exosomes).....	171
Supplemental Table 3.4 – Control experiments used to show exosome mediated immune activation effects in myometrial, decidual and BeWo cells .....	172
Appendix C: Supplemental Tables for Chapter 5 .....	173
Supplemental Table 5.1. Exosome concentration throughout gestation: Tukey's multiple comparisons.....	173
Supplemental Table 5.2. Proteins with Log <sub>2</sub> (Fold Change) of $\pm 0.6$ and $-\text{Log}(P\text{-value}) > 2.0$ for Volcano Plots.....	174

References .....	178
Curriculum Vita .....	205

## **List of Tables**

Table 2.1: p38 MAPK Activation (P-p38) and Cellular Senescence of Control and CSE treated AECs.....	45
Table 2.2- Size and quantity distribution of control & CSE exosomes .....	46
Table 5.1: Exosome Size and Concentration throughout Gestation .....	111
Table 5.2: Top 3 canonical pathways identified with IPA.....	114

## List of Figures

Figure 1.1: Invasion of the leukocytes into the fetal-maternal interface during pregnancy .....	24
Figure 1.2: Initiators and Effectors of Labor at Term.....	25
Figure 1.3: Exosome Biogenesis and Secretion.....	27
Figure 2.1: Cytokeratin staining of primary AECs. ....	44
Figure 2.2: Characterization of exosomes released from amnion cells grown under standard (control) and oxidative (CSE) conditions.....	47
Figure 2.3: Colocalization of exosome marker CD9 and P-p38 MAPK in AECs.....	48
Figure 2.5: Colocalization of exosome marker HSP70 and CD9 in AECs. ....	49
Figure 2.4: Colocalization of exosome marker H3 and CD9 in AECs. ....	49
Figure 2.6: Colocalization of HMGB1 in exosomes. ....	50
Figure 2.7: Colocalization of cffTF in exosomes. ....	51
Figure 2.8: Proteomic analysis of AEC-derived exosome proteins.....	52
Figure 2.9: Ingenuity pathway analysis of AEC-derived-exosomes proteins.....	54
Figure 2.10: Circular view of the readings of fragments along each chromosome in the (A) whole-genome and (B) mitochondria sequencing analysis of exosomal DNA isolated from amnion cells grown under standard (control) and OS (CSE) conditions.....	55



Figure 2.11: Characterization of AEC Exosomes .....	59
Figure 3.1: Characterization of control and oxidative stress exosomes.....	71
Figure 3.2 Localization of AEC derived exosomes (from control and oxidative stress treatments) inside gestational cells .....	72
Figure 3.3: ELISA data showing IL-6 (A), IL-8 (B) and PGE <sub>2</sub> (C) in myometrial cells .....	73
Figure 3.4: ELISA data showing IL-6 (A), IL-8 (B) and PGE <sub>2</sub> (C) in decidual cells .....	74
Figure 3.5: ELISA data showing IL-6 (A) and PGE <sub>2</sub> (B) in BeWo cells .....	75
Figure 3.6: Activation of NF- $\kappa$ B as determined by RelA/p65 Phosphorylation.....	77
Figure 3.7: Immunohistochemical localization of NANOG (amniotic stem cell marker constitutively expressed in AEC derived exosomes) in term labor and term not in labor gestational tissues.....	78
Figure 4.1: Illustration of exosomes injected into the amniotic cavity of pregnant mice.....	89
Figure 4.2: Characterization of two representative exosome samples isolated from primary amnion cells .....	91
Figure 4.3: In vivo imaging of pregnant mouse 24 hours post injection .....	92
Figure 4.4: Maternal and fetal sides of the placenta collected from injected mice on gestational day 18 .....	93

Figure 4.5: In vivo imaging of uterine tissues collected from gestational day18 .....	94
Figure 5.1: Experimental model: maternal plasma collection and injection timelines in a CD-1 mouse model of pregnancy. ....	101
Figure 5.2: Characterization of exosomes isolated from maternal plasma. ....	110
Figure 5.3: Proteomic and bioinformatic analysis of maternal plasma exosomes throughout gestation. ....	113
Figure 5.4: Volcano plots and molecular networks of differentially-expressed proteins.....	117
Figure 5.5: The injection of E18 exosomes causes preterm birth.....	119
Figure 5.6: Exosome-induced preterm labor is not associated with systemic progesterone withdrawal or systemic inflammation. ....	120
Figure 5.7: Exosomes injected into pregnant mice traffic to the cervix, uterus, fetal membranes and placenta. ....	122
Figure 5.8: Exosomes injected into pregnant mice induce labor-associated changes in the cervix.....	124
Figure 5.9: Exosomes injected into pregnant mice induce labor-associated changes in the uterus.....	126
Figure 5.10: Exosomes injected into pregnant mice traffic to the fetal tissues and induce inflammatory changes in the fetal membranes but not the placenta. ....	128

Figure 6.1: Maternal-Fetal Exosome Trafficking and Cre-Reporter Transgenic Mouse Model .....	138
Figure 6.2: Fluorescence microscopy of the placenta and fetal membranes from WT female mated with mT/mG expressing male .....	142
Figure 6.3: Immunoprecipitation and nanoparticle tracking analysis of mT expressing exosomes from maternal plasma.....	143
Figure 6.5: Colocalization of exosomes expressing tdTomato (mT) with macrophages in the maternal tissues.....	144
Figure 6.4: Exosomes expressing mT localize in maternal cervix and uterus.....	144
Figure 6.6: Fluorescence microscopy of the placenta and fetal membranes from mice injected Cre-enriched exosomes .....	145
Figure 6.7: Flow cytometry of exosomes isolated from maternal plasma after immunoprecipitation for mG .....	146
Figure 6.8: Exosomes expressing mG localize in maternal cervix and uterus .....	147
Figure 6.9: Maternal-Fetal Exosome Trafficking and Cre-Reporter Transgenic Mouse Model .....	148

## List of Abbreviations

AEC	Amnion epithelial cells	LC/MS-MS	Liquid chromatography/mass spectrometry
Baf A1	bafilomycin A1	LPS	Lipopolysaccharide
BSA	bovine serum albumin	LXR/RXR	liver X receptor/retinoid X receptor
C <sub>12</sub> FDG	5-dodecanoylamino fluorescein di-β-D-galactopyranoside	MAPK	Mitogen activated protein kinase
CAN	acetonitrile	mT/mG	Membrane-targeted tdTomato/EGFP
cffTF	Cell free fetal telomere fragments	MVB	multivesicular body
CFSE	Carboxyfluorescein succinimidyl ester	MVE	multivesicular endosome
CRH	corticotrophin releasing hormone	NANOG	Transcription factor of self-renewing embryonic stem cells
CSE	Cigarette smoke extract	NBF	Neutral Buffered Formalin
DAMPs	Damage associated molecular pattern markers	NF-κB	Nuclear factor kappa B
DAPI	4',6-diamidino-2-phenylindole	NTA	Nanoparticle Tracking Analysis
DiR	1,1-dioctadecyl-3,3,3,3-tetramethylindotricarbocyanine iodide	OCT	optimal cutting temperature
DMEM/F12	Dulbecco's Modified Eagle Medium: Nutrient Mixture F-12 media	OS	Oxidative stress
E#	Gestation day #	PBS	Phosphate buffered saline
EGF	epidermal growth factor	PFA	Paraformaldehyde
EGFP	Enhanced green fluorescent protein	PGE	Prostaglandin E
ELISA	Enzyme Linked Immunosorbent Assay	PLAP	placental alkaline phosphatase
EM	Electron Microscopy	PNA	peptide nucleic acid
EMT	Epithelial to mesenchymal transition	PR	progesterone receptor
ESCRT	endosomal sorting complex required for transport	PRR	pattern recognition receptors
FA	formic acid	PTA	Phosphotungstic Acid

FasL	Fas ligand	PTB	Preterm birth
FDR	False discovery rate	PTL	Preterm labor
FFPE	Formalin-fixed paraffin-embedded	RelA	RELA Proto-Oncogene, NF- $\kappa$ B Subunit
FITC	fluorescein isothiocyanate	RFU	relative fluorescence units
GO	gene ontology	RIPA	radioimmunoprecipitation assay
H&E	hematoxylin and eosin	SASP	Senescence associated secretory phenotype
H3	Histone 3	SA- $\beta$ -Gal	senescence-associated $\beta$ -galactosidase
HBSS	Hanks Balanced Salt Solution	TEM	Transmission electron microscope
HMGB	High mobility group box	tdTomato	Tandem dimer tomato (red fluorescent protein)
HPA	hypothalamic–pituitary–adrenal axis	TGF $\beta$	Transforming growth factor beta
HSP	Heat shock protein	TNF- $\alpha$	Tumor necrosis factor alpha
IACUC	Institutional Animal Care and Use Committee	UTMB	University of Texas Medical Branch
IPA	Ingenuity Pathway Analysis		

## **CHAPTER 1: GENERAL INTRODUCTION**

### **Preterm Birth Is a Significant Problem**

Preterm birth (PTB), defined as birth before 37 weeks of gestation, complicates approximately 10% of pregnancies in the US, is the leading cause for childhood morbidity and mortality [1], and cost more than \$26 billion annually [2]. Even with survival, many preterm babies face a lifetime of significant disability, including cerebral palsy, mental retardation, visual and hearing impairment and developmental delays [3–5]. Although survival rates for babies born prematurely have improved in recent years, preterm birth rates are increasing in most countries [1,6,7] due to our lack of understanding of the precise etiologies and initiating mechanisms of term and preterm labor.

Current treatments used for preterm labor can only delay labor temporarily [8], and are focused on the final stage of labor, specifically the initiation of contractions, which occurs primarily on the maternal side. Maintenance of pregnancy and parturition (either at term or preterm) are processes that involve constant communication (biochemical signaling) between the mother and the fetus. Hence, trying to control preterm parturition at the maternal side alone without considering the fetal contributions is often futile. [1,6,9]. To prevent preterm birth effectively, we need to better understand the feto-maternal signaling at term that transitions a quiescent uterus to an activated state to initiate the process of labor and delivery.

### **Initiators and Effectors of Labor**

It is widely accepted that labor is an inflammatory process initiated by environmental, endocrine and physiological factors [10]. This process requires the uterus to transition from a quiescent state to an activated phenotype in which it develops coordinated contractility and cervical dilation [8]. It also requires that the fetal organs have

matured for survival outside the uterus. Therefore, it is not surprising that the initiation of labor requires communications between both the fetus and the mother indicating fetal organ maturity occurs prior to initiation of parturition.

### ***Fetal Signals of Organ Maturity***

It has long been thought that signals from the growing fetus to the mother induce the cascade of events required for parturition. These include signals of organ maturity – signals indicating fetal readiness for survival outside the womb. The final fetal organ to fully develop is the lungs, as the lungs are largely unnecessary for a fetus while still in the uterus. The lungs begin to produce surfactant protein A, which allows the air sacs in the lungs to inflate and expand. Many hypothesize this protein, which is secreted from the lungs into the amniotic fluid, is a major player in the initiation of labor by causing fetal macrophages to traffic to the myometrium [9,11]. Other signals of fetal organ maturity include platelet-activating factor released from the lungs, endothelin from the kidneys, and cortisol from fetal adrenals, all of which are released into the amniotic fluid and function to increase inflammation.

### ***Fetal-Derived Endocrine Signals***

In addition to signals of fetal organ maturity, fetal endocrine signals are also under investigation as initiators of labor. In particular, corticotrophin releasing hormone (CRH), released from the placenta, that increases in maternal plasma drastically prior to the initiation of labor [12] and has been shown to activate the myometrium [13,14]. In addition to placental CRH, activation and increased expression of genes in the fetal hypothalamic–pituitary–adrenal (HPA) axis results in increased output of fetal cortisol [15]. Fetal cortisol increases maturation of the fetal lungs, that in turn produce surfactant proteins, described above.

### ***Maternal-Derived Endocrine Signals***

Progesterone is considered the main hormone associated with pregnancy. It is important in keeping uterine quiescence throughout pregnancy by decreasing myometrial contractility and promoting relaxation [6,16,17]. It is generally considered that natural labor is initiated by either systemic (in most mammals) or functional (in humans) progesterone withdrawal [18]. In humans, the high progesterone levels are maintained at term and it is hypothesized that human parturition is mediated by a decrease in myometrial progesterone responsiveness, rather than a decrease in progesterone levels, due to progesterone receptor (PR) expression changes from PR-B dominance (anti-inflammatory) to PR-A (pro-inflammatory) in the myometrium [17,18]. In addition to progesterone, estrogen has also been investigated as an endocrine mediator for the initiation of labor. At term, estrogen levels are significantly increased and it has been shown that there is a functional estrogen activation in the myometrium that correlates with the functional progesterone withdrawal [16]. Overall, these mechanisms increase uterine inflammatory load.

### ***Immune Cell Activation***

Because parturition is an inflammatory process, it is logical that immune cells be present in this process. As discussed above, fetal macrophages have been linked to the initiation of labor that can cargo surfactant proteins to the myometrium. Additionally, leukocytes and other immune cells (T, B, and Mast cells) have been investigated as propagators of the labor process [19,20] (Figure 1.1), in which chemotaxic signals recruit leukocytes and other immune cells to the uterine compartment where they release cytokines, chemokines, matrix degrading enzymes and other effectors [21]. This creates a feed-forward loop such that the cells of the uterus and cervix, as well as other leukocytes, amplify the original signals, leading to the overwhelming inflammation associated with the initiation of labor [20].



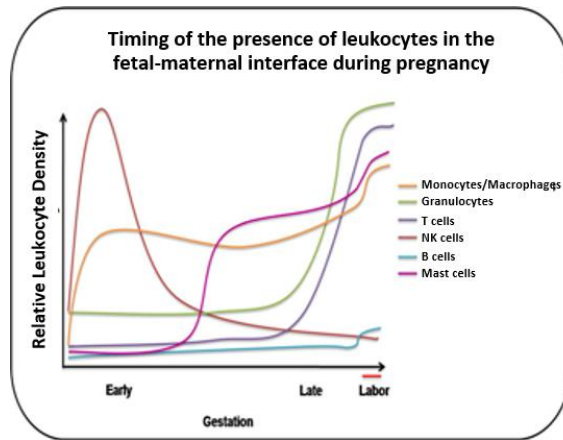


**Figure 1.1: Invasion of the leukocytes into the fetal-maternal interface during pregnancy**

Leukocytes are present throughout pregnancy, but the subpopulations change in a coordinated manner. (From Gomez-Lopez, et al., 2010)

### *Changes in Maternal Physiology*

While there are endocrine signals that may be the initiators of labor, localized changes in the uterus and cervix are important contributors to the process of labor. Mechanical stretch of the myometrium due to fetal growth has been shown to induce expression of pro-inflammatory cytokines mediated by NF- $\kappa$ B activation, and COX-2 expression [22,23]. While different from the uterus, remodeling of the cervix must be coordinated with the initiation of contractions. The cervix must remain closed during pregnancy, yet at term the cervix must become pliable and open sufficiently to allow delivery of the fetus. Cervical remodeling occurs through the breakdown of the collagenous extracellular matrix by increased expression of matrix degrading enzymes [7,24,25].

### **Parturition Is an Inflammatory Process**

As stated earlier, the process of parturition is multifactorial and as such, the above pathways and mediators work in tandem to initiate labor at term (Figure 1.2). Both fetal and maternal signals and pathways activate NF- $\kappa$ B, a major transcriptional activator of inflammatory genes, to cause the massive inflammatory response associated with

parturition, mediated by pro-inflammatory cytokines, such as IL-1 $\beta$ , TNF- $\alpha$ , IL-6 and IL-8, as well as activation of COX-2 and production of prostaglandins [26–28]. Generation of

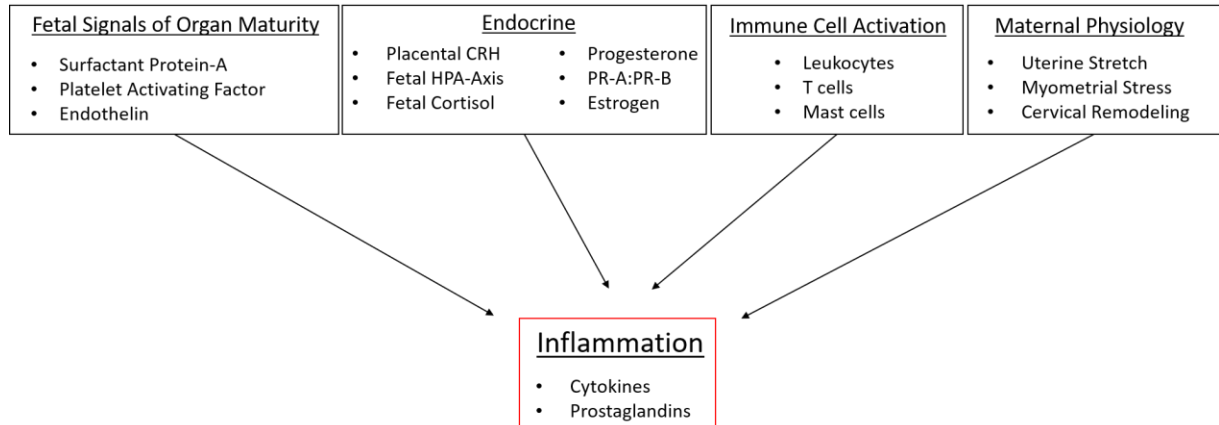


**Figure 1.2: Initiators and Effectors of Labor at Term**

At term, all these pathways work together to increase intra-uterine inflammation mediated by cytokines and prostaglandins to cause labor.

sterile inflammatory markers contribute to term parturition, whereas in preterm birth the same biomarkers are reported to be higher in response to infectious inflammation (~50% of preterm birth have an infectious association) or inflammation in response to other risk factors [29–31].

### **Fetal Membrane Senescence Leads to Parturition**

Our lab has looked at the initiation of labor at term from a fetal tissue perspective. Specifically, generation of sterile inflammation at term in fetal derived tissue like fetal membranes (amniochorion). We have shown a telomere dependent cellular senescence of the fetal membranes mediated by p38 mitogen activated kinase (MAPK) leading to sterile inflammation inside the amniotic cavity [32–35]. Amnion epithelial cells (AECs), mesenchymal cells and chorion cells have all been shown to undergo senescence in response to oxidative stress at term [34,36–38]. Similarly, progressive development of senescence mediated by telomere dependent p38 MAPK activation was shown in mouse

parturition [37]. Senescence, or the irreversible arrest of cell proliferation, is a physiological and biomolecular mechanism associated with the natural aging of a living organism [38,39] and can be accelerated by oxidative stress and other pathologies. Senescent cells do not undergo apoptosis or autophagy [40–43]. Instead, they persist; continuously secreting growth factors, pro-inflammatory cytokines, chemokines and matrix degrading enzymes, termed the senescence associated secretory phenotype (SASP) [44–46]. Senescence also causes cellular injury and release damage-associated molecular patterns (DAMPs), which are bioactive molecules released from dying cells that communicate cellular damage [47–50]. These DAMPs include High Mobility Group Box 1 (HMGB1), histone proteins, heat shock proteins, DNA and RNA [48,49]. Although SASP and DAMP signal action is predominantly localized, these signals of cellular stress may get carried to distant tissues, signaling fetal maturity and prompting delivery of the fetus. We propose aging of the fetal membranes is synchronous with fetal organ maturity and other pathways discussed above. Therefore, endocrine factors together with senescent paracrine signaling may determine the timing of labor. Based on these data, we have generated a model showing fetal membrane senescence generating sterile inflammatory signals (SASP and DAMPs) that are propagated from the fetal membranes to the maternal decidua, which is an immunocompetent tissue with several resident immune cells. The decidua can act as an amplifier of inflammation propagating these signals further to the cervix and myometrium where this inflammatory load can disrupt homeostasis that maintains pregnancy.

Yet, how these paracrine signals reach the maternal tissues is still unknown, although it could be a diffusion process or via specific carriers. Diffusion is less effective due the avascular nature of the fetal membranes and the potential of swift degradation. The latter mechanism caused us to propose that intercellular vesicles, such as exosomes may function as carriers of fetal tissue derived inflammatory cargo for signaling between fetal and maternal tissues [51,52].

## Exosomes are Unique Messengers for Intercellular Communication

Exosomes are 30-150 nm endosome-derived vesicles with specific characteristics that separate them from other larger particles such as microvesicles and apoptotic bodies [53,54]. Exosomes are formed from the inward budding of the late endosome and are secreted during the process of exocytosis (Figure 1.3). In addition to common cell-membrane and cytosolic proteins and lipids, exosomes also cargo proteins, lipids and nucleic acids specific to the cell of origin.

Due to the size of exosomes and overlap of other extracellular vesicles, many techniques have been developed for the isolation of exosomes. Methods have been adapted to increase exosome purity and yield, as well as decrease cost and amount of time required to isolate exosomes. Each technique exploits a unique characteristic of exosomes, such as their density, shape, size, and surface proteins. The most commonly used method for exosome isolation is differential ultracentrifugation [55,56], which consists of multiple centrifugation steps of increasing centrifugal force and duration culminating in a high-speed centrifugation step, which pellets crude exosomes. This pellet is often subjected to either a PBS wash, in which the pellet is resuspended in PBS and re-centrifuged at high

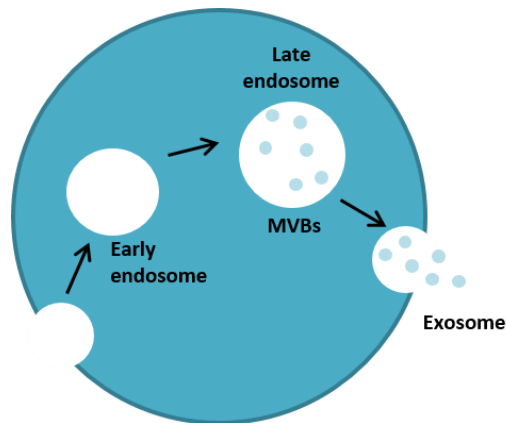


**Figure 1.3: Exosome Biogenesis and Secretion**

Following endocytosis into the early endosome, the cargo is packaged within multivesicular bodies (MVBs) via the inward budding of the membrane of the late endosome. Upon fusion with the cell membrane, the MVBs are released into the extracellular matrix as exosomes.

speeds, or a gradient [56,57] where exosomes are separated from other contaminants by density. Other methods include precipitation reagents, filtration and size exclusion chromatography. While there are advantages and disadvantages to each method used exclusively or in combination with others, current isolation methods are yet to be standardized [58]. Due to heterogeneity in particles obtained after differential centrifugation approaches, size exclusion purifications are recommended to avoid confounding higher sized particles in the preparations.

Exosomes have emerged as molecules of interest in recent years as they contain a fingerprint of the parental cells from which they are originated. While the biological function of exosomes remains elusive, current research has indicated that exosomes play an essential role in multiple cellular processes, including but not limited to waste management, immune cell modulation and are now being considered a central component to a new form of cell-cell communication [56,59]. For example, exosomes have recently been highlighted in immune signaling, senescence, proliferation, differentiation, and have been implicated in multiple diseases, including neurodegenerative diseases and cancer [60–62]. Additionally, there is increasing evidence suggesting exosomes as mediators of tumorigenicity and metastasis [58,63,64].

Characteristics of exosomes and their ability to act as carriers of signals susceptible to degradation, such as proteins modified by acetylation or oxidation, to distant cells and tissues [65,66], makes them ideal candidates for carriers of fetal senescent signals to distant maternal tissues

### **Exosomes as Channels of Fetal-Maternal Communication**

While exosome function and trafficking have been heavily studied in diseases such as cancer, they have not been as reported in pregnancy. Current research on exosomes and pregnancy have focused on placenta-derived exosomes, have been isolated from human maternal circulation using a placenta-specific protein called placental alkaline phosphatase

(PLAP). It has been shown that PLAP-expressing exosomes increase as gestation progresses [67,68] and cargo changes are reflective of changes in the placental microenvironment, such as hypoxia and glucose concentration changes [68–70]. Thus, changes in placenta-derived exosome cargo may be exploited to diagnose placental dysfunction and pregnancy outcomes.

Several reports have shown placenta-derived exosomes can modulate the maternal immune system and regulate immune tolerance by suppressing the maternal immune response [71]. For example, Stenqvist, et al. found that Fas ligand (FasL) and TRAIL, two physiologically relevant death messengers involved in the regulation of apoptosis, were expressed on the membranes of placenta-derived exosomes and showed they were functionally active by inducing apoptosis in vitro [72]. Their data provide a potential mechanism for fetal tolerance during pregnancy.

In pregnancy, exosomes have been investigated during implantation [72–74], placental development [73,75], and maintenance of pregnancy [76–79]. Ongoing studies in our lab have suggested exosomes play a role as paracrine communication channels between fetal and maternal tissues, specifically at term to initiate labor.

## **Objectives of The Dissertation**

Exosomes carry a wide range of signaling molecules, and their roles in physiology and pathophysiology during pregnancy and parturition remain to be fully elucidated, particularly in the fetal membranes. Few studies exist on fetal membrane-derived exosomes, their characteristics and potential function during pregnancy. Therefore, the objectives of this dissertation are to 1) isolate and characterize exosomes from primary amnion epithelial cells and determine functional effects when exposed to maternal cells in culture; 2) determine fetal exosome trafficking to maternal tissues in animal models; 3) isolate and characterize total exosomes from maternal plasma throughout gestation and demonstrate the functional role of exosomes in producing preterm labor in mouse models;

4) develop a Cre-reporter mouse model to determine maternal-fetal-maternal exosome communication and functional effects during pregnancy.

Together, the experimental data in this dissertation will add to the understanding of the initiation of labor at term and advance the perinatal field by providing important clues to the feto-maternal signaling in the initiation of labor. It is hoped that this information can contribute to the identification of new biomarkers or interventions to combat preterm labor.

## CHAPTER 2: AMNION-EPITHELIAL-CELL-DERIVED EXOSOMES

### DEMONSTRATE PHYSIOLOGIC STATE OF CELL UNDER OXIDATIVE STRESS

Modified in part from:

**Amnion-Epithelial-Cell-Derived Exosomes Demonstrate Physiologic State of Cell under Oxidative Stress**

**Samantha Sheller**, John Papaconstantinou, Rheanna Urrabaz-Garza, Lauren Richardson, George Saade, Carlos Salomon, Ramkumar Menon  
Published: *PLoS One* (2016)

And

**Damage-Associated Molecular Pattern Markers HMGB1 and Cell-Free Fetal Telomere Fragments in Oxidative-Stressed Amnion Epithelial Cell-Derived Exosomes**

**Samantha Sheller-Miller**, Rheanna Urrabaz-Garza, George Saade, Ramkumar Menon  
Published: *Journal of Reproductive Immunology* (2017)

### Introduction

Normal term human parturition is initiated between 37 and 40 weeks of gestation when in utero fetal growth and development are completed [4,15,80]. The signals from mature fetal organs prompt uterine readiness for delivery by transitioning quiescent myometrium to an active stage (contractile phenotype) [15,81,82]. Various endocrine, immune and mechanical signals from feto-maternal compartments enhance overall uterine inflammatory load leading to functional progesterone withdrawal causing myometrial contractility [8,83,84]. Therefore, term labor and delivery results from well-orchestrated activities of various endocrine and paracrine factors. Nonetheless, the signature of these signals and their precise mechanisms in initiating parturition are still unclear and under investigation by many laboratories. Understanding the mechanisms of these signals in normal term pregnancies can provide insights into pathologic activation that can cause spontaneous preterm parturitions.

Recently, our laboratory has reported fetal membrane (amniochorionic membrane) senescence as a mechanism associated with normal term parturition [34]. Placental membrane cells multiply and fully develop by the 12<sup>th</sup> week of gestation, providing



protection to the growing fetus [85]. Placental membranes undergo an oxidative stress associated telomere dependent cellular senescence at term [86–88]. In addition, placental membrane senescence is also associated with sterile inflammation in the amniotic fluid [34,89]. The unique inflammation seen in senescent cells is defined senescence associated secretory phenotype (SASP) that are linked to initiation of labor [88,90–92]. Besides cytokines, chemokines, and other inflammatory mediators of SASP, sterile inflammation within the fetal membrane includes damage-associated molecular pattern (DAMPs) markers [34,93]. DAMPs are molecules with defined intracellular functions, but outside of the cell, DAMPs are proinflammatory mediators. Examples of such DAMPs include high-mobility group box 1 (HMGB1), a nonhistone nuclear protein [94,95]; HSP70, a chaperon protein [96,97]; fragments of cell-free DNA [98–100]; telomere fragments [88]; and uric acid [101]. DAMPs are often recognized by pattern recognition receptors (PRRs) that are located in the cell membranes [102]. Ubiquitous expression enables PRRs to recognize and ligate DAMPs to promote signaling cascades causing inflammation, complement activation, cell necrosis, and apoptosis [103]. We postulate that SASP and DAMPs constitute sterile inflammatory signals from the fetus with uterotonic properties and overwhelming production, and propagation of these signals between fetomaternal compartments constitute a novel paracrine signaling mechanism to initiate parturition.

The findings in clinical specimens have been reproduced in vitro in primary amnion epithelial cells in culture exposed to oxidative stress induced by cigarette smoke extract (CSE) [87]. Generation of senescence and SASP were reduced by inhibiting p38 mitogen activated kinase (MAPK), a stress associated pro-senescence protein, suggesting that sterile inflammation can be generated by senescent cells [32,87,89].

It is still unclear how proinflammatory SASP signals from senescent fetal membranes can reach distant myometrium or whether they are confined to enforcing local (fetal) tissue damage and inflammation until parturition. Senescent signals may be transported to distant tissues indicating a dysfunctional fetal membrane status that prompts

delivery of the fetus, as well as placenta and membrane. Although localized activities of SASP can be achieved through direct cell-cell contact or through ligand-receptor interactions, distant feto-maternal communication is likely facilitated through specific carriers that can transport and deliver signals from senescent cells. Thus, prior to projecting senescent fetal cells signaling parturition at a distant myometrium, the mode of delivery of such signals must be established. Several recent reports and reviews propose a role for exosomes as such carriers of parturition signals to utero-placental compartments [51,64,65,104].

Exosomes are 30-150 nm endosome-derived vesicles with specific characteristics that separate them from other larger particles such as microvesicles and apoptotic bodies [57,105–107]. Exosome biogenesis is a process that begins with the endocytosis of transmembrane proteins [108,109]. Once sorted to late endosomes, the endosomal sorting complex required for transport (ESCRT) complex, recruits proteins and other cargo, while also mediating the inward budding of the late endosome, creating the intraluminal vesicles inside the multivesicular body (MVB) [59,76,78,110]. The MVB can either follow a degradation pathway fusing with lysosomes or proceed to release the intraluminal vesicles into the extracellular space through exocytosis as exosomes [76,110]. Placental derived exosomes have been well characterized during normal and abnormal pregnancies and their functional roles have also been documented [67,68,71,111–116]. Their size facilitates easy transportation between cells and tissues, while their contents reflect the state of the source cell and regulate the phenotype of the target cell [69,79,106,113,114,117]. Exosomes interact with the target cell by direct fusion with the cell membrane, thus releasing the contents directly into the cytosol; through active uptake via endocytosis or by binding to the target cell via receptor-ligand interactions thereby inducing a signaling cascade which changes the phenotype of the target cell.

No reports exist on fetal membrane- derived exosomes or their contents. Therefore, the objectives of this study are: 1) determine the generation of exosomes from primary

amnion epithelial cells and characterize their contents, 2) determine the changes in specific exosome contents in primary amnion cells in response to oxidative stress. Since p38 MAPK was identified as a crucial stress response-signaling pathway that activates oxidative stress induced senescence at term, we specifically examined exosomal p38 MAPK cargo. Using an in vitro primary amnion epithelial cell (AEC) model of oxidative stress induced by cigarette smoke extract, a well characterized model of in vitro oxidative stress, and using Liquid Chromatography (LC)/ Mass Spectrometry (MS) and Next Generation Sequencing, we characterize the contents of AEC -derived exosomes and their potential role in parturition.

## **Materials and Methods**

Placental samples were obtained for this study from John Sealy Hospital at The University of Texas Medical Branch (UTMB) at Galveston, TX, USA. No subjects were recruited or consented for this study as we used discarded placenta from normal term, not in labor cesarean sections. The study protocol was submitted and approved by the institutional review board at UTMB, whereby placental samples could be collected without consenting subjects. Placentae from women (18–40 years old) undergoing elective repeat cesarean delivery (between 37 and 41 weeks of gestation) prior to the onset of labor were included in the study. Women with prior history of preterm labor and delivery, preterm premature rupture of the membranes, preeclampsia, placental abruption, intrauterine growth restriction, and gestational diabetes were excluded. Additionally, group B *streptococcus* carriers, treated for urinary tract infection, sexually transmitted diseases, chronic infections like HIV, hepatitis, and women who smoked cigarettes or reported drug and alcohol abuse, were also excluded.

### **Isolation and Culture of Human Amnion Epithelial Cells (AECs)**

All reagents and media were warmed to 37°C prior to use. The amniotic membrane was processed as described previously [87,89]. Briefly, the amnion membrane was manually peeled from normal, term, not in labor caesarean section placentas, rinsed in saline and transferred to a petri dish containing Hanks Balanced Salt Solution (HBSS; Mediatech Inc., Manassas, VA). After cutting the amnion into 2 cm x 2 cm pieces, they were digested twice in 0.25% trypsin and 0.125% Collagenase A (Sigma – Aldrich, St. Louis, MO) in HBSS for 35 minutes at 37°C. After each digestion, the tissue was filtered through a 70 µm cell strainer (Thermo Fisher Scientific, Waltham, MA) and trypsin was inactivated using complete Dulbecco's Modified Eagle Medium: Nutrient Mixture F-12 media (DMEM/F12; Mediatech Inc.) supplemented with 15% fetal bovine serum (FBS; Sigma-Aldrich), 10% Penicillin/Streptomycin (Mediatech Inc.) and 100 µg/mL epidermal growth factor (EGF; Sigma-Aldrich). The collected filtrate was centrifuged for 10 minutes at 3000 RPM and the pellet was resuspended in 3.0 mL complete DMEM/F12. Once cells were counted, approximately 3-5 million cells per flask were cultured in T75 flasks containing complete DMEM/F12 media at 37°C, 5% CO<sub>2</sub>, and 95% air humidity to 70-80% confluence.

### **Stimulation of AECs with Cigarette Smoke Extract (CSE)**

To induce oxidative stress in AECs, CSE was used as detailed in our prior studies, [87,118,119] with modifications. Smoke from a single lit commercial cigarette (unfiltered Camel<sup>TM</sup>, R.J. Reynolds Tobacco Co, Winston Salem, NC) was infused into 25 mL of exosome-free media, consisting of DMEM/F12 supplemented with 10% exosome-free FBS (System Biosciences, Mountain View, CA). The stock CSE was sterilized using 0.25 mm Steriflip® filter unit (Millipore, Billerica, MA). CSE concentrate was diluted 1:10 in exosome-free media prior to use. Once cells reached 70-80% confluence, each flask was

rinsed with sterile 1x PBS followed by treatment with exosome-free media (control) or CSE containing media and incubated at 37°C, 5% CO<sub>2</sub>, and 95% air humidity for 48 hours.

### **Activation of p38 MAPK in AECs Using Flow Cytometry**

Activation of p38 MAPK was also performed. After harvesting cells using trypsin EDTA and centrifugation for 10 minutes at 3000 RPM, the pellet was resuspended in 500  $\mu$ L 4% paraformaldehyde and vortexed. After incubation for 10 minutes at room temperature, cells were placed on ice for 1 minute then centrifuged for 5 minutes at 2000 RPM at 4°C. The supernatant was removed and the pellet was resuspended in 500  $\mu$ L 90% ice cold methanol, gently vortexing while adding methanol slowly. Once the pellet was completely resuspended, the cells were incubated on ice for 10 minutes then stored at -20°C until use. All centrifugations were performed at 2000 RPM for 5 minutes at 4°C. Cells in 90% methanol were centrifuged and washed twice with 5% BSA in PBS. After the second centrifugation, the pellet was resuspended in P-p38 MAPK primary antibody (Cell Signaling) diluted 1:200 in 5% BSA and incubated at room temperature for 2 hours. Cells were washed twice with 5% BSA in PBS then resuspended in Alexa Fluor conjugated secondary antibody (Life Technologies) diluted 1:400 in PBS and incubated for 1 hour at room temperature in the dark. Cells were centrifuged and resuspended in 400  $\mu$ L PBS and run immediately on the Cytoflex flow cytometer (Beckman Coulter). After gating for single cells, data analysis based was performed using Cytexpert (Beckman Coulter).

### **Senescence-Associated B-Galactosidase (SA-B-Gal) Activity**

Senescence was assessed with the commonly used biomarker senescence-associated  $\beta$ -galactosidase (SA- $\beta$ -Gal) activity, adapted for flow cytometry [120,121] with modifications. Cells were incubated for 1 hour in complete DMEM growth medium supplemented with 100nM bafilomycin A1 (baf A1). After 1 hour, 5-

dodecanoylaminofluorescein di- $\beta$ -D-galactopyranoside (C<sub>12</sub>FDG) was added for a final concentration of 6 $\mu$ M and incubated at 37°C, 5% CO<sub>2</sub>, and 95% air humidity for 1 hour. Cells were harvested by trypsinization and centrifugation at 3000 g for 10 minutes at 4°C. The cell pellet was resuspended in 500- $\mu$ L Coulter DNA Prep Stain (Beckman Coulter, Indianapolis, IN) and run immediately on the CytoFlex flow cytometer (Beckman Coulter). Unstained, control AECs were used as negative controls for gating. Data analysis was performed using Cytexpert (Beckman Coulter).

### **Isolation of Exosomes from Control and CSE-Treated Amnion Cell**

The culture media were collected and centrifuged at 300g for 10 minutes and 2,000g for 20 minutes at 4°C then stored at -80°C until exosome isolation. Media was thawed overnight at 4°C then isolated using differential ultracentrifugation as described previously, with modifications [57,122–125]. Briefly, the supernatant was transferred to Amicon Ultra 15 centrifugation filters (Millipore, Billerica, MA) and centrifuged at 2000 g for 90 minutes. The concentrate was collected and centrifuged at 10,000 g for 30 minutes. The supernatant was transferred to ultracentrifugation tubes and centrifuged at 100,000 g for 2 hours. The supernatant was discarded, and the pellet was resuspended in cold 1x PBS then centrifuged at 100,000 g for 1 hour. The final pellet was resuspended in RIPA (Western Blot) or 1x PBS (electron microscopy, Flow Cytometry, DNA quant and sizing) and stored at -80°C until use.

### **Transmission Electron Microscopy (TEM) Of Whole Mounted Exosomes**

For TEM studies, 5  $\mu$ L suspended exosomes in PBS were dropped onto a formvar-carbon coated 300-mesh copper grid and left to dry at room temperature for 10 min. Grids were treated with 10 seconds of Hydrogen-Oxygen plasma in a Gatan Solarus 950 plasma cleaning system (Gatan, Inc., Pleasanton, CA) prior to use. After three washes in purified

water, the exosome samples were negatively stained using PhosphoTungstic Acid (PTA). The grids were dried at room temperature then viewed in a 120 keV JEM 1400 electron microscope (Jeol, Peabody, MA). A minimum of 10 frames were viewed per sample.

### **Nanoparticle Tracking Analysis**

Exosome total size distribution and concentration was determined using the Nanosight NS300 (Malvern Instruments, Worcestershire, UK). Samples were diluted 1:500 in distilled water and run following the manufacturer's instructions. For all samples, we used a camera level of 15–16 and automatic functions for all postacquisition settings except for the detection threshold, which was fixed at 5. The camera focus was adjusted to make the particles appear as sharp dots. Using the script control function, three 30-second videos for each sample were recorded.

### **Western Blot Analysis**

Exosomal pellets were resuspended in RIPA lysis buffer (50 mM Tris pH 8.0, 150 mM NaCl, 1% Triton X-100, and 1.0 mM EDTA pH 8.0, 0.1% SDS) supplemented with protease and phosphatase inhibitor cocktail and PMSF. After centrifugation at 10,000 RPM for 20 minutes, the supernatant was collected and protein concentrations were determined using BCA (Pierce, Rockford, IL). The protein samples were separated using SDS-PAGE on a gradient (4–15%) Mini-PROTEAN1TGX™ Precast Gels (Bio-Rad, Hercules, CA) and transferred to the membrane using iBlot1Gel Transfer Device (Thermo Fisher Scientific). Membranes were blocked in 5% nonfat milk in 1x Tris buffered saline-Tween 20 (TBS-T) buffer for a minimum of 1 h at room temperature then probed (or re-probed) with primary antibody overnight at 4°C. The membrane was incubated with suitable secondary antibody conjugated with horseradish peroxidase and immunoreactive proteins were visualized using Luminata Forte Western HRP substrate (Millipore, Billerica, MA).

The stripping protocol followed the instructions of Restore Western Blot Stripping Buffer (Thermo Fisher). No blots were used more than three times. The following anti-human antibodies were used for Western blot: exosome markers CD9 (Abcam, Cambridge, United Kingdom) diluted 1:400, CD81 (Abnova, Taiwan) diluted 1:500 and Alix (Abcam) diluted 1:500, Nanog (Cell Signaling, Beverly, MA) diluted 1:400 to confirm AEC specificity of exosomes, Heat shock protein (HSP) 70 (Abcam), a damage associated molecular pattern, was diluted 1:500. Total p38 MAPK and phospho p38 MAPK (Cell Signaling) were diluted 1:400.

### **Flow Cytometry Analysis for Exosome Markers**

For flow cytometry analysis of exosome tetraspanin markers CD9, CD63 and CD81, a total of five samples per condition were prepared using the ExoFlow kit (System Biosciences) protocol with modifications. Briefly, exosomes isolated from treated and untreated amnion cell cultures were resuspended in 150  $\mu$ L 1x PBS and all kit reagent volumes were halved. Streptavidin coated 9.1 $\mu$ m beads were washed then incubated with biotinylated anti-CD9, CD63 or CD81 for 2 hours on ice, flicking intermittently to mix. Beads were washed and resuspended in 200  $\mu$ L bead wash buffer prior to incubation overnight at 4°C with 50  $\mu$ L exosomes (total volume 250  $\mu$ L). The following day, samples were washed and stained using the Exo-FITC exosome stain according to manufacturer then run on the Cytoflex flow cytometer (Beckman Coulter). Negative controls with isotype-matched antibodies were used for gating, applied according to manufacturer instructions. Data analysis based on fluorescein isothiocyanate (FITC) signal shift was performed using Cytexpert (Beckman Coulter).

### **Immunofluorescence Staining and Microscopy**



Oxidative stress induction of AECs activates pro-senescence marker p38 MAPK by phosphorylation while also releasing HMGB1 from the cells' nuclei to cytoplasm. Both are expected to be packaged into exosomes. To colocalize HMGB1 and P-p38 MAPK inside exosomes, IF staining was performed for colocalization with exosome marker CD9. Once cells reached confluence, culture media were removed, and cells were rinsed with PBS, harvested with trypsin EDTA (Corning, Corning, NY), and centrifuged for 10 minutes at 3000 RPM. Cells were resuspended in complete media and seeded on glass coverslips at a density of 30,000 cells per slip and incubated overnight. Cells, untreated and CSE-treated (48 hours), were fixed with 4% paraformaldehyde (PFA), permeabilized with 0.5% Triton X, and blocked with 5% bovine serum albumin (BSA, Fisher Scientific, Waltham, MA) in PBS prior to incubation with primary antibodies HMGB1 (Cell Signaling), P-p38 MAPK (Cell Signaling) and CD9 (Abcam, Cambridge, United Kingdom) diluted 1:300 in 5% BSA overnight at 4°C. After washing with PBS, slides were incubated with Alexa Fluor 488- or 594-conjugated secondary antibodies (Life Technologies, Carlsbad, CA) diluted 1:1000 in 5% BSA for 30 minutes in the dark. Slides were washed with PBS, treated with NucBlue® Live ReadyProbes® Reagent (Life Technologies) for 2 minutes, and mounted using Mowiol 4-88 mounting medium (Sigma-Aldrich). Slides were dried at room temperature and stored in the dark until imaging.

#### **Exosomal localization of cffTF using fluorescent in situ hybridization (FISH)**

To colocalize cffTF in exosomes, cells were harvested as described above and seeded in Millicell EZ slides 4-well glass slides (Millipore, Billerica, MA) at a density of 65,000 cells/well overnight. After 48-hour treatment, cells were fixed and permeabilized with ice cold 100% methanol (stored at -20°C) for 10 minutes at -20°C and blocked with 5% BSA in PBS. Cells were incubated with primary antibody CD9 diluted 1:300 in 5% BSA at 4°C overnight while gently rocking. After washing with PBS, slides were incubated

with Alexa Fluor 594-conjugated secondary antibody (Life Technologies) diluted 1:1000 in 5% BSA in the dark for 30 minutes. Cells were washed with PBS then refixed using 4% PFA and permeabilized with 70% EtOH overnight at 4°C. Wells of the slides were removed, and cells were dehydrated by 2-minute incubation in 85% and 100% ethanol. Slides were air-dried at room temperature for 10 minutes.

Leading strand (C-rich) telomere peptide nucleic acid (PNA) probe conjugated with Alexa Fluor 488 (PNA Bio, Newbury Park, CA) lyophilized powder was resuspended in 100- $\mu$ L formamide to make a 50 $\mu$ M stock, which was aliquoted and stored at -80°C. The stock was diluted in prewarmed hybridization buffer (Thermo Fischer) to a final concentration of 200nM, and 50  $\mu$ L was added to each prewarmed slide, covered with a coverslip, and heated at 85°C for 10 minutes. For in situ hybridization, slides were incubated at room temperature for 2 hours in a humidity chamber. After hybridization, slides were placed in 2x SSC with 0.1% Tween to remove the coverslips and washed twice in 2x SSC with 0.1% Tween heated to 55°C–60°C and again at room temperature. Slides were treated with NucBlue® Live ReadyProbes® Reagent (Life Technologies) for 2 minutes and then washed in 2x SSC, 1x SSC, and DI H<sub>2</sub>O for 2 minutes each. Slides were dried at room temperature for 10 minutes then mounted using Mowiol 4-88 mounting medium (Sigma-Aldrich). Slides were dried at room temperature and stored in the dark until imaging.

### **Image Processing and Analysis**

Confocal images were acquired using a Zeiss LSM-510 Meta confocal microscope with a 63  $\times$  1.20 numerical aperture water immersion objective. The images were obtained using 3 excitation lines (364, 488, and 543), line emissions were collected with 385–470-nm, 505–530-nm, and 560–615-nm filters, respectively. All images were collected using 8-frame-Kallman-averaging with a pixel time of 2.51  $\mu$ s, a pixel size of 160 nm, and an

optical slice of 1  $\mu\text{m}$ . Z-stack acquisition was carried out with 0.8- $\mu\text{m}$  z-steps. Image processing and analysis were performed with Image J (open source) to set the low and high thresholds for measurement of immunofluorescent intensity. After discounting background in each channel, we traced a linescan over the areas where we saw the highest intensity of colocalized signal. A graphic of raw fluorescence intensity vs calibrated distance in micrometers along the linescan (indicated by arrows on every figure) was plotted.

### **Proteomic Analysis of AEC-Derived Exosomes by Mass Spectrometry**

Protein profile of exosomes isolated from AEC culture under normal or oxidative stress conditions were established by Liquid Chromatography (LC)/ Mass Spectrometry (MS) as previously described with modifications [69,117]. Briefly, exosome pellets were lysed in 500 $\mu\text{L}$  modified RIPA buffer (2.0% SDS, 150mM NaCl, 50mM Tris, pH 8.5, 1X Complete Protease inhibitor (Roche)) at 100°C for 15 minutes. The lysate was clarified by centrifugation and the protein concentration determined by Qubit fluorometry (Invitrogen). 10  $\mu\text{g}$  of extracted protein was processed by SDS-PAGE using 10% Bis Tris NuPage mini-gel (Invitrogen) in the MES buffer system. The migration window (2cm lane) was excised and in-gel digestion performed using a ProGest robot (DigiLab) using ammonium bicarbonate (25mM), dithiothreitol (reduction step, 10mM at 60°C) and iodoacetamide (alkylation step, 50mM). Samples were digested with sequencing grade trypsin (Promega) at 37°C for 4h and quenched with formic acid. The supernatant was analyzed directly without further processing. Digested samples were analyzed by nano LC-MS/MS with a Waters NanoAcquity HPLC system interfaced to a ThermoFisher Q Exactive. Peptides were loaded on a trapping column and eluted over a 75 $\mu\text{m}$  analytical column at 350nL/min using a 2hr reverse phase gradient; both columns were packed with Jupiter Proteo resin (Phenomenex). The mass spectrometer was operated in data-dependent mode, with the Orbitrap operating at 60,000 FWHM and 17,500 FWHM for MS and MS/MS respectively.

The fifteen most abundant ions were selected for MS/MS. False discovery rate (FDR) was estimated using a reversed sequence database.

Proteins identified by MS/MS were analyzed by PANTHER (Protein Analysis THrough Evolutionary Relationships; <http://www.pantherdb.org>) as previously described [69,117]. Differentially identified proteins were analyzed further by bioinformatic pathway analysis (Ingenuity Pathway Analysis [IPA]; Ingenuity Systems, Mountain View, CA; [www.ingenuity.com](http://www.ingenuity.com)).

### **NGS to Determine Exosomal cffTF and Other Cell-Free Amnion Cell DNA Specificity**

DNA libraries were created using the Nextera tagmentation technology (Illumina, San Diego, CA). Tagmentation uses a transposon-based approach that fragments the target DNA and introduces a partial adapter sequence in a single step. All DNA samples were quantified using a Qubit fluorometric assay (Thermo Fisher Scientific). DNA quality was assessed using a high-sensitivity DNA chip on an Agilent 2100 Bioanalyzer (Agilent Technologies, Santa Clara, CA). Creation of DNA libraries was performed using 50 ng of genomic DNA and Nextera tagmentation reagents as recommended by the manufacturer. Limited PCR (5 cycles: 95C x 10 seconds/ 62C x 30 seconds/ 72C x 3 minutes) amplification was performed to complete the adapter sequence and index the final library. All NGS libraries were indexed independent of the planned complexity of the sequence analysis. The final concentration of all NGS libraries was determined using a Qubit fluorometric assay, and the DNA fragment size of each library was assessed using a DNA 1000 high-sensitivity chip and an Agilent 2100 Bioanalyzer.

We created an artificial telomere sequence by concatenating 50 copies of the consensus sequence TTAGGG. Adapter sequences were trimmed from the reads in fastq format using the program Trimmomatic, version 0.36, without quality trimming. Reads

were then aligned in paired end format to the telomere reference using Bowtie2, version 2.2.5, in the local alignment mode with default parameters. The number and percentage of mapped reads were reported in the Bowtie2 output [126,127]. Circular representations of the readings of fragments along each chromosome in the whole-genome and mitochondria were created using Circos [128].

### **Statistical Analysis**

SPSS software (IBM, Armonk, NY) was used for statistical evaluation. Samples were analyzed using independent sample t test, and a P value less than .05 was considered statistically significant.

## **Results**

### **Primary AEC Cultures Are Positive for Cytokeratin**

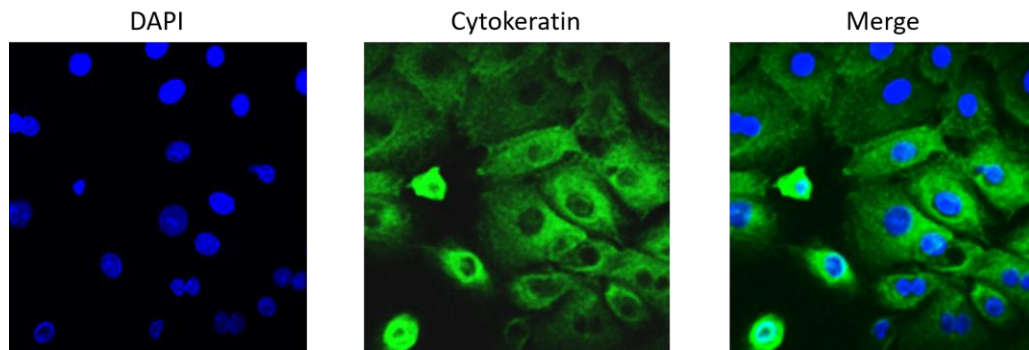


**Figure 2.1: Cytokeratin staining of primary AECs.**

Primary AECs were fluorescently labeled for cytokeratin 18 to show cultures were predominantly epithelial cells. AEC- amnion epithelial cell.

Primary amnion cells isolated from term, not in labor C-sections were positive for cytokeratin 18, a commonly used marker for epithelial cells (Figure 2.1).

### **CSE Activates p38 MAPK and Induces Cellular Senescence in Primary AECs**

We examined p38 MAPK activation, an oxidative stress response indicator activated by various stressors, and beta-galactosidase activity using flow cytometry. AECs treated with CSE showed higher p38 MAPK activation than control cells (Table 2.1), indicating CSE AECs were undergoing oxidative stress and cellular senescence. To determine cellular senescence, control and CSE-treated cells were analyzed for SA- $\beta$ -Gal activity using flow cytometry [44,120,121,129]. As shown in Table 1, control cells (9.5%) had significantly ( $p < 0.0001$ ) less senescent cells compared to CSE-treated cells (38.0%). This finding confirmed our prior histology-based reports that CSE causes AEC senescence [34,87–89].

**Table 2.1: p38 MAPK Activation (P-p38) and Cellular Senescence of Control and CSE treated AECs**

	P-p38 MAPK	SA- $\beta$ -Gal
Control (untreated) AEC	1.8%	9.5%
CSE Treated AEC	35.9%	38.0%

### **Characterization of Exosomes from Control and CSE-Treated AECs**

Exosomes isolated from AECs under standard (control) and oxidative (CSE) conditions were characterized using four different methods—electron microscopy (for shape and morphology), nanoparticle tracking analysis (size), western blot and flow cytometry (specific markers and cargo contents) and Next Generation Sequencing (DNA cargo).

TEM studies (Figure 2.2A) showed, regardless of treatment, amnion exosomes exhibited cup-shaped morphology and a size distribution of 50–150 nm [67,130]. Nanoparticle tracking analysis was performed to confirm size distribution and quantify the number of exosomes per sample (Figure 2.2B). There was no significant difference ( $P = 0.474$ ) seen in the size distribution of exosomes derived from control (138.6 nm) and

CSE-treated (137.8 nm) AECs. Additionally, after quantifying the number of exosomes in each prep, we calculated the number exosomes released per cell in each experiment. We did not see significant difference ( $P=0.53$ ) in number of exosomes secreted in control (2727 exosomes per cell) and CSE-treated (2926 exosomes per cell) cells (Table 2.2).

**Table 2.2- Size and quantity distribution of control & CSE exosomes**

	Mean Size (nm)	Exosomes/cell
Control	138.6	2727
CSE	137.8	2926

Western blot was performed to characterize common exosome markers and cell-type-specific markers in each sample (Figure 2.2C). Regardless of condition, AEC-derived exosomes were positive for exosome markers CD9, CD81, and Alix, as well as embryonic stem cell marker Nanog. Flow cytometry was performed to further characterize the exosomes using tetraspanin markers CD9 and CD63 (Figure 2D), common markers used for exosome identification [131]. The shift in FITC intensity on the representative histograms in Figure 2E indicates beads positive for either CD9 or CD63 exosomes (pink peaks) relative to the negative control (no exosomes) (green peaks). By graphing forward scatter versus FITC intensity, we calculated the percentage of beads positive for exosome markers. After subtracting the negative control to account for background, results are expressed as percentage of beads positive for CD9 or CD63 expressing exosomes. Exosomes from control AECs showed an average of 70% for CD9 compared to 38% in CSE treated AEC exosomes. Similar decrease was also seen for CD63 (64% and 19% in controls vs CSE respectively). Difference in exosome marker expression was found to be statistically significant ( $P < 0.05$ ).

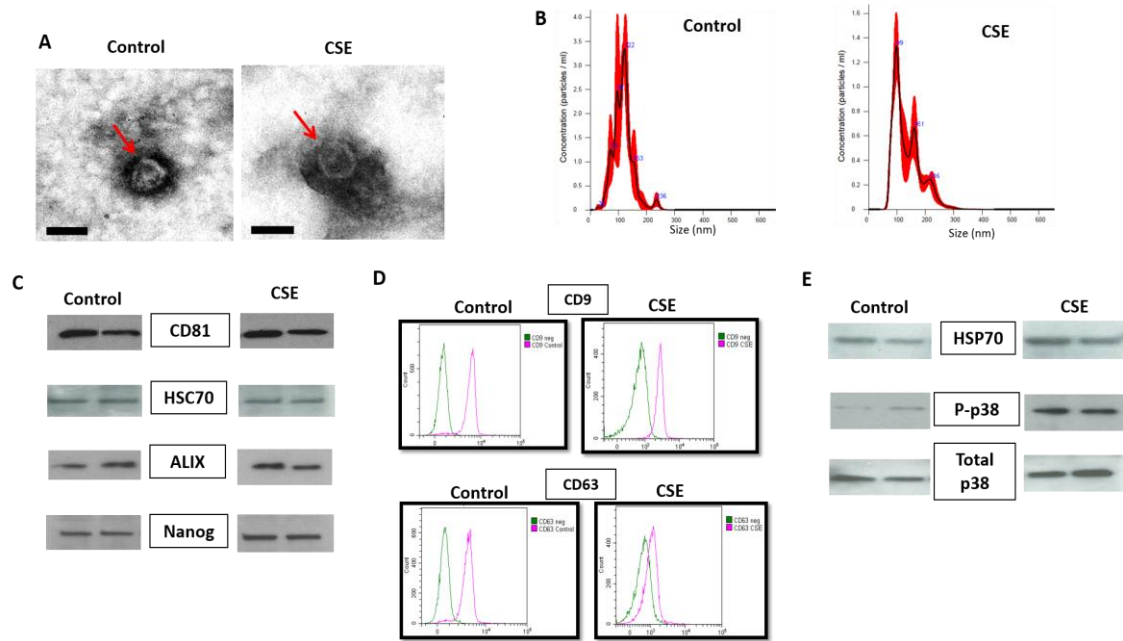


**Figure 2.2: Characterization of exosomes released from amnion cells grown under standard (control) and oxidative (CSE) conditions.**

A: Electron microscopy showing cup-shaped vesicles that have a size distribution of 30–150 nm (arrow indicates exosomes; scale bar represents 50 nm). B: Representative images from nanoparticle tracking analysis (NTA) of control and CSE exosomes. All our preparations showed particles <140 nm. C: Western blot analysis showed the presence of exosome markers CD81, HSC70 and ALIX, as well as embryonic stem cell marker, Nanog, indicating amnion epithelial cell origin. D: Flow cytometric characterization of exosome tetraspanin markers exosome markers CD9 and CD63. X-axis is FITC intensity, y-axis is count, or number of beads positive for exosomes. Green represents negative control (neg). E: Western blot analysis showing differences in specific markers. Presence of stress responsive and pro-senescence marker p38 mitogen activated protein kinase (MAPK) and one of the DAMP) markers, HSP70, in exosomes from both control and CSE treated AECs. Expression of P-p38 MAPK was higher in exosomes from AECs treated with CSE compared to control.

### Characterization of Exosomal Cargo from Control and CSE Treated AECs

Western blot analysis showed the presence of active forms of pro-senescence and parturition associated marker p38 MAPK (P-p38 MAPK) and one of the damage associated molecular pattern (DAMP) molecules HSP70 in exosomes from both control and CSE treated AECs. As shown in Figure 2E HSP70, P-p38 MAPK and total p38 MAPK were



seen in both untreated and treated exosomes. However, the intensity of bands for P-p38 MAPK was higher in exosomes from AECs treated with CSE.

P-p38 MAPK (Figure 2.3), Histone 3 (H3, Figure 2.4), and HSP70 (Figure 2.5) were colocalized with exosome marker CD9 using immunofluorescent microscopy to determine whether exosomes reflect the physiologic state of AECs. All studied markers are associated with oxidative stress response and activation of p38 MAPK in amnion cells, which is the signaler in senescence response to CSE. H3 and HSP70 are p38 MAPK responder genes in stress associated cellular signaling [132,133]. Colocalization was quantified using Pearson's correlation coefficient and graphed comparing control and CSE mean values. Colocalization of all three markers were significantly higher in CSE treated AEC exosomes compared to control AEC exosomes (mean Pearson's correlation coefficients for each were statistically significant ( $p < 0.05$ )) confirming CSE causes increased cargo of these markers by exosomes. CSE induced oxidative stress damage leads

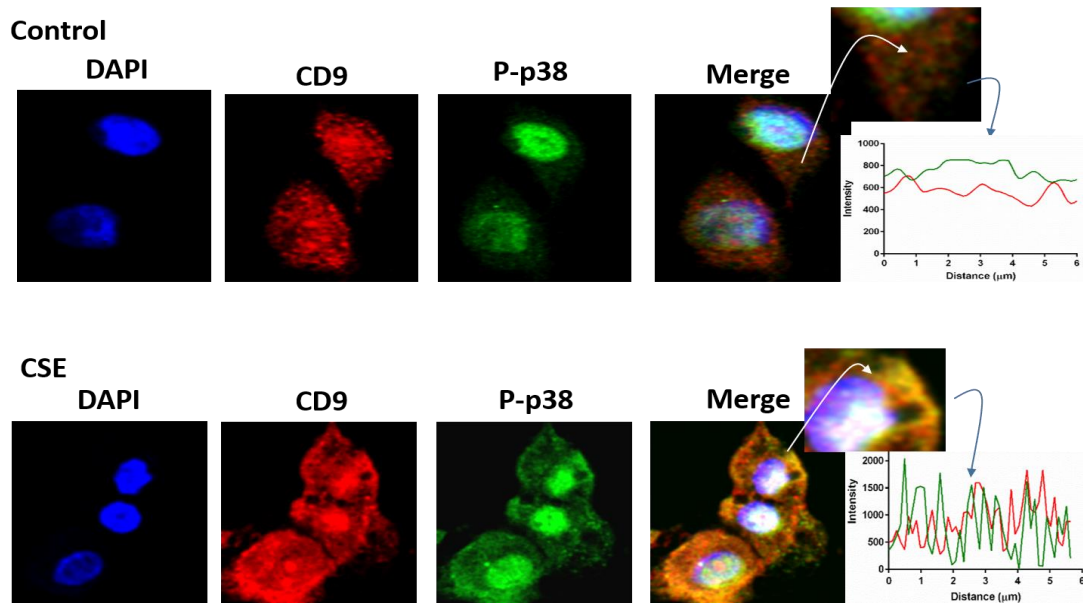


**Figure 2.3: Colocalization of exosome marker CD9 and P-p38 MAPK in AECs.**

Colocalization of pro-senescence marker P-p38 MAPK and CD9: Immunofluorescence imaging of control (top panel) and CSE treated amnion cells (bottom panel) show colocalization differences of P-p38 MAPK (green) and CD9 (red).

to senescence of AEC through p38 MAPK signaling [87] and current data confirm that P-p38 MAPK and its responder proteins H3 and HSP70 can also get packaged inside

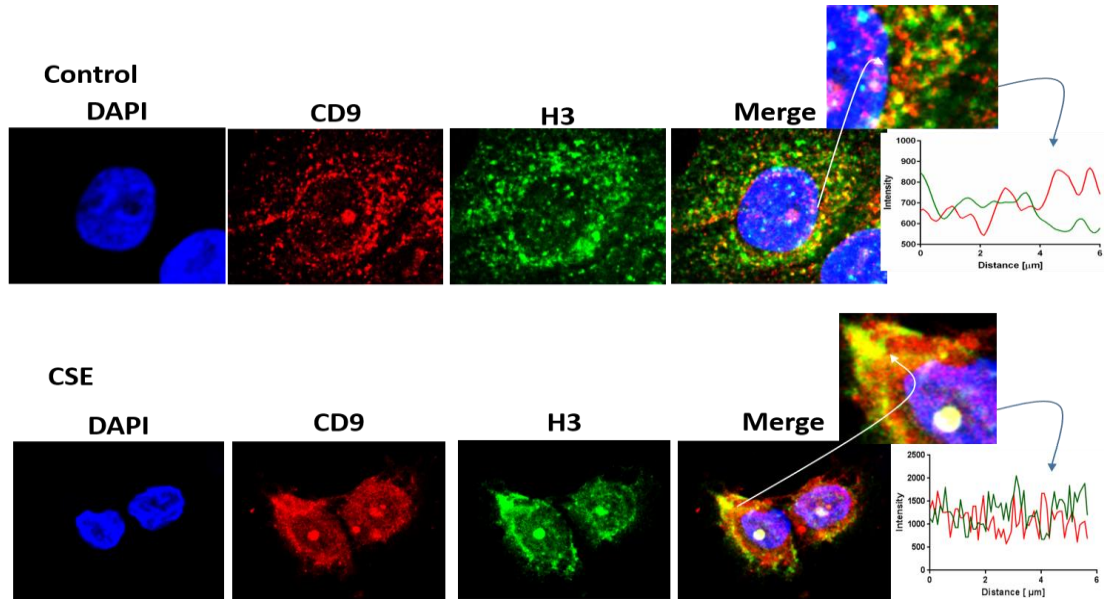


**Figure 2.4: Colocalization of exosome marker H3 and CD9 in AECs.**

Immunofluorescence imaging of control (top panel) and CSE treated amnion cells (bottom panel) show colocalization differences of H3 (green) and CD9 (red).

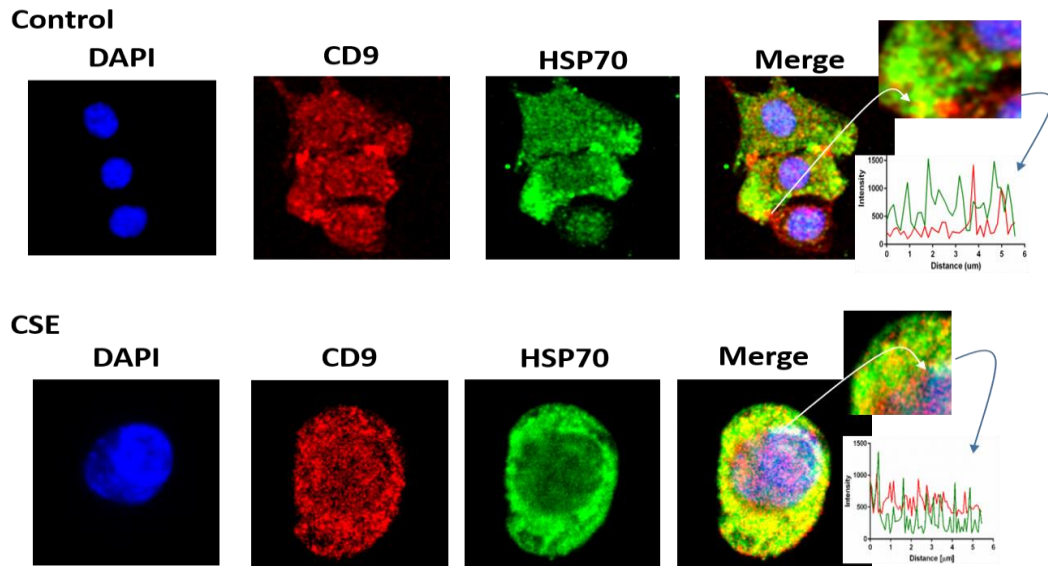


**Figure 2.5: Colocalization of exosome marker HSP70 and CD9 in AECs.**

Immunofluorescence imaging of control (top panel) and CSE treated amnion cells (bottom panel) show colocalization differences of HSP70 (green) and CD9 (red).

exosomes at a higher level reflecting the physiologic state of AECs.

HMGB1, a nonhistone nuclear protein, was localized in the nucleus (green staining) in control cells (Figure 2.6A). Oxidative stress induced by CSE, however, caused translocation of HMGB1 from the nucleus to cytoplasm (Figure 2.6B). Red staining in the cells represent CD9+ exosomes. Next, we determined colocalization of HMGB1 within the exosomes in both control and CSE-treated AECs. Control amnion cells displayed only a few overlapping spots in a cell, whereas CSE treatment produced cytoplasmic localization

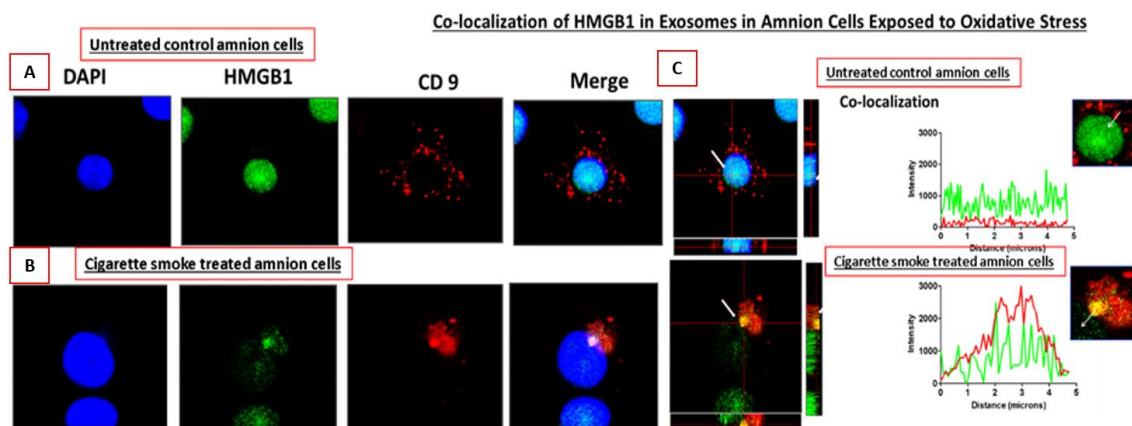


**Figure 2.6: Colocalization of HMGB1 in exosomes.**

A: Colocalization of HMGB1 and CD9+ exosomes in untreated amnion cells compared to CSE treated amnion cells. B: Confocal xy-planes of the z-stack. Intensity profile graphs show the topographical profile of the pixel intensity levels of each antibody labelling along the freely positioned arrow. The maximum height represents the brightest possible pixel in the source image.

of HMGB1 and multiple areas of colocalization (Figure 2.6C). A linescan confirmed that colocalization of HMGB1 in exosomes was higher in the cytoplasm after CSE treatment compared to controls AECs. This finding confirms that exosomes and HMGB1 are colocalized, and they can potentially escort off the cell together.

FISH was performed to colocalize cffTF and exosome marker CD9. Under standard cell culture conditions, telomeres are localized in the AEC nucleus (Figure 2.7A). Treatment of AECs with CSE caused fragmentation of telomeres (as reported previously)

and telomere fragment translocation from the nucleus to the cytoplasm (Figure 2.7C). A linescan was performed to determine colocalization of telomere fragments with exosome marker CD9. As shown in Figure 2.7B and 2.7D, colocalization of cffTF in exosomes was higher in CSE-treated AECs compared to control.

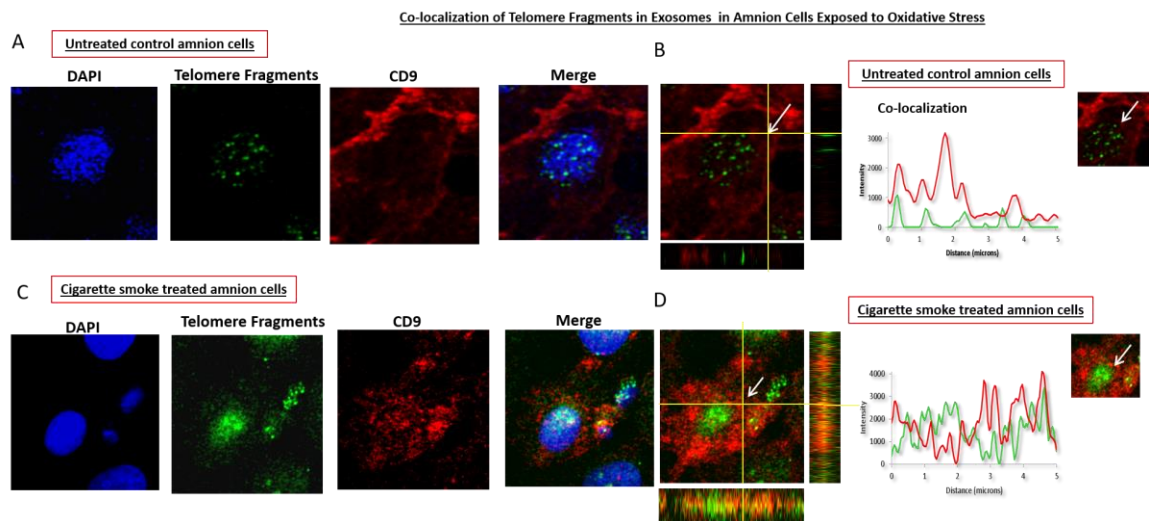


**Figure 2.7: Colocalization of cffTF in exosomes.**

A: Colocalization of telomere fragments in untreated amnion cells compared to CSE treated amnion cells. B: Confocal xy-planes of the z-stack. Intensity profile graphs show the topographical profile of the pixel intensity levels of each antibody labelling along the freely positioned arrow.

## Proteomic Analysis of AEC-Derived Exosomes by Mass Spectrometry

Mass spectrometry analysis identified over 200 exosomal proteins (Appendix Table 1). We also identified unique proteins for each condition (Figure 2.8A; See Appendix 1: Supplemental Tables 2.1 and 2.2). The number of proteins identified in exosomes isolated from AEC exposed to CSE was higher (193) compared to control (173). We investigated the molecular network that can be activated by the proteins identified in exosomes isolated from AEC cultured under normal (Figure 2.8B) and oxidative stress conditions (Figure

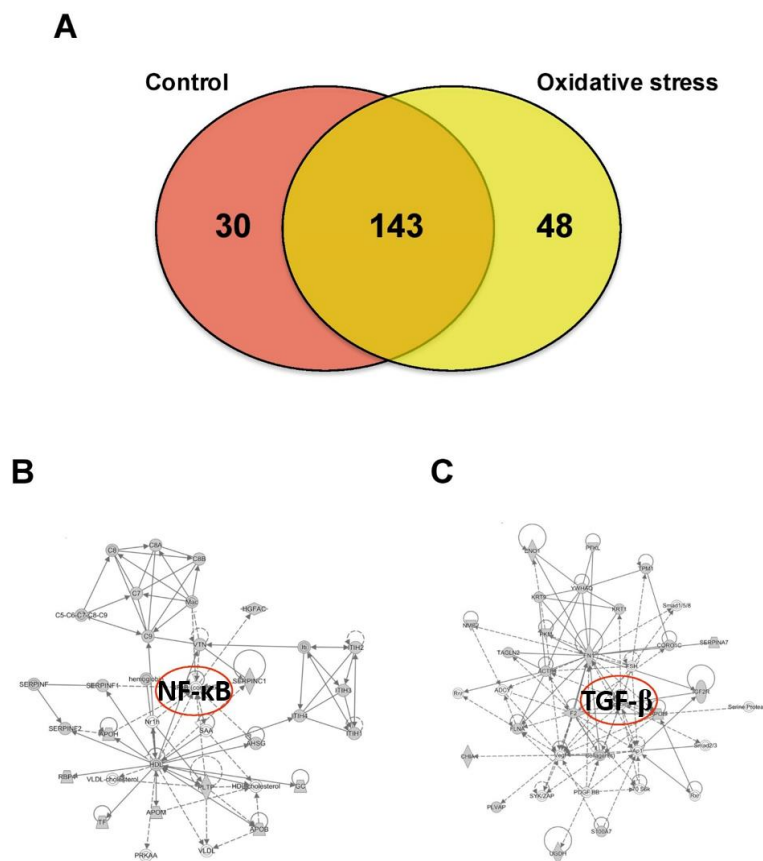


**Figure 2.8: Proteomic analysis of AEC-derived exosome proteins.**

A: The Venn diagram represents the distribution of common and unique proteins identified by nanospray LC-MS/MS in exosomes released from AEC cultured under normal or stress conditions (n=2 per treatment). List contain 221 unique proteins. B and C: Proteins identified in exosomes isolated from AEC under normal (B) or oxidative stress (C) conditions were submitted to IPA network analysis. Red circle: central molecules involved in the signaling pathways.

2.8C). Interestingly, NF- $\kappa$ B complex seems to be a central regulator in the molecular network that can be activated by exosomes network from exosomes from AEC treated with CSE. We have already reported that CSE treatment produces minimal activation of NF- $\kappa$ B compared to control and the exosomal proteomic analysis further supports our earlier findings [93]. We have also seen evidence of epithelial-mesenchymal transition (EMT) of amnion epithelial cells under oxidative stress conditions. TGF- $\beta$  is a major mediator of EMT [134–138]. Molecular networks in CSE treated exosomes suggests that TGF- $\beta$

mediated EMT may be functional in AECs under oxidative stress. Using Ingenuity Pathway Analysis (IPA), a bioinformatics approach, we examined the biological pathways represented by differentially expressed proteins from our proteomic analysis. The canonical pathways determined by exosomal cargo contents showed ERK/MAPK (Figure 2.9A), PI3K/AKT (Figure 2.9B) and epithelial adherent junctions (Figure 2.9C) was significantly higher in exosomes from AEC under oxidative stress conditions compared to the control. On the other hand, canonical pathways as LPS/IL-1 mediated inhibition of the nuclear receptor retinoid X receptor (RXR) function and IL-6 signaling were significantly lower and unchanged in exosomes from AEC cultured under oxidative stress conditions compared to control, respectively. Finally, analysis of diseases and functions showed that exosomes isolated from AEC under oxidative stress conditions might significantly increase the eosinophilic inflammation compared to control. Interestingly, higher amount of eosinophil cells in the amniotic fluids has been associated with preterm labor [139].

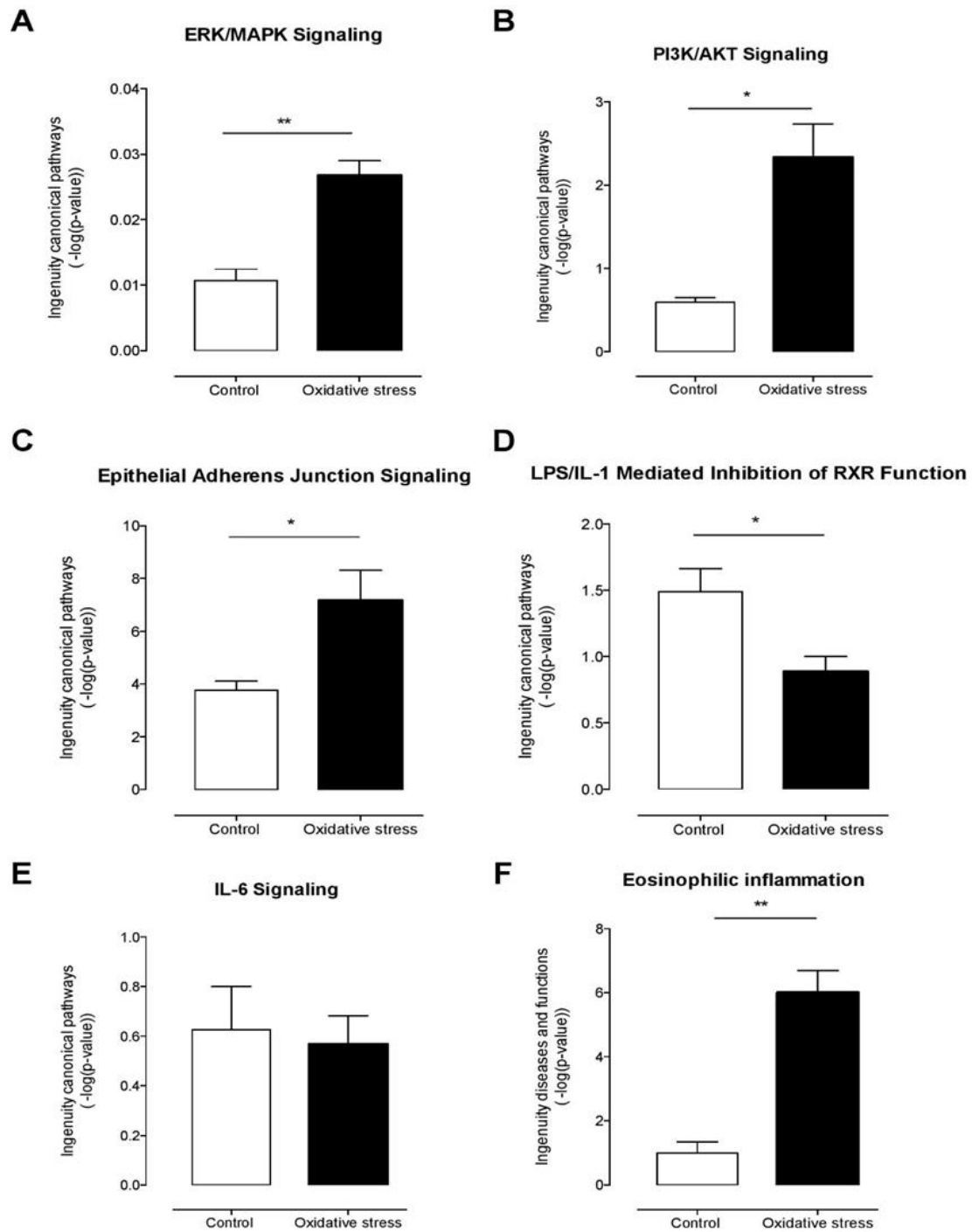


**Figure 2.9: Ingenuity pathway analysis of AEC-derived-exosomes proteins**

Exosomal protein identified under normal (control) or oxidative stress conditions were analyzed using the IPA software. Comparison of canonical pathways: (A) ERK/MAPK, (B) PI3K/AKT, (C) epithelial adherens junctions, (D) LPS/IL-1 mediated inhibition of RXR function and (E) IL-6 signaling. Diseases and functions analysis: (F) eosinophilic inflammation.



## Exosomes Released from AECs Contain Genomic and Nongenomic DNA

DNA extracted from control and CSE exosomes was analyzed by high throughput sequencing. DNA sequencing was done to confirm the above reported findings using FISH. By creating an artificial telomere sequence using 50 copies of the consensus sequence TTAGGG, we determined that CSE exosomes carry nongenomic DNA and their telomere fragment specificity. Quantitative assessment of any differences in cffTF between normal and CSE-derived AEC exosomes were not attempted in this approach.

In addition to determining cffTF in exosomes, we also report the presence of genomic DNA in exosomes. Reads from control and CSE AEC exosomes were aligned to the whole genome (Figure 2.10A). While we did not find an overrepresentation of a specific chromosome in either treatment, we did see that CSE exosomes had significantly higher GC content than control exosomes ( $P=0.023$ ). Control and CSE DNA reads were also aligned to mitochondrial DNA (Figure 2.10B), and we report the packaging of mitochondrial DNA in exosomes derived from AECs. Previously, we reported that DNase digestion is not necessary in AEC exosomes studies because DNA fragments sticking to exosomes are not seen in our preparations [125].

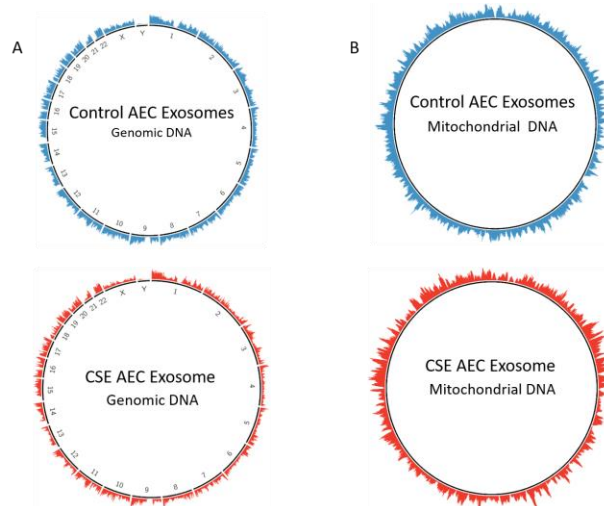


**Figure 2.10: Circular view of the readings of fragments along each chromosome in the (A) whole-genome and (B) mitochondria sequencing analysis of exosomal DNA isolated from amnion cells grown under standard (control) and OS (CSE) conditions.**



## Discussion

Ongoing studies suggest the development of fetal membrane senescence as a mechanism associated with term parturition [34,87,89]. Oxidative stress, antioxidant depletion, oxidative stress induced senescence, stress associated p38 MAPK activation, and sterile inflammation, are associated with normal term human parturition [33,34,87,140]. These findings in *in vivo* clinical samples were recapitulated *in vitro* using normal term not in labor fetal membrane explant cultures or AECs where oxidative stress induced transition of fetal membranes to a senescence phenotype mimicked term labor status [87–89]. This suggests that exogenous oxidative stress at term promotes senescence and senescent fetal membrane cells to signal parturition by enhancing the overall inflammatory load in the uterine cavity. In this study, we demonstrated that AEC-derived exosomes may serve as carriers of signals of communication between various tissue layers by senescent fetal cells. Exosomes, generated as a consequence of multivesicular endosome (MVE) fusion with the plasma membranes [54,141,142], and their contents (protein, DNA, and all forms of RNAs), represent the character and physiologic state of the cell of origin that makes them good vectors of paracrine signaling.

The primary aim of this study was to isolate, characterize and demonstrate that AEC derived exosomes reflect the physiological status of the cells of origin. Our key findings are as follows: 1) AEC derived exosomes demonstrated classic shape, size and markers (CD9, 63, 81, HSC 70, ALIX) along with amnion cell-stem cell specific transcription factor Nanog, regardless of treatment. 2) AEC derived exosomes do not show the presence of amnion cell stem cell marker Oct-4 in their cargo. 3) CSE treatment caused increased colocalization of H3, HSP70, HMGB1, active p38 (P-p38) MAPK and telomere fragments in AEC exosomes. Increased localization of these cargo demonstrated a pathophysiological phenotype of AECs in response to CSE induced oxidative stress. Although the functional relevance is unclear, this is the first report to demonstrate P-p38 MAPK as an exosomal

cargo. We propose that AEC-derived exosomes demonstrate the characteristics of a pathophysiological state of the cell of origin and that the presence of P-p38 MAPK, a marker of inflammation, is a key mediator of senescence induction and sterile inflammation. Our studies suggest the importance of AEC derived exosome cargo in causing potential functional changes in fetomaternal compartments. Although we do not report any functional role of AEC exosomes during pregnancy, ongoing research is focused on determining such a role.

The impact of p38 MAPK activation is well documented in fetal tissues but no data exist on its functional contributions on myometrial side whose contractility determines pregnancy outcome. Functional progesterone withdrawal and subsequent myometrial activation (i.e. increased contractility and excitability) are key events in the initiation of labor [16,18,143,144]. Functional progesterone withdrawal, which is mediated, in part, by switching of the PR-A:PR-B ratio in myometrial cells from PR-B-dominance (mediates anti-inflammatory and relaxing actions of progesterone) to PR-A-dominance (inhibits the anti-inflammatory actions of progesterone and increase contractility) [16,18,143,144]. A key finding in breast cancer cell lines is that the PR-A: PR-B ratio is determined by the stability of the PR-A and PR-B proteins, which is caused by post-translational modifications, especially phosphorylation by MAPKs at specific serine residues in the N-terminal domain [145–148]. Khan et al found that PR-A stability is increased by MEKK1-induced p38 MAPK activation, which increased the PR-A: PR-B ratio; whereas PR-B stability was increased by activation of ERK1/2, leading to a decrease in the PR-A: PR-B ratio. Our unpublished data (performed in collaboration with Dr. Sam Mesiano) in myometrial cells demonstrate that CSE can cause functional progesterone withdrawal in myocytes through p38 MAPK mediated mechanism, a process reversed by p38 MAPK inhibitor SB203580. This determined the impact of p38 MAPK in human parturition. Therefore, exosomal transport of fetal cell derived P-p38 MAPK to the maternal side may be influential in determining the status of pregnancy. This is also dependent on the number

of exosomes and load of p38 MAPK that can reach the maternal side. Exosomes may carry other inflammatory molecules (SASP) from senescent fetal cells and they may also enhance the inflammatory load on the maternal side. We postulate that based on the physiologic state of cell, exosome cargo and signaling may determine the outcome of pregnancy. Placental derived exosomes have been well documented in maternal liquid biopsies and their changes (quantity and contents) have been implicated in various pregnancy associated pathologies [67,69,71–73,75,79,111–115,123,149–162].

Although AEC exosomes demonstrated the consistent presence of classical exosomal markers and the amnion stem cell marker Nanog, we did not show one of the ESCRT class of proteins, Alix. ESCRT complex dependent and independent mechanisms of exosomal assembly and secretion have been described as a tissue/cell specific physiological phenomenon [110]. We have documented three of the tetraspanin protein markers (CD9, CD63 and CD81), as well as ESCRT protein ALIX, that can participate in exosomal assembly and release of cargo.

In summary, we have demonstrated AECs produce exosomes and that their cargo reflects the status of the cell (Figure 2.11). Furthermore, we identified active p38 MAPK as one of the cargo proteins in exosomes derived from oxidative stress-treated AECs. Our studies highlight the significance of AEC derived exosomes as donors of p38 MAPK which plays a major role in determining the fate of pregnancy. This study demonstrated a limited number of markers and further characterization of AEC exosome cargo using proteomic and genomics approaches are warranted to elucidate the functional role of exosomes in human parturition and feto-maternal communication.

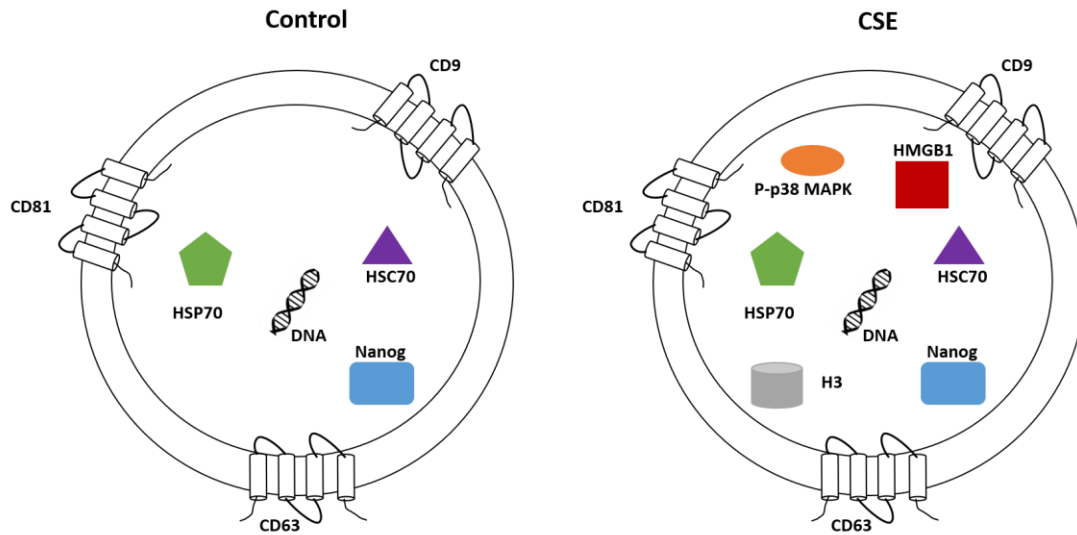


**Figure 2.11: Characterization of AEC Exosomes**

The exosomes isolated from untreated (control) and CSE treated primary AEC carry cargo representative of the state of the origin cell. AEC exosomes contain tetraspnins (CD9, CD63 and CD81), Nanog, HSC70, HSP70 and DNA regardless of treatment, while CSE exosomes contain significantly increased amounts of P-p38 MAPK, HMGB1, H3, and an increase in telomere fragments compared with control exosomes.

## CHAPTER 3: PARACRINE MEDIATORS OF PARTURITION: EXOSOMES

### DERIVED FROM AMNION EPITHELIAL CELLS

Modified in part from:

**Paracrine mediators of parturition: Exosomes derived from amnion epithelial cells**

Emily E Hadley, **Samantha Sheller-Miller**, George Saade, Carlos Salomon, Sam Mesiano,  
Robert N Taylor, Brandie D Taylor, Ramkumar Menon

Published: *Manuscript under review at AJOG* (2018)

### Introduction

A substantial body of evidence supports the hypothesis that parturition is sustained by an inflammatory process. Labor in humans and other mammals is associated with infiltration and activation of leukocytes, mainly neutrophils and macrophages, into the fetal (amniochorion) and uterine tissues (decidua myometrium and cervix) [19,20]. Clinical and animal (mainly mouse) studies have identified key roles of specific cytokines, chemokines and immune cell types in the parturition process [11,31,163]. Endocrine signals arising from the fetus, such as corticotropin-releasing hormone and adrenocorticotrophic hormone, are postulated to function as a biologic clock translating organ maturation and triggering labor at term. These hormones are known to have pro-inflammatory effects on various tissues in vitro [164–166]. However, the precise mechanisms by which signals from the fetus initiate human parturition remain a mystery.

Our recent findings support the core hypothesis that oxidative stress and cellular senescence of the fetal (amniochorionic) membranes trigger human parturition by activating intrauterine inflammation. We have shown that human fetal membranes undergo a telomere-dependent process of progressive senescence throughout gestation, which is correlated with fetal growth [34,89]. Studies of senescence using human fetal membranes and cell culture have been corroborated in murine pregnancy models indicating that in utero cell senescence is driven by a p38 mitogen activated protein kinase (MAPK) pathway

[32,87,88]. Senescence of the fetal membranes peaks at term resulting in dysfunctional fetal membranes. We postulate that signals arising from senescent fetal membranes are a proxy for completion of fetal growth and may trigger parturition. Premature senescence activation in the amniochorion is associated with preterm parturition [167,168]. Examination of signals arising from senescent fetal membranes at term has identified two key classes of inflammatory factors: senescence associated secretory phenotype (SASP) and damage associated molecular pattern markers (DAMPs) arising due to cell and cellular organelle injury [34,88]. SASPs and DAMPs mediate sterile (non-infectious) inflammation in fetal compartments at term during normal gestation. Many of the SASPs (inflammatory cytokines, chemokines, matrix degrading enzymes and growth factors) are activated in parturition [169–171]. Two DAMPs released from senescent fetal cells, high mobility group box (HMGB) 1 and cell free fetal telomere fragments (cffTF), induce an inflammatory response in decidua and myometrium suggesting a paracrine communication from the senescing fetal membrane to uterine effector tissues of labor [32,88,171–173]. Furthermore, in animal models injection of these DAMPs cause preterm birth [174]. Based on these data, we hypothesize that sterile inflammatory signals from senescent fetal membranes are propagated from fetal to maternal compartments in a paracrine fashion to initiate labor.

Exosomes are bioactive, spherical, cell-derived vesicles which are 30–150 nm in size and are secreted via exocytosis [71,109,175]. Exosomes are comprised of bi-layered plasma membranes and contain molecular constituents of their cell of origin, including proteins, DNA, and RNA that reflect the physiological state of their parent cell. In addition to common membrane and cytosolic molecules, exosomes harbor unique, cell specific subsets of proteins. They contain high concentrations of cholesterol and detergent resistant lipid membranes, making them extremely stable and efficient carriers of molecules across tissue layers [109]. Exosomes mostly act as transporters of paracrine signals between

tissues, but can regulate intracellular pathways by sequestering signaling molecules from the cytoplasm, reducing their bioavailability [114,162,176].

It has recently been shown that senescent amnion epithelial cells (AECs) at term produce exosomes containing pro-inflammatory factors [124,125]. This finding supports the hypothesis that pro-inflammatory signals are transmitted from fetal to maternal tissues via AEC-derived exosomes. Importantly, animal model studies have shown that exosomes injected into the amniotic fluid cavity access the maternal tissues by local and systemic routes [124]. There are several studies which have reported exosome trafficking between tissues [177,178] and that indicate exosomes are released from cells from both the apical and basolateral compartments [179–183]. Although these data support the core hypothesis that exosomes from the fetus access maternal tissues, the capacity for fetal exosomes to induce inflammatory changes in the maternal tissues remains unknown.

The objectives of this study were to: 1) determine whether exosomes derived from AECs grown under normal cell culture conditions (control exosomes) and under oxidative stress conditions (oxidative stress (OS) exosomes) enter maternal uterine cells (decidua and myometrium) and fetal (syncytiotrophoblast) cells, and 2) determine whether oxidative stress affects the capacity for AEC-derived exosomes to induce an inflammatory response in decidual, myometrial and syncytiotrophoblast cells.

## **Materials and Methods**

This study is basic science study utilizing fetal membrane derived cells, primary decidual cells, and myometrial and trophoblast cell lines. The University of Texas Medical Branch (UTMB) in Galveston, TX, USA, under an approved Investigational Review Board protocol, allowed the use of discarded placentas after delivery. Placentae were collected from women (18–40 years old) undergoing an elective repeat cesarean delivery at term (37–41 weeks gestation) prior to onset of labor. Exclusion criteria included: a history of preterm labor and delivery, premature rupture of the membranes, preeclampsia, placental

abruption, intrauterine growth restriction, gestational diabetes, Group B *streptococcus* carrier status, history of treatment for urinary tract infection, sexually transmitted diseases during pregnancy, chronic infections like HIV and hepatitis, and history of cigarette smoking or reported drug and alcohol abuse.

### **Human amnion epithelial cell isolation and culture**

Amniotic membrane was processed as described in Chapter 2 to produce AEC monolayer cultures.

### **Primary amnion epithelial cells under normal (control) and oxidative stress cell culture conditions**

Cigarette smoke extract (CSE) was used to induce oxidative stress in amnion cells as detailed in Chapter 2.

### **Exosome isolation**

Prior to exosome isolation, cell supernatant media were thawed overnight and exosomes were isolated using differential ultracentrifugation as described in Chapter 2.

### **Transmission electron microscopy**

Exosome shape was determined using a JEOL transmission electron microscope (TEM) as described in Chapter 2.

### **Nanoparticle tracking analysis with ZetaView**

Nanoparticle tracking analysis was performed using the ZetaView PMX 110 (Particle Metrix, Meerbusch, Germany) and its corresponding software (ZetaView 8.02.28). Frozen exosomes in 1x PBS were thawed on ice. A 1:500 dilution of the exosome sample was made with Millipore water. Samples of control or oxidative stress exosomes were loaded in the ZetaView Nanoparticle Tracking Analyzer and number of particles/ml



and size distribution were counted for each sample. The machine was cleaned between samples using filtered water. The results of the ZetaView were used to calculate the number of exosomes produced per amnion cell for the two treatment types (control or oxidative stress).

### **Myometrial cell culture**

Myometrial cells were obtained from the hTERT-HM<sup>A/B</sup> myometrial cell line (a gift from Dr. Sam Mesiano, Case Western Reserve University, Cleveland, OH). The hTERT-HM<sup>A/B</sup> is a clonal sub-line of hTERT-HM, a telomerase immortalized myometrial cell line produced from uterine fundus obtained from a premenopausal woman [184]. The cells express the smooth muscle cell-specific genes calponin, h-caldesmon and smoothelin. They also express the oxytocin receptor and respond to oxytocin with increased intracellular calcium, which is typical of the myometrial cell phenotype. Myometrial cells were plated in a T75 flask and cultured in media containing DMEM, 1X (Corning Cellgro, Manassas, VA) supplemented with 10% charcoal stripped-FBS (Sigma-Aldrich), 10% Penicillin/Streptomycin plus L-glutamine (Sigma-Aldrich), gentamicin (Mediatech), hygromycin B (Life technologies, Carlsbad, CA), blastocidin (Invitrogen, Carlsbad, CA) at 37°C, and 5% CO<sub>2</sub>, and grown to 80% confluence.

### **Decidual cell culture**

Decidua cells were isolated from placentas collected from women undergoing elective cesarean delivery at term who were not in labor. The method for isolation was adapted from a protocol described by Mills et al. 2006.<sup>56</sup> Briefly, fetal membrane was cut from placenta and amnion was removed. The tissue was washed with in pre-warmed 0.9%NaCl to remove blood and then cut into 2 inch squares. Blunt dissection of the decidua from chorion was performed using forceps and scalpel. The tissue was minced into small pieces and incubated in a digestion buffer (Hanks BSS with trypsin and DNase I) and at

37° C for 30 minutes. The tissue was then centrifuged at 2,000 rpm for 10 minutes at room temperature (RT). The supernatant was removed and pellet was re-suspended in a digestion buffer (Hank's BSS with trypsin, DNase I and collagenase type IA) and incubated for 1 hour at 37° C. The digestion was neutralized and filtered through four layers of sterile gauze. The collected cells were centrifuged at 2,000 rpm x 10 minutes at RT and the pellet was re-suspended in DMEM. Next a pre-prepared Optiprep "column" was used with steps ranging from 4%-40% of 4 mL each. The processed decidua cells were added to the top of the gradient, then centrifuged at 1,000g x 30 minutes at RT. Decidual cells were collected between densities of 1.027 – 1.038g/mL (between 4-6%). The decidual cells were collected and washed with DMEM/F-12 50/50, 1X and then centrifuged at 2,000 rpm x 10 minutes at RT. The pellet was re-suspended in DMEM/F12 and placed in T25 flasks. The primary cells were grown in media containing complete DMEM/F12 media plus 10% heat inactivated (HI) FBS (Sigma-Aldrich), penicillin/streptomycin, and endothelial growth factor at 37°C, 5% CO<sub>2</sub>, and 95% air humidity to 70–80% confluence. The purity of the cells was tested using antibodies to vimentin and cytokeratin. We found that the cultured decidual cells were vimentin positive and cytokeratin negative.

### **BeWo cell culture**

BeWo cells are a human choriocarcinoma cell line (provided by Dr. Robert N Taylor, Wake Forest University, Winston-Salem, NC). Despite being a cell line BeWo cells continue to reveal physiological characteristics of the villous trophoblast [185,186]. Cells were plated in a T75 flask and cultured in media containing Roswell Park Memorial Institute (RPMI) 1640, 1X (Corning Cellgro) media with Penicillin/Streptomycin and 10% HI-FBS at 37°C, 5% CO<sub>2</sub>, and 95% air humidity and grown to 70–80% confluence.

### **Immunofluorescence staining of exosomes and confocal microscopy to localize exosomes in recipient cells**

Isolated control and oxidative stress AEC exosomes were labeled with carboxyfluorescein succinimidyl ester (CFSE) by re-suspending the final exosome pellet in 7.5  $\mu$ M CFSE. Exosomes were incubated at 37°C for 30 minutes then diluted with media containing 10% exosome-depleted FBS. Exosomes were ultracentrifuged overnight (>16 hours) at 4°C and pellets were re-suspended in cold PBS. Myometrial, decidual and BeWo cells were plated on glass coverslips at a density of 20-50,000 cells per slip and incubated overnight prior to treatment with CFSE labeled control or oxidative stress exosomes. After a 4 hour incubation with the labeled exosomes, cells were fixed with 4% paraformaldehyde (PFA), permeabilized with 0.5% Triton X and blocked with 3% BSA in PBS. To counter stain and to visualize cell morphology, cells were incubated with primary antibodies to  $\alpha$ -smooth muscle actin (Affymetrix, Santa Clara, CA) (for myometrial and decidua) or anti- $\beta$  actin (Sigma-Aldrich) (for BeWo cells) overnight at 4°C 3% BSA in PBS. After washing the slides several times with PBS, slides were incubated with secondary antibody Alexa Fluor 488 or 594 (Life Technologies) diluted 1:400 in PBS for 1 hour in the dark. Slides were then washed with PBS and treated with 4', 6-diamidino-2-phenylindole (DAPI) (Invitrogen by Thermo Scientific) then washed and then mounted using MOWIOL 4-88 (Sigma-Aldrich) mounting medium. Slides were allowed to dry overnight and then the cells were imaged using the LSM 510 Meta UV confocal microscope (63x) (Zeiss, Germany). Multiple (at least 5) cells on each slide were imaged with the confocal microscope. Images were obtained and analyzed using Image J (open source) to visualize z-stacks and confirm the location of the exosomes in regards to the cells. 3D reconstructions of the cells were created to further confirm the location of the exosomes in relation to the target cell.

### **Exosome treatments of cells**

Myometrial, decidual and BeWo cells were placed in 6 well plates and grown overnight. The next day the cell media was removed, cells were washed with PBS and media was replaced with exosome free cell media. Cell treatments with control and

oxidative stress exosomes were performed by adding them to the wells. Exosomes from either control or oxidative stress conditions were added in 3 titrations of  $2 \times 10^5$ ,  $2 \times 10^7$ , and  $2 \times 10^9$  exosomes/well. The cells were allowed to incubate with the exosomes for 24 hours. A negative control well was included that consisted of exosome free media only and a positive control well was included which was treated with LPS (100 ng/mL). At the completion of the treatment, media was collected from each well and stored at  $-80^\circ \text{C}$ . The cells were collected from the wells after being washed with PBS. To collect the cells, wells were treated with radio immunoprecipitation assay buffer including phenylmethanesulfonyl fluoride (Fluka), protease inhibitor cocktail (Sigma-Aldrich) and Halt phosphatase inhibitor cocktail (Thermo-Scientific) and cells were manually scraped from the well using a cell scraper. The cells were then placed on ice for 10 minutes, vortexed for 10 seconds, sonicated for 30 seconds, vortexed an additional 10 seconds, and placed on ice for 10 minutes. The lysed cells were then flash frozen using liquid nitrogen and stored at  $-80^\circ \text{C}$ . This experiment was repeated a total of 7 times.

### **Exosome blocking experiments**

To determine if the effects in recipient cells were mediated by exosomes, several control experiments were performed. These included cold incubation of recipient cells and treatment with heat inactivated and sonicated exosomes. For the cold incubation treatment, the exact treatments as explained in the last section were performed, with the following changes: cells treated with exosomes were incubated at  $4^\circ \text{C}$  for 6 hours. For heat inactivation and sonication treatments, the above described treatments were performed with the following changes: the exosomes (both control and oxidative stress) were either heated in a  $65^\circ \text{C}$  water bath for 30 minutes or sonicated for 30 minutes prior to being added for the exosome treatment.<sup>59</sup> A total of  $4 \times 10^7$  exosomes were added per well and treatment type. The cell media and cells were collected at the end of the 24 hour treatment as described above.

## **Enzyme Linked Immunosorbent Assay for determining inflammatory marker response**

All of the media collected from exosome treatments and exosome blocking treatments were analyzed using an enzyme-linked immunosorbent assay (ELISA) for 5 common inflammatory cytokines/mediators: IL-1 $\beta$ , TNF- $\alpha$ , IL-6, IL-8, and PGE<sub>2</sub>. These inflammatory cytokines were chosen based on the results of a systematic review, performed by our lab, which indicated that these cytokines/mediators are present at the time of labor in all the gestational tissues included in this report [187]. The ELISA was performed after media was thawed and spun to remove cellular and other debris. The media was pipetted into the ELISA plate wells as per kit instructions (R&D Systems- Quantikine ELISA). The results of the ELISA were obtained by using the Synergy H4 microplate reader (BIO-TEK).

## **Western Blot**

Western blot was performed to determine total and phosphorylated NF- $\kappa$ B (Rel-A) from the myometrial, decidual and BeWo cells, which had been treated with  $2 \times 10^9$  exosomes from control or oxidative stress induced cells. Cell samples, which had previously been suspended in RIPA, were thawed and then centrifuged at 10,000 rpm for 20 minutes. The supernatant was collected and then a bicinchoninic acid assay (BCA) (Pierce, Rockford, IL) was performed to determine protein concentrations of the samples. Then samples were run as described in Chapter 2 with primary antibodies to Phospho Rel-A, total Rel-A, or total actin.

## **Immunohistochemical analysis of amnion exosomes in maternal gestational tissues**

To determine that fetal cell derived material can reach maternal gestational tissue during parturition, we collected myometrial tissues and decidual tissues from pregnant women undergoing cesarean delivery (not in labor) or vaginal delivery (term labor) and looked for the presence of an amnion stem cell marker (NANOG). Dual staining was

performed for NANOG and CD9 (background marker). Tissues were fixed in 10% Neutral Buffered Formalin (NBF) for 24 hours at room temperature before embedding them in paraffin blocks and sectioning 4µm slices. Formalin-fixed paraffin-embedded (FFPE) were baked overnight at 50°C and tissue slides were re-hydrated the next day, by immersing in Xylene three times for 10 minutes each followed by 100% EtOH, 95% EtOH, 70% EtOH, 50% EtOH, distilled water; each step performed twice for 5 minutes. Antigen retrieval was then carried out in 2100 Antigen Retriever (Electron Microscopy Sciences, USA) with citrate buffer, pH 6.0 for 20 minutes followed by cooling for approximately 2 hours and rinsed in TBS buffer. Endogenous peroxidase activity was quenched by incubation with 0.3% hydrogen peroxide for 10 minutes. The tissue was then blocked for non-specific signals using Protein Block buffer (Abcam) in a moist chamber for 1 hour at room temperature. Sequential dual staining was performed with primary antibody NANOG (Rabbit, 1:400, Cell signaling, Danvers, MA) followed by second primary antibody CD9 (Rabbit, 1:100, Novus Biologicals, Littleton, CO). Secondary antibody incubation was carried out for 30 minutes at room temperature with each antibody. NANOG was stained using DAB substrate (Abcam, Cambridge, United Kingdom) for 5 minutes. Slides were then washed in TBS-tween20, antigen retrieved and re-blocked prior to second primary antibody staining. CD9 staining was developed using AP substrate (Vector Blue) for 10 minutes. The Olympus light microscope BX43 (OLYMPUS) was used to image the slide and images were captured using software Q Capture Pro.

### **Statistical analysis**

Each cell type (BeWo, Myometrial and Decidua) was either untreated (negative controls) or treated with exosomes at  $2 \times 10^5$ ,  $2 \times 10^7$  and  $2 \times 10^9$  from either normal or CSE conditions to examine the distribution of inflammatory markers between untreated (negative controls) and exosome treated cells (from both conditions). For each cell type, there were a total of 4 negative controls which served as the reference group and for each

exosome treatment ( $2 \times 10^5$ ,  $2 \times 10^7$  and  $2 \times 10^9$ ) there were 5 observations under normal conditions and 5 under CSE. Normality for each inflammatory marker (IL-6, IL-8 and PGE2) was tested using the Kolmogorov-Smirnov test, with a p-value of  $<0.05$  indicating that the distribution was non-normal. No markers had a normal distribution. The distribution of inflammatory markers were compared between controls (untreated cells) and exosome treated cells (from both normal and oxidative stress conditions) using non-parametric Wilcoxon-Mann-Whitney test (non-parametric analog to the independent samples t-test). These analyses were conducted for each cell type. A  $P$ -value  $<0.05$  was considered statistically significant. All analyses were conducted using SAS V9.2 (Cary, NC).

## **Results**

### **Exosome Quantification and Characterization**

The size and quantity of exosomes were determined using Zetaview analysis (Figure 3.1). Electronic microscopy of exosomes isolated from conditioned media samples showed round, cup-shaped exosomes with a size range between 50–150 nm (Figure 3.1A). AECs under normal cell culture (control) conditions produced an average of  $9.4 \times 10^9$  particles/ml which correlates with 899 exosomes/cell, while AECs under oxidative stress conditions produced  $1.5 \times 10^{10}$ /ml which correlated with 1211 exosomes/cell (Figure 3.1B and C). The average size of exosomes from control and oxidative stress treatments were 112 nm and 101 nm respectively. AEC exosomes were shown in a previous experiment to contain exosome markers CD9, CD81 along with AEC marker NANOG (Figure 3.1D).

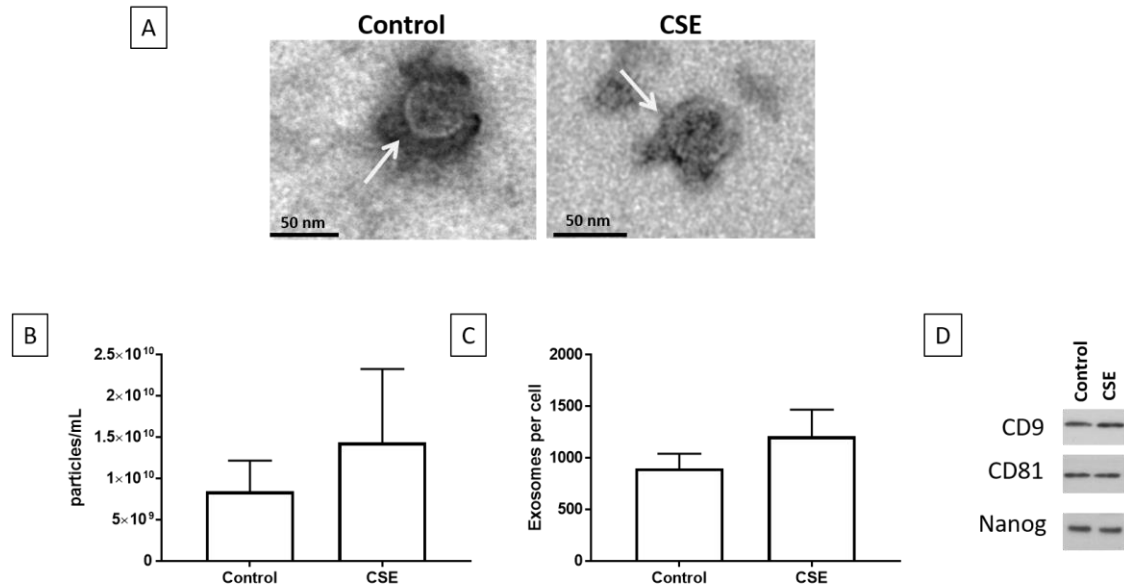


**Figure 3.1: Characterization of control and oxidative stress exosomes**

A: Transition electron micrograph of control and oxidative stress exosomes show round/cup shaped exosomes. B: Total number of particles/ml of media show no difference in exosomes between treatments. C: Number of exosomes/AEC from both control and oxidative stress treatments were not different. D: Both control and oxidative stress derived AEC exosomes showed exosome markers CD9, CD81 and stem cell marker NANOG.

### Exosomes were localized in recipient cells

Confocal microscopy and z-stack analysis was used to localize exosomes in recipient myometrial, decidual and placental cells. As shown in Figure 3.2, CFSE labeled control and oxidative stress exosomes were detected within myometrial, decidual and BeWo cells. The location of the exosomes within cells, as opposed to adjacent to the cells, was confirmed using z-stack analysis and 3D reconstructions as shown in Appendix B Supplemental Figure 3.1.



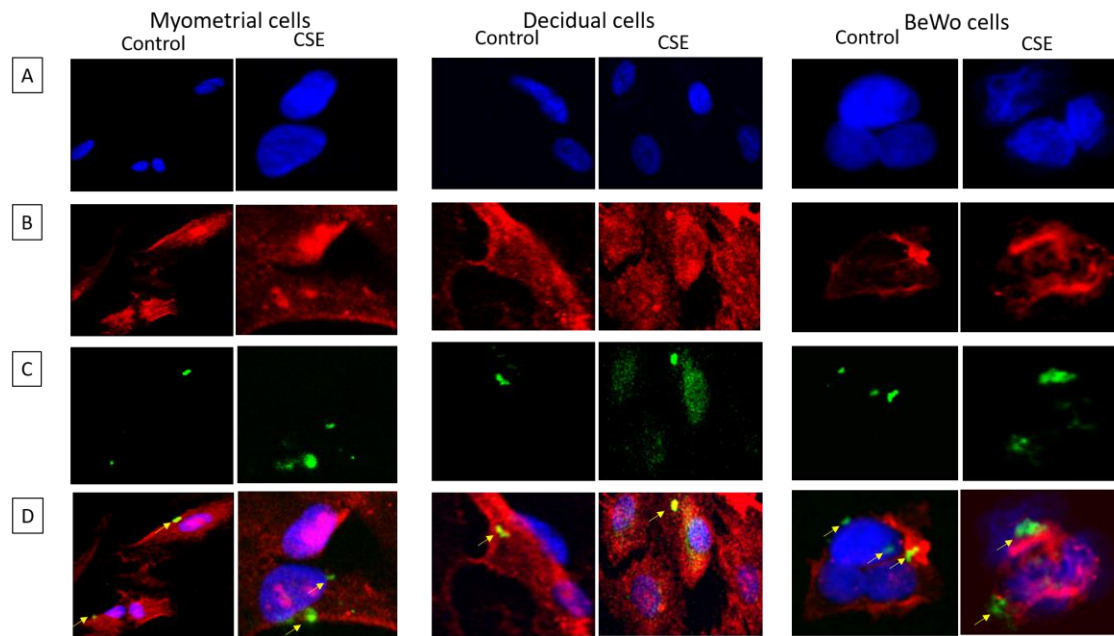


**Figure 3.2 Localization of AEC derived exosomes (from control and oxidative stress treatments) inside gestational cells**

Carboxyfluorescein succinimidyl ester (CFSE) labelled exosome localization inside myometrial, decidual and BeWo cells. Left panel: Myometrial cells; Middle panel: Decidual cells; and Right panel: BeWo cells. A: DAPI; B: Cell specific marker:  $\alpha$ -smooth muscle actin (myometrium and decidua) or  $\beta$ -actin (BeWo); C: CFSE labelled exosomes; D: merged images.

### **AEC exosomes induce a pro-inflammatory response in myometrial and decidual cells**

To determine the effect of AEC derived exosomes to cause functional changes, we determined inflammatory cytokines and prostaglandin levels in cell culture supernatants after treatment with various doses of control and oxidative stress exosomes and compared them to the analytes from normal, untreated, cell cultures. The markers studied were shown to be associated with human parturition in each of these cell types. Control and oxidative stress AEC exosomes significantly increased the concentration of IL-6, IL-8 and PGE<sub>2</sub> but not IL-1 $\beta$  or TNF- $\alpha$  in the media of myometrial and decidual cells compared to normal (untreated) cells in culture (Figures 3.3-3.4, Appendix B Supplemental Tables 3.1-3.2).

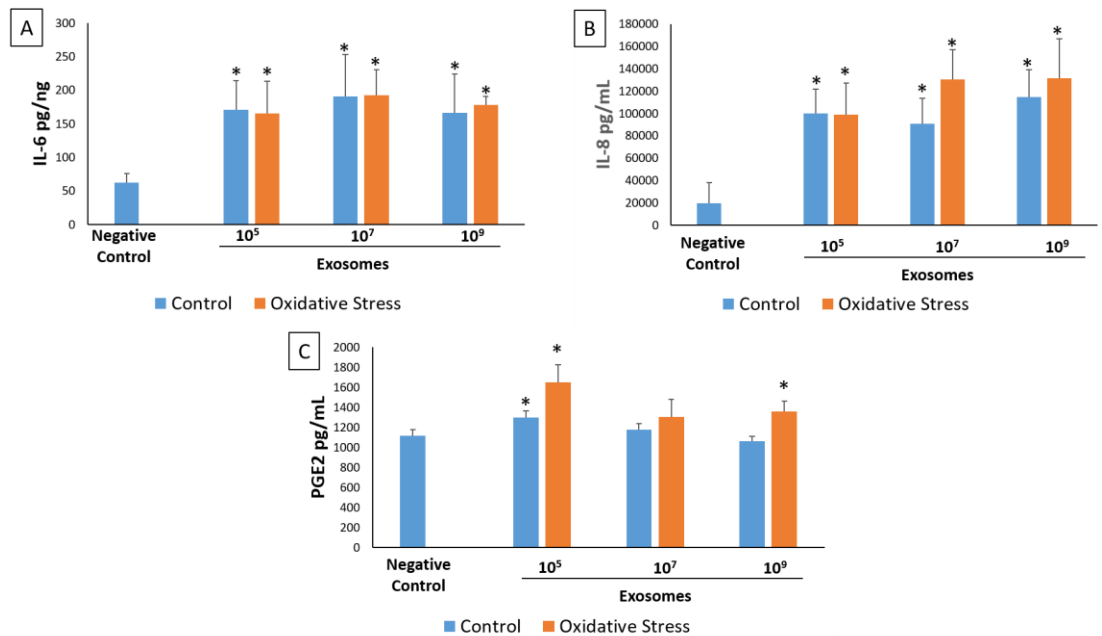


**Figure 3.3: ELISA data showing IL-6 (A), IL-8 (B) and PGE<sub>2</sub> (C) in myometrial cells**

Comparisons were made between IL-6, IL-8, or PGE<sub>2</sub> analyte concentrations in negative control cell media and concentrations in media after treatment of myometrial cells with each dose (Exosomes 10<sup>5</sup>, 10<sup>7</sup>, 10<sup>9</sup>) of either control (blue) or oxidative stress (orange) AEC derived exosomes. All experiments include n=5. Significant results (p<0.05) between specific treatment compared to untreated control cell media are marked with an asterisk (\*).

The capacity for oxidative stress exosomes to increase myometrial and decidual cell media IL-6, IL-8 and PGE<sub>2</sub> levels appeared to be slightly higher compared to control AECs. A dose dependent effect of exosomes (control or oxidative stress) to stimulate inflammatory response was not observed in our experiments. BeWo cells only produced detectable levels of IL-6 and PGE<sub>2</sub> and none of the other cytokines studied. Control and oxidative stress exosomes had no effect on BeWo cell media IL-6, IL-8, PGE<sub>2</sub>, IL-1 $\beta$  and TNF- $\alpha$  levels (Figure 3.5, and Appendix B Supplemental Table 3.3).

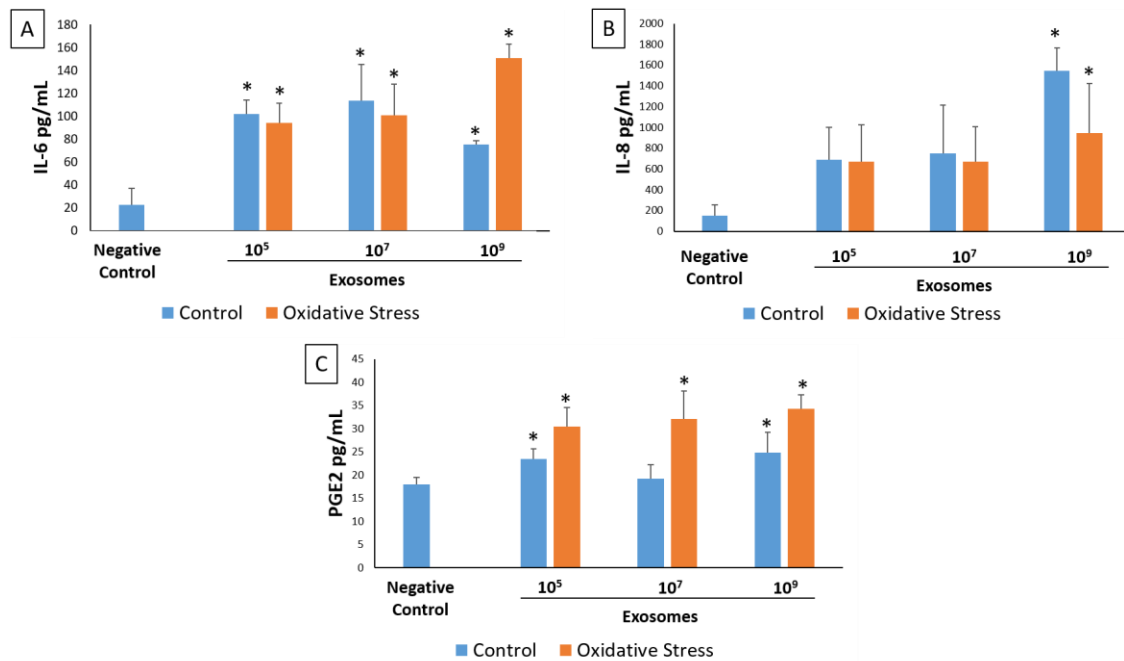


**Figure 3.4: ELISA data showing IL-6 (A), IL-8 (B) and PGE<sub>2</sub> (C) in decidual cells**

Comparisons were made between IL-6, IL-8, or PGE<sub>2</sub> analyte concentrations in negative control cell media and concentration in media after treatment of decidual cells with each dose (Exosomes 10<sup>5</sup>, 10<sup>7</sup>, 10<sup>9</sup>) of either control (blue) or oxidative stress (orange) AEC derived exosomes. All experiments include n=5. Significant results (p<0.05) between specific treatment compared to untreated control cell media are marked with an asterisk (\*).

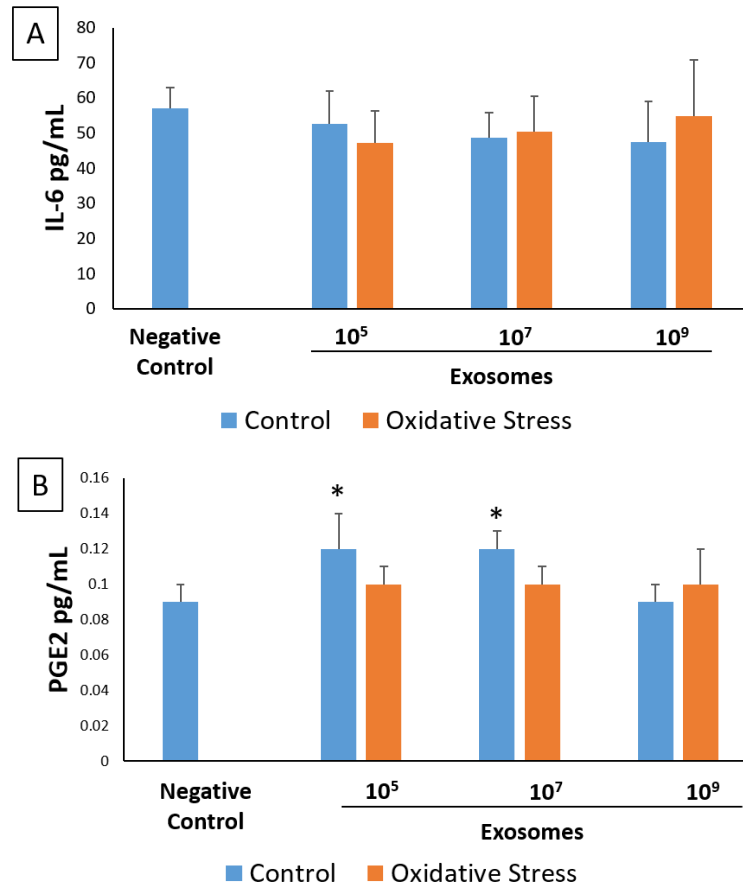


**Figure 3.5: ELISA data showing IL-6 (A) and PGE<sub>2</sub> (B) in BeWo cells**

Comparisons were made between IL-6 or PGE<sub>2</sub> analyte concentrations in negative control cell media and concentration in media after treatment of BeWo cells with each dose (Exosomes 10<sup>5</sup>, 10<sup>7</sup>, 10<sup>9</sup>) of either control (blue) or oxidative stress (orange) AEC derived exosomes. All experiments include n=5. Significant results (p<0.05) between specific treatment compared to untreated control cell media are marked with an asterisk (\*).

### Positive control experiments show exosome-mediated effect

To confirm that cells are responding to the treatments and that the effects are truly mediated by exosomes, multiple control experiments were performed. LPS treatment (100 ng/ml) was used as a positive control to confirm inflammatory responses from each cell type. LPS produced significant increase in cytokine production from all cell types compared to untreated cells. A sample of these data are shown in Appendix B Supplemental

Figure 3.1. IL-6 levels after LPS treatment were higher in all cell types compared to control. However, IL-6 concentrations after LPS treatment was similar to that observed after exosome treatment. In BeWo cells, LPS significantly increased only IL-6, but not IL-8 or PGE<sub>2</sub>. Control data from LPS treatments are also graphically represented in Appendix B Supplemental Table 3.4.

### **Determination of exosome mediated cytokine response**

To confirm exosome specificity of stimulation, media samples from the exosome blocking experiments were subjected to ELISA. Incubation of cells in cold lead to decreased IL-6, IL-8 and PGE<sub>2</sub> production by all three cell types. This suggests that exosome entry into these cells were blocked due to reduced endocytosis at 4°C. Two other experiments were performed to disrupt exosomes and cargo. Media samples from cells treated with a single dose of exosomes (10<sup>7</sup>) whose cargo was inactivated by either heat inactivation or sonication were compared to control and control or oxidative stress exosome treatments. Heating and sonicating the exosomes prior to treatment lead to no change in IL-6, IL-8, and PGE<sub>2</sub> levels which were similar to negative control treatments. This suggests that the exosome's cargo, either destroyed or disrupted, were not sufficient to cause inflammatory mediator response from these cells (Appendix B Supplemental Figure 3.1 and Appendix B Supplemental Table 3.4). These data partly confirmed exosome mediated effects.

### **Exosomes increase NF-κB activation in myometrial and decidual cells**

Exosomes, regardless of source (control or oxidative stress) produced inflammatory response by increasing IL-6, IL-8 and PGE<sub>2</sub> release suggesting activation of NF-κB, a key transcription activator by exosomes. To test this, we performed western blot analysis for p-RelA/p65, total RelA/p65, and actin on cells collected from myometrial, decidual, and BeWo cells. Myometrial and decidual cells increased p-RelA in response to exosomes

(regardless of control or oxidative stress) and BeWo cells increased less. Densitometry (based on the ratio of active/total [mean arbitrary units]) (Figure 3.6 bar graphs) corroborated that myometrial and decidual cells had higher p-RelA than controls after treatment with both control and oxidative stress exosomes (Figure 3.6); however, RelA baseline activation was similar between normal BeWo cells compared to cells exposed to exosomes (see bar graphs). This further verifies the previous cytokine data presented which indicates that increased cytokine and PGE2 levels induced by both control and oxidative

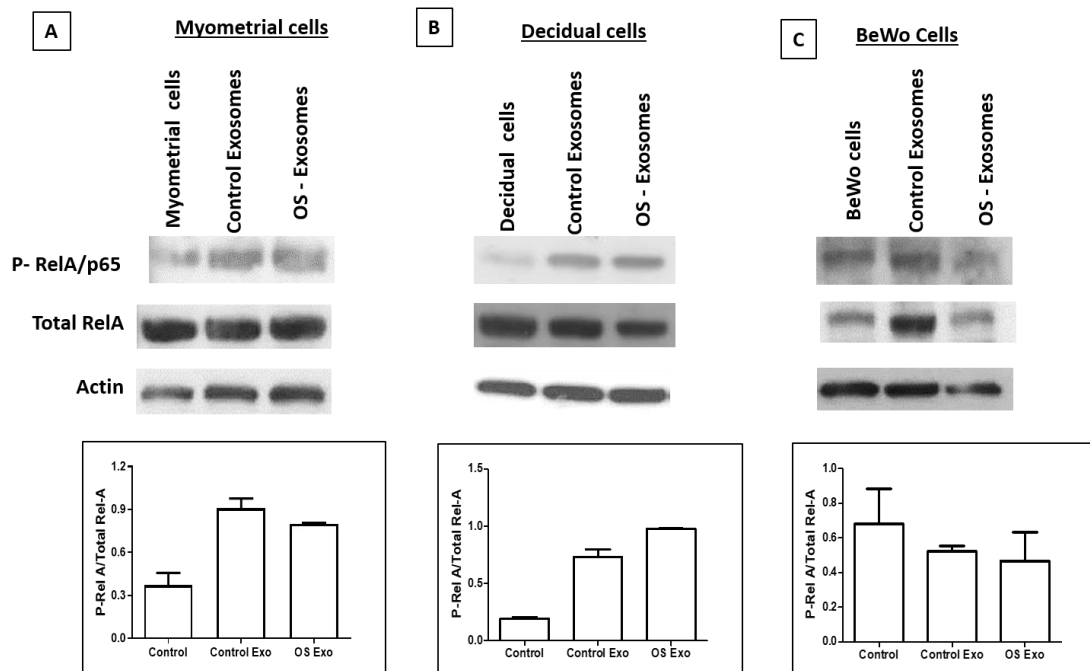


**Figure 3.6: Activation of NF- κB as determined by RelA/p65 Phosphorylation**

Top panel P-RelA/p65; Middle panel – Total RelA/p65; Bottom Panel – Actin; A: Myometrial cells- normal myometrial cells in culture; Control exosomes- myometrial cells treated with exosomes (dose  $2 \times 10^9$ ) from AEC grown under normal cell culture conditions; OS exosomes: myometrial cells treated with oxidative stress exosomes (dose  $2 \times 10^9$ ). B: Decidual cells: normal decidual cells in culture; Control exosomes: decidual cells treated with exosomes (dose  $2 \times 10^9$ ) from AEC grown under normal cell culture conditions; OS exosomes: decidual cells treated with oxidative stress exosomes (dose  $2 \times 10^9$ ). C: BeWo cells: normal BeWo cells in culture; Control exosomes: BeWo cells treated with exosomes (dose  $2 \times 10^9$ ) from AEC grown under normal cell culture conditions; OS exosomes: BeWo cells treated with oxidative stress exosomes (dose  $2 \times 10^9$ ).

stress exosomes are likely mediated by increased phosphorylation of NF- $\kappa$ B by exosomal cargo. BeWo cells are refractory to NF- $\kappa$ B activation by AEC exosomes.

### **Increased localization of NANOG in myometrial and decidual tissues at term labor**

Immunohistochemical analysis and dual staining of NANOG (AEC stem cell marker) showed increased staining of NANOG (brown) in myometrial tissues and decidual tissues from term delivery samples compared to not in labor deliveries (Figure 3.7). This

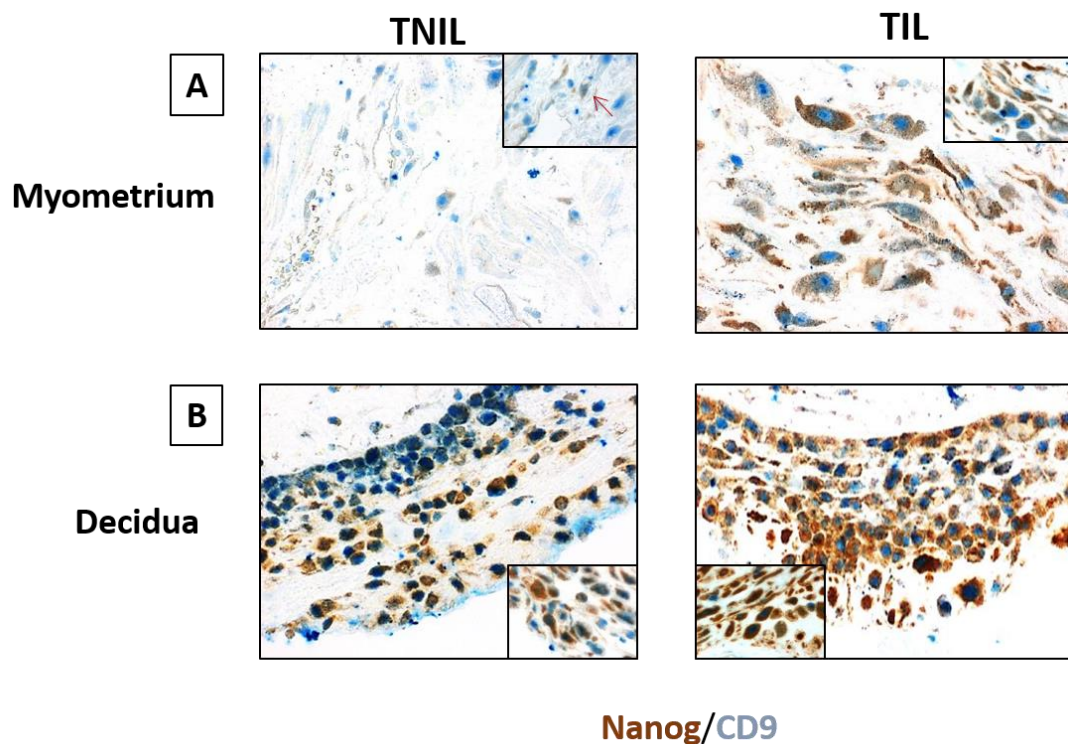


**Figure 3.7: Immunohistochemical localization of NANOG (amnion stem cell marker constitutively expressed in AEC derived exosomes) in term labor and term not in labor gestational tissues**

A: Term not in labor (TNIL) and term in labor (TIL) myometrium – Brown staining indicates NANOG (fetal amnion stem cell marker) and blue staining indicates CD9 (background marker). NANOG expression was higher in term labor myometrium than term not in labor myometrium. B: Term not in labor (TNIL) and Term in labor (TIL) decidua (attached to chorion layer of fetal membranes) – Brown staining indicates NANOG (fetal amnion stem cell marker) and blue staining indicates CD9 (background marker). NANOG expression was higher in term labor decidua than term not in labor decidua.

is indicative of increased influx of fetal-derived exosomes in myometrium and decidua, likely contributing to the functional changes described above.

## **Discussion**

### **Principal findings of the study**

This study tested if senescent fetal amnion epithelial cell derived exosomes can cause inflammatory changes in maternal and placental tissues. Our main findings are: 1. AECs produce exosomes that are quantitatively the same regardless of cell culture conditions; 2. AEC exosomes are taken up by myometrial, decidual and BeWo cells; 3. Treatment with control and oxidative stress AEC exosomes increase production of pro-labor inflammatory mediators (IL-6, IL-8 and PGE<sub>2</sub>) and cause activation of NF- $\kappa$ B in maternal myometrial and decidual cells; 4. Production of pro-inflammatory mediators was reduced when exosome uptake was blocked; 5. Fetal derived exosomes (expressing NANOG) are increased in laboring myometrium and decidua.

Although feto-maternal endocrine mediators have been reported to be associated with initiation of labor [83,144,188,189], the exact pathway of labor initiation remains a mystery [66]. Inflammatory activation is one of the functional facilitators of parturition in all gestational tissues, as an imbalanced inflammatory state transitions quiescent gestational tissues to an active state [190–193]. Thus, factors that increase inflammatory load, directed either by endocrine signals or paracrine signals, can cause mechanistic activation of the labor process [90,194]. This process ideally occurs when fetal growth and maturation are sufficient to ensure newborn survival. Based on recent findings of senescence in various gestational tissues that coincide with fetal growth, and our findings in fetal membrane models showing that membrane senescence and damage are associated with parturition, we hypothesized that senescent fetal membranes generate inflammatory mediators to signal fetal readiness for parturition [37,195]. We propose that these signals



are propagated from fetal tissues to the uterine parturition effector tissues (decidua and myometrium) via fetal cell derived exosomes.

We believe that AEC exosomes as well as other cell membrane derived vesicles can reach maternal tissues in multiple ways; 1. Basolateral secretion of AEC derived exosomes than can traverse through layers and reach the uterine tissues 2. Apical secretion of exosomes into amniotic fluid, taken up by fetus and reaching maternal systemic circulation 3. Exosomes reaching maternal circulation and thus reaching maternal reproductive tissues by crossing placental barriers, specifically those exosomes released from membrane cells overlaying the placenta. Our lab has shown in animal models that exosomes in the fetal compartment can reach the maternal compartment either via systemic spread or by diffusion through tissue layers. Fluorescently labeled AEC exosomes injected into the amniotic cavity of pregnant mice were identified in maternal gestational tissues and blood stream, indicating that exosomes are able to traverse the maternal fetal barrier [124]. Several studies in other labs have reported exosome trafficking between tissues [177,178]. There is also evidence in multiple studies to indicate that exosomes are released from cells from both the apical and basolateral compartments [179–183].

**Fetal exosomes, irrespective of the physiologic status of cell of origin, cause inflammatory activation in maternal cells**

The number of exosomes released from cells under normal culture conditions or after CSE treatments were similar. This can partly be explained by the fact that the same number of cells were treated for each treatment type. Additionally, CSE treatment alone is not sufficient to cause an increase in exosome quantity but does lead to a change in exosome cargo content reflecting the physiologic state of cells [125]. A key finding to highlight is that regardless of the source of exosomes (from cells grown under normal or oxidative stress conditions), exosome treatments produced inflammation in recipient maternal cells (myometrial and decidual cells).

It is not totally unexpected that exosomes from control environments would cause an inflammatory response as we have reported in a proteomic analysis of AEC exosomes derived under control conditions that they contain markers suggestive of NF- $\kappa$ B signaling [125]. Oxidative stress treatment with CSE also resulted in exosome cargo with inflammatory signals but mostly contained inflammation mediated by transforming growth factor (TGF) $\beta$  pathway. TGF $\beta$  is produced in fetal membrane cells in response to CSE treatment and oxidative stress and it is a well-known activator of epithelial mesenchymal transition (EMT) [196–198]. EMT is an inflammatory state [199] and Chaudhuri et al. has shown fetal membrane EMT occurring at term [200]. Similar findings were reported by Mogami H et al in fetal membranes rupture models [200]. Ongoing data from our laboratory suggest exosomes can alter the fetal membrane microenvironment at term enhancing senescence, EMT and inflammation.

Exosomes are generated by cells and propagated throughout gestation. It is plausible that minimal levels of inflammation generated by normal cell exosomes during gestation are used for tissue remodeling and their quantity and cargo are insufficient to cause labor related inflammation. We speculate that oxidative stress build up at term produces an exclusive group of exosomes that can induce unique inflammatory conditions resulting in parturition. As shown in Figure 3.6, oxidative stress derived exosomes induced NF- $\kappa$ B activation in myometrial cells, which is known to be associated with inflammation and functional progesterone withdrawal. Our previous work has also shown that CSE induced oxidative stress leads to packaging of p38 MAPK, an activated form of stress signaler, into AEC exosomes. p38 MAPK has been shown to be a potential mediator of functional progesterone withdrawal [92,201].

In this study we used primary decidual cells and myometrial and placental cell lines. It can be argued that primary vs cell line differences may impact our observed outcome. However, similarities in response to exosomes between decidual primary cells and myometrial cell line cells' suggest that comparable outcomes can be expected irrespective

of cell types. We acknowledge that more studies are needed using primary cells as well as intact tissues to verify our data.

### **Placental cells are refractory to immune response by amnion exosomes**

Placental cells were found to be refractory to stimulation by AEC exosomes. Regardless of concentration or exosome origin (control vs oxidative stress), placental (BeWo) cells did not respond to exosomes or show any inflammatory change. It is possible that AEC derived exosomes are not capable of generating an inflammatory response from placenta. It is also possible that the inflammatory response may be different in primary cells as compared to the BeWo cell line. A study by Koh et al. found while BeWo cells will produce IL-6 after stimulation with OS, they will not produce IL-8 or IL-1 $\beta$  [202]. Our results indicated no increase in IL-6 production by placental (BeWo) cells after treatment with exosomes which makes the conclusion that placental cells may be refractory to AEC exosomes more plausible. We speculate that exosomes show tropism and they are capable of causing functional impact in specific target tissues and likely at specific times. The mechanism of exosomal tropism and its selection of target tissues are yet to be determined. Specific surface proteins acquired by exosomes under distinct physiologic state of a cell may determine tissue tropism and the functional role of exosomes. Proximity of placenta and fetal membranes makes placenta less likely to respond to inflammatory challenges produced by membranes because any inflammatory response by membranes spread via exosomes can be detrimental to the survival of placenta and thus the fetus. We do not rule out that refractoriness of BeWo cells may be attributed to transitioned state of trophoblast cells and primary cytotrophoblast cells may have yield different results.

### **Determining fidelity of exosomal functions**

In this current study, multiple experiments were conducted where exosome uptake was blocked. Exosome uptake or functional contribution of exosomes are mostly

manifested by the following routes: 1. Endocytosis of exosomes and cytoplasmic delivery of cargo [202] 2. Specific ligand (markers on exosomes) – receptor (on recipient cell) interaction [203,204] 3. Fusion of exosomes directly with plasma membrane and release of cargo [205] 4. Delivery of cargo into the environment of the target cell after undergoing lysis outside the recipient cell [206]. We primarily tested the endocytosis effect, a well reported mechanism of exosome entry. Energy dependent endocytosis was stopped by incubating cells at 4° C, as described in prior studies of exosome uptake and function [205,207–209], which lead to a reduced production of IL-6, IL-8 and PGE<sub>2</sub> by all cell types. This indicates that exosomes are contributing to the increased inflammatory mediator production, predominantly via endocytosis. We also either heated or sonicated the exosomes prior to treatment [69]. Heating can denature the surface proteins of the exosome while sonication breaks the exosome open. Heating or sonicating the exosomes prior to treatment reduces the number of routes through which the exosome can be taken up by the target cell, but likely releases the contents of the exosomes into the recipient cell extracellular environment. There was not a significant increase in cytokine production after treating with heated or sonicated exosomes. This indicates that the AEC exosomes can exert effects via several different routes in gestational cells.

Exosomes may contain various molecules and it was theoretically possible that the AEC exosomes contained the inflammatory analytes of interest. To test this, as a part of an ongoing study in our laboratory, we verified whether exosomes from control and oxidative stress exosomes carried cytokines contributing to the observed data. For this, a proteomic analysis of the exosomes was conducted by Dr. Salomon's laboratory using LC/MS-MS approach and we report that none of the analytes measured in this study (IL-6, IL-8 and PGE<sub>2</sub>) were detectable in our exosomes preparations from control or oxidative stress conditions.

**Oxidative stress of amnion epithelial cells leads to production of exosomes with pronounced effect on target cells**

Exosomes produced under oxidative stress conditions have a more dominant effect than those produced under normal cell conditions (control exosomes) as almost all treatments using oxidative stress exosomes increased pro-parturient biomarkers in decidua and myometrium. Dose dependent effect was not seen at the end of a 24 hour incubation and it is likely that all doses used are either saturating the response or that additional doses or longer incubation may be necessary to show the true kinetics of cytokine response.

The results of our study indicate that exosomes produced by AECs are capable of being taken up by other gestational tissue cells and cause inflammatory, labor-promoting changes in maternal gestational cells. This indicates that AEC derived exosomes may be involved in the labor cascade by functioning as messengers carrying specific signals between the fetal and maternal compartments. We conclude that AEC exosomes are a novel paracrine mechanism of fetal-maternal communication.

## **CHAPTER 4: FETO-MATERNAL TRAFFICKING OF EXOSOMES IN MURINE PREGNANCY MODELS**

Modified in part from:

**Feto-Maternal Trafficking of Exosomes in Murine Pregnancy Models**

Samantha Sheller-Miller, Jun Lei, George Saade, Carlos Salomon, Irina Burd and  
Ramkumar Menon

Published: *Frontiers in Pharmacology* (2016)

### **Introduction**

Human parturition is widely accepted as an inflammatory process initiated by environmental, endocrine and physiological factors, although the precise mechanisms involved are still unclear [10,25]. Normal term parturition consist of well-orchestrated events involving both fetal and maternal compartments [8,9]. On the maternal side, activation of the decidua, myometrial functional progesterone withdrawal, and cervical ripening are all considered mechanistic signals associated with parturition [4,84]. Both endocrine and paracrine fetal biochemical signals and released from matured organs, such as surfactant protein-A from fetal lungs, can induce parturition [9,10]. Our laboratory has investigated a new fetal signaling mechanism initiated by fetal membrane senescence in response to inflammation and oxidative stress that builds up in the amniotic cavity at term [33,34,89,92]. This leads to senescence-associated sterile inflammation through the release of inflammatory cytokines, chemokines, matrix degrading enzymes and growth factors, termed senescence-associated secretory phenotype (SASP) [33,34,87,91]. Senescent cells also secrete damage associated molecular patterns (DAMPs), which are well known inflammatory mediators released from dying cells communicating cellular damage [48,49]

Although the senescent signal action is predominantly localized, these signals of cellular stress may get carried to maternal tissues, signaling fetal maturity and prompting delivery of the fetus [51,52]. Distant senescent signaling is likely facilitated through

intercellular signaling vesicles called exosomes [125]. Exosomes are 30-100 nm endosome-derived vesicles with specific characteristics that separate them from other larger particles such as microvesicles and apoptotic bodies [53,54]. First described as modulators of the immune response to cancer cells, exosomes have also been found to contribute to angiogenesis and metastasis [59,210]. The current research involving exosome signaling in tumorigenesis via immune cell modulation has increased interest in their role in inflammatory disorders, such as asthma, arthritis and inflammatory bowel disease [78,175,210]. Since inflammation is an underlying theme in the initiation and progression of labor [10,33,84,211,212], it is likely that exosomes play an important role in cell signaling during term labor.

Exosome size facilitates transport between cells and tissues, while their contents, which reflect the functional state of the cell of their origin, may regulate the phenotype of the target cell [162,206,213]. Ongoing studies in our laboratory have shown that myometrial cells treated with exosomes from amnion epithelial cells cultured under oxidative stress conditions induce a contractile phenotype through the activation of NF $\kappa$ B and gene transcription activation of contraction associated proteins COX-2 and Connexin-43.

Although studies show exosomes can induce functional changes in myometrial cells, we do not know if the fetal membrane-derived exosomes can reach the maternal tissues to induce labor. The objective of this study was to determine the biodistribution of exosomes *in vivo* in pregnant animal models. By injecting fluorescently-labeled amnion cell-derived exosomes into the amniotic fluid of pregnant CD-1 mice, we will observe the migration of exosomes from the fetal to the maternal tissues.

## **Materials and Methods**

### **Patient exclusion criteria**

Placental samples obtained for this study were from John Sealy Hospital at The University of Texas Medical Branch (UTMB) at Galveston, TX, USA. No subjects were recruited or consented for this study as we use discarded placenta from normal term, not in labor cesarean sections described in Chapter 2.

### **Isolation and Culture of human Amnion Epithelial Cells (AECs)**

All reagents and media were warmed to 37°C prior to use. The amniotic membrane was processed as described in Chapter 2. Cells were cultured in T75 flasks containing complete media consisting of Dulbecco's Modified Eagle Medium: Nutrient Mixture F-12 media (DMEM/F12; Mediatech Inc., Manassas, VA) supplemented with 10% fetal bovine serum (FBS; Sigma-Aldrich, St. Louis, MO), 10% Penicillin/Streptomycin (Mediatech Inc.) and 100 µg/mL epidermal growth factor (EGF; Sigma-Aldrich) at 37°C, 5% CO<sub>2</sub>, and 95% air humidity to 60-65% confluence.

### **Exosome isolation**

Culture media was removed and cells were serum starved for 1 hour in DMEM/F12 with 5% pen/strep prior to treatment with exosome-depleted media (DMEM/F12, 5% pen/strep and 10% exosome-depleted FBS) for 48 hours. FBS (Sigma-Aldrich) was depleted of exosomes by ultracentrifugation at 100,000 g for 18 hours then filter-sterilized with 0.22 µm filter (Millipore, MA, USA) [162,214]. Culture media were collected and stored at -80°C until exosome isolation. Media was thawed overnight then isolated using differential ultracentrifugation as described in Chapter 2 with the following modifications. After the 2-hour 100,000 g centrifugation, the sample was split: half was resuspended in PBS and centrifuged for 1 hour at 100,000 g while the other half was labeled with DiR. The final pellets were resuspended in cold PBS and stored at -80°C.

### **Labeling of Exosomes with DiR**



To fluorescently label exosomes for *in vivo* imaging, the pellet from centrifugation at 100,000 g for 2 hours was resuspended in 7.0 mL 7.5  $\mu$ M 1,1-dioctadecyl-3,3,3,3-tetramethylindotricarbocyanine iodide (DiR) (Life Technologies, Carlsbad, CA) in PBS. After mixing, the exosomes were incubated in the DiR/PBS solution for 15 minutes at room temperature in the dark, then ultracentrifuged at 100,000 g for 1 hour. The final pellet was resuspended in 50  $\mu$ L PBS and stored at -80°C.

### **Exosome Characterization Using Transmission Electron Microscopy (TEM) And Western Blot**

To show exosomes isolated from primary AECs exhibit classic exosome shape and morphology, TEM studies were performed as described previously [125], with the following modification. Exosomes were fixed in 5% buffered formalin then 5  $\mu$ L of exosome suspension were dropped onto the grid and left to dry at room temperature for 10 min. To show exosome and amnion cell markers, western blot was performed as described previously [125].

### **Animals**

All animal procedures were approved by the Animal Care and Use Committee of Johns Hopkins University. Timed - Pregnant CD-1 mice, outbred mice reflecting diverse genetic background in humans, were purchased from Charles River Laboratories (Houston, TX) and received on gestational day 9 (E9). Animals had access to food and water ad libitum freely during the housing and experimental period. To determine the biodistribution of exosomes *in vivo*, we anesthetized pregnant CD-1 mice on 17 (n=9) with continuous isoflurane in oxygen and performed intrauterine injections of DiR in PBS (vehicle), DiR-labeled exosomes or phosphate-buffered saline solution (PBS).

Mice were subjected to mini-laparotomy as cartooned in Figure 4.1, using a Hamilton syringe, 2  $\mu$ L of DiR in PBS (n=2 E17), saline (n=3) or DiR-labeled exosomes

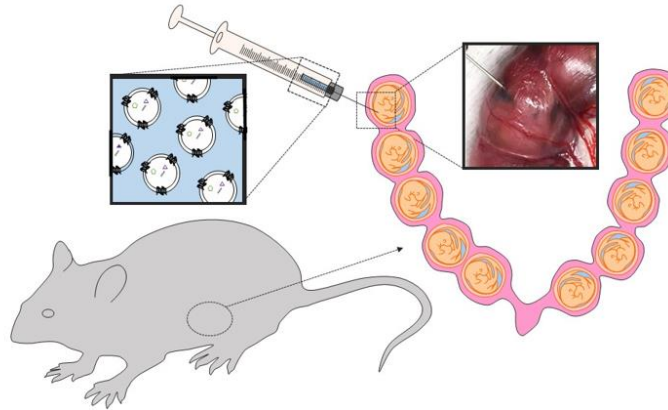


**Figure 4.1: Illustration of exosomes injected into the amniotic cavity of pregnant mice.**

in PBS (n=6) were injected intra-amniotically into each gestational sac on the right side of the cervix (maximum of 5 injections). The left side of the uterus was not injected and served as an internal control. Surgical incisions were closed, and the dams were recovered in individual cages.

After 24 hours, animals were imaged under anesthesia on both dorsal (after hair removal) and abdominal sides using the Bruker MS FX PRO In Vivo Imager (Bruker, Billerica, MA). Once live imaging was performed, animals were sacrificed by carbon dioxide inhalation according to the IACUC and American Veterinary Medical Association guidelines. The fetus contained within the uterus was collected in 4% paraformaldehyde (Sigma – Aldrich) and analyzed by histology for the presence of exosomes. The uterus was also removed from saline and exosome injected mice and imaged using IVIS 200 (PerkinElmer, Inc., Waltham, MA). Any image modifications (brightness, contrast, and smoothing) were applied to the entire image using Image J (open source). Maternal plasma was collected for exosome isolation.

Embryos were removed and fixed in 4% PFA at 4°C overnight. The next day, specimens were washed with PBS extensively and immersed in 30% sucrose until saturation, followed by cryosection at 20  $\mu$ m thickness. All photographs were taken with

Zeiss AxioPlan 2 Microscope System (Jena, Germany). Routine hematoxylin and eosin (H&E) histochemical staining was performed on the neighbor sections.

### **Maternal Plasma Exosome Isolation to Localize Trafficking of Exosomes**

To determine whether exosomes injected into the amniotic cavity can reach maternal side through systemic route, serum samples were analyzed for fluorescently labeled exosomes in maternal serum. Exosomes were isolated from maternal plasma as described above and the final pellet was resuspended in 100  $\mu$ L 1:1 glycerol/ethanol solution. To determine if the isolated exosomes contained fluorescence, 50  $\mu$ L of each sample was pipetted into a black 96 well plate (Corning) and imaged on the Biotek Synergy H4 Hybrid (Biotek, Winooski, VT). Wavelength was set for excitation at 745 nm and emission at 779 nm. A serial dilution of DiR in 1:1 glycerol/ethanol solution was used as the positive control, while the glycerol/ethanol solution was used as a negative control. Values were determined using relative fluorescence units (RFU).

## **Results**

### **Amnion Epithelial Cell-Derived Exosome Characterization**

Isolated exosomes were characterized using transmission electron microscope (TEM) and western blot for exosome and amnion markers as described previously [125]. TEM analysis revealed vesicles with classic exosome size and morphology (Figure 4.2A), consistent with previously published reports for exosomes [71,113,155,159]. Western blot analysis was performed to determine exosome-enriched markers HSC70, CD81, and HSP70, as well as embryonic stem cell marker, Nanog (Figure 4.2B).

### **Exosome Trafficking in Pregnant Mice**

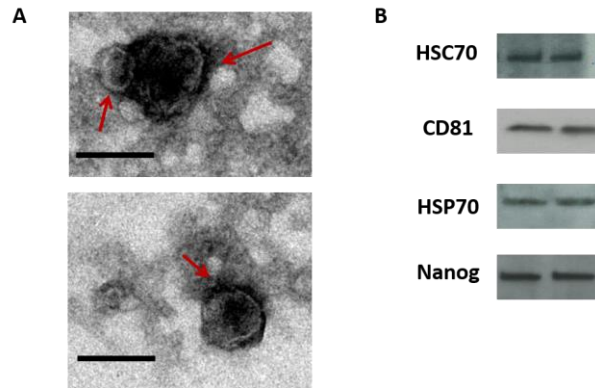


**Figure 4.2: Characterization of two representative exosome samples isolated from primary amnion cells**

A: Electron microscopy showing cup-shaped vesicles that have a size distribution of 30–150 nm (arrow indicates exosomes; scale bar represents 100 nm). B: Western blot analysis showing the presence of exosome markers HSC70, CD81 and HSP70, as well as embryonic stem cell marker, Nanog, indicating amnion epithelial cell origin.

To determine the trafficking of exosomes injected into the amniotic cavity, animals were imaged after 24 hours of injection. As a negative control, saline was injected into the amniotic cavity and imaged after 24 hours. Fluorescent signals could not be seen in saline-injected mice when imaged (data not shown).

Fluorescently labeled exosomes were injected into mice and imaged after 24 hours. Regardless of the gestational day, exosome injected mice images showed fluorescence on the dorsal side (Figure 4.3A), although the signal remained on the injected side. When the uterus was removed and imaged (Figure 4.3B), fluorescent signal was seen only on the injected side and not on the uninjected side, confirming the dye stays contained within the exosomes and does not leak from the membrane of the exosomes. On gestational day 18, images of the maternal kidneys from saline-injected and exosome injected mice were also taken (Figure 4.3C). No fluorescent signal can be seen in the saline-injected kidney while fluorescence was seen in the kidney of the exosome injected mice.

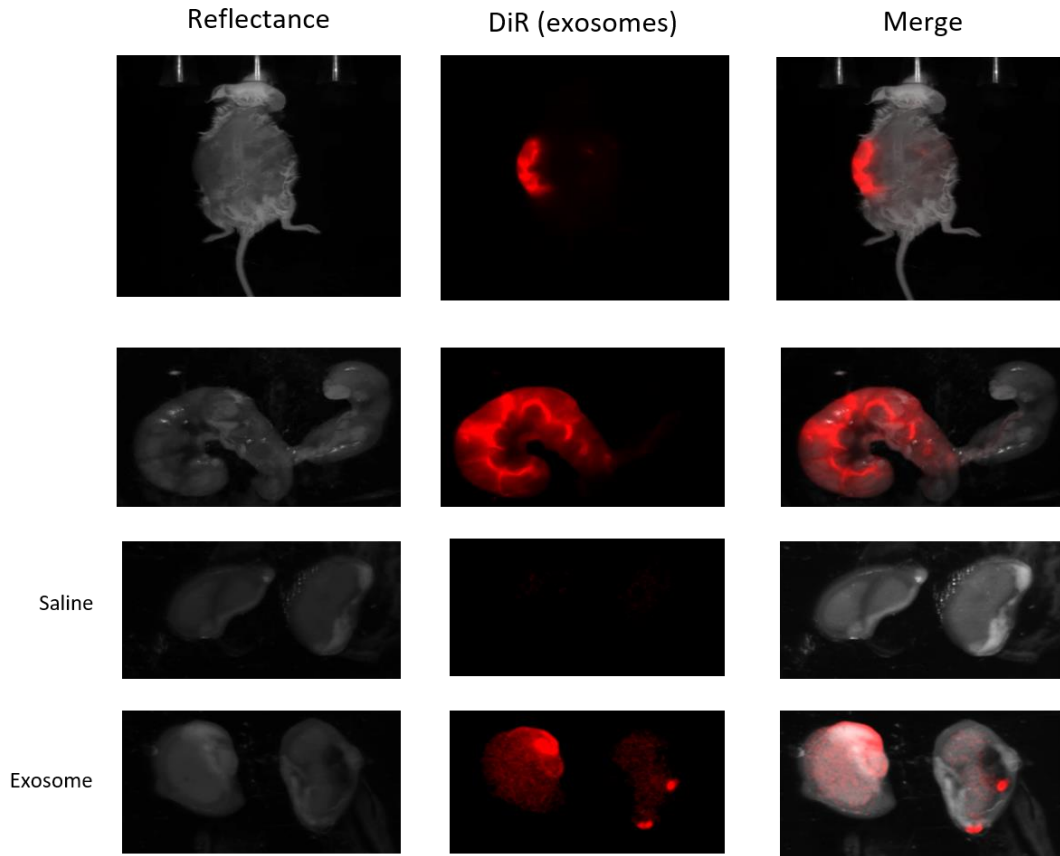


**Figure 4.3: In vivo imaging of pregnant mouse 24 hours post injection**

Exosomes stained with DiR (red) were injected into five different embryonic sacs on one side of the uterus. A: Dorsal image after removal of hair using Nair. B: Uterus was removed post sacrifice. Red fluorescence indicated embryonic localization of DiR labeled exosomes. Uninjected side (right) lacks fluorescence. C: Kidneys from saline-injected mice (top) do not have fluorescent signal while kidneys from exosome injected mice (bottom) have fluorescent signal. Merge is an overlay of reflectance and DiR.

Histologic analysis of placental and uterine tissues was performed to observe exosome trafficking in the reproductive tissues. On E18, signal emerging from exosomes can be seen on the maternal side of the placenta, whereas signal was not seen on the fetal side or in the saline-injected placenta (Figure 4.4). *In vivo* imaging of the uterine tissue showed saline-injected uterine tissue did not have fluorescent signal, whereas uterine

tissues from the exosome injected animals showed fluorescent signal (Figure 4.5). The fluorescent signal was validated using the Biotek Synergy H4 Hybrid in which the exosome-injected uterine tissues had almost 30-fold higher RFU than the saline injected tissues (data not shown).

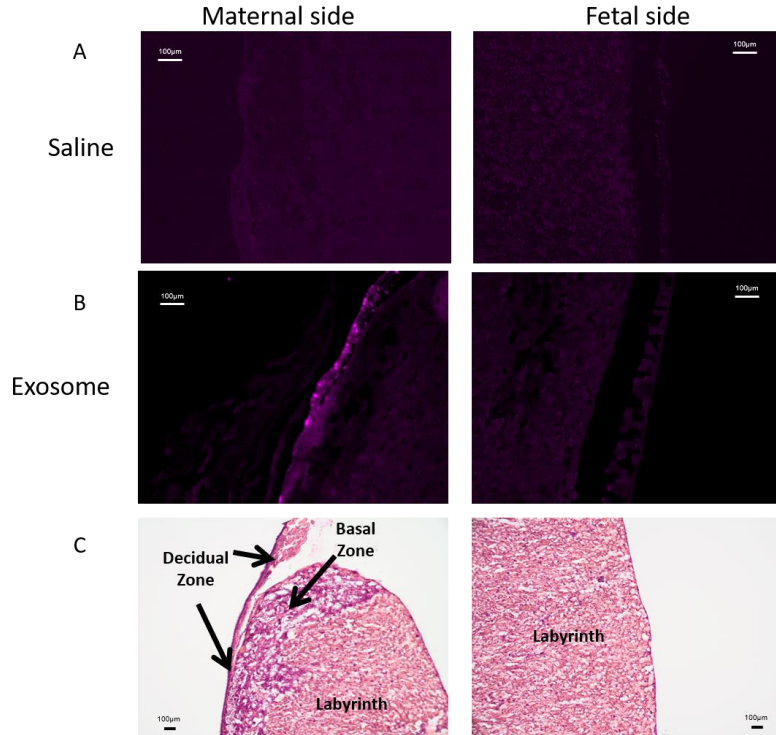


**Figure 4.4: Maternal and fetal sides of the placenta collected from injected mice on gestational day 18**

A: Saline injected mouse placenta showed no fluorescence on maternal or fetal sides. B: Exosome injected mouse placenta showed fluorescence on maternal side but lacks signal on the fetal side of the placenta. C: H&E staining of maternal and fetal sides of the placenta (scale bars represent 100 nm).

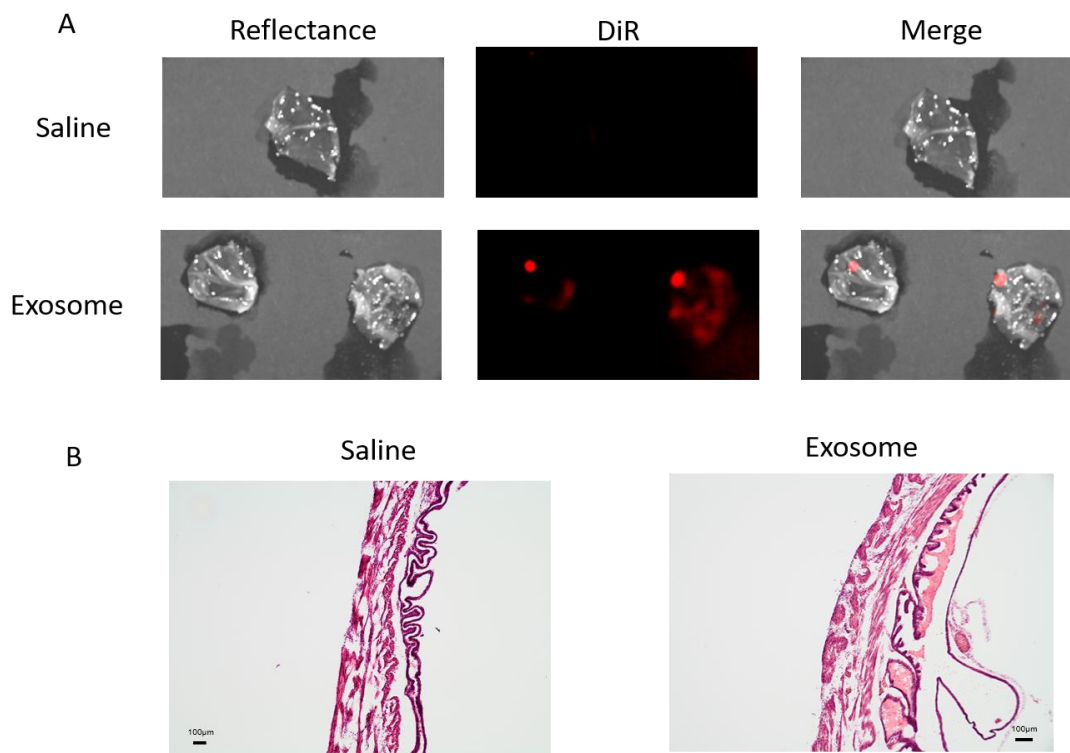


**Figure 4.5: In vivo imaging of uterine tissues collected from gestational day18**

A: Saline-injected (top) mouse uterus showed no fluorescent signal, while exosome-injected (bottom) mouse uterus showed fluorescence, indicating exosomes traffic to the maternal tissues. B: H&E staining of uterus tissue from saline (left) and exosome (right) injected mice (scale bars represent 100µm). Merge is an overlay of reflectance and DiR.

### Exosomes Traffic to The Maternal Serum

To validate the observations above and trafficking of exosomes through a systemic route, exosomes isolated from maternal serum were analyzed for fluorescence. Exosome injection solution was also analyzed for fluorescence to ensure exosomes were successfully labeled. Serum from mice injected with saline on E17, RFU below 50, similar to the negative control (glycerol/ethanol solution). The serum from the mice injected with exosomes on day 17 had an RFU above 50, indicating the exosomes from the amniotic

fluid can traffic through the maternal serum later in pregnancy and may be dependent on timing.

In summary, we demonstrate that exosomes may diffuse to the placental side where it can reach maternal tissues through a systemic route.

## Discussion

It is generally considered that the timing and initiation of labor are well orchestrated by communications between the fetus and the mother [15,81]. However, how these signals are communicated between the fetal and maternal compartments is poorly understood. As intercellular signaling vesicles that can travel long distances through tissues and fluids [64,109,153,215], exosomes may be carriers of these signals.

This study was performed to observe exosome trafficking *in vivo*. After labeling exosomes with the near infrared dye DiR, we determined that exosomes injected intra-amniotically into pregnant mice can be imaged and monitored for their migration. DiR-labeled exosomes injected on E17 were observed in the maternal plasma and kidneys and on the maternal side of the placenta and uterus on E18, indicating migration from the amniotic cavity to the maternal side. Our study shows that exosomes, which can potentially carry signals for the initiation of parturition, can traffic from the amniotic fluid into the placenta, and can have a systemic spread through circulation.

Exosomes are characterized by their contents, which reflect the physiological status of the origin cell and can regulate the phenotype of the target cell [125,152,215,216]. At term, oxidative stress and inflammation build up in the amniotic cavity, causing cellular senescence of the fetal membranes and subsequent release of signals of cellular damage [33,34,88,91,92]. Senescent signal action is primarily localized, although we have shown signals of cellular damage are also packaged into exosomes from amnion epithelial cells treated with the oxidative stress inducer cigarette smoke extract [125]. It is likely that



exosomes carrying signals of cellular damage can reach maternal tissues and contribute to parturition.

Though our study answers basic questions about exosome trafficking *in vivo*, it does not include activation of inflammatory pathways involved in the initiation and progression of labor. We only allowed for 24 hours prior to imaging and tissue collection, which may not be sufficient time for exosomes to migrate to the target tissues or cause functional changes. Determination of initiation of parturition at term or preterm based on signals carried by exosomes was beyond the scope of this study. The number of exosomes injected was random, which may influence the trafficking and eventual response to exosome signaling. Our ongoing studies using a specific number of exosomes will determine the effect of the quantity required to cause a functional change and specific pregnancy outcomes like preterm or term parturition. Future studies using live imaging will also determine the timing required for exosome migration between fetomaternal compartments. We will also understand differences between exosomes from amnion cells grown under standard conditions and oxidative stress conditions, including activation of inflammatory pathways related to parturition and preterm birth rates.

In summary, we have demonstrated that exosomes injected into the amniotic cavity of pregnant mice can traffic to the maternal tissues. Specifically, exosomes injected on gestational day 17 migrated to the maternal side of the placenta, the maternal serum, and the maternal kidneys. This study demonstrated that fetal signals can be carried as exosomal cargo through either diffusion between tissues or through systemic route from fetal to maternal side during pregnancy. This supports the postulate that fetal signals that can contribute to the initiation of human parturition can be delivered via exosomes.

## **CHAPTER 5: EXOSOMES CAUSE PRETERM BIRTH IN MICE: EVIDENCE FOR PARACRINE SIGNALING IN PREGNANCY**

Modified in part from:

### **Exosomes Cause Preterm Birth in Mice: Evidence for Paracrine Signaling in Pregnancy**

**Samantha Sheller-Miller**, Jayshil Trivedi, Steven M. Yellon, Ramkumar Menon

Published: *Manuscript under review at PNAS* (2018)

### **Introduction**

Parturition is an inflammatory process involving both fetal and maternal tissues and is initiated by fetal endocrine signals as well as signals arising from organ maturation at term (i.e., around 37-40 weeks of gestation) [3,15]. In humans, the inflammatory signals of fetal readiness for delivery lead to functional progesterone withdrawal [16,18], the recruitment and activation of immune cells, and the development of an inflammatory overload in the uterine cavity [19,217], which disrupts the homeostatic factors that maintain pregnancy and leads to the promotion of fetal delivery. Although fetal endocrine signals are a component of the biological clock that signals organ maturation and determines the timing of birth [9,11,218], paracrine signaling by intercellular signaling vesicles (called exosomes) may also contribute to the initiation of labor. However, knowledge gaps exist in understanding the signature of paracrine mediators, how they are generated, and how they are propagated to initiate labor and delivery [116,153]. How paracrine mediators regulate cervical remodeling and maturation of uterine contractile capabilities is essential for understanding the premature activation of such factors that are often postulated to be associated with spontaneous preterm birth, which complicates approximately 10.5% of all pregnancies [219–221]

At term, inflammatory mediators, often referred to as sterile inflammation, that are capable of contributing to labor-associated changes are elevated in both fetal and maternal gestational tissues [174,222]. Senescent fetal (amniochorionic membranes) or maternal (decidua) tissues produce inflammatory markers [34,195,223,224] termed the senescence-associated secretory phenotype (SASP) [45,46] as part of the molecular mechanism for sterile inflammation [32,89,90]. In addition to SASP, senescent fetal cells release damage-associated molecular patterns (DAMPs) [88,90]. SASP and DAMPs are postulated to constitute a set of sterile inflammatory signals that can be propagated from fetal to maternal tissues to indicate fetal readiness for delivery [66]. In addition, this inflammatory overload in maternal gestational tissues can create labor-associated changes [222,225,226]. Unlike endocrine mediators, senescence and the senescence-associated development of inflammatory paracrine signaling are similar in both human and rodent pregnancy and labor, thus suggesting that natural and physiological fetal tissue aging is an independent process and is unlikely to be regulated by endocrine mediators of pregnancy [72–74]. Senescence of the fetal membrane tissues is a physiological event in fetal membranes throughout gestation and is well correlated with fetal growth and organ maturation. Oxidative stress that builds up in the amniotic cavity at term accelerates senescence and the production of senescence-associated sterile inflammation [37,87] and this mechanism is considered as a contributor of labor and delivery.

The propagation of sterile inflammatory signals between fetal and maternal tissues can occur as simple diffusion through tissue layers or, more efficiently and in a protected manner, through extracellular vesicles (e.g. exosomes) [124]. Exosomes are 30-150 nm membrane vesicles that are formed by the inward budding of the late endosome [76,227]. Exosomes are released by cells and carry cellular metabolic byproducts including, but not limited to, proteins, nucleic acids, and lipids, and they represent the metabolic state of the cell that releases them [125,228]. Thus exosomes represent the biological and functional state of the origin cell, and studying them can provide evidence for the underlying status

of the organ [229,230]. Evidence suggests that exosomes play a role in the paracrine communication between fetal and maternal tissues. Specifically, (1) senescent fetal cells produce exosomes and carry fetal specific markers, SASPs, and DAMPs [125,231]; (2) irrespective of the experimental conditions (normal cell culture vs. oxidative stress conditions), exosomes carry inflammatory mediators; however, the inflammatory markers are unique depending on the type of treatment [232]; (3) fetal-derived exosomes can traffic from the fetal to the maternal side [124]; and (4) fetal exosomes may be capable of causing inflammatory activation in maternal gestation cells (myometrium and decidua) but not in placental cells. Besides this data, the current literature on exosomes during pregnancy has focused on placental exosomes and their potential effect on maternal tissues [67,68,70–72,112,153]. Several studies have explored the biomarker potential of exosomes and their cargo in adverse pregnancies, including preeclampsia and diabetes [75,111,117,151,155]. Although these descriptive observations suggest a courier or biomarker role for exosomes, a functional role of exosomes was lacking in processes associated with parturition or pregnancy-associated pathologies. Therefore, the primary objective of this study was to test the hypothesis that late gestational exosomes induce preterm parturition in mouse models of pregnancy. Little is known about exosomes during normal mouse pregnancy, therefore total maternal plasma exosomes were also characterized at various stages of mouse gestation prior to testing the functional role.

## **Materials and Methods**

### **Animal care**

Procedures were approved by the Institutional Animal Care and Use Committee (IACUC) at the University of Texas Medical Branch, Galveston. Timed-pregnant CD-1 mice (Charles River Laboratories, Houston, TX) were received on gestational day 4 (E4) or 14 (E14). Mice were housed in a temperature- and humidity-controlled facility with

automatically controlled 12:12-h light and dark cycles with regular chow and drinking solution provided ad libitum. Certified personnel and veterinary staff provided regular maintenance and animal care according to IACUC guidelines. The animals were sacrificed by CO<sub>2</sub> inhalation according to the IACUC and American Veterinary Medical Association guidelines.

### **Maternal plasma collection**

Maternal blood (0.5-1.0 mL) from timed-pregnant CD-1 mice was collected by cardiac puncture in tubes that contained EDTA (Becton Dickinson, Franklin Lakes, NJ) on gestation day (E) 5, 9, 13, 15, 18, and 19 and on postpartum day 7 (Figure 5.1A), as well as from nonpregnant mice. Mice were sacrificed by CO<sub>2</sub> asphyxiation. Plasma was harvested after centrifugation ( $2000 \times g$  for 10 min at 4°C) and stored at -80°C.

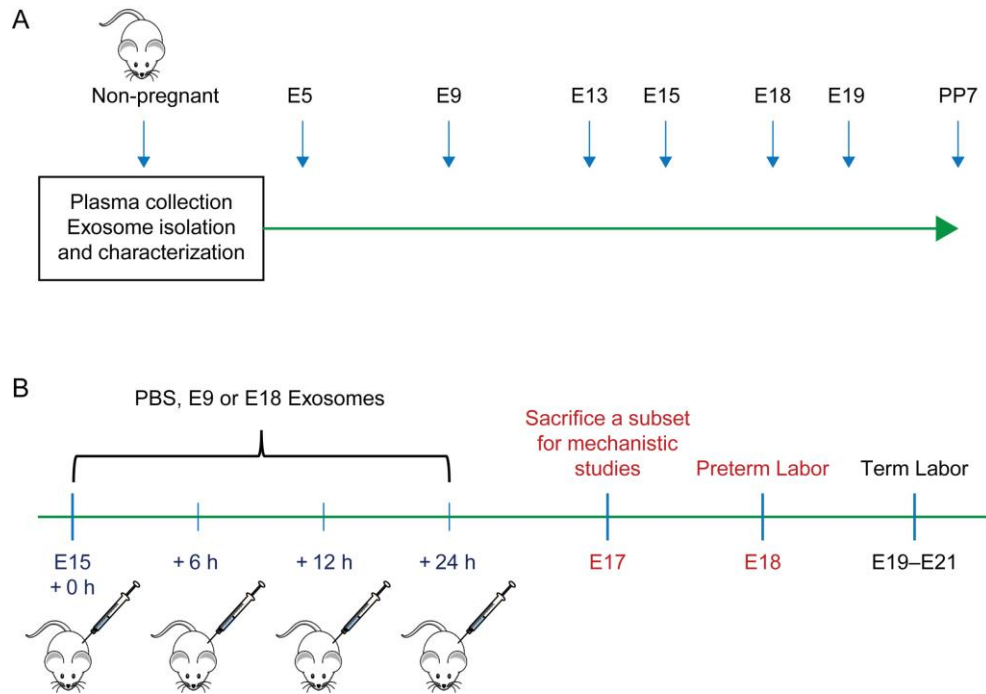


**Figure 5.1: Experimental model: maternal plasma collection and injection timelines in a CD-1 mouse model of pregnancy.**

**A:** Experimental Design. Plasma from nonpregnant mice and pregnant mice was collected on gestation day (E)5, 9, 13, 15, 18, 19, and postpartum day 7 for exosome isolation and characterization. **B:** Experimental design for PBS and exosome injections to determine the functional role of early (E9), and late gestation (E18) exosomes in vivo. PBS, E9 exosomes, or E18 exosomes were injected every 6 h on E15 and once more on E16. Mice were monitored for preterm labor and delivery prior to the expected delivery day (E19). Tissue samples and maternal plasma collected on E17 were analyzed for inflammatory markers associated with labor and delivery.

### Maternal plasma exosome isolation

Exosomes from maternal plasma were isolated as described previously with modifications [55,126,233]. Briefly, plasma samples were thawed on ice, diluted in 1.0 mL of cold 1x phosphate buffered saline (PBS), and centrifuged at 2000 x g for 10 min at 4°C. Supernatants were transferred to clean microcentrifuge tubes then filtered through Nalgene™ Syringe Prefilter Plus (Thermo Fisher, Waltham, MA). After filtration, samples were centrifuged at 10,000 x g for 30 min. The supernatant was transferred to ultracentrifuge tubes and centrifuged at 100,000 x g for an additional 2 h. The supernatant

was subsequently discarded, and the pellet was resuspended in 100  $\mu$ L of cold 1x PBS. The final pellet was passed through an Exo-spin<sup>TM</sup> column (Cell Guidance Systems, St. Louis, MO) following the manufacturer's instructions. Samples were aliquoted and stored at  $-80^{\circ}\text{C}$ .

### **Determination of exosome shape using cryo-electron microscopy**

To determine the shape of exosomes in maternal plasma, 3  $\mu$ L of prepared exosome suspension was pipetted onto a copper grid with quantifoil support film (QUANTIFOIL, Germany). The support film was patterned with a regular array of circular holes. When the excess liquid was blotted away from the grid, a 60-120 nm-thick film of sample suspension remained in these holes. The grid was then plunged into a small crucible of liquid ethane that was cooled to its melting point by liquid nitrogen. In the liquid ethane, the sample suspension was cooled at over 10,000 degrees/s, solidifying the water in an amorphous state. This "vitrification" process preserves the exosomes in their native state without distorting their geometry by crystallization and density change [230]. The vitrified sample on the grid was then placed in a Gatan 626 specimen holder (Gatan, Pleasanton, CA), which was placed in a JEOL 2100 TEM (JEOL, Osaka, Japan). The samples were imaged with a 200 kV electron beam from a LaB6 emission source, and images were recorded on a Gatan US4000 CCD camera. Images were captured at 15,000-30,000 magnification.

### **Determination of exosome size and quantification**

The size distribution and concentration of exosomes were determined using the Nanosight NS300 (Malvern Instruments, Worcestershire, UK). Samples were diluted (1:500) in distilled water and run following the manufacturer's instructions. A camera level of 12 and automatic functions were used for all postacquisition settings, except for the detection threshold which was fixed at seven. The camera focus was adjusted to make the

particles appear as sharp dots. Three 30 s videos were recorded for each sample using the script control function.

### **Flow cytometry analysis for exosome markers**

For flow cytometry analysis of exosome tetraspanin marker CD63, samples were prepared using the ExoFlow kit (System Biosciences, Mountain View, CA) protocol with modifications. Briefly, 9.1  $\mu\text{m}$  streptavidin-coated beads were washed and incubated with biotinylated anti-CD63 (clone MX-49.129.5, Novus Biologicals, Littleton, CO) for 2 h on ice, flicking intermittently to mix. The beads were washed and resuspended in 200  $\mu\text{L}$  of bead wash buffer prior to overnight incubation (4°C) with 100  $\mu\text{L}$  of exosomes. The following day, samples were washed and stained using the Exo-FITC exosome stain according to the manufacturer's instructions, before being run on the Cytotflex flow cytometer (Beckman Coulter, Brea, CA). Negative controls were beads incubated with antibody but without exosomes, and these controls were used for gating according to the manufacturer's instructions. Data analysis based on the fluorescein isothiocyanate (FITC) signal shift was performed using Cytexpert (Beckman Coulter).

### **Proteomic analysis of maternal plasma exosomes by mass spectrometry**

#### ***Exosome protein clean-up and digestion***

The protein profile of maternal plasma exosomes was established by liquid chromatography (LC) and mass spectrometry (MS). Exosomes (n=3/gestation day) in 1x PBS (12.5  $\mu\text{L}$ ) were lysed in 12.5  $\mu\text{L}$  of 10% SDS in 0.1 M TEAB by sonicating on ice for 10 min. A total of 1  $\mu\text{L}$  of 0.25 M TCEP was added to each tube to attain a final concentration of 0.01 M, and samples were incubated at 55°C for 1 h. The samples were allowed to cool before 1  $\mu\text{L}$  of 20 mM iodoacetamide was added to each tube and the samples were incubated for 45 min in the dark. The samples were subsequently transferred to tubes containing 8 M dry urea and vortexed. A total of 2.7  $\mu\text{L}$  of 12% phosphoric acid



was added, and 165  $\mu$ L of S-Trap buffer (90% MeOH, 100 mM TEAB, pH 7.5) was added to the acidified lysate. The lysate was added to the S-Trap microcolumn (Protifi, Huntington, NY) and centrifuged at 4000 x g for 2 min. The flow-through was discarded and the column was washed with 150  $\mu$ L of S-Trap buffer before being centrifuged at 4000 x g for 2 min. Columns were transferred to new tubes and incubated with 16 ng/mL of trypsin for 2 h at 47°C. Proteins were eluted by centrifugation at 4000 x g for 2 min with 50 mM TEAB, 0.2 % formic acid (FA), 50% acetonitrile (ACN)/0.2% formic acid, and finally 80% acetonitrile/0.1% formic acid. After the elutions, the final elute was dried.

### ***LC-MS/MS analysis of plasma exosomes***

Nano LC-MS/MS data acquisition was performed on the OrbiTrap Fusion mass spectrometer system (Thermo Fisher Scientific, San Jose, CA) coupled to a Dionex Ultimat 3000 nano-HPLC with a 40-well standard tray autosampler. The sample (5  $\mu$ L) was injected onto a trap column (300  $\mu$ m i.d. x 5 mm, C18 PepMap 100) and then a C18 reverse-phase nano LC column (100 75  $\mu$ m X 25 cm, Acclaim PepMap), which was heated to 50°C in a chamber. The loading pump flow rate was set to 8  $\mu$ L/min. The nano pump flow rate was set to 400 nL/min with a 130-min LC gradient, where the mobile phases were A (99.9% water and 0.1% FA) and B (99.9% ACN and 0.1% FA). The gradient was 0-5 min at 2% of B, 6-100 min at 4%-32% of B, an increase to 50% at 108 min, 5 min of 90% B wash, and 15 min equilibrium. Mass spectrometer parameters included tip spray voltage at +2.2 kV, sweep gas 1, and an ion-transfer tube temperature of 275°C. FTMS mode for the MS full scan from 350-1500 Da was used for the acquisition of precursor ions (resolution 120,000), ITMS top-speed (3 s) mode was used for MS/MS, and MS/MS was accomplished via HCD with collision energy of 32%.

All MS/MS samples were analyzed using Proteome Discoverer 1.4.1.14, which was set up to search UniProt-mouse.fasta (downloaded April 2016). Proteome Discoverer was searched using a fragment ion mass tolerance of 0.60 Da and a parent ion tolerance of 10.0

PPM. Peptide charges considered were +2, +3, and +4. Scaffold (version 4.8.4, Proteome Software Inc., Portland, OR) was used to validate MS/MS-based peptide and protein identifications. Peptide identifications were accepted if they could be established at >99.0% probability to achieve a false discovery rate (FDR) <1.0% by the Peptide Prophet algorithm [234,235] with Scaffold delta-mass correction, if they could be established at >99.0% probability and contained at least two identified peptides. Proteins that contained similar peptides and could not be differentiated based on MS/MS analysis alone were grouped to satisfy the principles of parsimony. Proteins were annotated with gene ontology (GO) terms from NCBI (downloaded on September 1, 2017) [236]. Proteins were normalized to nonpregnant samples (median area under curve) and considered significantly different when  $P < 0.01$  and the fold change was  $\pm 1.5$ .

### **Ingenuity pathway analysis (IPA) of identified proteins**

Pathway enrichment analyses were performed with IPA (Qiagen, Hilden, Germany) using Fisher's exact test. IPA was performed to identify canonical pathways, biological functions, and protein networks. Heatmap and hierarchical cluster analyses (ClusterMaker, open source) were used to demonstrate the expression patterns of the differentially-expressed proteins and pathways based on fold change and Z-scores. Significantly enriched pathways for the proteins and scenarios were identified using  $P < 0.01$ .

### **Injection of E9 and E18 exosomes to determine trafficking and labor-associated functional changes**

To test the functional effects of exosomes, maternal plasma exosomes from E18, typically the day prior to birth on E19.5) in this strain, and E9 (early gestation control) were used. Exosomes from these days were chosen based on data showing that E9 exosomes have minimal levels of inflammation and E18 have maximum levels of

inflammation (see results section). On E15, mice were injected three times at 6-h intervals and 12-h later on E16 with exosomes ( $3.33\text{--}9.16 \times 10^{10}$  in 250  $\mu\text{L}$  PBS, Figure 5.1B) of PBS. Treatment on E15 was chosen based upon other models of inflammation-induced preterm birth [24,29,237]. Multiple doses of exosomes were administered to sustain systemic concentrations because exosome half-life is relatively short and a single dose does not affect pregnancy duration [60,61]. Mice were monitored for preterm birth, which was defined as delivery on or before E18, compared to the expected delivery date of E19-E21 in controls. To further understand the functional effects of exosomes, tissues were obtained from four mice per treatment group on E17 as described above, fixed in 10% neutral-buffered formalin or flash frozen in liquid nitrogen.

#### **Fluorescent labeling of exosomes for determining in vivo trafficking and localization**

Maternal plasma exosomes from E9 and E18 were isolated and labeled with carboxyfluorescein succinimidyl ester (CFSE) by resuspending them in 100  $\mu\text{L}$  of 7.5  $\mu\text{M}$  CFSE. Exosomes were incubated at 37°C for 30 min before being diluted in PBS containing 5% BSA. Exosomes were run through the Exo-spin™ column (as described above) to remove excess CFSE.

#### **Immunofluorescent imaging for exosome trafficking**

Tissue samples collected in 10% neutral-buffered formalin were stored overnight (4°C) before being washed twice with 1x PBS and transferred to a 15% sucrose solution overnight (4°C). Samples were then transferred to 30% sucrose and stored at 4°C until they were embedded in optimal cutting temperature (OCT) and cut into 5- $\mu\text{m}$  sections. Sections were washed twice in water and treated with FITC Block (Abcam) for 15 min at room temperature. After a further two washes in water, tissues were mounted using Mowiol 4-88 mounting medium. Exosomes were visualized using the Olympus BX43 fluorescent microscope (Olympus, Tokyo, Japan) at 40x magnification, and images were captured

using Q Capture Pro software. Brightness, contrast, and smoothing were applied to the entire image using FIJI (open source).

### **Enzyme-linked immunosorbent assay (ELISA) for progesterone levels in maternal plasma**

Maternal plasma samples were collected on E17 and analyzed for progesterone levels. Plasma progesterone levels were determined using the Mouse Progesterone ELISA kit (Biotang Inc., Lexington, MA) following the manufacturer's instructions. Concentrations below the assay detection limits (0.5 ng/mL) were considered as one-tenth of each value

### **Immunohistochemistry for macrophage infiltration and activation**

To determine that exosomes can cause inflammatory changes in maternal gestational tissues, cervix and uterus were fixed in 10% neutral buffered formalin for 24 h at 4°C overnight before paraffinization, sectioning (10 µm), and processing as previously described [238]. Sections were stained with the F4/80 antibody to visualize mature macrophages (1:800 BM8; BMA Biomedicals, Switzerland) and counterstained with a 1% methyl green solution to identify cell nuclei. Macrophages were clearly identified by dark brown stain against low background and in association with a methyl green counterstained cell nucleus.

### **Western blot analysis**

#### ***Western blot analysis for exosome markers***

Exosomes in PBS were lysed by the addition of 10x radioimmunoprecipitation assay (RIPA) lysis buffer (50 mM Tris pH 8.0, 150 mM NaCl, 1% Triton X-100, 1.0 mM EDTA pH 8.0, and 0.1% SDS) supplemented with protease and phosphatase inhibitor cocktails and PMSF. Western blot samples were subsequently processed as described previously [124,125,231]. The anti-mouse antibodies used included exosome markers CD9

(1:400; Abcam, Cambridge, United Kingdom), CD81 (1:500; Cell Signaling, Beverly, MA), and Alix (1:1000; Abcam).

### ***Western blot analysis of fetal and maternal tissues***

Tissues flash frozen in liquid nitrogen were homogenized in RIPA buffer supplemented with protease and phosphatase inhibitors using a bullet blender (Next Advance, Averill Park, NY) as described previously [37]. Blots were incubated overnight with primary antibodies against total NF- $\kappa$ B (1:1000; Cell Signaling, Danvers, MA), phosphorylated (P)-NF- $\kappa$ B (1:400; P-RelA; Abcam), total p38 MAPK (1:1000; Cell Signaling), P-p38 MAPK (1:400; Cell Signaling), COX-2 (1:800; Abcam), or connexin-43 (1:3000; Abcam). Samples for the same experiment were run on the same gel for a given marker to avoid interassay variability between blots. The blots were all reprobed with antibodies to GAPDH (1:1000; Santa Cruz Biotechnology, Dallas, TX), and all proteins were normalized to GAPDH prior to densitometry analysis. Semi-quantitated data on western blots (based on densitometry readings) are expressed in arbitrary units in the result sections.

### **Luminex assay to determine inflammatory markers in tissue and plasma**

Plasma and tissues collected from mice on E17 were assayed for IL-6 and TNF- $\alpha$  (n = 4 per group) using MILLIPLEX Mouse Cytokine Panel 1 (Millipore) following the manufacturer's protocol. For tissues, equal amounts of protein (25  $\mu$ g) were loaded into each well. Standard curves were developed using duplicate samples of known-quantity recombinant proteins that were provided by the manufacturer. Sample concentrations were determined by relating the absorbance of the samples to the standard curve using linear regression analysis. Concentrations below the assay detection limits (IL-6 = 1.1 pg/mL; TNF- $\alpha$  = 2.3 pg/mL) were considered as one-tenth of each value.

### **Statistical analysis**

Western blot (n = 4), bioplex and ELISA (n = 4), macrophage quantitation (n=3) and exosome size and concentration (n = 8) data were analyzed using a one-way ANOVA with Tukey's post hoc test using GraphPad Prism (GraphPad, San Diego, CA).  $P < 0.05$  was considered significant. Proteomic comparison between all gestation days (n = 3) was analyzed using the Kruskal-Wallis test with Benjamini-Hochberg correction using Scaffold 4 Viewer. Comparison between two gestation days was analyzed using the nonparametric Mann-Whitney test with Benjamini-Hochberg correction using Scaffold 4 Viewer.  $P < 0.01$  was considered significant.

A post hoc power analysis was performed using G\*Power [239] based on group means, standard deviation, and effect size ( $f = 1.1$  for western blot and cytokine data, 0.81 for progesterone and exosome size and concentration, and 0.93 for preterm birth rates). This analysis revealed that the study had  $>80\%$  power for the ANOVA to detect differences between groups at a 0.05 significance level.

## **Results**

### **Plasma exosomes exhibit classic exosome characteristics**

To understand the changes associated with exosome quantity and characteristics, total exosomes were isolated from maternal plasma samples at various gestational days and compared to nonpregnant and postpartum day 7 animals. Regardless of pregnancy or gestation day, exosomes isolated from maternal plasma were round double-membrane vesicles (Figure 5.2A). Western blot analysis indicated that exosomes contained tetraspanin markers CD9 and CD81, as well as the multivesicular body protein ALIX (Figure 5.2B). As evidenced by flow cytometry, exosomes were also positive for another tetraspanin exosome marker, CD63 (Figure 5.2C).

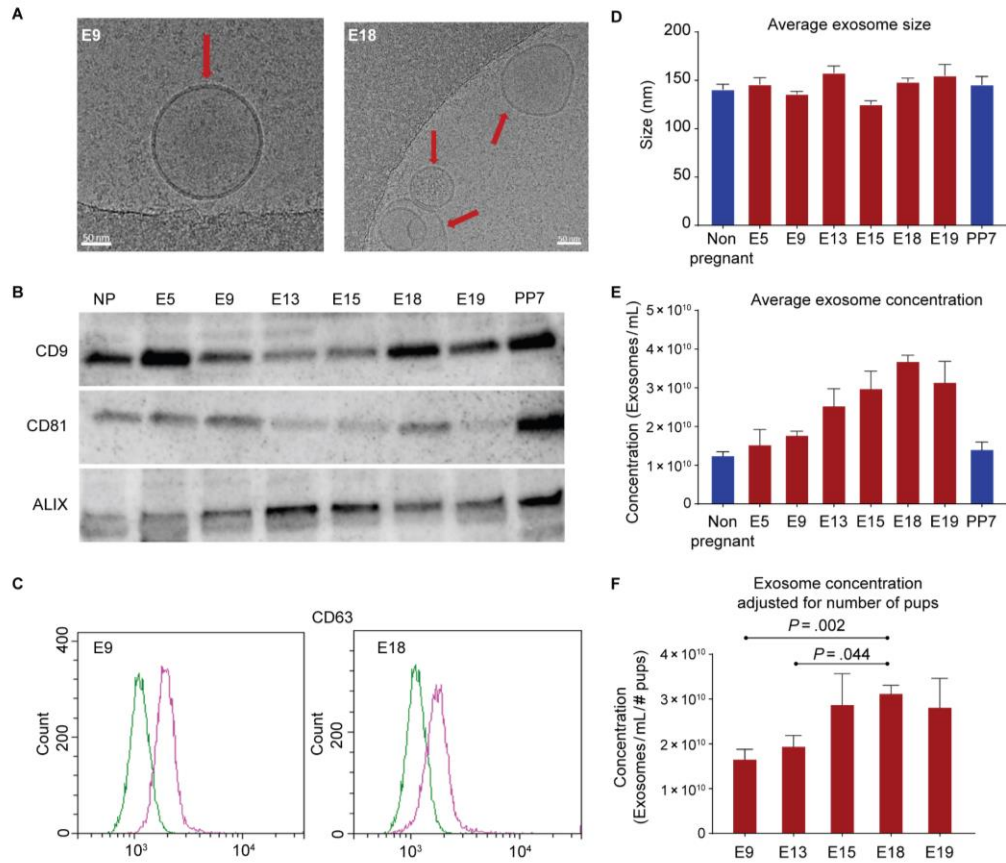


**Figure 5.2: Characterization of exosomes isolated from maternal plasma.**

**A:** Representative cryo-electron microscopy image showing classic exosome characteristics of double-membrane vesicles from early gestation (E9) and late gestation (E18). The arrow indicates exosomes, and the scale bar represents 50 nm. **C:** Regardless of gestation day or pregnancy status, there was consistent expression of exosome markers CD9, CD81, and ALIX. **D:** Representative flow cytometry histogram for maternal plasma exosome marker CD63 from E9 and E18 exosomes. X-axis, FITC intensity; y-axis, count or the number of beads positive for exosomes. Green represents the negative control; pink represents beads containing exosomes positive for CD63. **E:** Exosome size was not significantly different between gestation days. **F:** The average exosome concentration increased significantly throughout gestation (E5 through E19) compared to the nonpregnant state. **G:** The average exosome concentration for each gestation day was adjusted to the average number of pups per mouse to determine if the increase in exosome concentration throughout gestation was dependent on the number of pups each mouse was carrying. The number of pups per mouse was not significantly different between each gestation day and exosome concentration per pup on E18 was still the maximum concentration observed. Exosome concentration per pup was significantly higher on E18 compared to E9 ( $P = 0.002$ ) and E13 ( $P = 0.04$ ) when adjusted for the number of pups.

### Exosome concentration increases throughout gestation

Exosomes isolated from maternal plasma did not differ significantly in size throughout gestation (Figure 2D, Table 5.1). However, a significant increase in exosome quantity (see Appendix C Supplemental Table 5.2) was seen between E5 ( $1.52 \times 10^{11}$  exosomes/mL) and E19 ( $3.13 \times 10^{11}$  exosomes/mL), with the maximum concentration seen at E18 ( $3.66 \times 10^{11}$  exosomes/mL, Table 5.1) (Figure 5.2E). The trend remained the same after adjusting for the number of pups, with E18 showing the maximum number of exosomes (Table 5.1). As shown in Figure 5.2, significant differences were noted (Figure 5.2F) between E18 and E9 ( $P = 0.002$ ) and E18 and E13 ( $P = 0.044$ ).

**Table 5.1: Exosome Size and Concentration throughout Gestation**

Gestation Day	Mean Size	Mean Concentration	Average Number of Pups	Adjusted for Number of Pups
Nonpregnant	140.9 ( $\pm 11.4$ )	$1.24 \times 10^{11}$ ( $\pm 2.41 \times 10^{10}$ )	N/A	N/A
E5	146.0 ( $\pm 15.0$ )	$1.52 \times 10^{11}$ ( $\pm 9.03 \times 10^{10}$ )	N/A	N/A
E9	136.1 ( $\pm 8.9$ )	$1.75 \times 10^{11}$ ( $\pm 4.48 \times 10^{10}$ )	12 ( $\pm 3$ )	$1.65 \times 10^{10}$ ( $\pm 7.74 \times 10^9$ )
E13	157.9 ( $\pm 19.6$ )	$2.53 \times 10^{11}$ ( $\pm 1.27 \times 10^{11}$ )	13 ( $\pm 2$ )	$1.94 \times 10^{10}$ ( $\pm 6.99 \times 10^9$ )
E15	131.3 ( $\pm 12.4$ )	$2.97 \times 10^{11}$ ( $\pm 1.03 \times 10^{11}$ )	10 ( $\pm 4$ )	$2.87 \times 10^{10}$ ( $\pm 1.56 \times 10^{10}$ )
E18	148.6 ( $\pm 17.2$ )	$3.66 \times 10^{11}$ ( $\pm 8.31 \times 10^{10}$ )	12 ( $\pm 3$ )	$3.11 \times 10^{10}$ ( $\pm 9.11 \times 10^9$ )
E19	155.1 ( $\pm 29.8$ )	$3.13 \times 10^{11}$ ( $\pm 1.47 \times 10^{10}$ )	12 ( $\pm 2$ )	$2.81 \times 10^{10}$ ( $\pm 1.73 \times 10^{10}$ )
PP7	145.7 ( $\pm 18.6$ )	$1.39 \times 10^{11}$ ( $\pm 4.60 \times 10^{10}$ )	N/A	N/A

### Proteomic analysis of maternal plasma exosomes throughout gestation

Proteomic analysis of maternal plasma exosomes identified 1283 differentially-expressed proteins. A heat map (Figure 5.3A) was created of the 912 differentially expressed proteins that were used for bioinformatics analysis using IPA. Proteomic analysis of exosomal cargo determined that molecules involved with inflammation were the predominant pathway that



increased during late gestation. Specifically, acute-phase response signaling, liver X receptor/retinoid X receptor (LXR/RXR), and coagulation canonical pathways (Figure 5.3B) increased between E13 and E18, peaked at E18, and returned to levels seen in nonpregnant animals in the postpartum samples (Table 5.2). Analysis of the top biological functions associated with exosomal cargo on each gestation day (Figure 5.3C) included inflammatory pathways related to increased recruitment of leukocytes and other immune cells throughout gestation, peaking on E18 and decreasing postpartum. The biological functions associated with the proteins identified in late-gestation exosomes included chemotaxis, the inflammatory response, cell movement, leucocyte activation, and neutrophil infiltration, all of which have been linked to physiological changes associated with prepartum processes related to cervix remodeling and initiation of labor [163,211,212,240].

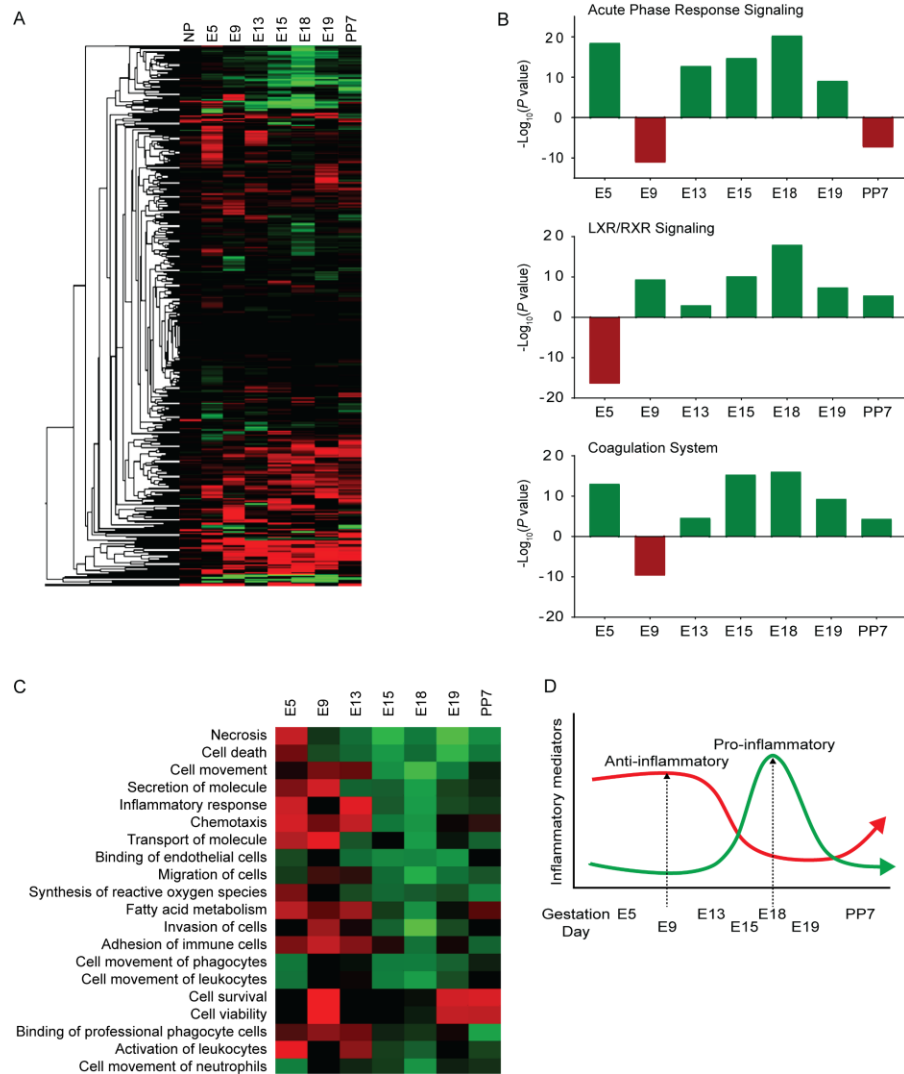


**Figure 5.3: Proteomic and bioinformatic analysis of maternal plasma exosomes throughout gestation.**

**A:** Heatmap to visually represent differentially-expressed exosome proteins (912) throughout gestation. Green is an increased fold change, while red is a decreased fold change. **B:** Graphical representation of the top three canonical pathways identified during late gestation: acute-phase response signaling (top), liver X receptor/retinoid X receptor (LXR/RXR, middle), and coagulation (bottom). The x-axis represents gestation day, and the y-axis represents  $-\log(P\text{-value})$ . Green represents a positive Z-score (upregulation), while red represents a negative Z-score (downregulation). **C:** Heatmap of the top biological functions associated with exosomal cargo on each gestation day shows inflammatory pathways and recruitment of leukocytes and other immune cells increasing throughout gestation, peaking on E18, and decreasing postpartum. Green represents a positive Z-score (upregulation), while red represents a negative Z-score (downregulation). **D:** Graphical representation of well-reported inflammatory changes during mouse pregnancy, which are also reflected in exosomes throughout gestation. Gestation days are not drawn to scale.

**Table 5.2: Top 3 canonical pathways identified with IPA**

<b>Acute Phase Response Signaling</b>				
Gestation Day	-Log (P-value)	Z-score	# Molecules Identified	Molecules
E5	18.387	0	13	ITIH3, AMBP, SERPINA3, SAA2-SAA4, FGG, SERPINF2, F2, ALB, ITIH4, CRP, FGB, SERPINA1, FGA
E9	11.032	-1.89	10	KLKB1, ALB, APOA2, SERPINA3, FGB, FGA, A2M, FGG, RBP4, AGT
E13	12.645	0	10	SERPING1, HP, APOA1, APOA2, CRP, SERPINA3, FGB, A2M, FGG, C5
E15	14.62	1.89	13	TTR, ITIH3, APOA2, VWF, SERPINA3, FGG, F2, PLG, C4A/C4B, ALB, ITIH4, SERPINA1, A2M
E18	20.202	1.414	18	APOH, C1S, APOA2, SERPINF1, VWF, SAA2-SAA4, F2, SERPIND1, PLG, C4A/C4B, TF, ITIH4, CRP, SERPINA1, FGB, LBP, A2M, AGT
E19	8.965	1.342	9	ITIH4, APOA2, SERPINF1, VWF, SERPINA3, SERPINA1, FGB, A2M, FGG
PP7	7.272	-2	7	HP, APOA2, AHSG, SERPINA3, SERPINA1, A2M, RBP4
<b>Liver X Receptor/Retinoid X Receptor (LXR/RXR)</b>				
Gestation Day	-Log (P-value)	Z-score	Molecules Identified	Molecules
E5	16.345	-2.111	11	KNG1, APOE, ALB, APOB, LCAT, ITIH4, AMBP, SERPINA1, FGA, GC, SERPINF2
E9	9.29	0.707	8	KNG1, ALB, APOB, APOA2, VTN, FGA, RBP4, AGT
E13	2.922	0	3	APOA1, APOA2, GC
E15	10.089	1	9	C4A/C4B, PON1, TTR, ALB, ITIH4, APOA2, VTN, SERPINA1, A1BG
E18	17.898	2.324	15	KNG1, APOB, APOH, APOA2, VTN, SERPINF1, C4A/C4B, PON1, LCAT, TF, ITIH4, SERPINA1, LBP, CLU, AGT
E19	7.324	0.378	7	KNG1, PON1, ITIH4, APOA2, SERPINF1, SERPINA1, A1BG

PP7	5.311	0.447	5	APOC4, APOA2, AHSG, SERPINA1, RBP4
<b>Coagulation System</b>				
Gestation Day	-Log (P-value)	Z-score	Molecules Identified	Molecules
E5	12.962	1.89	7	KNG1, SERPINA1, FGB, FGA, FGG, F2, SERPINF2
E9	9.624	-1.633	6	KNG1, KLKB1, FGB, FGA, A2M, FGG
E13	4.521	0	3	FGB, A2M, FGG
E15	15.208	1	9	C4A/C4B, PON1, TTR, ALB, ITIH4, APOA2, VTN, SERPINA1, A1BG
E18	15.957	0.632	10	PLG, KNG1, F5, VWF, SERPINA1, FGB, F7, A2M, F2, SERPIND1
E19	9.237	0	6	KNG1, VWF, SERPINA1, FGB, A2M, FGG
PP7	4.292	0	3	SERPINA1, F13B, A2M

The specific scenarios associated with different gestation points were evaluated by investigating the molecular networks that were activated by proteins with a  $\pm 1.5$ -fold change ( $\log_2$  fold change =  $\pm 0.6$ ) and a  $P$ -value  $< 0.01$  ( $-\log P$ -value = 2). When comparing E18 (late gestation) to E5 (early gestation), plasminogen (PLG) was identified as a central molecule in the molecular network (Figure 5.4A). PLG activates matrix-degrading enzymes MMP-2 and MMP-9, as well as TGF- $\beta$ . These molecules have been implicated in parturition at term and in preterm birth [241,242]. TGF- $\beta$  is also a major mediator of epithelial-mesenchymal transition, a mechanism that has been implicated in labor [200,243]. Identified proteins are listed in Appendix C Supplemental Table 5.2. E18 was also compared to E9 (Figure 5.4B) as these two gestation days seemed to have the most differences in canonical pathways and biological processes. TNF- $\alpha$  was identified as a central molecule in the network comparing exosomal proteins on E18 to E9. TNF- $\alpha$  is a pro-inflammatory cytokine shown to be upregulated in the myometrium at term and can activate smooth muscle contractions [225]. Additionally, TNF- $\alpha$  can activate pro-

senescence marker p38 MAPK in epithelial cells [232]. Identified proteins are listed in Appendix C Supplemental Table 5.2. Exosome cargo were also compared between E18 (term not in labor) and E19 (term in labor) (Figure 5.4C) and the central molecule identified was epidermal growth factor receptor, which activates the mitogen-activated protein kinase family (i.e., ERK, JUN, and p38) and other inflammatory pathways (i.e., STAT3 and the NF- $\kappa$ B complex). Multiple data have shown the mechanistic roles of these factors in term labor [15,84,92,100,244]. Identified proteins are listed in Appendix C Supplemental Table 5.2.

In summary, the exosomal cargo reflected a gradual buildup of inflammation during the later stages of pregnancy and nonspecific inflammation peaking on the penultimate day before the expected delivery in this mouse model. Delivery day exosomal cargo was characterized by senescence, necrosis, and other cell death pathways and markers as expected [37]. All these indicators returned to normal in postpartum animals. These data suggest that exosomal proteins reflect distinct phases of pregnancy and functional changes that are activated to promote labor and delivery.

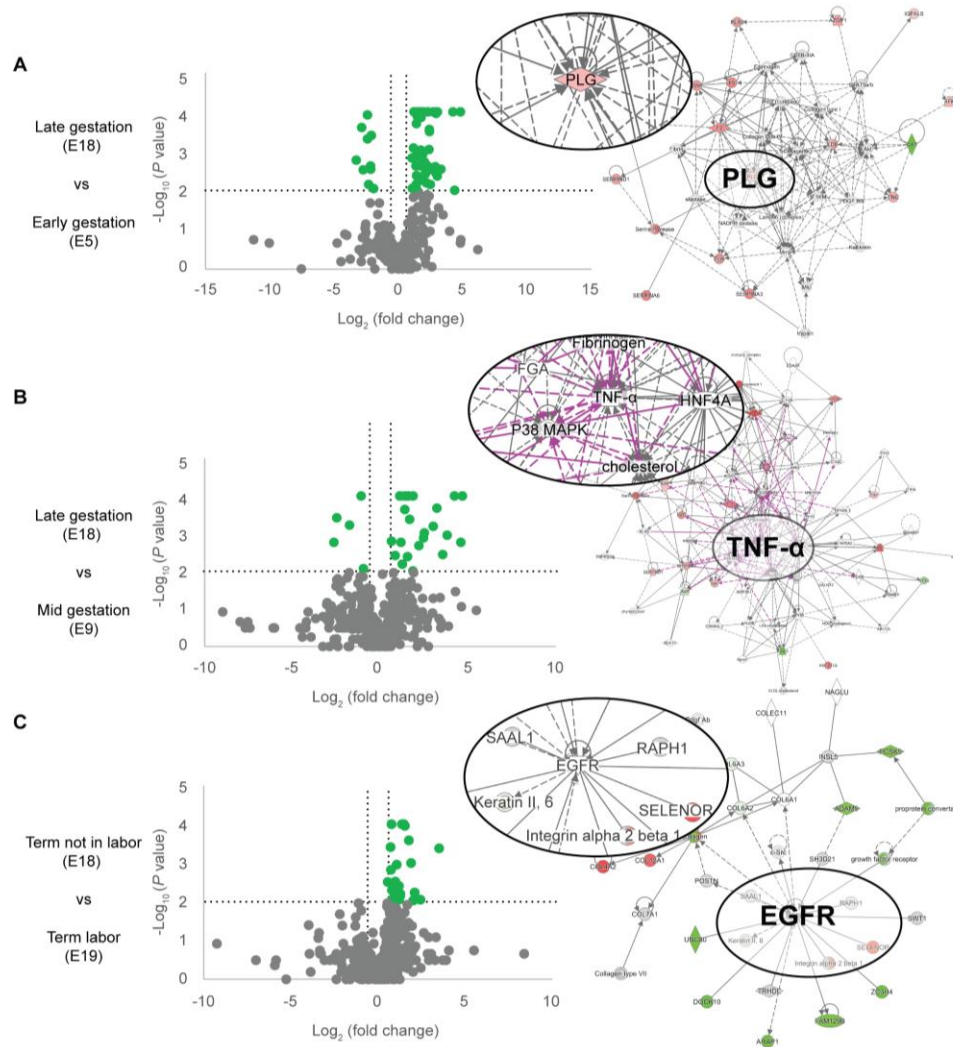


**Figure 5.4: Volcano plots and molecular networks of differentially-expressed proteins.**

Molecular networks were identified using IPA network analysis based on proteins with a  $\pm 1.5$ -fold change ( $\log_2$  fold change =  $\pm 0.6$ ) and a P-value  $< 0.01$  ( $-\log P\text{-value} = 2$ ). Circular insets are a zoomed in view of the central molecules identified. **A:** Comparison of E18 (late gestation) and E5 (early gestation) identified plasminogen (PLG) as a central molecule in the molecular network. PLG has been shown to activate matrix-degrading enzymes MMP-2 and MMP-9, as well as TGF- $\beta$ , and is associated with inflammation and tissue remodeling. **B:** Comparison of E18 and E9 identified TNF- $\alpha$  as a central molecule in the molecular network. TNF- $\alpha$  is a pro-inflammatory cytokine upregulated during parturition. It is also an activator of p38 MAPK, a pro-senescence marker in the fetal membranes and known activator of other inflammatory pathways. **C:** Comparison of E18 (term not in labor) and E19 (term in labor) exosome cargo identified epidermal growth factor receptor (EGFR) as the central molecule. EGFR activates MAPK pathways and other inflammatory pathways shown to have mechanistic roles in parturition.

### **Intraperitoneal injections of E18 exosomes induce preterm birth independent of systemic progesterone withdrawal or inflammation**

To determine the role of late-gestation exosomes in labor, exosomes from E18 mice were injected into pregnant mice on E15. E18 was chosen based on data that showed that E18 (the penultimate day of labor and delivery in CD-1 mouse models) had the maximum number of exosomes carrying nonspecific inflammatory mediators. Therefore, the hypothesis that an increased quantity of inflammatory cargo may contribute to labor and delivery was tested in this model. Exosomes from E9 mice were chosen as the control group as they contained a low number of exosomes and a minimal number of inflammatory mediators (Figures 5.2 and 5.3). In support of the abovementioned hypothesis, 80% (4/5) of mice injected with E18 exosomes delivered preterm (Figure 5.5B), which was defined as the delivery of at least one pup on or before E18. Preterm labor occurred on average 48 hours after the final exosome injection. Conversely, E9- and PBS-injected mice (Figure 5.5A) delivered on E19.5 (Table 5.3). The number of pups was not different between E18-, E9-, or PBS-injected animals (data not shown). All pups were viable upon delivery and had normal weaning periods as they were born close to term.

**Table 5.3 Preterm birth rates in PBS, E9 and E18 exosome injected mice**

Treatment	Number of Animals	PTB	Term Birth	PTB (%)
PBS	5	0	5	0%
E9 Exosomes	5	0	5	0%
E18 Exosomes	5	4	1	80%

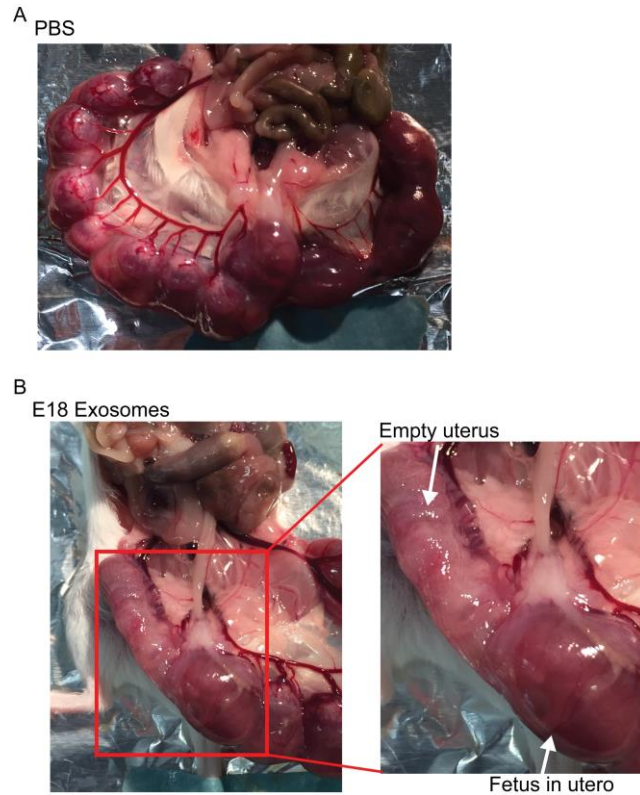


**Figure 5.5: The injection of E18 exosomes causes preterm birth.**

A: Representative photograph of a nonlaboring pregnant mouse on E18 has a full uterus. B: Representative photograph of a preterm delivering mouse. After delivery of at least one pup, the mouse was sacrificed and the uterus was exposed. The fetuses contained on the right side of the uterus have been delivered while the left side still contained fetuses.

Although systemic progesterone withdrawal is a key mechanistic event in mice that contributes to inflammation [16,26,245], exosome-mediated preterm labor was not associated with systemic progesterone withdrawal or an increase in key inflammatory markers in circulation. Maternal plasma progesterone levels did not differ between mice injected with PBS and E9 exosomes ( $76.16 \pm 7.09$  vs.  $70.07 \pm 23.88$  ng/mL;  $P = 0.83$ ), PBS and E18 exosomes ( $89.73 \pm 5.57$  pg/mL;  $P = 0.43$ ), or E9 and E18 exosome ( $P =$



0.20) (Figure 5.6A). Although E18 exosomes isolated from maternal plasma carry mediators of inflammation, injecting these exosomes did not result in systemic maternal

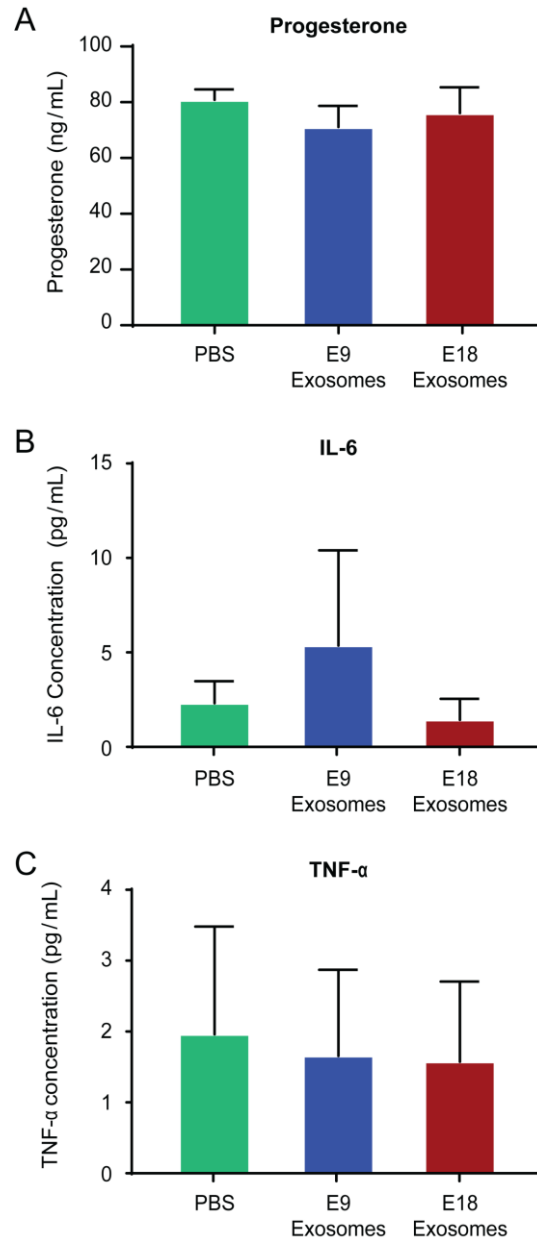


**Figure 5.6: Exosome-induced preterm labor is not associated with systemic progesterone withdrawal or systemic inflammation.**

A: Maternal plasma were analyzed for progesterone levels using ELISA. Plasma progesterone levels were not significantly different regardless of the treatment. B: Bioplex analysis of maternal plasma showed no significant difference in for IL-6 levels in PBS, E9, and E18-injected mice. C: Bioplex analysis of maternal plasma showed no significant difference in TNF- $\alpha$  levels in PBS, E9, and E18-injected mice.

inflammation. As shown in Figure 5.6B, there were no significant differences in the levels of the inflammatory cytokines, IL-6 and TNF- $\alpha$  (Figure 5.6B, all  $P > 0.98$  and Figure 5.6C, all  $P > 0.65$ , respectively), in maternal plasma regardless of the treatment. Exosomes not only encapsulate degradation-susceptible signals, but they also carry these signals to specific sites to induce a localized, rather than a systemic, inflammatory response. The tropism exhibited by exosomes was not a part of this study, and the chemotactic signals attracting inflammatory exosomes to specific uterine sites were not investigated. It is speculated that inflammatory mediators required for parturition are protected and delivered at sites where they have specific functions to avoid systemic inflammation that can be detrimental to the maintenance of pregnancy.

### **Exosome trafficking to intrauterine tissues to cause labor-associated changes**

#### ***CFSE-labeled exosomes localize in maternal and fetal tissues***

Exosomes from both E9 and E18 mice were found to reach specific and relevant reproductive tissues. Intraperitoneal injection of E9 and E18 exosomes labeled with CFSE were localized in the maternal cervix (green fluorescence in Figure 5.7). As expected, PBS-injected mice did not show any green fluorescence in any of the tissues investigated (Figure 5.7). CFSE diluted in PBS (7.5  $\mu$ M) was injected as a vehicle control to show nonspecific dye localization in tissues. As shown in Figure 5.7, localization of the dye was not found in maternal or fetal tissues, thus suggesting that the localization data were exosome specific. These results were observed on E17.

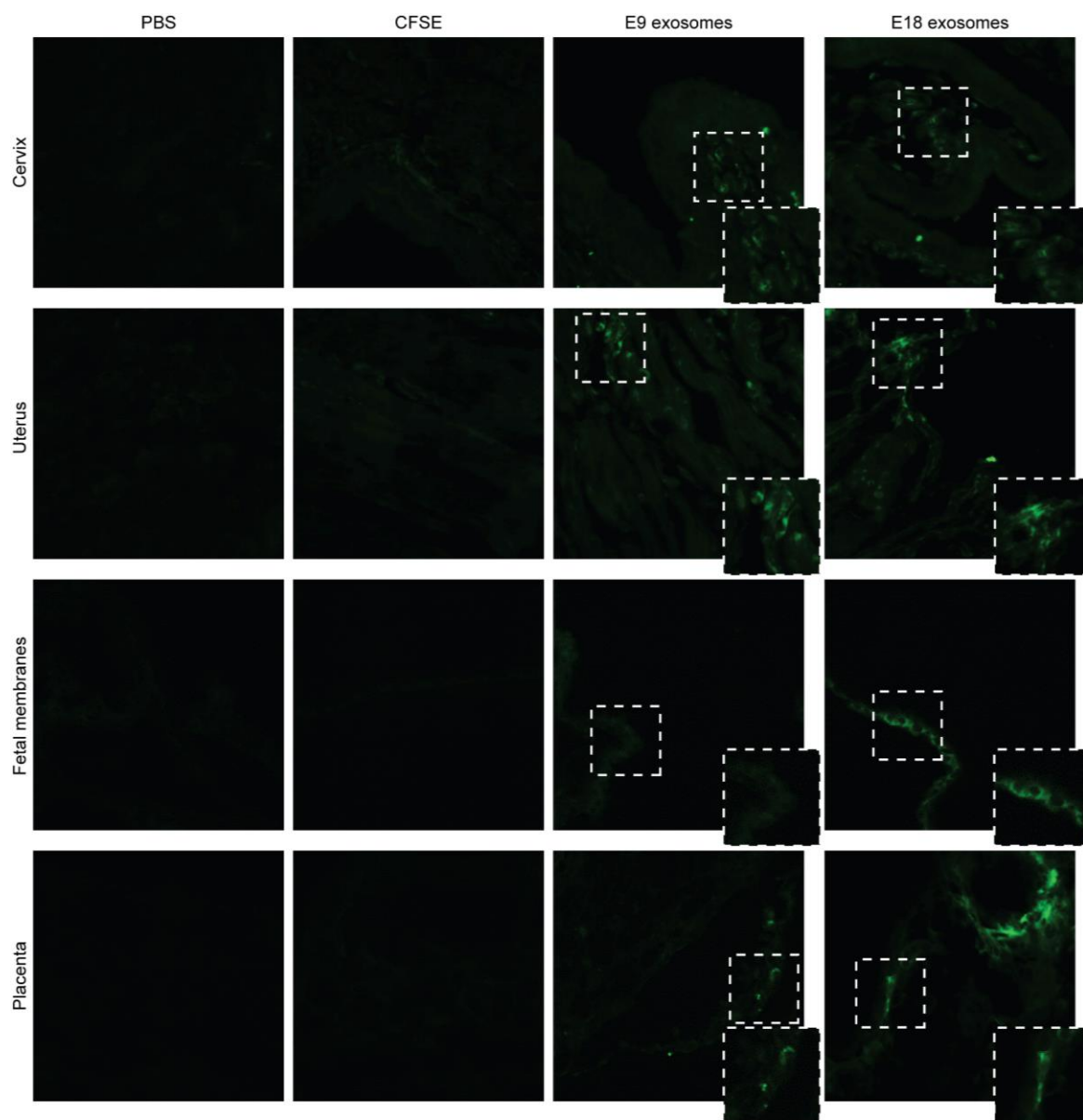


**Figure 5.7: Exosomes injected into pregnant mice traffic to the cervix, uterus, fetal membranes and placenta.**

Exosomes were fluorescently labeled with carboxyfluorescein succinimidyl ester (CFSE), as well as PBS and CFSE in PBS (7.5  $\mu$ M) then injected into mice on E15. Maternal and fetal tissues were collected and analyzed for fluorescent signal emerging from exosomes. PBS- and CFSE-injected mice show no fluorescent signals, while fluorescent signals from labeled exosomes (E9 and E18; green) can be seen in both maternal and fetal tissues tested. The inset is an enlargement of the tissue area marked by white boxes. All images were taken at 40x magnification.

### **E18 exosomes promote proinflammatory processes to prepare the cervix and uterus for parturition**

Based on the effect of day 15-16 treatments with E18 exosomes to induce preterm birth on E18, maternal tissues were analyzed for labor-associated inflammatory changes on E17 (the day prior to preterm birth in this model). In the cervix (Figure 5.8A and 5.8B), E18 exosome-injected mice had significantly higher NF- $\kappa$ B activation (expressed as arbitrary units) compared to the PBS controls ( $1.011 \pm 0.51$  vs.  $0.3135 \pm 0.22$ ;  $P = 0.022$ ). COX-2 expression in E18-injected mice ( $1.458 \pm 0.22$ ) was also significantly higher than in E9 exosome- and PBS-injected mice ( $0.6874 \pm 0.1637$ ;  $P < 0.005$  and  $0.8219 \pm 0.23$ ,  $P < 0.0001$ , respectively). Cytokine analysis (Figure 5.8C) showed a significant increase in the labor- and delivery-associated cytokine, IL-6, in E18 exosome-injected mice ( $8.20 \pm 1.72$  pg/mL) compared to E9 exosome- and PBS-injected mice ( $0.89 \pm 4.30$  pg/mL;  $P = 0.01$  and  $1.11 \pm 0.87$  pg/mL;  $P = 0.02$ , respectively). Similarly, the TNF- $\alpha$  concentration was also significantly higher ( $P < 0.0005$ ) in E18 exosome-injected mice ( $1.14 \pm 0.84$  pg/mL) compared to E9 exosome- (not detectable) and PBS- (not detectable) injected mice. Histologic analysis and quantitation of macrophage infiltration and activation in cervix of E18, E9 exosome and PBS injected mice (Figure 5.8D and 5.8E) showed significantly increased numbers of cells positive for macrophage marker F4/80 in E18-injected ( $0.066 \pm 0.083$ ) mice compared to E9- ( $0.006 \pm 0.007$ ,  $P=0.02$ ) and PBS- ( $0.005 \pm 0.009$ ,  $P=0.02$ ) injected mice (Figure 5.8E).

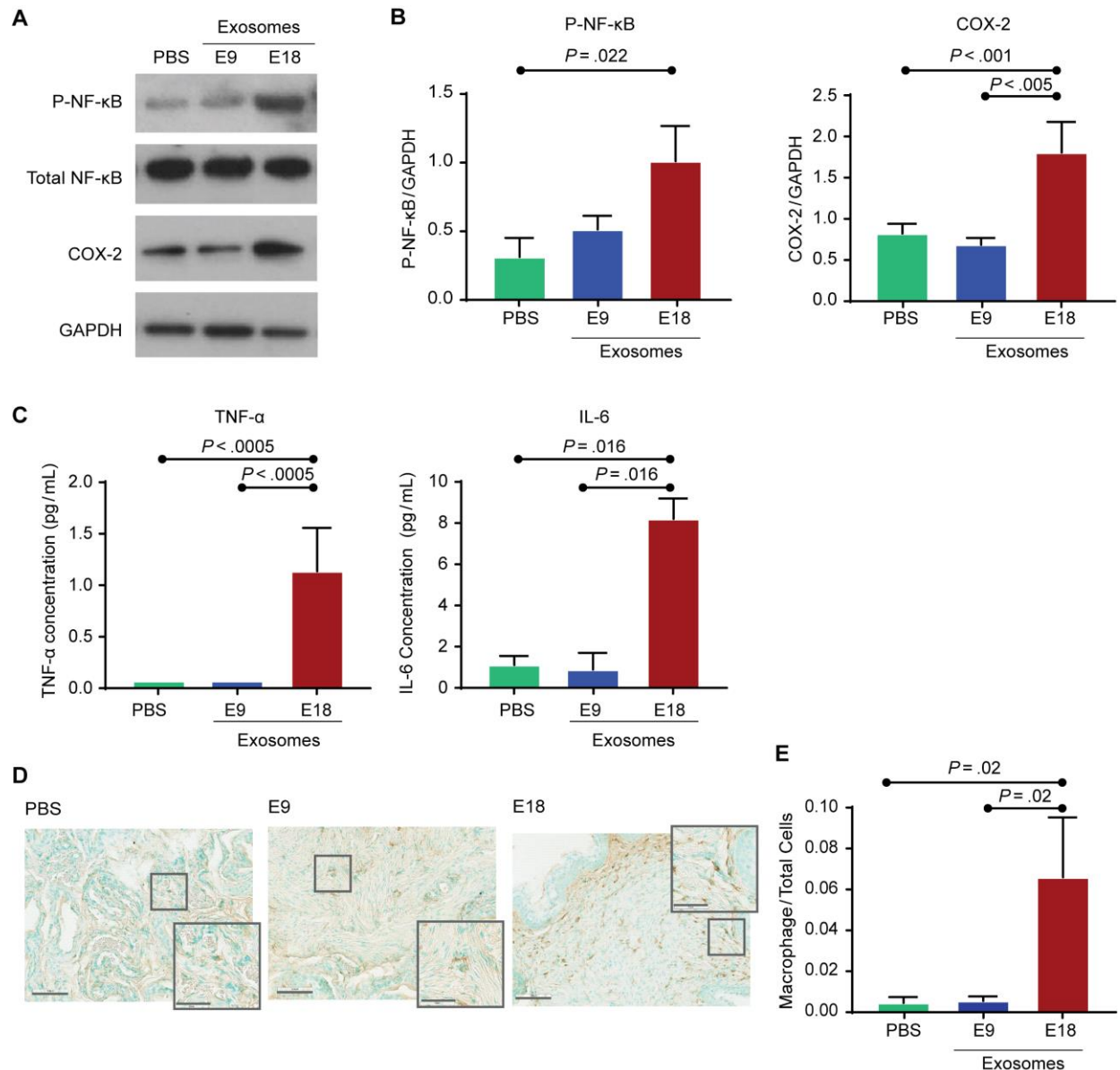


**Figure 5.8: Exosomes injected into pregnant mice induce labor-associated changes in the cervix.**

A-C: Western blot analysis and densitometry quantitation show a significant increase in the activation of the inflammatory signalers NF-κB (as determined RelA phosphorylation) and COX-2 in E18 exosome-injected mice compared to PBS- and E9 exosome-injected mice. Inflammatory cytokines IL-6 and TNF-α were significantly increased in E18 exosome-injected mice compared to PBS- and E9 exosome-injected mice. D-E: Histological analysis and quantitation of macrophages in cervix: Histology showing that macrophage activation marker F4/80 were significantly increased in E18 exosome injected mouse cervix compared to E9 and PBS control injected mice. Nuclei were stained green by methyl green and macrophages were stained brown. For a semi-quantitative estimation of macrophage activation, total cells and macrophages were counted to determine macrophage to total cell ratio (bar graph).

In the uterus, E18 exosome-injected mice did not exhibit significantly different NF- $\kappa$ B activation compared to PBS- or E9 exosome-injected mice (Figure 5.9A and 5.9B); however, there was a significant increase in the expression of CX-43 (Figure 5.9A and 5.9B) in E18 exosome-injected mice ( $1.300 \pm 0.350$ ) compared to PBS- and E9 exosome-injected mice ( $0.495 \pm 0.230$ ;  $P < 0.05$  and  $0.496 \pm 0.440$ ;  $P < 0.05$ , respectively). No significant differences were seen in the tissue levels of IL-6 and TNF- $\alpha$  between the various injected groups (Figure 5.9C). Histologic analysis and quantitation of macrophage infiltration and activation in uterus of E18, E9 exosome and PBS injected mice (Figure 5.9D and 5.9E) showed no significant increase in number of cells positive for macrophage marker F4/80 in E18-injected ( $0.075 \pm 0.045$ ) mice compared to E9- ( $0.031 \pm 0.015$ ,  $P=0.07$ ) and PBS- ( $0.070 \pm 0.061$ ,  $P=0.10$ ) injected mice.

***E18 exosomes promote prepartum proinflammatory processes in fetal membranes but not in the placenta***

In fetal membranes, western blot analysis of p38 MAPK activation, RelA phosphorylation, and COX-2 expression indicate fetal tissue response to exosomes injected on the maternal side (Figure 10A). Quantification was performed using densitometry (expressed as arbitrary units) (Figure 10B). E18 exosome-injected mice had significantly increased p38 MAPK activation ( $0.787 \pm 0.166$ ) compared to E9 exosome- and PBS-injected mice ( $0.220 \pm 0.172$ ;  $P = 0.01$  and  $0.214 \pm 0.057$ ;  $P = 0.003$ ). This supports previous reports that showed that accelerators of fetal membrane senescence via p38 MAPK can cause sterile inflammation and lead to labor and delivery. P-RelA was significantly higher after E18 exosome injection compared to PBS ( $1.557 \pm 0.787$  vs.  $0.664 \pm 0.229$ ;  $P = 0.04$ ); however, although P-RelA was increased in E18 exosome- compared to E9 exosome-injected mice, it was not significant. In addition, COX-2 expression was also higher in E18 exosome-injected mice ( $0.623 \pm 0.258$ ) compared to E9 exosome- and PBS-injected mice ( $0.359 \pm 0.310$ ;  $P = 0.04$  and  $0.253 \pm 0.053$ ;  $P = 0.04$ , respectively).

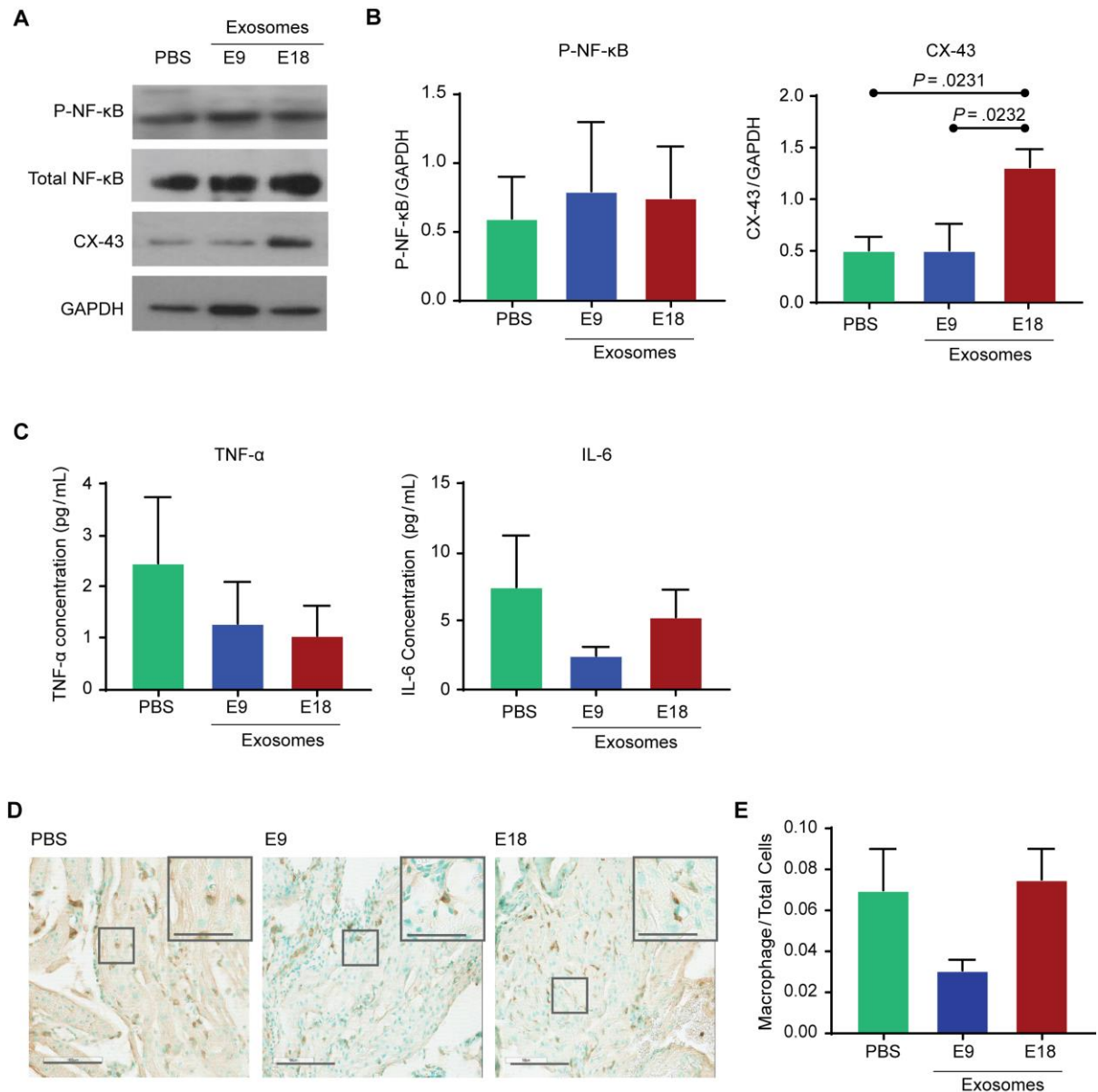


**Figure 5.9: Exosomes injected into pregnant mice induce labor-associated changes in the uterus.**

A-C: Western blot and densitometry quantitation of NF-κB activation (as determined by RelA phosphorylation) and connexin-43 (CX-43) expression show that NF-κB activation is not significantly different between treatments, while CX-43 expression is significantly increased in E18 exosome-injected mice compared to PBS- or E9 exosome-injected mice. CX-43 is a gap-junction protein important for smooth muscle contractions. Inflammatory cytokines IL-6 and TNF-α were not significantly increased in E18 exosome-injected mice compared to PBS- and E9 exosome-injected mice. D-E: Histological analysis and quantitation of macrophages in uterus: Histology showing that macrophage activation marker F4/80 were not significantly different regardless of treatment. Nuclei were stained green using methyl green and macrophages were stained brown. Total cells and macrophages were counted to determine macrophage to total cell ratio (bar graph).

IL-6 was not different between the treatment groups (Figure 10C), and TNF- $\alpha$  was not detectable.

Both E18 and E9 exosomes were localized in the placental tissue (Figure 8), thus confirming its trafficking to both fetal tissues; however, western blot analysis for P-p38, P-RelA, and COX-2 (Figure 10D and 10E) and cytokine analysis for IL-6 (10F) in placental tissue was not significantly different between E18-, E9-, and PBS-injected mice. In addition, TNF- $\alpha$  was not detectable, thus indicating that placental tissue did not respond to exosome-induced inflammation. These data suggest minimal placental changes associated with exosome-induced labor and delivery in this mouse model.



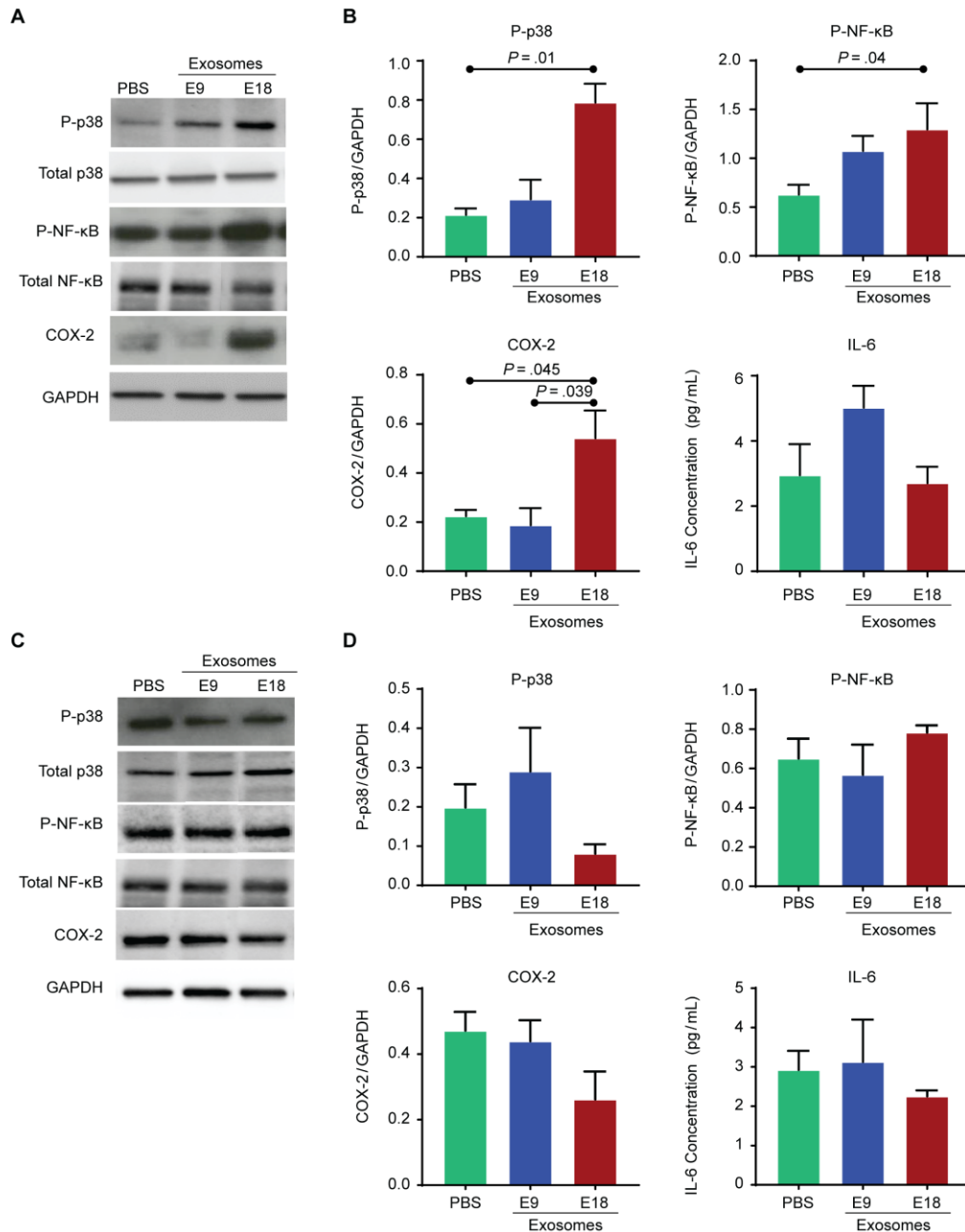


**Figure 5.10: Exosomes injected into pregnant mice traffic to the fetal tissues and induce inflammatory changes in the fetal membranes but not the placenta.**

A-C: Western blot analysis and densitometry quantitation show significant activation of NF-κB (as determined by RelA phosphorylation), COX-2, and the prosenescence marker p38 MAPK in E18 exosome-injected mice compared to PBS- or E9 exosome-injected mice. No significant difference in proinflammatory cytokine IL-6 levels was observed regardless of the treatment. D-F: Western blot and densitometry analysis of NF-κB activation (as determined by RelA phosphorylation), COX-2, and p38 MAPK expression in the placenta show no significant difference in the activation of the prosenescence marker p38 MAPK and inflammatory markers NF-κB, COX-2, and IL-6 between the treatment and control groups.

## Discussion

This report tested the hypothesis that exosomes can act as paracrine signals that traffic between maternal and fetal tissues, cause functional inflammatory changes, and induce labor and delivery in a CD-1 mouse model. The 5 major findings of this study were: (1) the injection of E18 exosomes caused preterm birth; (2) by E17, there was evidence of inflammation related to characteristics of maternal cervix remodeling and uterine activation, as well as premature senescence of fetal membranes; (3) the size and shape of maternal plasma exosomes remained constant throughout pregnancy; however, their quantity increased as gestation progressed, with the maximum number seen on E18 (the day before the expected delivery date), before returning to normal 7 days after pregnancy; (4) exosome protein cargo varied at different gestational days, as evidenced by E9 exosome treatments had little or no effects on endpoints of inflammation in reproductive tract tissues; (5) E18 exosome-induced preterm birth was independent of changes in placental function or systemic progesterone withdrawal as plasma levels did not change after treatment. Thus, findings suggest that E18 exosomes provided information that prepares the reproductive tract for parturition at term because when this exosomal cargo is provided on E15-16, preterm birth results.

As seen in this mouse study, human pregnancy is also associated with a progressive increase in maternal plasma exosome concentrations as gestation progresses [112]. Exosomes in the maternal plasma are of both fetal and maternal origin, and the increased concentration throughout gestation is likely contributed to by the growing fetus, the placenta, and fetal membranes [112]. Ongoing studies in our lab (data not shown) suggest that the fetus and fetal tissues (membranes and placenta) contribute approximately 20% of exosomes on E18. The maternal plasma exosome concentration also increases as gestation progresses in mouse pregnancies, peaking on E18 and decreasing postpartum. This is similar to data reported by Salomon et al. in human pregnancies and suggests that the days

preceding labor and delivery are marked by an increased number of exosomes in the maternal plasma [68].

Irrespective of the species, inflammation is the mechanistic effector of labor and delivery, and labor inducing inflammation is not systemic but is localized to intrauterine tissues [6,25,27,226,246]. Proteomic and bioinformatic analysis determined that exosomal cargo on E18 included proteins linked with the inflammatory response and immune cell migration, which are physiological effectors of labor [4,211,212,245]. An influx of proinflammatory cargo-rich exosomes (E18 exosomes) in uterine tissues, and the biological pathways likely elicited by these cargo contents, eventually cause preterm birth in animals. This is supported by the data reported here, where NF- $\kappa$ B activation and cytokines increased in feto-maternal tissues. The lack of systemic progesterone withdrawal indicates that paracrine mediators can cause labor-associated changes that are independent of endocrine signals. Findings raise the possibility that the quantity of exosomes or specificity of cargo of mature E18 exosomes on critical components in the mechanism for parturition have yet to be examined. Major roles for prostaglandin dehydrogenase and progesterone receptor isoforms in prepartum cervix and uterus have been proposed for parturition [247–249]. Clearly, inflammatory signal carrying exosomes are sufficient to cause labor. These exosomes likely override proposed immunosuppressive effects of progesterone in the cervix and the uterus. In a related study, exosomes from oxidative stress-induced human amnion epithelial cells caused functional progesterone withdrawal (progesterone receptor [PR]A:PRB ratio switch) in human myometrial cells, which is a theorized mechanism associated with human labor [249–251]. Therefore, the possibility that exosomes may also cause endocrine disruption to ensure labor and delivery cannot be excluded.

In mice, cervical ripening and distention begin long before the initiation of labor. In the present study, a greater inflammatory response to E18 exosomes was found in the cervix compared to uterine tissues. This is an expected event before labor and delivery as

cervical ripening precedes uterine changes [238,252]. Increased presence of macrophages occur by E17, 2-3 days before birth [253,254]. NF- $\kappa$ B activation likely induces proinflammatory cytokines and an increase in COX-2 in the cervix, thus supporting ripening-associated changes. The CX-43 increase was the only statistically relevant observation in the uterus. NF- $\kappa$ B activation trended in the same direction as seen in the cervix; however, the increase was not sufficient to reach statistical significance. This was likely due to the uterine tissues slowly responding to the changes in the ripening cervix on E17. Activation and infiltration of immune cells was also not significantly different in the uterus. This trends with current literature indicating leukocyte infiltration of the uterus does not increase until active labor [255,256]. The lack of systemic inflammation (no change in plasma IL-6 and TNF- $\alpha$  irrespective of exosome or PBS injection) indicates that inflammation in the cervix and uterus is highly localized and that signals propagate within this region to exclusively modify the environment to prime specific target tissues for labor. The timing of preterm labor is also worthy of discussion. In E18 exosome-treated animals, multiple injections were necessary to compensate for the short circulating lifespan of exosomes and to mimic the consistent influx and concentration of exosomes from both the fetus and the mother as term approaches. The lack of systemic inflammation and the gradual development of inflammation (as observed in E17 tissues) was archetypal of such changes during pregnancy before labor. Hence the delivery on E18 was as expected in this model.

We expected exosomes to cause changes in both maternal and fetal side. As shown in our results, exosomes (E9 and E18) injected on the maternal side were shown to traffic to the fetal compartment (placenta and fetal membranes). Although no functional changes associated with labor and delivery were seen in the placenta, increased inflammation and activation of prosenescence marker p38 MAPK was observed in mice injected with E18 exosomes. Previous studies showed that fetal membrane senescence is regulated by p38 MAPK in humans [34,91] and mice [37]. Activation of p38 leads to fetal membrane

senescence, a mechanism shown to be associated with the initiation of labor at term and is accompanied by the release of SASP and DAMPs, which may be carried to the maternal tissues by exosomes and support fetal-maternal crosstalk to prepare for labor. Thus, increased p38 MAPK in the fetal membranes on E17 (the day prior to observed preterm labor in this model) may be an important mechanistic contributor to the preterm labor observed in this study.

This study determined the contribution of total plasma exosomes in the initiation of labor; however, the specific or independent contributions by either fetal or maternal exosomes are still unknown. Therefore, it is still not possible to elucidate which paracrine signal (the mother, the fetus, or both) initiates labor. This is primarily due to the lack of fetal-specific exosome markers in mouse models, unlike in humans where exosome-expressed placental alkaline phosphatase is used to differentiate fetal (placental)-derived signals [70,72,151]. A transgenic mouse model has been developed in which fetal exosomes are tagged and can be sorted from maternal blood. Further characterization of these exosomes and similar studies using maternal- and fetal-specific exosomes may determine the requirement of feto-maternal specific signals in the initiation of labor in mice.

The lack of systemic progesterone withdrawal or systemic inflammation supports an independent functional role for exosomes in labor and delivery. In addition, trafficking of exosomes was also observed from the maternal side to the fetal side, where they produced functional changes (i.e., senescence and sterile inflammation) in fetal membranes as expected at this gestational age [37,92]. Exosomal cross talk between mother and the fetus and the functional changes they can cause may be one of the non-endocrine mechanisms that will determine the timing of pregnancy. Unlike pathological stimulants (e.g., LPS, TNF, and IL-1 injections) [257–259], exosomes are more physiologically representative. Slow development of labor (preterm in this model) associated changes in cervix and uterus (48-h post injection) suggests a gradual, natural, and physiological

buildup of exosomes (quantitatively and qualitatively), reflects tissue-level changes exerted by exosomes, and a progressive programming of uterine tissue for labor and delivery. It should be noted that the exosome doses used for the injections (E9 vs. E18) were different. This was done to mimic the systemic exposure experienced on those specific days.

Exosomes, as paracrine signalers, can induce labor associated change in fetomaternal uterine tissues leading to labor and delivery in the absence of systemic progesterone withdrawal. This is the first study to report exosome characterization throughout murine pregnancy, and the results show that exosomes on the maternal side can cross the placenta to reach the fetal side. In addition, this study suggests a potential role for exosomes in the initiation and progression of labor. Further studies must be performed to determine the maternal and fetal contribution to better understand the communication during pregnancy and specifically during labor and delivery. Human studies on term and preterm parturition are restricted mostly to endocrine or cytokine mediated labor initiation signals. Knowledge of exosome mediated paracrine signaling of labor associated changes and induction labor provides new avenues of research on how exosomes may contribute to normal and adverse labor events.

## **CHAPTER 6: CRE-REPORTER MOUSE MODEL TO DETERMINE MATERNAL-FETAL EXOSOME COMMUNICATION AND FUNCTIONAL EFFECTS**

### **Introduction**

Interest in the field of extracellular vesicles has increased due to their importance in intercellular communication by transfer of proteins, nucleic acids and lipids. Exosomes, which are the smallest of the extracellular vesicles, have received the most attention for their role in physiological and pathophysiological functions [215,260–262]. Exosome size facilitates easy transport of their contents between local and distant tissues, while their cargo represents the physiological status of the cell of origin and can regulate the phenotype of the target cell. Current research has indicated that exosomes are important in multiple cellular processes, including waste management, immune cell modulation and are now being considered a central component to a novel paracrine mechanism of cell-cell communication [56,59]. Since their discovery, exosomes have been widely investigated for their potential functional roles in neurodegenerative diseases [60,215,263], viral and bacterial pathogenicity [264–266], and especially cancer progression [267–269]. Exosomes from cancer cells act as communication channels that transfer cancer-promoting cellular molecules (proteins, RNAs and lipids) to surrounding cells or through the circulation to distant sites, promoting cancer progression and metastasis [269,270].

While exosomes have been classically studied as intercellular communication networks in diseases and infection, they are less reported during pregnancy, a unique system involving implantation [72–74], placental development [73,75], and maintenance of pregnancy [76–79]. Placenta-specific exosomes have been studied for their role in maternal immune cell regulation for fetal tolerance [72], pre-eclampsia [151,271], and other placental dysfunction-associated diseases. The majority of these studies have been

performed in humans or in human cells using placenta-specific protein marker placental alkaline phosphatase (PLAP). PLAP is enriched in placenta-derived exosomes and can be used to easily identify and immunoprecipitate placental exosomes. Current literature on exosomes during pregnancy has focused on placental exosomes and their potential effect on maternal tissues [67,68,70–72,112,153]. While these studies are important for identifying potential biomarkers for placental dysfunction associated with various pregnancy pathologies in humans, a functional role of exosomes was lacking in processes associated with parturition or pregnancy-associated pathologies.

Characteristics of exosomes, including size and membrane proteins and lipids, and their ability to act as carriers of signals that are otherwise susceptible to degradation to distant cells and tissues [65,66] makes them ideal candidates for fetal signalers to distant maternal tissues and vice versa. However, mechanistic and functional studies during pregnancy are impractical to perform in humans and thus animal models have been developed to understand the processes associated with pregnancy, parturition and preterm labor [27,174,272,273]. Although mouse parturition differs from humans with respect to endocrine signaling, progesterone levels decreasing at term in the mouse but remaining high in humans [274–276], there are enough similarities to make the mouse a viable model to study parturition, specifically exosome-mediated paracrine signaling mechanisms for fetomaternal communication [112,124].

Exosomes have been under investigation in our lab as potential paracrine signaling mechanism for term labor initiation [124,125,231]. We have shown that exosomes injected intraamniotically can traffic from the fetal compartment to maternal tissues in murine models of pregnancy [124]. , Additionally, maternal plasma exosomes from gestational day 18 of mouse pregnancy (normal gestational period 19-20 days) cause preterm birth in mouse models when they were injected intraperitoneally on gestational day 15. This suggests a pro-parturition functional role for exosomes. The total plasma exosomes used for this study contained both maternal and fetal exosomes and therefore contributions



specifically by fetal or maternal exosomes in parturition are still unclear. To fully elucidate the feto-maternal communication during pregnancy and parturition, a fetal-specific protein marker is essential to identify the fetal contribution.

The primary objective of this study is to develop a model with which we can isolate and characterize fetal specific exosomes from maternal plasma that will allow us to study fetal contributions during pregnancy and parturition. In addition, examination of fetal exosome cargo and quantity will allow us to understand fetal physiology in response to adverse pregnancy environments associated with pregnancy complications. The secondary objective is to examine functional changes produced by exosome trafficking between maternal and fetal tissues during pregnancy.

To achieve this, we established a mouse model where the fetal tissues express a marker that was not expressed in maternal tissues. Therefore, exosomes generated from these tissues are expected to carry these markers. Our model utilizes a transgenic mouse with a membrane-targeted, two-color fluorescent Cyclic recombinase (Cre)-reporter allele where tandem dimer Tomato (mT) fluorescence is expressed in the plasma membrane of all cells and tissues. In the presence of Cre, mT is excised and cells express membrane-localized enhanced green fluorescent protein (mG) that replaces mT (Figure 1A) [277]. When mated with a wild type female, the fetal tissues will express this construct while the maternal tissues will not. Using this approach, we developed and validated a mouse model to determine trafficking of exosomes between maternal-fetal tissues and confirmed functional changes produced in fetal tissues by exosomes from the maternal compartment using exosomes enriched with Cre.

## **Materials and Methods**

### **Animal care**

All animal procedures were approved by the Institutional Animal Care and Use Committee (IACUC) at the University of Texas Medical Branch, Galveston. Mice were housed in a temperature- and humidity-controlled facility with 12:12-h light and dark cycles. Regular chow and drinking solution were provided ad libitum. We used a transgenic C57BL/6J mouse with a plasma membrane-targeted, two-color fluorescent Cre-reporter allele (Figure 6.1A) where tandem dimer Tomato (mT) fluorescence is expressed in the cell membrane of all cells and tissues but in the presence of Cre, mT is excised and cells express membrane-targeted enhanced GFP (mG) on the cell membrane (stock 007676, Jackson Laboratory, Bar Harbor, ME). The mT/mG transgenic mouse model utilizes two highly photostable fluorescent proteins with low cytotoxicity. The red fluorescent protein tdTomato, which is expressed in the absence of Cre, has increased brightness and photostability compared to other red fluorescent proteins, as well as deeper penetration using longer wavelengths of light [277] allowing for easier imaging of intrauterine tissues by in vivo imaging. Breeding was performed in our facility in which wild type (WT) C57BL/6J (stock 000664, Jackson Laboratory) 8-12 weeks old were mated with males homozygous for the mT/mG construct (Figure 1B). Female mice were checked daily between 8:00 am and 9:00 am for the presence of a vaginal plug, indicating gestation day (E) 0.5. Females positive for a plug were housed separately from the males, their weight was monitored and a gain of at least 1.75 g by E10.5 confirmed pregnancy. Animals were sacrificed by CO<sub>2</sub> inhalation according to the IACUC and American Veterinary Medical Association guidelines prior to tissue collection.

### **Injection of Cre-enriched exosomes to determine maternal to fetal exosome trafficking**

On E12.5, pregnant WT mice were intraperitoneally injected with either PBS, naïve exosomes or Cre-enriched exosomes ( $1 \times 10^{10}$  exosomes in 250  $\mu$ L, Figure 6.1B). Exosomes were produced in the laboratory of Dr. Chulhee Choi in human embryonic kidney

(HEK293) cells. Naïve exosomes are exosomes produced by cells under standard conditions and were used as an exosome control. E12.5 was selected as the date for

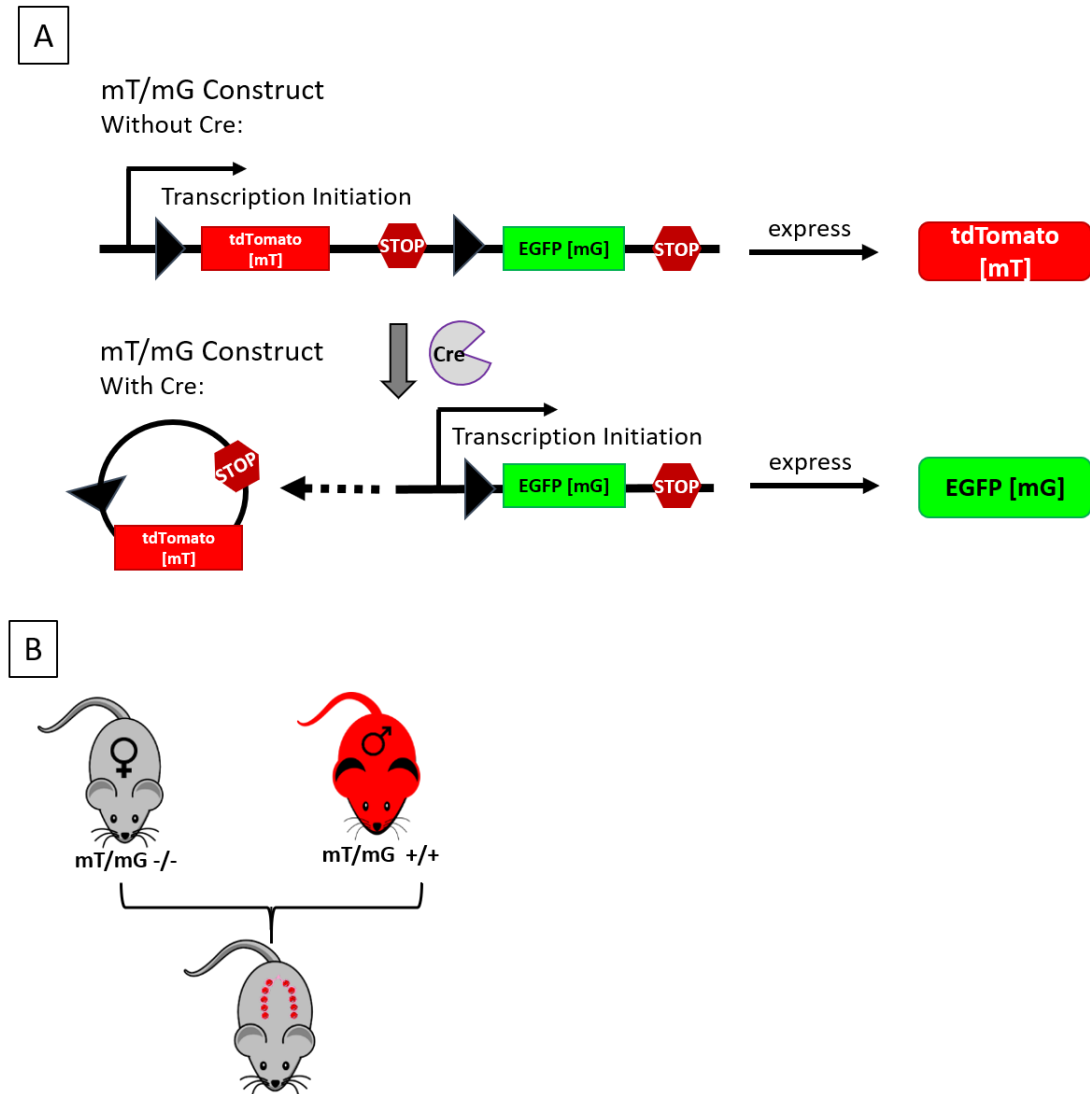


**Figure 6.1: Maternal-Fetal Exosome Trafficking and Cre-Reporter Transgenic Mouse Model**

A: TOP: The two-color fluorescent Cre-reporter allele (mT/mG construct) has a membrane-targeted tandem dimer Tomato (mT) red fluorescent protein (red) in all cells and tissues, while eGFP is not expressed. BOTTOM: In the presence of Cre, mT is excised and cells express enhanced green fluorescent protein (mG), which replaces mT expression. B: Female wild type (WT) mice were mated with males homozygous for the mT/mG construct such that all fetal tissues express mT/mG construct. Maternal tissues are negative.

injection to maximize the red to green changes that occur in the fetal tissues. Since E12.5 is post-placentation but pre-senescence in the mouse fetal membranes [37], exosomes would need to cross the placenta barrier and cells affected by Cre recombinase would still be proliferative and not yet undergoing senescent changes. 72 hours post-injection (E15.5), females were sacrificed for plasma and tissue collection.

### **Immunofluorescent imaging for exosome trafficking**

Tissue samples collected in 4% paraformaldehyde (PFA) were stored overnight (4°C) before being washed twice with 1x PBS and transferred to a 15% sucrose solution overnight (4°C). Samples were then transferred to 30% sucrose and stored at 4°C until they were embedded in optimal cutting temperature (OCT) and cut into 5-µm sections. Sections were incubated at room temperature for 30 minutes then washed twice in water to remove OCT. Sections were incubated with DAPI for nuclear staining for 2 minutes at room temperature then washed twice in water. To reduce the autofluorescence, tissues were incubated for 10 seconds with TrueVIEW™ Autofluorescence Quenching Kit (Vector Laboratories, Burlingame, CA) then washed twice with 1x Tris buffered saline-Tween 20 (TBS-T). Slides were air-dried at room temperature for 10 minutes then mounted using Mowiol 4-88 mounting medium. Tissues were visualized using the Olympus BX43 fluorescent microscope (Olympus, Tokyo, Japan) at 40x magnification, and images were captured using Q Capture Pro software. Brightness, contrast, and smoothing were applied to the entire image using FIJI (open source).

For macrophage colocalization with tdTomato, after removing OCT, sections were incubated with blocking buffer (3% BSA in TBS-T) for 1 hour at room temperature in a humidity chamber. Blocking buffer was removed and macrophages were labeled with Alexa Fluor 488 conjugated anti-F4/80 (50-167-58, ThermoFisher, Hampton, NH) diluted 1:100 in blocking buffer. After 1-hour incubation at room temperature in a humidity chamber, slides were washed twice with TBS-T, stained with DAPI, incubated with

TrueVIEW and mounted as described above. Confocal images were captured using Zeiss LSM 880 with Airyscan (Oberkochen, Germany). Brightness, contrast, and smoothing were applied to the entire image and colocalization of tdTomato-expressing exosomes and macrophages was performed using FIJI.

### **Maternal plasma collection**

Maternal blood was collected by cardiac puncture in tubes containing EDTA (Becton Dickinson, Franklin Lakes, NJ) and plasma was harvested after centrifugation ( $2000 \times g$  for 10 min at  $4^{\circ}\text{C}$ ) then stored at  $-80^{\circ}\text{C}$ .

### **Maternal plasma exosome isolation**

Exosomes from maternal plasma were isolated as described in Chapter 5.

### **Exosome Immunoprecipitation (IP) and flow cytometry analysis**

The tdTomato (mT) and EGFP (mG) proteins are membrane-targeted allowing for IP of exosomes expressing either mT or mG. IP was performed using Exo-Flow (System Biosciences, Mountain View, CA) as described previously [125] with modifications. Briefly, magnetic beads coated with streptavidin were incubated with 500 ng/mL either biotinylated anti-tdTomato (ab3477, Abcam, Cambridge, United Kingdom) or biotinylated anti-EGFP (ab6658, Abcam) for 2 hours on ice flicking intermittently to mix. Beads were washed then incubated with exosomes rocking overnight at  $4^{\circ}\text{C}$ . The following day, before removing exosomes from the beads, we validated the IP using flow cytometry. Beads were washed then stained using the reversible Exo-FITC exosome stain according to manufacturer instructions. Negative controls incubated with antibody/Exo-FITC stain and without exosomes were used for gating, applied according to manufacturer instructions. Data analysis based on FITC signal shift of 10,000 events per sample was performed using CytExpert (Beckman Coulter). Once flow cytometry validated our IP, exosome elution

buffer was used to remove FITC stain and collect exosomes from beads following manufacturer instructions. The supernatant containing mT exosomes was collected for NTA.

### **Determination of exosome size and concentration**

The size distribution and concentration of exosomes were determined using the Nanosight NS300 (Malvern Instruments, Worcestershire, UK) as described in Chapter 5. To determine the percentage of fetal-specific exosomes (mT<sup>+</sup>), the mean mT<sup>+</sup> exosome concentration was divided by the total exosome concentration.

## **Results**

### **Validation of the tdTomato exosome mouse model**

#### ***Expression of mT in fetal tissues***

Female WT mice were mated with males homozygous for the mT/mG construct so that all fetal tissues express the construct while all maternal tissues do not. To validate this model, we collected fetal tissues and analyzed them using fluorescence microscopy for mT expression in the placenta and fetal membranes (Figure 6.2). Expression of red fluorescence indicated the mT/mG construct was expressed in the fetal tissues. While there is green fluorescence, indicative of mG bleed through, mT expression was predominant in the fetal tissues.

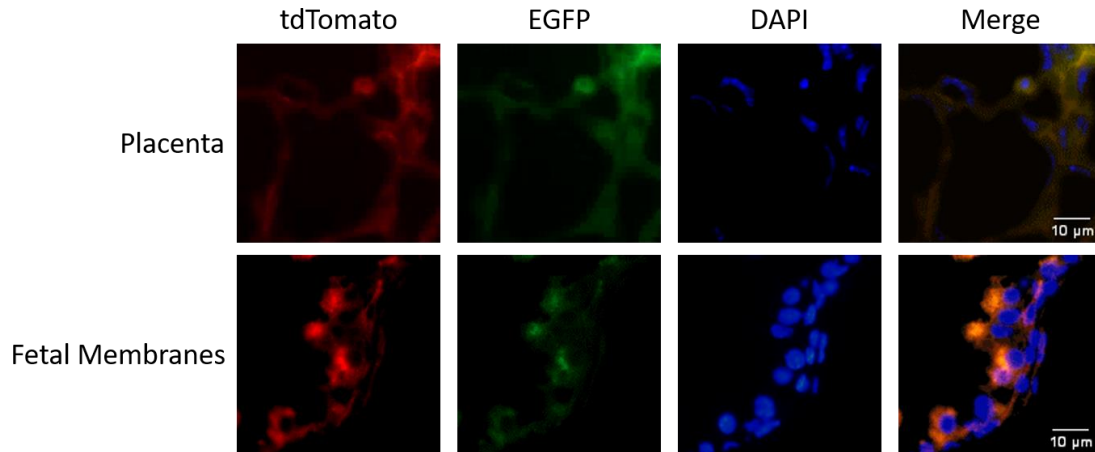


**Figure 6.2: Fluorescence microscopy of the placenta and fetal membranes from WT female mated with mT/mG expressing male**

Placenta (TOP) and fetal membranes (BOTTOM) have a dominant expression of tdTomato (mT) with limited expression of EGFP (mG).

#### ***Maternal plasma exosomes express mT***

Maternal plasma of WT mice mated with mT/mG males was collected and exosomes expressing mT were analyzed using flow cytometry and nanoparticle tracking analysis (Figure 6.3A). Flow cytometry analysis showed 13.07% beads were positive for mT-expressing exosomes. After flow cytometry analysis confirming IP of mT-expressing exosomes, exosomes were removed from the beads and analyzed using NTA (Figure 6.3B). Exosome concentration in maternal plasma was  $6.95 \times 10^{10}$  exosomes/mL with an average size of 109.9 nm. The concentration of exosomes expressing mT with  $5.93 \times 10^9$  exosomes/mL with an average size of 113.3 nm. Using these concentrations, we were able to determine the fetal contribution in maternal plasma to be about 9%, validating our flow cytometry data.

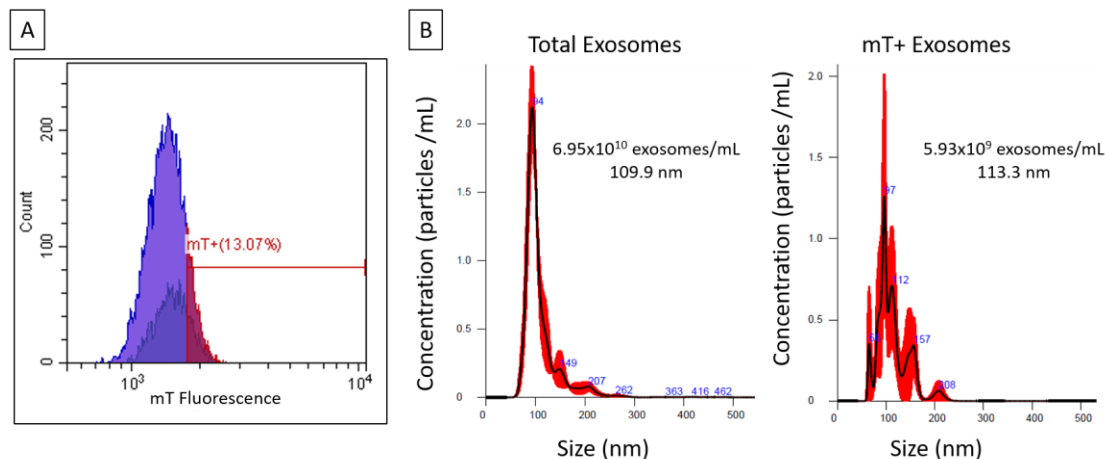


**Figure 6.3: Immunoprecipitation and nanoparticle tracking analysis of mT expressing exosomes from maternal plasma**

A: Maternal plasma from female mice mated with mT/mG males had 13.07% beads positive for mT expressing exosomes indicating fetal exosomes cross to the maternal side. B: Nanoparticle tracking analysis of total maternal plasma exosomes (LEFT) and mT expressing exosomes (RIGHT). Of the total exosomes in maternal plasma, 9% were mT-expressing exosomes.

#### ***mT expression in WT maternal uterus and cervix***

Since exosomes containing mT were in maternal plasma, we used fluorescence microscopy to determine if mT expressing exosomes could localize in maternal reproductive tissues, specifically the cervix and uterus (Figure 6.4). Exosomes expressing mT were localized in maternal uterus and cervix. Additionally, as previous studies indicate exosomes are immune regulators [141,278,279], we also colocalized mT-expressing exosomes with macrophages in the maternal tissues using murine macrophage marker F4/80 (Figure 6.5). Not only were fetal exosomes trafficking to the maternal cervix and uterus, they were also interacting with the resident macrophages in these tissues.



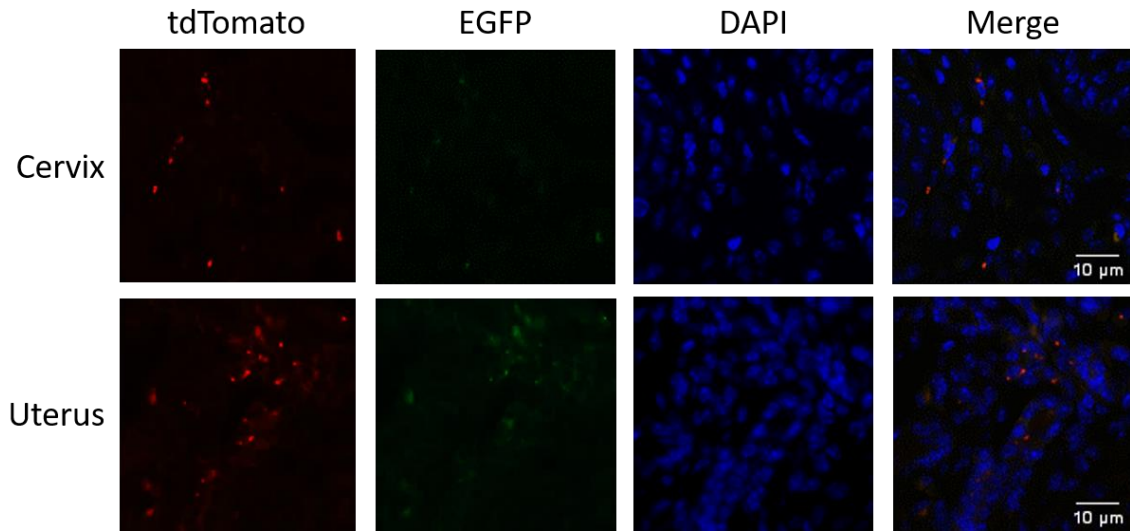


**Figure 6.4: Exosomes expressing mT localize in maternal cervix and uterus**

Female WT mice mated with males homozygous for the mT/mG construct have localization of tdTomato (mT) signal in the maternal cervix (TOP) and uterus (BOTTOM).

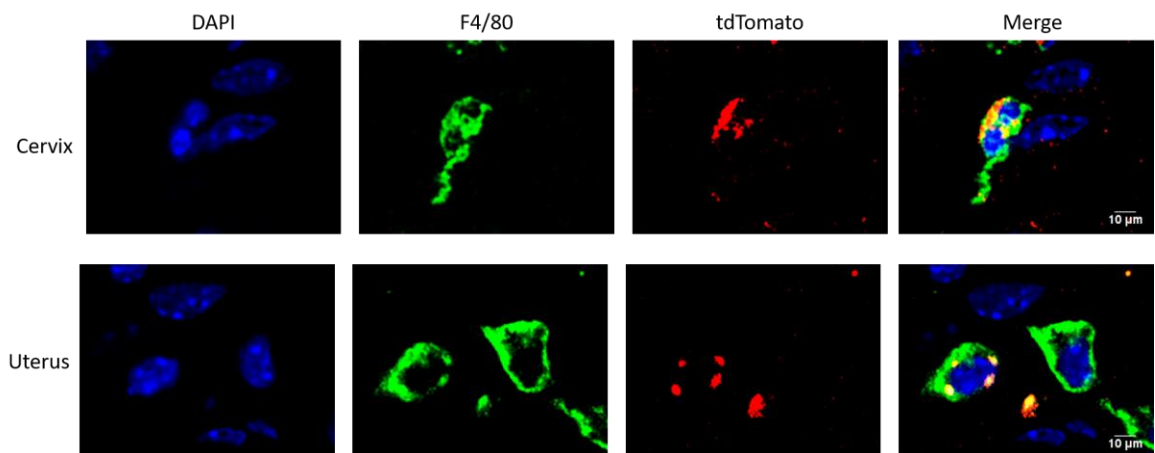


**Figure 6.5: Colocalization of exosomes expressing tdTomato (mT) with macrophages in the maternal tissues**

Macrophages in the maternal cervix (TOP) and uterus (BOTTOM) were labeled using murine macrophage marker F4/80 (green) and colocalized with fetal exosomes expressing mT (red).

## Cre-enriched exosomes injected on the maternal side traffic to the fetal tissues and induce a functional change

Cre-containing exosomes were injected into pregnant mice intraperitoneally to determine maternal to fetal communication via exosomes. Fetal tissues were collected and evaluated for mT or mG fluorescence (Figure 6.6). Placenta and fetal membranes had increased expression of mG and decreased mT signal (Figure 6.6) compared to PBS and naïve exosomes. These results indicate exosomes on the maternal side can cross to the fetal tissues and cause functional changes (red to green fluorescence change).

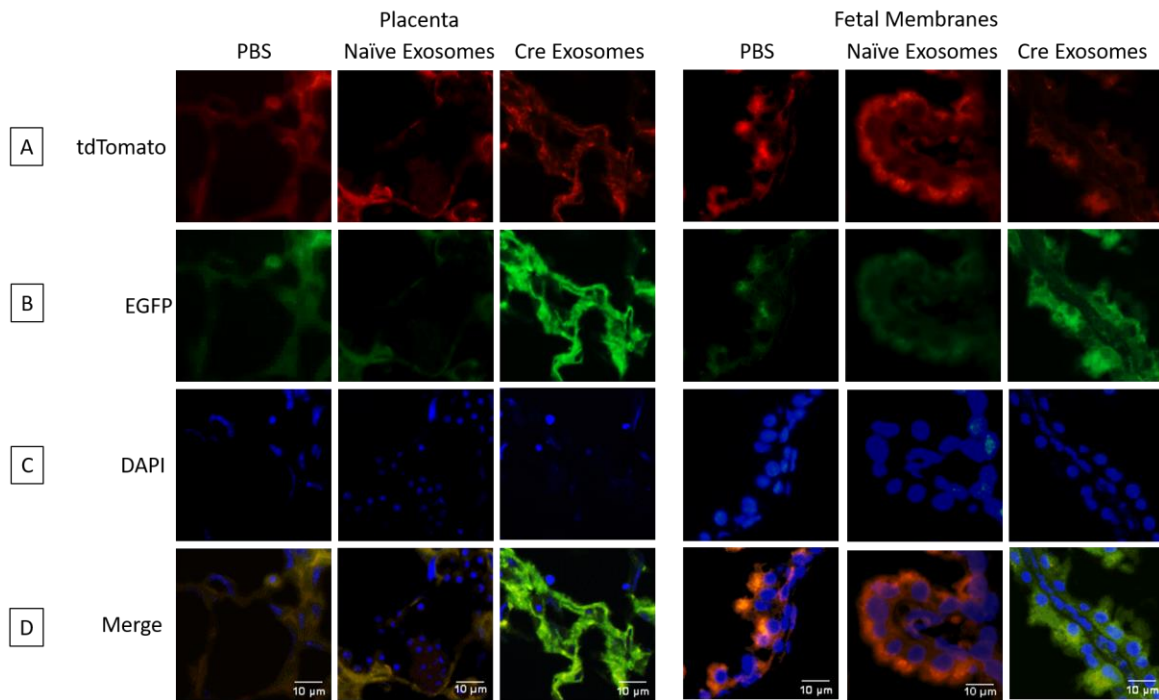


**Figure 6.6: Fluorescence microscopy of the placenta and fetal membranes from mice injected Cre-enriched exosomes**

tdTomato and EGFP expression in placenta and fetal membranes after PBS, naïve and Cre-enriched exosome injections. Left panel – placenta; Right panel – fetal membranes. A –tdTomato; B – EGFP; C – DAPI; D: merged images. Scale bar is 10 μm.

## Fetal exosomes in maternal plasma express mG

Fetal tissues responded to maternally-derived Cre-containing exosomes that cause mT to mG change expression change. To determine if the exosomes in maternal plasma reflected this functional change, exosomes from maternal plasma of Cre exosome-injected mice were isolated and analyzed by flow cytometry for mT and mG expression (Figure 6.7). Cre exosome-injected mice had 15.2% beads positive for mG-expressing exosomes (Figure 6.7). As maternal tissues do not express the mT/mG construct, this change in mT

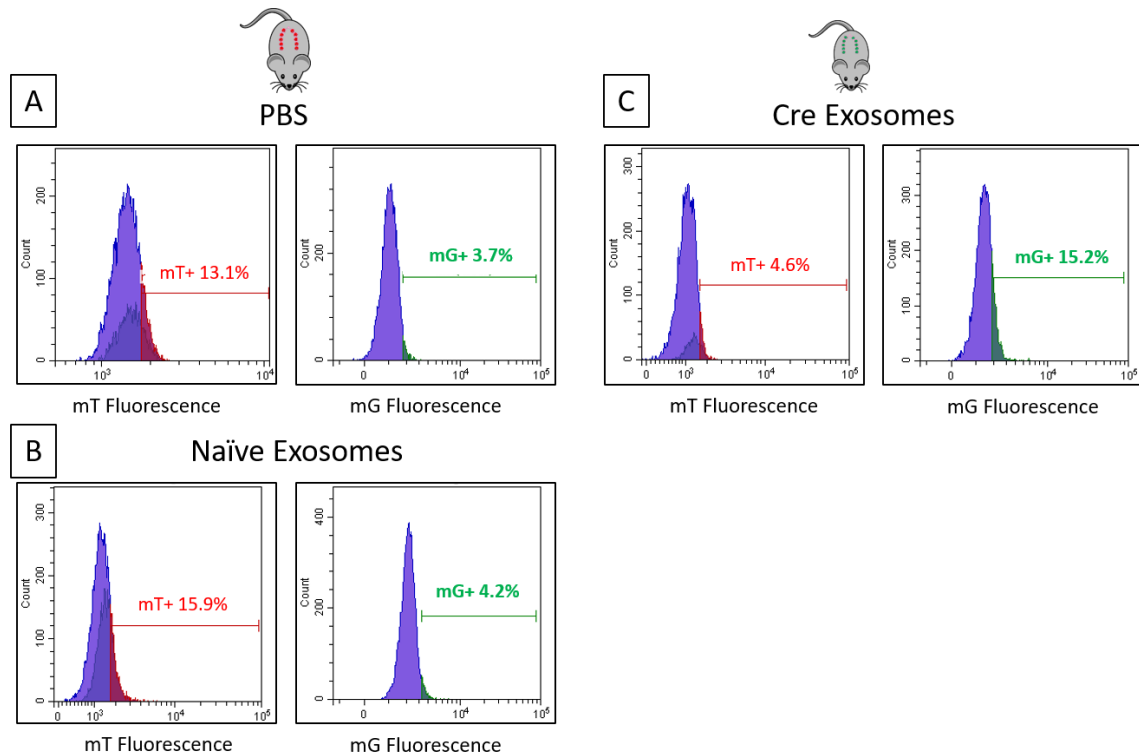


**Figure 6.7: Flow cytometry of exosomes isolated from maternal plasma after immunoprecipitation for mG**

A-B: PBS- and naïve exosomes injected mice have dominant expression of mT-expressing exosomes (13.1% and 15.9% beads respectively, LEFT) with minimal expression of mG-expressing exosomes (3.7% and 4.2% beads respectively, RIGHT). C: Cre-exosome injection decreased expression of mT exosomes (LEFT, 4.6% beads) and showed mG-expressing exosomes (RIGHT, 15.2% beads) in maternal plasma confirming Cre exosome induced functional changes on the fetal side and crossing of exosomes from fetal to maternal circulation.

to mG expression after Cre-exosome injection is due to the functional change caused by Cre in the fetal tissues.

### **Fetal-derived exosomes traffic to maternal reproductive tissues**

Fetal exosomes containing mG were isolated from maternal plasma. To determine if these mG-expressing exosomes were also localized in maternal tissues, we analyzed maternal uterus and cervix after Cre-injection using fluorescence microscopy (Figure 6.8). After Cre-exosome injection, fetal-exosome signal emerging from mG fluorescence was seen in uterus and cervix (Figure 6.8). The changes in fluorescent signal reflect changes seen in the fetal tissues and maternal plasma after Cre-enriched-exosome injection.

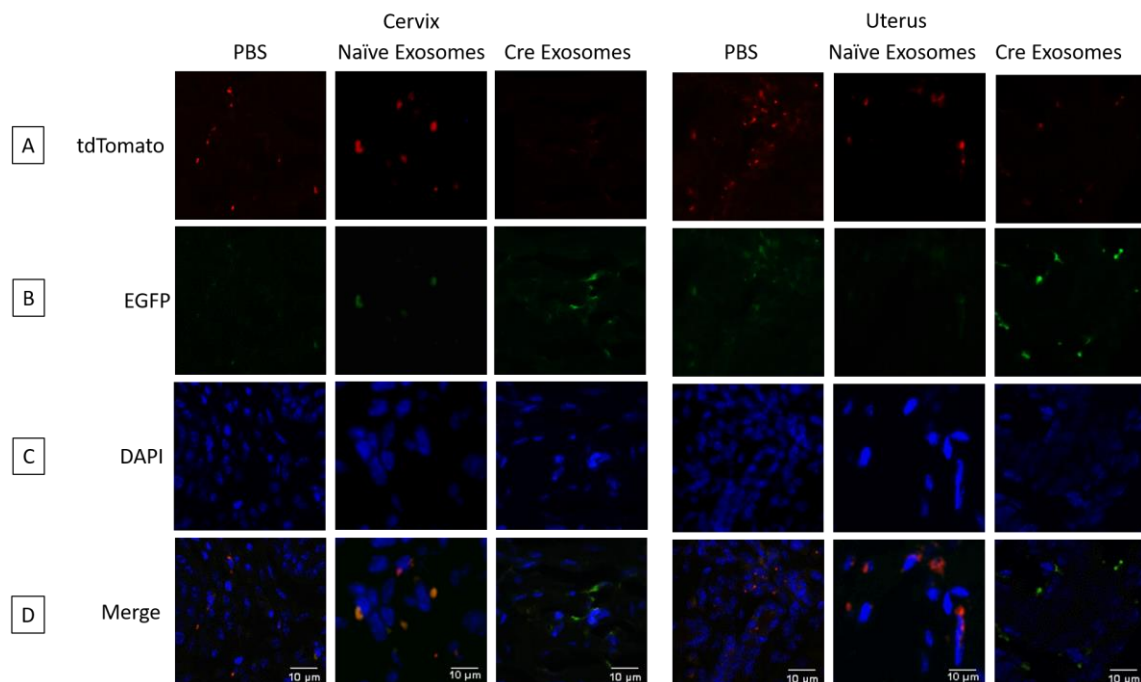


**Figure 6.8: Exosomes expressing mG localize in maternal cervix and uterus**

tdTomato and EGFP expression in cervix and uterus after PBS, naïve and Cre-enriched exosome injections. Left panel – cervix; Right panel – uterus. A –tdTomato; B – EGFP; C – DAPI; D: merged images. Scale bar is 10  $\mu$ m.

## Discussion

Our study sought to validate a model to determine the feto-maternal communication via exosomes utilizing a transgenic mouse model that expresses mT. Cross breeding of mT expressing male with a null female produced all fetal tissues expressing Cre reporter system. This model allowed us to test functional changes in feto-maternal tissues mediated by exosome signaling. Our principle findings are 1) development of a model where fetal exosomes can be sorted from a pool of maternal and fetal exosomes using a marker expressed on exosome membranes (mT+) 2) Cre enriched exosomes injected on maternal side can cross the placental barrier (maternal-fetal trafficking), reach the fetal tissues and produce functional changes in fetal tissues expressing mT+ where it excised mT+ to express mG+ (Figure 6.9) 3) fetal exosomes expressing mT can be colocalized with macrophages in the maternal tissues, indicating exosomes may be targeting the resident immune cells in the maternal uterus and cervix; 4) fetal exosomes reflecting the mT to mG switch traffic to the maternal compartment and can be seen in circulation as well as in tissues.

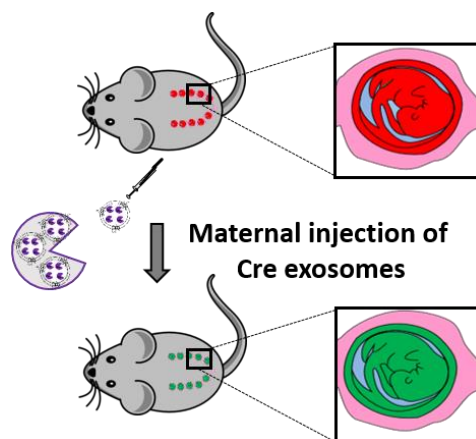


**Figure 6.9: Maternal-Fetal Exosome Trafficking and Cre-Reporter Transgenic Mouse Model**

**TOP:** PBS injected mice expressing mT in fetal membranes. **BOTTOM:** Cre- exosomes injected on the maternal side caused mG expression in the fetal membranes replacing mT expression.

Conditional gene targeting using site-specific recombinase systems, such as the Cre/loxP system in the mT/mG transgenic mouse in this study, is being applied to study gene function in multiple disease models [280]. This system is primarily used for to study tissue-specific loss of function in mice by linking the Cre/loxP genes with a tissue-specific protein to allow for conditional gene targeting. Unfortunately, a protein specific to the fetal tissues in the mouse does not currently exist. The Cre-enriched exosomes makes the use of this model possible for the study of exosome communication in our unique system of two individuals. While multiple methods for enrichment of nucleic acids, proteins and lipids in exosomes have been developed, the Cre exosomes in this study were developed using a novel and robust technique called Exosomes for protein loading via optically reversible protein-protein interaction (EXPLOR). This technique was developed to overcome the limitations of conventional methods used to load proteins into exosomes, including simple incubation, freeze-thaw, sonication, and extrusion, all of which are based on mechanical dispersion, and cannot be applied for use as therapeutics due to the potential development of unstable proteins [281]. Our model illustrated successful delivery of Cre to fetal tissues via bioengineered exosomes. We were able to enrich exosomes with functionally stable Cre to be delivered to the fetal side and produce desired changes. This approach can be used for delivery of specific molecules, such as treatments for preterm labor. EXPLOR technology can be adapted to carry protein therapeutics, such as inhibitors of NF- $\kappa$ B to reduce inflammation commonly associated adverse pregnancy outcomes and increase drug delivery efficiency and efficacy.

Optimization of this model is still ongoing in our laboratory and the approaches employed to determine optimal doses to obtain desired effects as well as monitoring for any adverse effects associated with the Cre-enriched exosomes. We acknowledge that the Cre-enriched exosomes also carry other cellular cargo. While the focus of this study was on the Cre functional effects, it must be noted that other functional effects may be occurring due to additional cargo contained in the exosomes. Injection of naïve exosomes did not

show any adverse outcomes and therefore we are confident that the observed effects are indeed produced by Cre. The model we developed is advantageous to study the functional roles of exosomes during pregnancy and parturition. Limitations of this study include the endocrine regulation differences [26,282] and multifetal pregnancy in the mouse compared to humans. Despite these differences, fetal membrane senescence [34,37,168] and paracrine signaling via exosomes [68,112,124] are similar mechanisms associated with labor in humans and mice. Thus, this model can further our understanding of the role fetal and maternal exosomes play in the initiation of labor and provide a platform to test potential therapeutics for treating preterm labor by monitoring fetal responses via exosomes. While this model allows for the selection of fetal vs maternal exosomes, the fetal exosome origin could be fetal membranes, placenta and the fetus. Another limitation of the model is the increased occurrence of high GFP background before Cre recombination, known as bleeding effect of GFP gene expression irrespective of dominant suppressive effect of mT. As expected, minimal levels of mG were observed even in the presence of dominant mT protein before Cre recombination. However, by including the TrueView quenching reagent, we were able to reduce the green fluorescent background that could potentially confound our results. However, we did not observe any mG effect on the maternal side. Additionally, the mT/mG efficiency of exosome transfer to induce the functional effects seen was not 100%, as evidenced by mT expression in fetal tissues before and after Cre enriched exosome injection. However, we do not expect 100% efficiency with injection on the maternal side. Better efficiency will most likely be seen using intra-amniotic injections, which is more invasive and less ideal if using this to mimic potential treatments for women at risk for preterm labor. More studies to determine the optimal exosome dose for full efficiency are needed, especially if 100% transfer is required for fetal survival.

The study of pregnancy and labor involves multiple obstacles, including the uniqueness of the maternal-fetal system of dealing with two individuals, which is not seen in any other system. This is the first mouse model to allow for the study of feto-maternal

exosome trafficking and function using the membrane-targeted, two-color fluorescent Cre-reporter construct. Being able to selectively analyze fetal vs maternal exosomes allows the opportunity to further our understanding of the feto-maternal communication during pregnancy and labor. The photostability of both fluorescent reporter proteins and the membrane-targeting aspect of this transgenic mouse will pave the way for future research investigating the role of exosomes in normal and adverse complications of pregnancy.



## CHAPTER 7: SUMMARY AND CONCLUSIONS

Complications due to preterm birth are the leading cause of death among children under 5 years of age and responsible for approximately 1 million neonatal deaths/year [283]. While there has been no reduction in preterm birth rates (they are rising in most countries), the development of neonatal intensive care units has significantly increased fetal survival [1,3], yet even with survival, babies born prematurely face a lifetime of significant disability. In order to address the problem of preterm birth, a better understanding of the mechanisms that activate the labor process is required.

Labor is a multifactorial inflammatory process activated by environmental, endocrine and physiological factors from both the fetal and maternal compartments. The current understanding is that fetal signals of organ maturity and fetal endocrine signals act in tandem with maternal endocrine changes that alters maternal physiology, preparing the uterine and cervical tissues for labor. Yet decades of research have not yielded interventions to delay preterm labor by more than 48 hours [8] because they focus on the maternal contribution to the process of labor.

While many laboratories are studying endocrine signals for the initiation of parturition, including progesterone withdrawal and the PRA: PRB switch in maternal tissues [16,284], our laboratory is studying the fetal paracrine signaling contribution to the initiation of labor. We have shown a novel signaling mechanism associated with senescence, or aging, of the fetal membranes that is telomere dependent and mediated by p38 MAPK [34,88,167]. Senescent fetal tissues release sterile inflammatory mediators, SASP and DAMPs, that can act either locally or be carried to maternal tissues via intercellular signaling vesicles called exosomes [124,125,285]. This mechanism has been reproduced in our laboratory by treating primary amnion epithelial cells from term, not in labor fetal membranes with the oxidative stress inducer cigarette smoke extract [34,125,167,285]. The purpose of this dissertation was to gain a better understanding of

the role exosomes play in the initiation of labor in cell culture and in murine models of pregnancy.

### **Exosomes carry signals of sterile inflammation to maternal tissues**

Using the well-established in vitro model of amnion cell senescence, we showed in chapter 2 that primary amnion epithelial cells can produce exosomes with classic size, shape and markers [106,279,286,287], including embryonic stem cell marker Nanog. While exosome characteristics were similar in those released from cells cultured under standard and oxidative stress conditions, oxidative stress-induced exosomes carry increased DAMPs, in the form of HMGB1 and cell free fetal telomere fragments. They also carry phosphorylated p38 MAPK, all of which are indicative of cellular stress. Additionally, bioinformatic analysis demonstrated NF- $\kappa$ B complex may be a central regulator in the molecular network that can be activated by exosomes from AEC cultured under normal conditions, whereas TGF- $\beta$  might regulate the molecular network from exosomes from AEC treated with CSE. While both are inflammatory pathways, TGF- $\beta$  is a major mediator of the epithelial-mesenchymal transition, a mechanism in the fetal membranes that has been implicated in labor [200,243].

Since their discovery, exosomes have been widely investigated for their potential functional roles in various diseases [60,215,263], infections [264–266], and cancer [267–269] as mediators of cellular communication and transfer of disease-promoting molecules [269,270]. The ability of exosomes to carry signals to distant sites provides a channel with which the fetus can communicate with the mother via exosomes. To determine if fetal exosomes can interact with and cause functional changes in maternal cells, we treated myometrial cells and decidual cells with exosomes isolated from primary amnion cell culture. Chapter 3 highlights that exosomes from control and oxidative stress-treated cells can be taken up by maternal cells and induce an inflammatory response in the form of

increased cytokine and prostaglandin production; however, placental cells had no response associated with exosome treatment despite being taken into the cells.

Due to the ability of exosomes to produce functional changes in maternal cells and the trafficking of exosomes in other disease models, we investigated fetal-exosome trafficking in murine models of pregnancy in chapter 4. Fluorescently labeled exosomes were intra-amniotically injected into pregnant mice and imaged for exosome trafficking. After 24 hours, exosomes were localized in maternal plasma, kidney, uterus and on the maternal side of the placenta, indicating exosomes can travel through tissues and systemically to the maternal compartment. Our studies support exosomes have the potential to act as carriers of fetal-derived signals for the initiation of parturition.

### **Exosomes as paracrine signalers in pregnancy and parturition**

To further understand the potential characteristics and mechanism of exosomes that may be inducing the changes necessary for the initiation of labor, we characterized total maternal plasma exosomes at various stages of mouse gestation and tested the functional role associated with late-gestation exosomes in chapter 5. The concentration of exosomes in maternal plasma, which consists of both fetal and maternal origin based on our previous studies [124], increased significantly from E5 through E19, with a maximum seen on E18, then decreased to nonpregnant levels 7 days postpartum. Exosome concentration also increases during human pregnancy, peaking during late gestation [67,68]. Additionally, exosome cargo changes associated with upregulation of inflammatory pathways, cell death and immune cell recruitment were increased on E18 compared to early gestation. Thus, when injected into pregnant mice on E15, we were able to induce preterm labor. To determine potential mechanisms associated with E18 exosome-induced preterm labor, we sacrificed mice the day before preterm labor on E17. E18 exosomes were localized in maternal and fetal tissues where they induced parturition-associated changes, except in the placenta. These changes were induced independent of endocrine or systemic inflammation.

While this study determined the function of total exosomes in the maternal plasma, we were unable to differentiate between fetal and maternal contribution to the functional changes observed. Therefore, we developed a mouse model to select for fetal-specific exosomes in maternal plasma.

### **Transgenic mouse model to determine exosome trafficking and function during pregnancy**

We used a transgenic mouse to develop a model to determine fetomaternal communication via exosomes in chapter 6. The transgenic mouse model utilizes a plasma membrane-targeted, two-color fluorescent Cre-reporter allele where tandem dimer Tomato (mT) fluorescence is expressed in the cell membrane of all cells and tissues but in the presence of Cre, mT is excised and cells express membrane-targeted enhanced GFP (mG) on the cell membrane [277]. To exploit this construct, we used Cre-enriched exosomes injected on the maternal side to determine maternal-to-fetal communication and functional effects such that when Cre-containing exosomes crossed from the maternal to the fetal side, the fetal tissues switch from red fluorescence to green fluorescence. Our model showed for the first time maternal to fetal to maternal exosome trafficking.

### **Concluding Remarks**

The work described in this dissertation provides novel insights into exosomes as a paracrine signaling mechanism for fetomaternal communication, specifically at term to initiate labor. Our findings indicate the involvement of exosomes in parturition by carrying signals of inflammatory mediators to maternal and fetal tissues. Exosomes are under investigation by many labs in human pregnancy and we have shown similar trends using cell culture models and mouse models, which are highly utilized models to study preterm labor. While there are differences in mouse and human pregnancy, we have shown senescence and exosome signaling are commonalities we can exploit to further our

understanding of the initiation of labor both at term and preterm. The primary conclusions of the work presented in this dissertation are that 1) primary amnion epithelial cells produce exosomes whose cargo reflects the physiological status of the cell of origin, making them ideal biomarkers for fetal and fetal tissue status; 2) fetal exosomes can traffic to maternal tissues through a systemic route and through tissues (placenta membrane) and cause parturition-associated changes in maternal cells; 3) exosomes in maternal plasma, which constitute a fetal and maternal contribution, prime the maternal tissues for labor initiation by gradual increase in concentration and change in cargo to pro-inflammatory mediators at term; 4) our transgenic mouse model of feto-maternal exosome trafficking can provide a novel avenue for the study of fetal and maternally-derived exosomes in term and preterm labor. While we are still lacking the mechanism of fetal and maternal exosome tissue specificity, our model can provide a method to study the mechanistic aspects of exosome-mediated communication.

My work raises the question about how scientists have been studying the timing and initiation of labor. While endocrine signals from both the fetal and maternal compartments have been the predominantly studied factors in the timing of birth, my work has shown paracrine factors may also play a role. In fact, exosomes may bypass the function of the endocrine signaling pathways to initiate labor. It is hoped that my work will change the way we think about preterm labor and will open new avenues of research beyond endocrine function determining the timing of labor. We hope to view exosome signaling between the fetus and the mother as a new communication network establishing pregnancy, maintaining pregnancy and determining the timing of birth.

For continuation of the work presented in this dissertation and to further advance the study of the initiation of labor, I recommend the following future studies to complement the findings reported here: 1) our transgenic mouse model allows for the easy immunoprecipitation of fetal-specific exosomes. Therefore, future studies should fully characterize fetal exosomes (size, concentration, cargo) throughout gestation using NTA

and proteomics analysis; 2) the transgenic mouse model can also allow for the evaluation of the fetal vs maternal contribution to initiate labor at term by injecting fetal, maternal and fetal+maternal exosomes into pregnant mice; 3) it was shown that p38 MAPK activation was increased in the fetal membranes of mice injected with late gestation exosomes the day before preterm labor. Additionally, studies have suggested that p38 activation in myometrium and cervix is necessary for the initiation of labor [288,289]. Therefore, using the EXPLORS technology, a biological inhibitor to p38 can be bioengineered into exosomes to block p38 MAPK activation in fetal and maternal compartments; 4) our in vitro and in vivo studies have shown placenta cells do not have a pro-inflammatory response to exosomes, regardless of origin or cargo. Further studies to understand this phenomenon could lead to potential methods for blocking exosome function in cells, as current methods to inhibit exosome function require pharmaceutical agents that are cytotoxic and may confound results.

Although further studies are needed, we provide a potential role for exosomes in the initiation and progression of labor. Knowledge of exosome mediated paracrine signaling of labor associated changes and induction labor provides new avenues of research on how exosomes may contribute to normal and adverse labor events and will aid in the discovery of biomarkers and potential treatments to delay preterm labor.

## Appendix A: Supplemental Tables for Chapter 2

**Supplemental Table 2.1. Proteomics analysis of exosomal cargo identified 30 unique markers in exosomes derived from amnion epithelial cells grown in normal culture conditions.**

ID	Symbol	Entrez Gene Name	Function	Location	Type(s)
ADK_HUMAN	ADK	adenosine kinase	metabolism	Nucleus	kinase
AK1A1_HUMAN	AKR1A1	aldo-keto reductase family 1, member A1 (aldehyde reductase)	metabolism	Cytoplasm	enzyme
ASSY_HUMAN	ASS1	argininosuccinate synthase 1	metabolism	Cytoplasm	enzyme
CADH5_HUMAN	CDH5	cadherin 5	cell adhesion	Plasma Membrane	other
COBA1_HUMAN	COL11A1	collagen, type XI, alpha 1	cell adhesion	Extracellular Space	other
COR1A_HUMAN	CORO1A	coronin 1A	structural	Cytoplasm	other
DYH8_HUMAN	DNAH8	dynein, axonemal, heavy chain 8	structural	Cytoplasm	enzyme
DESP_HUMAN	DSP	desmoplakin	cell adhesion	Plasma Membrane	other
URP2_HUMAN	FERMT3	fermitin family member 3	cell adhesion	Cytoplasm	enzyme
FMOD_HUMAN	FMOD	fibromodulin	structural	Extracellular Space	other
GSTA2_HUMAN	GSTA2	glutathione S-transferase alpha 2	metabolism	Cytoplasm	enzyme
HGD_HUMAN	HGD	homogentisate 1,2-dioxygenase	metabolism	Cytoplasm	enzyme
HORN_HUMAN	HRNR	hornerin	structural	Cytoplasm	other
IBP7_HUMAN	IGFBP7	insulin like growth factor	cell adhesion	Extracellular Space	transporter

		binding protein 7			
KPRP_HUMAN	KPRP	keratinocyte proline-rich protein	other	Cytoplasm	other
LYSC_HUMAN	LYZ	lysozyme	immune response	Extracellular Space	enzyme
MAOX_HUMAN	ME1	malic enzyme 1, NADP(+)-dependent, cytosolic	metabolism	Cytoplasm	enzyme
NCAM1_HUMAN	NCAM1	neural cell adhesion molecule 1	cell adhesion	Plasma Membrane	other
NELL2_HUMAN	NELL2	neural EGFL like 2	cell adhesion	Extracellular Space	other
PARVA_HUMAN	PARVA	parvin alpha	cell adhesion	Cytoplasm	other
PROF1_HUMAN	PFN1	profilin 1	cell adhesion	Cytoplasm	other
PROS_HUMAN	PROS1	protein S (alpha)	cell migration	Extracellular Space	other
PYGB_HUMAN	PYGB	phosphorylase, glycogen; brain	metabolism	Cytoplasm	enzyme
S10A8_HUMAN	S100A8	S100 calcium binding protein A8	inflammation	Cytoplasm	other
HEP2_HUMAN	SERPIND1	serpin peptidase inhibitor, clade D (heparin cofactor), member 1	cell migration	Extracellular Space	other
SHBG_HUMAN	SHBG	sex hormone-binding globulin	transport	Extracellular Space	other
SPRR3_HUMAN	SPRR3	small proline-rich protein 3	structural	Cytoplasm	other
ST1E1_HUMAN	SULT1E1	sulfotransferase family 1E member 1	metabolism	Cytoplasm	enzyme
VCAM1_HUMAN	VCAM1	vascular cell adhesion molecule 1	cell adhesion	Plasma Membrane	transmembrane receptor
VNN1_HUMAN	VNN1	vanin 1	cell adhesion	Plasma Membrane	enzyme



**Supplemental Table 2.2. Proteomics analysis of exosomal cargo identified 48 unique markers in exosomes derived from amnion epithelial cells grown under oxidative stress conditions**

ID	Symbol	Entrez Gene Name	Function	Location	Type(s)
ACES_HUMAN	ACHE	acetylcholinesterase (Yt blood group)	signaling	Plasma Membrane	enzyme
ACTN1_HUMAN	ACTN1	actinin, alpha 1	structural	Cytoplasm	transcription regulator
AOC3_HUMAN	AOC3	amine oxidase, copper containing 3	cell adhesion	Plasma Membrane	enzyme
APOA4_HUMAN	APOA4	apolipoprotein A-IV	binding	Extracellular Space	transporter
RIMB1_HUMAN	BZRAP1	benzodiazepine receptor (peripheral) associated protein 1	binding	Cytoplasm	other
CR063_HUMAN	C18orf63	chromosome 18 open reading frame 63	other	Other	other
CO2_HUMAN	C2	complement component 2	immune response	Extracellular Space	peptidase
CAB39_HUMAN	CAB39	calcium binding protein 39	cell cycle	Cytoplasm	enzyme
CADH6_HUMAN	CDH6	cadherin 6	cell adhesion	Plasma Membrane	other
CFAB_HUMAN	CFB	complement factor B	immune response	Extracellular Space	peptidase
CNDP2_HUMAN	CNDP2	CNDP dipeptidase 2 (metallopeptidase M20 family)	cell cycle	Cytoplasm	peptidase
COR1C_HUMAN	CORO1C	coronin 1C	signaling	Cytoplasm	other
DPYS_HUMAN	DPYS	dihydropyrimidinase	metabolism	Cytoplasm	enzyme
FILA_HUMAN	FLG	filaggrin	structural	Cytoplasm	other

FILA2_HUMAN	FLG2	filaggrin family member 2	structural	Cytoplasm	other
GDIB_HUMAN	GDI2	GDP dissociation inhibitor 2	signaling	Cytoplasm	other
GSTM5_HUMAN	GSTM5	glutathione S-transferase mu 5	metabolism	Cytoplasm	enzyme
HS90B_HUMAN	HSP90AB1	heat shock protein 90kDa alpha family class B member 1	inflammation	Cytoplasm	enzyme
IGF2_HUMAN	IGF2	insulin like growth factor 2	signaling	Extracellular Space	growth factor
ITA2_HUMAN	ITGA2	integrin subunit alpha 2	cell adhesion	Plasma Membrane	transmembrane receptor
LAMC1_HUMAN	LAMC1	laminin subunit gamma 1	cell adhesion	Extracellular Space	other
MYH2_HUMAN	MYH2	myosin, heavy chain 2, skeletal muscle, adult	structural	Cytoplasm	enzyme
NDKB_HUMAN	NME2	NME/NM23 nucleoside diphosphate kinase 2	metabolism	Nucleus	kinase
PCLO_HUMAN	PCLO	piccolo presynaptic cytomatrix protein	signaling	Cytoplasm	transporter
PFKAL_HUMAN	PFKL	phosphofructokinase, liver	metabolism	Cytoplasm	kinase
PAFA_HUMAN	PLA2G7	phospholipase A2 group VII	inflammation	Extracellular Space	enzyme
PLVAP_HUMAN	PLVAP	plasmalemma vesicle associated protein	signaling	Plasma Membrane	other
PPIB_HUMAN	PPIB	peptidylprolyl isomerase B	structural	Cytoplasm	enzyme
PRDX1_HUMAN	PRDX1	peroxiredoxin 1	inflammation	Cytoplasm	enzyme
PRDX2_HUMAN	PRDX2	peroxiredoxin 2	inflammation	Cytoplasm	enzyme

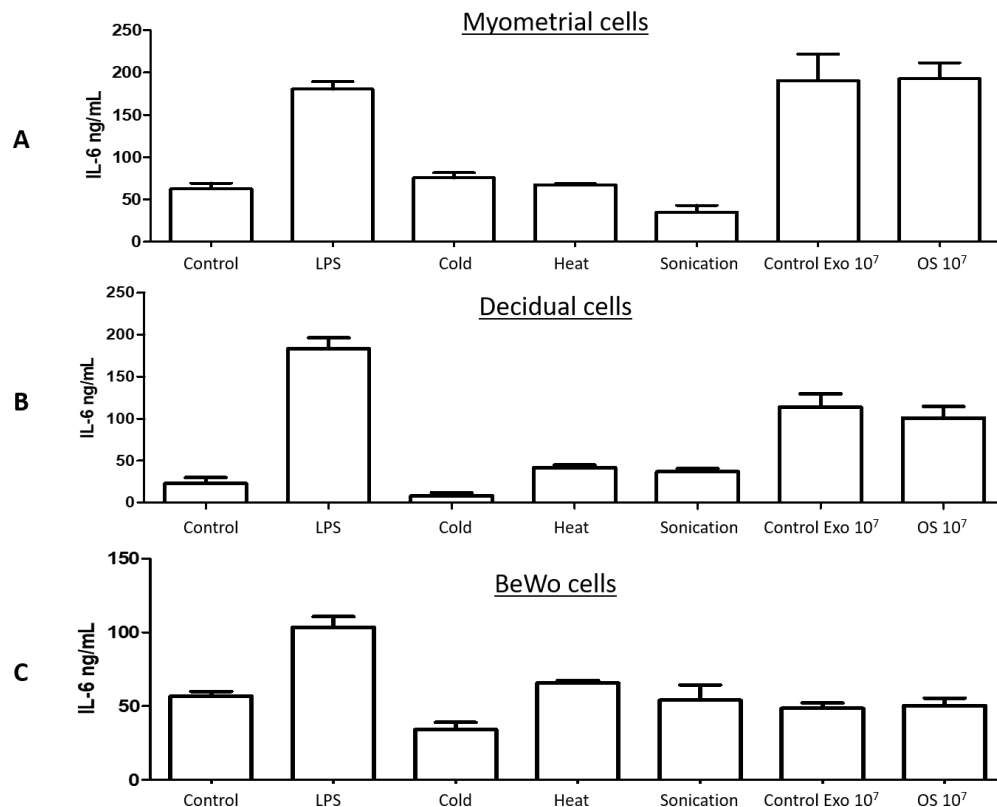
PSA1_HUMAN	PSMA1	proteasome subunit alpha 1	cell cycle	Cytoplasm	peptidase
PSA4_HUMAN	PSMA4	proteasome subunit alpha 4	cell cycle	Cytoplasm	peptidase
PSA6_HUMAN	PSMA6	proteasome subunit alpha 6	cell cycle	Cytoplasm	peptidase
PSA7_HUMAN	PSMA7	proteasome subunit alpha 7	cell cycle	Cytoplasm	peptidase
PSMD5_HUMAN	PSMD5	proteasome 26S subunit, non-ATPase 5	cell cycle	Other	other
PYGL_HUMAN	PYGL	phosphorylase, glycogen, liver	metabolism	Cytoplasm	enzyme
RAN_HUMAN	RAN	RAN, member RAS oncogene family	cell cycle	Nucleus	enzyme
RAP1B_HUMAN	RAP1B	RAP1B, member of RAS oncogene family	transport	Cytoplasm	enzyme
S10A7_HUMAN	S100A7	S100 calcium binding protein A7	inflammation	Cytoplasm	other
S10A9_HUMAN	S100A9	S100 calcium binding protein A9	inflammation	Cytoplasm	other
TAGL2_HUMAN	TAGLN2	transgelin 2	binding	Cytoplasm	other
TFR1_HUMAN	TFRC	transferrin receptor	transport	Plasma Membrane	transporter
TENX_HUMAN	TNXB	tenascin XB	cell adhesion	Extracellular Space	other
TPM1_HUMAN	TPM1	tropomyosin 1 (alpha)	structural	Cytoplasm	other
TBA4A_HUMAN	TUBA4A	tubulin alpha 4a	structural	Cytoplasm	other
RL40_HUMAN	UBA52	ubiquitin A-52 residue ribosomal protein fusion product 1	inflammation	Cytoplasm	enzyme

WDR1_HUMAN	WDR1	WD repeat domain 1	transport	Extracellular Space	other
1433T_HUMAN	YWHAQ	tyrosine 3-monooxygenase/tryptophan 5-monooxygenase activation protein, theta	signaling	Cytoplasm	other

## Appendix B: Supplemental Materials for Chapter 3

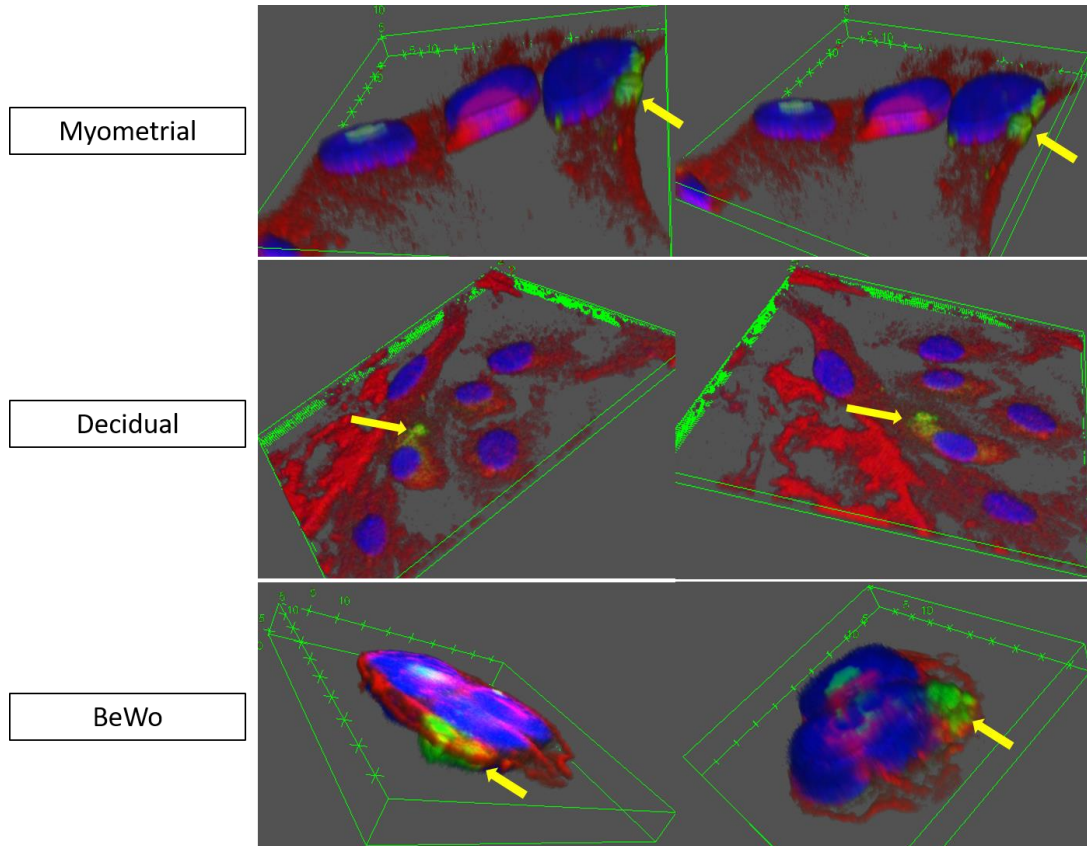
### Supplemental Figure 3.1: IL-6 concentration in media from various control experiments performed to confirm exosome specific activation of inflammatory mediators

Treatments are on the Y-axis; Control: negative control, Lipopolysaccharide (LPS) was used as a positive control, Cold – cold treatment of cells to prevent endocytosis of exosomes, Heat inactivation – to disrupt exosomal membrane and denature proteomic cargo, Sonication - to disrupt exosomal membrane and denature proteomic cargo, Control and oxidative stress exosomes treatments at a dose of  $10^7$ ; A: Myometrial cells treated with LPS and control and oxidative stress exosomes show increased IL-6 compared to control. Cold, heat and sonication did not change IL-6 compared to negative control; B: Decidual cells treated with LPS and control and oxidative stress exosomes show increased IL-6 compared to control. Cold treatment reduced IL-6 more than negative control settings whereas heat and sonication did not change IL-6 compared to negative control. C: BeWo cells increase IL-6 in response to LPS. No change was seen with any other conditions including exosome treatment.



### Supplemental Figure 3.2. 3D reconstructions of confocal images of each target cell studied

Blue is DAPI which shows the nucleus. Red is a cytoplasmic protein either  $\alpha$  or  $\beta$  actin. Exosomes are shown in green. Exosomes are identified within each cell type (myometrial, decidual and BeWo) by yellow arrows.



**Supplemental Table 3.1A: Cytokine and PGE2 concentrations in  
myometrial cells treated with control exosomes**

<b>IL-6</b>	Control	Exo 10 <sup>5</sup>	Exo 10 <sup>7</sup>	Exo 10 <sup>9</sup>
Mean ± SD	62.5±13.3	171.3±43.1	190.6±62.6	166.4±58.0
Median (IQR)	60.3 (21.5)	190.4 (47.8)	190.4 (107.9)	147.7 (78.6)
<i>P</i> - Untreated cells vs control exosomes		0.03	0.03	0.03

<b>IL-8</b>	Control	Exo 10 <sup>5</sup>	Exo 10 <sup>7</sup>	Exo 10 <sup>9</sup>
Mean ± SD	19721±18210.7	99892.8±21968.2	90793.1±23044.6	114652.2±24259.5
Median (IQR)	11764.0 (200059)	103786.9 (31454)	88936.9 (37985.0)	24259.5 (119391.2)
<i>P</i> - Untreated cells vs control exosomes		0.03	0.03	0.03

<b>PGE<sub>2</sub></b>	Control	Exo 10 <sup>5</sup>	Exo 10 <sup>7</sup>	Exo 10 <sup>9</sup>
Mean ± SD	1120.1±60.5	1301.5±62.9	1179.8±60.5	1064.1±47.2
Median (IQR)	1097.8 (83.5)	1300.6 (97.4)	1184.6 (99.2)	1073.4 (69.3)
<i>P</i> - Untreated cells vs control exosomes		0.03	0.19	0.31

**Supplemental Table 3.1B: Cytokine and PGE2 concentrations in myometrial cells treated with exosomes derived from AEC exposed to cigarette smoke extract (Oxidative stress (OS) exosomes)**

<b>IL-6</b>	Control	OS Exo 10 <sup>5</sup>	OS Exo 10 <sup>7</sup>	OS Exo 10 <sup>9</sup>
Mean ± SD	62.5±13.3	165.2±48.4	192.7±37.67	178.6±12.31
Median (IQR)	60.3 (21.5)	149.9 (58.2)	186.3 (56.0)	178.7 (21.0)
<i>P</i> - Untreated cells vs OS exosomes		0.03	0.03	0.03

<b>IL-8</b>	Control	OS Exo 10 <sup>5</sup>	OS Exo 10 <sup>7</sup>	OS Exo 10 <sup>9</sup>
Mean ± SD	19721.4±18210.7	99177.3±27778.8	130680.0±26657.2	131687±35418
Median (IQR)	11764.0 (200059.0)	107778.5 (37597.0)	119572.0(29365.0)	137049.3(51333.0)
<i>P</i> - Untreated cells vs OS exosomes		0.03	0.03	0.03

<b>PGE<sub>2</sub></b>	Control	OS Exo 10 <sup>5</sup>	OS Exo 10 <sup>7</sup>	OS Exo 10 <sup>9</sup>
Mean ± SD	1120±60.5	1650.0±174.4	1304.9±174.4	1360.0±101.5
Median (IQR)	1097.8 (83.5)	1705.6 (240.0)	1337.4(154.8)	1373.2 (153.3)
<i>P</i> - Untreated cells vs OS exosomes		0.03	0.06	0.03



**Supplemental Table 3.2A: Cytokine and PGE2 concentrations in myometrial cells treated with exosomes derived from AEC exposed to cigarette smoke extract (Oxidative stress (OS) exosomes)**

<b>IL-6</b>	Control	Exo 10 <sup>5</sup>	Exo 10 <sup>7</sup>	Exo 10 <sup>9</sup>
Mean ± SD	22.8±14.1	101.8±12.1	113.6±31.8	75.1±3.290
Median (IQR)	18.4 (16.2)	104.8 (18.6)	119.3(45.6)	75.8 (4.6)
<i>P</i> - Untreated cells vs control exosomes		0.03	0.03	0.03

<b>IL-8</b>	Control	Exo 10 <sup>5</sup>	Exo 10 <sup>7</sup>	Exo 10 <sup>9</sup>
Mean ± SD	148.1±109.1	687.4±312.3	747.6±464.9	1546±217.8
Median (IQR)	150.4 (186.5)	800.5 (363.3)	818.1 (715.2)	1589.2 (274.2)
<i>P</i> - Untreated cells vs control exosomes		0.11	0.11	0.03

<b>PGE<sub>2</sub></b>	Control	Exo 10 <sup>5</sup>	Exo 10 <sup>7</sup>	Exo 10 <sup>9</sup>
Mean ± SD	18.0±1.5	23.5±2.2	19.2±3.1	24.8±4.4
Median (IQR)	18.3 (2.4)	23.3 (3.5)	18.7 (4.7)	22.7 (4.5)
<i>P</i> - Untreated cells vs control exosomes		0.03	0.66	0.03

**Supplemental Table 3.2B: Cytokine and PGE2 concentrations in  
decidual cells treated with exosomes derived from AEC exposed to  
cigarette smoke extract (Oxidative stress (OS) exosomes)**

<b>IL-6</b>	Control	OS Exo 10 <sup>5</sup>	OS Exo 10 <sup>7</sup>	OS Exo 10 <sup>9</sup>
Mean ± SD	22.8±14.1	94.2±17.4	100.7±27.5	150.8±12.4
Median (IQR)	18.4 (16.2)	92.8 (27.2)	104.9 (39.7)	148.6 (18.3)
<i>P</i> - Untreated cells vs OS exosomes		0.03	0.03	0.03

<b>IL-8</b>	Control	OS Exo 10 <sup>5</sup>	OS Exo 10 <sup>7</sup>	OS Exo 10 <sup>9</sup>
Mean ± SD	148.1±109.1	672.8±351.7	673.1±334.7	946.9±478.3
Median (IQR)	150.4 (186.5)	676.9(505.8)	772.6 (482.6)	936.1 (703.4)
<i>P</i> - Untreated cells vs OS exosomes		0.06	0.11	0.03

<b>PGE<sub>2</sub></b>	Control	OS Exo 10 <sup>5</sup>	OS Exo 10 <sup>7</sup>	OS Exo 10 <sup>9</sup>
Mean ± SD	18.0±1.5	30.4±4.2	32.1±6.1	34.24±3.1
Median (IQR)	18.3 (2.4)	29.2(6.4)	32.9 (8.5)	33.4 (3.9)
<i>P</i> - Untreated cells vs OS exosomes		0.03	0.03	0.03

**Supplemental Table 3.3A: Cytokine and PGE2 concentrations in BeWo cells treated with control exosomes**

<b>IL-6</b>	Control	Exo 10 <sup>5</sup>	Exo 10 <sup>7</sup>	Exo 10 <sup>9</sup>
Mean ±SD	57.0±6.0	52.6±9.4	48.6±7.2	47.4±11.6
Median (IQR)	55.4 (8.3)	50.6 (11.5)	46.5 (10.3)	47.1 (14.8)
<i>P</i> - Untreated cells vs control exosomes		0.31	0.19	0.19

<b>PGE<sub>2</sub></b>	Control	Exo 10 <sup>5</sup>	Exo 10 <sup>7</sup>	Exo 10 <sup>9</sup>
Mean ±SD	0.09± 0.01	0.12± 0.02	0.12± .01	0.09 ± 0.01
Median (IQR)	0.10 (0.01)	0.12 (0.03)	0.12 (0.01)	0.09 (0.02)
<i>P</i> - Untreated cells vs control exosomes		0.03	0.03	0.89

**Supplemental Table 3.3B: Cytokine and PGE2 concentrations in BeWo cells treated with exosomes derived from AEC exposed to cigarette smoke extract (Oxidative stress (OS) exosomes)**

<b>IL-6</b>	Control	OS Exo 10 <sup>5</sup>	OS Exo 10 <sup>7</sup>	OS Exo 10 <sup>9</sup>
Mean ±SD	57.0±6.0	47.1±9.1	50.5±10.1	54.7±16.1
Median (IQR)	55.4 (8.3)	46.0 (14.9)	54.3 (13.1)	50.2 (22.7)
<i>P</i> - Untreated cells vs OS exosomes		0.19	0.67	0.67

<b>PGE<sub>2</sub></b>	Control	OS Exo 10 <sup>5</sup>	OS Exo 10 <sup>7</sup>	OS Exo 10 <sup>9</sup>
Mean ±SD	0.09±0.01	0.10±0.01	0.10±0.01	0.10±0.02
Median (IQR)	0.10 (0.01)	0.10 (0.02)	0.10 (0.02)	0.10 (0.02)
<i>P</i> - Untreated cells vs OS exosomes		0.56	0.67	0.19

**Supplemental Table 3.4 – Control experiments used to show exosome mediated immune activation effects in myometrial, decidual and BeWo cells**

	LPS			Cold treatment of cells			Heat inactivation of exosomes			Sonication of exosomes		
	IL-6	IL-8	PGE <sub>2</sub>	IL-6	IL-8	PGE <sub>2</sub>	IL-6	IL-8	PGE <sub>2</sub>	IL-6	IL-8	PGE <sub>2</sub>
<b>Myometrium</b>	↑	↑	↑	↓	↓	↔	↔	↔	↔	↓	↔	↔
<b>Decidua</b>	↑	↑	↑	↓	↓	↓	↔	↔	↔	↔	↔	↔
<b>BeWo</b>	↑	↔	X	↓	↔	↓	↔	↔	↔	↔	↔	↔

↑ Increase

↓ Decrease

↔ No change

X not detectable

## Appendix C: Supplemental Tables for Chapter 5

**Supplemental Table 5.1. Exosome concentration throughout gestation:**

### **Tukey's multiple comparisons**

<b>Gestation Days</b>	<b><i>P</i> value</b>
Nonpregnant vs. E5	0.500
Nonpregnant vs. E9	0.478
Nonpregnant vs. E13	0.103
Nonpregnant vs. E15	0.031
Nonpregnant vs. E18	<0.0001
Nonpregnant vs. E19	0.007
Nonpregnant vs. PP7	0.500
E5 vs. E9	0.500
E5 vs. E13	0.253
E5 vs. E15	0.095
E5 vs. E18	<0.0001
E5 vs. E19	0.029
E5 vs. PP7	0.500
E9 vs. E13	0.274
E9 vs. E15	0.092
E9 vs. E18	<0.0001
E9 vs. E19	0.017
E9 vs. PP7	0.497
E13 vs. E15	0.494
E13 vs. E18	0.029
E13 vs. E19	0.446
E13 vs. PP7	0.178
E15 vs. E18	0.383
E15 vs. E19	0.500
E15 vs. PP7	0.059
E18 vs. E19	0.433
E18 vs. PP7	<0.0001
E19 vs. PP7	0.016

**Supplemental Table 5.2. Proteins with Log<sub>2</sub> (Fold Change) of  $\pm 0.6$  and – Log(*P*-value) >2.0 for Volcano Plots**

<b>Late Gestation (E18) vs Early Gestation (E5)</b>		
<b>Protein Name</b>	<b>Log<sub>2</sub> (Fold change)</b>	<b>-Log (<i>P</i>-value)</b>
Serotransferrin	1.38	3.59
Ceruloplasmin	2.3	4
Alpha-2-macroglobulin-P	2.76	4
Complement C4-B	1.47	4
Complement factor H	1.89	4
Plasminogen	1.63	4
Inter alpha-trypsin inhibitor, heavy chain 4	4.21	4
Apolipoprotein B-100	3	4
Hemopexin	1.46	3.8
Vitamin D-binding protein	1.73	3.8
Leukemia inhibitory factor receptor	4.78	4
Corticosteroid-binding globulin	2.96	2.43
Inter-alpha-trypsin inhibitor heavy chain H1	1.74	4
Protein Gm20547	1.49	4
Prothrombin	2.66	4
Gelsolin	1.16	4
Carboxypeptidase N subunit 2	1.19	4
Inhibitor of carbonic anhydrase	0.99	2.72
Haptoglobin	3.24	2.54
Mannan-binding lectin serine protease 1	1.04	2
Apolipoprotein A-IV	1.12	3
Beta-2-glycoprotein 1	1.86	2.62
Clusterin	1.3	2.74
Prolow-density lipoprotein receptor-related protein 1	1.78	2.16
Alpha-2-antiplasmin	1.72	2.96
Coagulation factor V	2.88	3.96
Vitronectin	2.36	3.47
Afamin	1.76	4
Insulin-like growth factor-binding protein complex acid labile subunit	1.33	2.62
Fetuin-B	1.62	2.29

von Willebrand factor	2.47	2.15
Mannan-binding lectin serine protease 2	1.33	2.11
Sulfhydryl oxidase 1	1.38	2.34
Plasma protease C1 inhibitor	1.85	2.92
Hemoglobin subunit beta-2	-2.84	3.6
Alpha-amylase 1	2.83	2.57
Extracellular matrix protein 1	2.38	3.49
Heparin cofactor 2	2.33	2.46
Tenascin	2.04	2.42
Proteasome subunit alpha type-7	-2.45	4
Serine protease inhibitor A3N	2.88	2.44
Zinc-alpha-2-glycoprotein	2.32	2.96
Hepatocyte growth factor activator	4.31	2
Carbonic anhydrase 2	-2.19	2.54
Proteasome subunit alpha type-2	-2.36	2.15
Proteasome subunit beta type-2	-1.94	2.05
Proteasome subunit alpha type-3	-2.18	2.62
Catalase	-3.3	2.77
Vascular non-inflammatory molecule 3	2.21	2.62
Complement C1q subcomponent subunit C	2.97	2.37
Proteasome subunit beta type-5	-2.44	3.31
Hyaluronan-binding protein 2	1.65	2.62
Phosphatidylcholine-sterol acyltransferase	2.15	2.19
Aspartyl aminopeptidase	-2.14	3.4
Secreted phosphoprotein 24	1.99	2.72
Ig kappa chain V-VI region XRPC 44	-2.75	2.52
Beta-2-microglobulin	1.4	2.41
<b>Late Gestation (E18) vs Mid Gestation (E9)</b>		
<b>Protein Name</b>	<b>Log<sub>2</sub> (Fold change)</b>	<b>-Log (P-value)</b>
Fibrinogen alpha chain	1.87	2.01
Complement component C8 beta chain	-0.95	2.07
Mannan-binding lectin serine protease 2	1.26	2.19
Coagulation factor V	1.56	2.39
Heparin cofactor 2	0.85	2.42
Complement C1q subcomponent subunit A	3.56	2.44
Pigment epithelium-derived factor	2.21	2.68
Protein Ighg3 (Fragment)	-2.64	2.77



Complement C1q subcomponent subunit C	4.6	2.77
Hyaluronan-binding protein 2	1.19	2.77
Plasminogen	0.65	2.8
Vascular non-inflammatory molecule 3	2.47	2.89
Complement C1q subcomponent subunit B	3.82	2.96
Complement C1r-A subcomponent	2.52	3.02
Alpha-amylase 1	3.02	3.19
Alpha globin 1	-1.75	3.22
Mannan-binding lectin serine protease 1	1.68	3.38
Hemoglobin subunit beta-2	-2.47	3.42
Thrombospondin-1	1.41	3.64
von Willebrand factor	3.23	3.68
Fibrinogen beta chain	4.24	4
Fibrinogen gamma chain	4.69	4
Ceruloplasmin	1.58	4
Alpha-2-macroglobulin-P	-1.09	4
Complement C4-B	1.5	4
Complement factor H	1.15	4
Inter alpha-trypsin inhibitor, heavy chain 4	1.88	4
Inter-alpha-trypsin inhibitor heavy chain H1	1.12	4
Prothrombin	1.62	4
Prolow-density lipoprotein receptor-related protein 1	1.45	4
78 kDa glucose-regulated protein	1.41	4
<b>E18 (Term not in Labor) vs E19 (Term in Labor)</b>		
<b>Protein Name</b>	<b>Log<sub>2</sub> (Fold change)</b>	<b>-Log (P-value)</b>
Alpha-2-macroglobulin-P	-0.95	4
Complement factor H	0.8	2.3
Inter alpha-trypsin inhibitor, heavy chain 4	1.49	4
Apolipoprotein B-100	0.78	4
Hemopexin	1.08	2.21
Inter-alpha-trypsin inhibitor heavy chain H1	0.77	2.82
Prothrombin	0.73	3.41
Apolipoprotein A-IV	1.08	2.96
Murinoglobulin-2	3.51	3.38
Carboxypeptidase N catalytic chain	1.28	2.21
Coagulation factor V	1.38	4
H-2 class I histocompatibility antigen, Q10 alpha chain	1.78	3.59

Insulin-like growth factor-binding protein complex acid labile subunit	1.55	3.96
Ig gamma-2A chain C region, membrane-bound form	2.44	2.06
von Willebrand factor	-1.09	3.85
Epidermal growth factor receptor	0.86	2.08
Complement C1q subcomponent subunit B	1.9	3
Hepatocyte growth factor activator	1.28	2.15
Vascular non-inflammatory molecule 3	1.2	2.41

## References

1. Blencowe H, Cousens S, Chou D, Oestergaard M, Say L, Moller A, Kinney M. Born Too Soon : The global epidemiology of 15 million preterm births. 2013;10(Suppl 1):1–14.
2. Hodek J-M, von der Schulenburg J-M, Mittendorf T. Measuring economic consequences of preterm birth - Methodological recommendations for the evaluation of personal burden on children and their caregivers. *Health Econ Rev* [Internet]. 2011;1(1):6. Available from: <http://www.healtheconomicsreview.com/content/1/1/6>
3. Smith R. Parturition. *N Engl J Med* [Internet]. 2007 Jan 18;356(3):271–83. Available from: <http://www.nejm.org/doi/abs/10.1056/NEJMr061360>
4. Romero R, Dey SK, Fisher SJ. Preterm Labor: One Syndrome, Many Causes. *Science* [Internet]. 2014 Aug 15 [cited 2015 Jun 13];345(6198):760–5. Available from: <http://www.sciencemag.org/content/345/6198/760.long>
5. Flood K, Malone FD. Prevention of preterm birth. *Semin Fetal Neonatal Med* [Internet]. 2012 Feb;17(1):58–63. Available from: <http://dx.doi.org/10.1016/j.siny.2011.08.001>
6. Rajagopal SP, Hutchinson JL, Dorward DA, Rossi AG, Norman JE. Crosstalk between monocytes and myometrial smooth muscle in culture generates synergistic pro-inflammatory cytokine production and enhances myocyte contraction, with effects opposed by progesterone. *Mol Hum Reprod* [Internet]. 2015;21(8):672–86. Available from: <http://www.molehr.oxfordjournals.org/lookup/doi/10.1093/molehr/gav027>
7. Catalano RD, Lannagan TRM, Gorowiec M, Denison FC, Norman JE, Jabbour HN. Prokineticins: novel mediators of inflammatory and contractile pathways at parturition? *Mol Hum Reprod* [Internet]. 2010 May 1 [cited 2015 Jun 22];16(5):311–9. Available from: <http://molehr.oxfordjournals.org/content/16/5/311.long>
8. Blackburn S. Maternal, fetal, & neonatal physiology: a clinical perspective. 4th ed. Elsevier Health Sciences; 2014. 768 p.
9. Gao L, Rabbitt EH, Condon JC, Renthal NE, Johnston JM, Mitsche MA, Chambon P, Xu J, O'Malley BW, Mendelson CR. Steroid receptor coactivators 1 and 2 mediate fetal-to-maternal signaling that initiates parturition. *J Clin Invest* [Internet]. 2015 Jul 1;125(7):2808–24. Available from: <http://www.jci.org/articles/view/78544>
10. Reinl EL, England SK. Fetal-to-maternal signaling to initiate parturition. *J Clin Invest* [Internet]. 2015 Jul 1;125(7):2569–71. Available from: <http://www.ncbi.nlm.nih.gov/pubmed/26098207>
11. Condon JC, Jeyasuria P, Faust JM, Mendelson CR. Surfactant protein secreted by the maturing mouse fetal lung acts as a hormone that signals the initiation of parturition. *Proc Natl Acad Sci*. 2004;101(14):4978–83.

12. McLean M, Bisits A, Davies J, Woods R, Lowry P, Smith R. A placental clock controlling the length of human pregnancy. *Nat Med*. 1995;1(5):460–3.
13. Grammatopoulos DK, Hillhouse EW. Role of corticotropin-releasing hormone in onset of labour. *Lancet*. 1999;354(9189):1546–9.
14. Linton EA, Woodman JR, Asboth G, Glynn BP, Plested CP, Bernal AL. Corticotrophin Releasing Hormone: Its Potential for a Role in Human Myometrium. *Exp Physiol* [Internet]. 2001 Mar;86(2):273–81. Available from: <http://doi.wiley.com/10.1113/eph8602183>
15. Challis JRG, Bloomfield FH, Booking AD, Casciani V, Chisaka H, Connor K, Dong X, Gluckman P, Harding JE, Johnstone J, Li W, Lye S, Okamura K, Premyslova M. Fetal signals and parturition. *J Obstet Gynaecol Res*. 2005;31(6):492–9.
16. Mesiano S, Chan EC, Fitter JT, Kwek K, Yeo G, Smith R. Progesterone withdrawal and estrogen activation in human parturition are coordinated by progesterone receptor A expression in the myometrium. *J Clin Endocrinol Metab*. 2002;87(6):2924–30.
17. Tan H, Yi L, Rote NS, Hurd WW, Mesiano S. Progesterone receptor-A and -B have opposite effects on proinflammatory gene expression in human myometrial cells: implications for progesterone actions in human pregnancy and parturition. *J Clin Endocrinol Metab* [Internet]. 2012 May;97(5):E719–30. Available from: <http://press.endocrine.org/doi/abs/10.1210/jc.2011-3251>
18. Merlino A a., Welsh TN, Tan H, Li JY, Cannon V, Mercer BM, Mesiano S. Nuclear progesterone receptors in the human pregnancy myometrium: Evidence that parturition involves functional progesterone withdrawal mediated by increased expression of progesterone receptor-A. *J Clin Endocrinol Metab*. 2007;92(5):1927–33.
19. Thomson AJ, Telfer JF, Young A, Campbell S, Stewart CJR, Cameron IT, Greer IA, Norman JE. Leukocytes infiltrate the myometrium during human parturition: further evidence that labour is an inflammatory process. *Hum Reprod* [Internet]. 1999 Jan;14(1):229–36. Available from: <http://www.ncbi.nlm.nih.gov/pubmed/10374126>
20. Osman I, Young A, Ledingham MA, Thomson AJ, Jordan F, Greer IA, Norman JE. Leukocyte density and pro-inflammatory cytokine expression in human fetal membranes, decidua, cervix and myometrium before and during labour at term. *Mol Hum Reprod*. 2003;9(1):41–5.
21. Gomez-Lopez N, Guilbert LJ, Olson DM. Invasion of the leukocytes into the fetal-maternal interface during pregnancy. *J Leukoc Biol* [Internet]. 2010;88(4):625–33. Available from: <http://www.jleukbio.org/cgi/doi/10.1189/jlb.1209796>
22. Hua R, Pease JE, Sooranna SR, Viney JM, Nelson SM, Myatt L, Bennett PR, Johnson MR. Stretch and inflammatory cytokines drive myometrial chemokine expression via NF- $\kappa$ B activation. *Endocrinology*. 2012;153(1):481–91.
23. Sooranna SR, Lee Y, Kim LU, Mohan AR, Bennett PR, Johnson MR. Mechanical

- stretch activates type 2 cyclooxygenase via activator protein-1 transcription factor in human myometrial cells. *Mol Hum Reprod* [Internet]. 2004 Feb;10(2):109–13. Available from: <http://www.ncbi.nlm.nih.gov/pubmed/14742695>
24. Mahendroo M. Cervical remodeling in term and preterm birth: Insights from an animal model. *Reproduction*. 2012;143(4):429–38.
  25. Gonzalez JM, Dong Z, Romero R, Girardi G. Cervical remodeling/ripening at term and preterm delivery: The same mechanism initiated by different mediators and different effector cells. *PLoS One*. 2011;6(11).
  26. Nielsen BW, Bonney EA, Pearce BD, Donahue LR, Sarkar IN. A Cross-Species Analysis of Animal Models for the Investigation of Preterm Birth Mechanisms. Vol. 23, *Reproductive Sciences*. 2016. p. 482–91.
  27. Timmons BC, Reese J, Socrate S, Ehinger N, Paria BC, Milne GL, Akins ML, Auchus RJ, McIntire D, House M, Mahendroo M. Prostaglandins are essential for cervical ripening in LPS-Mediated preterm birth but not term or antiprogesterone-driven preterm ripening. *Endocrinology*. 2014;155(1):287–98.
  28. Tang M, Hu X, Liu Z, Kwak-kim J, Liao A. What are the roles of macrophages and monocytes in human pregnancy ? *J Reprod Immunol* [Internet]. 2015;112:73–80. Available from: <http://dx.doi.org/10.1016/j.jri.2015.08.001>
  29. Shynlova O, Dorogin A, Li Y, Lye S. Inhibition of infection-mediated preterm birth by administration of broad spectrum chemokine inhibitor in mice. *J Cell Mol Med*. 2014;18(9):1816–29.
  30. Boardman JP. Preterm Birth: Causes, Consequences and Prevention. *J Obstet Gynaecol (Lahore)* [Internet]. 2008 Jan 2;28(5):559–559. Available from: <http://www.tandfonline.com/doi/full/10.1080/01443610802243047>
  31. Salminen A, Paananen R, Vuolteenaho R, Metsola J, Ojaniemi M, Autio-Harmainen H, Hallman M. Maternal endotoxin-induced preterm birth in mice: Fetal responses in toll-like receptors, collectins, and cytokines. *Pediatr Res*. 2008;63(3):280–6.
  32. Bredeson S, Papaconstantinou J, Deford JH, Kechichian T, Syed TA, Saade GR, Menon R. HMGB1 promotes a p38MAPK associated non-infectious inflammatory response pathway in human fetal membranes. *PLoS One*. 2014;9(12):e113799.
  33. Menon R. Oxidative stress damage as a detrimental factor in preterm birth pathology. *Front Immunol* [Internet]. 2014;5(November):567. Available from: <http://www.pubmedcentral.nih.gov/articlerender.fcgi?artid=4228920&tool=pmcentrez&rendertype=abstract>
  34. Behnia F, Taylor BD, Woodson M, Kacerovský M, Hawkins H, Fortunato SJ, Saade GR, Menon R. Chorioamniotic membrane senescence: a signal for parturition? *Am J Obstet Gynecol* [Internet]. 2015;(June):1–16. Available from: <http://linkinghub.elsevier.com/retrieve/pii/S0002937815005177>
  35. Menon R, Fortunato SJ, Yu J, Milne GL, Sanchez S, Drobek CO, Lappas M, Taylor RN. Cigarette smoke induces oxidative stress and apoptosis in normal term

- fetal membranes. Placenta [Internet]. 2011 Apr [cited 2015 Jun 23];32(4):317–22. Available from:  
<http://www.sciencedirect.com/science/article/pii/S0143400411000269>
36. Brighton PJ, Maruyama Y, Fishwick K, Vrljicak P, Tewary S, Fujihara R, Muter J, Lucas ES, Yamada T, Woods L, Lucciola R, Lee YH, Takeda S, Ott S, Hemberger M, Quenby S, Brosens JJ. Clearance of senescent decidual cells by uterine natural killer cells in cycling human endometrium. *Elife*. 2017;6:1–23.
  37. Bonney EA, Krebs K, Saade G, Kechichian T, Trivedi J, Huaizhi Y, Menon R. Differential senescence in feto-maternal tissues during mouse pregnancy. *Placenta* [Internet]. 2016 Jul;43:26–34. Available from:  
<http://dx.doi.org/10.1016/j.placenta.2016.04.018>
  38. Davalos AR, Kawahara M, Malhotra GK, Schaum N, Huang J, Ved U, Beausejour CM, Coppe JP, Rodoer F, Campisi J. p53-dependent release of Alarmin HMGB1 is a central mediator of senescent phenotypes. *J Cell Biol*. 2013;201(4):613–29.
  39. Campisi J. Aging, cellular senescence, and cancer. *Annu Rev Physiol* [Internet]. 2013;75:685–705. Available from:  
<http://www.pubmedcentral.nih.gov/articlerender.fcgi?artid=4166529&tool=pmcentrez&rendertype=abstract>
  40. Kuilman T, Michaloglou C, Mooi WJ, Peeper DS. The essence of senescence. *Genes Dev*. 2010;24(22):2463–79.
  41. Henson SM, Lanna A, Riddell NE, Franzese O, Macaulay R, Griffiths SJ, Puleston DJ, Watson AS, Simon AK, Tooze SA, Akbar AN. P38 signaling inhibits mTORC1-independent autophagy in senescent human CD8+ T cells. *J Clin Invest* [Internet]. 2014 Sep;124(9):4004–16. Available from:  
<http://www.ncbi.nlm.nih.gov/pubmed/25083993>
  42. Goehe RW, Di X, Sharma K, Bristol ML, Henderson SC, Valerie K, Rodier F, Davalos AR, Gewirtz D a. The Autophagy-Senescence Connection in Chemotherapy: Must Tumor Cells (Self) Eat Before They Sleep? *J Pharmacol Exp Ther* [Internet]. 2012 Dec 1;343(3):763–78. Available from:  
<http://www.pubmedcentral.nih.gov/articlerender.fcgi?artid=3500537&tool=pmcentrez&rendertype=abstract>
  43. García-Prat L, Martínez-Vicente M, Perdiguero E, Ortet L, Rodríguez-Ubreva J, Rebollo E, Ruiz-Bonilla V, Gutarra S, Ballestar E, Serrano AL, Sandri M, Muñoz-Cánoves P. Autophagy maintains stemness by preventing senescence. *Nature* [Internet]. 2016 Jan 7;529(7584):37–42. Available from:  
<http://www.nature.com/doi/10.1038/nature16187>
  44. Cahu J, Sola B. A sensitive method to quantify senescent cancer cells. *J Vis Exp* [Internet]. 2013 Jan [cited 2015 Oct 25];(78). Available from:  
<http://www.pubmedcentral.nih.gov/articlerender.fcgi?artid=3846801&tool=pmcentrez&rendertype=abstract>
  45. Rodier F, Coppé J-P, Patil CK, Hoeijmakers WAM, Muñoz DP, Raza SR, Freund A, Campeau E, Davalos AR, Campisi J. Persistent DNA damage signalling

- triggers senescence-associated inflammatory cytokine secretion. *Nat Cell Biol* [Internet]. 2009 Aug;11(8):973–9. Available from: <http://www.ncbi.nlm.nih.gov/pubmed/19597488>
46. Coppé JP, Patil CK, Rodier F, Krtolica A, Beauséjour CM, Parrinello S, Hodgson JG, Chin K, Desprez PY, Campisi J. A human-like senescence-associated secretory phenotype is conserved in mouse cells dependent on physiological oxygen. *PLoS One*. 2010;5(2).
  47. Sangiuliano B, Pérez NM, Moreira DF, Belizário JE. Cell Death-Associated Molecular-Pattern Molecules: Inflammatory Signaling and Control. *Mediators Inflamm* [Internet]. 2014;2014:821043. Available from: <http://www.pubmedcentral.nih.gov/articlerender.fcgi?artid=4130149&tool=pmcentrez&rendertype=abstract>
  48. Srikrishna G, Freeze HH. Endogenous damage-associated molecular pattern molecules at the crossroads of inflammation and cancer. *Neoplasia*. 2009;11(7):615–28.
  49. Garg a D, Martin S, Golab J, Agostinis P. Danger signalling during cancer cell death: origins, plasticity and regulation. *Cell Death Differ* [Internet]. 2014;21(1):26–38. Available from: <http://www.ncbi.nlm.nih.gov/pubmed/23686135>
  50. Schaefer L. Complexity of danger: the diverse nature of damage-associated molecular patterns. *J Biol Chem* [Internet]. 2014 Dec 19;289(51):35237–45. Available from: <http://www.ncbi.nlm.nih.gov/pubmed/25391648>
  51. Zhang B, Yin Y, Lai RC, Lim SK. Immunotherapeutic Potential of Extracellular Vesicles. *Front Immunol* [Internet]. 2014;5(October):1–11. Available from: <http://journal.frontiersin.org/article/10.3389/fimmu.2014.00518/abstract>
  52. Natasha G, Gundogan B, Tan A, Farhatnia Y, Wu W, Rajadas J, Seifalian AM. Exosomes as immunotheranostic nanoparticles. *Clin Ther* [Internet]. 2014;36(6):820–9. Available from: <http://dx.doi.org/10.1016/j.clinthera.2014.04.019>
  53. Akers JC, Gonda D, Kim R, Carter BS, Chen CC. Biogenesis of extracellular vesicles (EV): Exosomes, microvesicles, retrovirus-like vesicles, and apoptotic bodies. *J Neurooncol*. 2013;113(1):1–11.
  54. György B, Szabó TG, Pásztói M, Pál Z, Misják P, Aradi B, László V, Pállinger É, Pap E, Kittel Á, Nagy G, Falus A, Buzás EI. Membrane vesicles, current state-of-the-art: Emerging role of extracellular vesicles. *Cell Mol Life Sci*. 2011;68(16):2667–88.
  55. Zarovni N, Corrado A, Guazzi P, Zocco D, Lari E, Radano G, Muhhina J, Fondelli C, Gavrilova J, Chiesi A. Integrated isolation and quantitative analysis of exosome shuttled proteins and nucleic acids using immunocapture approaches. *Methods* [Internet]. 2015;87:46–58. Available from: <http://dx.doi.org/10.1016/j.ymeth.2015.05.028>
  56. Li P, Kaslan M, Lee SH, Yao J, Gao Z. Progress in exosome isolation techniques.

Theranostics. 2017;7(3):789–804.

57. Liga A, Vliegenthart ADB, Oosthuyzen W, Dear JW, Kersaudy-Kerhoas M. Exosome isolation: a microfluidic road-map. *Lab Chip* [Internet]. 2015;15(11):2388–94. Available from: <http://xlink.rsc.org/?DOI=C5LC00240K>
58. Sullivan R, Maresh G, Zhang X, Salomon C, Hooper J, Margolin D, Li L. The emerging roles of extracellular vesicles as communication vehicles within the tumor microenvironment and beyond. Vol. 8, *Frontiers in Endocrinology*. 2017.
59. Bobrie A, Colombo M, Raposo G, Théry C. Exosome Secretion: Molecular Mechanisms and Roles in Immune Responses. *Traffic*. 2011;12(12):1659–68.
60. Soria FN, Pampliega O, Bourdenx M, Meissner WG, Bezard E, Dehay B. Exosomes, an unmasked culprit in neurodegenerative diseases. *Front Neurosci*. 2017;11(JAN):1–12.
61. Sarko DK, McKinney CE. Exosomes: Origins and therapeutic potential for neurodegenerative disease. *Front Neurosci*. 2017;11(FEB):1–7.
62. Jan AT, Malik MA, Rahman S, Yeo HR, Lee EJ, Abdullah TS, Choi I. Perspective Insights of Exosomes in Neurodegenerative Diseases: A Critical Appraisal. *Front Aging Neurosci* [Internet]. 2017 Sep 29;9(September):1–8. Available from: <http://journal.frontiersin.org/article/10.3389/fnagi.2017.00317/full>
63. Zhou J, Li X-L, Chen Z-R, Chng W-J. Tumor-derived exosomes in colorectal cancer progression and their clinical applications. *Oncotarget* [Internet]. 2017;8(59):100781–90. Available from: <http://www.oncotarget.com/fulltext/20117>
64. De Toro J, Herschlik L, Waldner C, Mongini C. Emerging Roles of Exosomes in Normal and Pathological Conditions: New Insights for Diagnosis and Therapeutic Applications. *Front Immunol* [Internet]. 2015;6(May):1–12. Available from: <http://journal.frontiersin.org/Article/10.3389/fimmu.2015.00203/abstract>
65. Buzas EI, György B, Nagy G, Falus A, Gay S. Emerging role of extracellular vesicles in inflammatory diseases. *Nat Rev Rheumatol* [Internet]. 2014;10(6):356–64. Available from: <http://www.ncbi.nlm.nih.gov/pubmed/24535546>
66. Menon R, Mesiano S, Taylor RN. Programmed Fetal Membrane Senescence and Exosome-Mediated Signaling: A Mechanism Associated With Timing of Human Parturition. *Front Endocrinol (Lausanne)* [Internet]. 2017 Aug 17;8(AUG):1–5. Available from: <http://journal.frontiersin.org/article/10.3389/fendo.2017.00196/full>
67. Sarker S, Scholz-Romero K, Perez A, Illanes SE, Mitchell MD, Rice GE, Salomon C. Placenta-derived exosomes continuously increase in maternal circulation over the first trimester of pregnancy. *J Transl Med* [Internet]. 2014;12(1):204. Available from: <http://www.ncbi.nlm.nih.gov/pubmed/25104112>
68. Salomon C, Scholz-Romero K, Sarker S, Sweeney E, Kobayashi M, Correa P, Longo S, Duncombe G, Mitchell MD, Rice GE, Illanes SE. Gestational Diabetes Mellitus Is Associated With Changes in the Concentration and Bioactivity of Placenta-Derived Exosomes in Maternal Circulation Across Gestation. *Diabetes*



- [Internet]. 2016 Mar;65(3):598–609. Available from: <http://www.ncbi.nlm.nih.gov/pubmed/26718504>
69. Salomon C, Ryan J, Sobrevia L, Kobayashi M, Ashman K, Mitchell M, Rice GE. Exosomal Signaling during Hypoxia Mediates Microvascular Endothelial Cell Migration and Vasculogenesis. *PLoS One*. 2013;8(7):1–24.
  70. Truong G, Guanzon D, Kinhall V, Elfeky O, Lai A, Longo S, Nuzhat Z, Palma C, Scholz-Romero K, Menon R, Mol BW, Rice GE, Salomon C. Oxygen tension regulates the miRNA profile and bioactivity of exosomes released from extravillous trophoblast cells-Liquid biopsies for monitoring complications of pregnancy. Vol. 12, *PLoS ONE*. 2017.
  71. Mitchell MD, Peiris HN, Kobayashi M, Koh YQ, Duncombe G, Illanes SE, Rice GE, Salomon C. Placental exosomes in normal and complicated pregnancy. *Am J Obstet Gynecol* [Internet]. 2015;213(4):S173–81. Available from: <http://linkinghub.elsevier.com/retrieve/pii/S0002937815007176>
  72. Stenqvist A-C, Nagaeva O, Baranov V, Mincheva-Nilsson L. Exosomes secreted by human placenta carry functional Fas ligand and TRAIL molecules and convey apoptosis in activated immune cells, suggesting exosome-mediated immune privilege of the fetus. *J Immunol* [Internet]. 2013;191(11):5515–23. Available from: <http://www.ncbi.nlm.nih.gov/pubmed/24184557>
  73. Atay S, Gercel-Taylor C, Kesimer M, Taylor DD. Morphologic and proteomic characterization of exosomes released by cultured extravillous trophoblast cells. *Exp Cell Res* [Internet]. 2011;317(8):1192–202. Available from: <http://dx.doi.org/10.1016/j.yexcr.2011.01.014>
  74. Kusama K, Nakamura K, Bai R, Nagaoka K, Sakurai T, Imakawa K. Intrauterine exosomes are required for bovine conceptus implantation. *Biochem Biophys Res Commun* [Internet]. 2018;495(1):1370–5. Available from: <https://doi.org/10.1016/j.bbrc.2017.11.176>
  75. Mincheva-Nilsson L, Baranov V. The Role of Placental Exosomes in Reproduction. *Am J Reprod Immunol*. 2010;63:520–33.
  76. Urbanelli L, Magini A, Buratta S, Brozzi A, Sagini K, Polchi A, Tancini B, Emiliani C. Signaling pathways in exosomes biogenesis, secretion and fate. *Genes (Basel)*. 2013;4(2):152–70.
  77. Ng YH, Rome S, Jalabert A, Forterre A, Singh H, Hincks CL, Salamonsen LA. Endometrial exosomes/microvesicles in the uterine microenvironment: a new paradigm for embryo-endometrial cross talk at implantation. *PLoS One* [Internet]. 2013;8(3):e58502. Available from: <http://www.ncbi.nlm.nih.gov/pubmed/23516492>
  78. Corrado C, Raimondo S, Chiesi A, Ciccia F, De Leo G, Alessandro R. Exosomes as intercellular signaling organelles involved in health and disease: Basic science and clinical applications. *Int J Mol Sci* [Internet]. 2013 Jan 6 [cited 2015 Jun 19];14(3):5338–66. Available from: <http://www.mdpi.com/1422-0067/14/3/5338/htm>

79. Rice GE, Scholz-Romero K, Sweeney E, Peiris H, Kobayashi M, Duncombe G, Mitchell MD, Salomon C. The Effect of Glucose on the Release and Bioactivity of Exosomes From First Trimester Trophoblast Cells. *J Clin Endocrinol Metab* [Internet]. 2015;100(10):E1280–8. Available from: <http://press.endocrine.org/doi/10.1210/jc.2015-2270>
80. Casey ML, MacDonald PC. The endocrinology of human parturition. *Ann N Y Acad Sci* [Internet]. 1997 Sep 26;828:273–84. Available from: <http://www.ncbi.nlm.nih.gov/pubmed/9329848>
81. Smith R, Mesiano S, McGrath S. Hormone trajectories leading to human birth. *Regul Pept.* 2002;108(2–3):159–64.
82. Phaneuf S AGLBARJE-FG. Parturition: activation of stimulatory pathways or loss of uterine quiescence? *Adv Exp Med Biol* [Internet]. 1995;395:435–51. Available from: <http://www.ncbi.nlm.nih.gov/pubmed/8713997>
83. Shynlova O, Tsui P, Jaffer S, Lye SJ. Integration of endocrine and mechanical signals in the regulation of myometrial functions during pregnancy and labour. *Eur J Obstet Gynecol Reprod Biol* [Internet]. 2009 May;144:S2–10. Available from: <http://www.sciencedirect.com/science/article/pii/S0301211509001341%5Cnhttp://www.ncbi.nlm.nih.gov/pubmed/19299064>
84. Shynlova O, Lee Y-H, Srikhajon K, Lye SJ. Physiologic uterine inflammation and labor onset: integration of endocrine and mechanical signals. *Reprod Sci* [Internet]. 2013 Feb 4;20(2):154–67. Available from: <http://www.ncbi.nlm.nih.gov/pubmed/22614625>
85. Fox H, Faulk WP. The placenta as an experimental model. *Clin Endocrinol Metab* [Internet]. 1981 Mar;10(1):57–72. Available from: <http://www.ncbi.nlm.nih.gov/pubmed/6261997>
86. Menon R, Yu J, Basanta-Henry P, Brou L, Berga SL, Fortunato SJ, Taylor RN. Short fetal leukocyte telomere length and preterm prelabor rupture of the membranes. *PLoS One.* 2012;7(2):1–6.
87. Menon R, Boldogh I, Urrabaz-Garza R, Poletini J, Syed TA, Saade GR, Papaconstantinou J, Taylor RN. Senescence of primary amniotic cells via oxidative DNA damage. *PLoS One* [Internet]. 2013;8(12):e83416. Available from: <http://www.ncbi.nlm.nih.gov/pubmed/24386195%5Cnhttp://www.ncbi.nlm.nih.gov/pmc/articles/PMC3873937/pdf/pone.0083416.pdf>
88. Poletini J, Behnia F, Taylor BD, Saade GR, Taylor RN, Menon R. Telomere Fragment Induced Amnion Cell Senescence: A Contributor to Parturition? Sun K, editor. *PLoS One* [Internet]. 2015 Sep 23;10(9):e0137188. Available from: <http://dx.plos.org/10.1371/journal.pone.0137188>
89. Menon R, Boldogh I, Hawkins HK, Woodson M, Poletini J, Syed TA, Fortunato SJ, Saade GR, Papaconstantinou J, Taylor RN. Histological Evidence of Oxidative Stress and Premature Senescence in Preterm Premature Rupture of the Human Fetal Membranes Recapitulated in Vitro. *Am J Pathol* [Internet]. 2014;184(6):1740–51. Available from:

<http://linkinghub.elsevier.com/retrieve/pii/S0002944014001643>

90. Menon R, Behnia F, Polettini J, Saade GR, Campisi J, Velarde M, Menon R, Behnia F, Polettini J, Saade GR, Campisi J, Velarde M. Placental membrane aging and HMGB1 signaling associated with human parturition. *Aging (Albany NY)* [Internet]. 2016 Feb 4;8(2):216–30. Available from: <http://www.ncbi.nlm.nih.gov/pubmed/26851389>
91. Menon R, Behnia F, Polettini J, Saade GR, Campisi J, Velarde M. Placental membrane aging and HMGB1 signaling associated with human parturition. *Aging (Albany NY)* [Internet]. 2016 Feb;8(2):216–30. Available from: <http://www.ncbi.nlm.nih.gov/pubmed/26851389>
92. Menon R, Bonney EA, Condon J, Mesiano S, Taylor RN. Novel concepts on pregnancy clocks and alarms: redundancy and synergy in human parturition. *Hum Reprod Update* [Internet]. 2016 Sep;22(5):535–60. Available from: <http://humupd.oxfordjournals.org/lookup/doi/10.1093/humupd/dmw022>
93. Behnia F, Sheller S, Menon R. Mechanistic Differences Leading to Infectious and Sterile Inflammation. *Am J Reprod Immunol* [Internet]. 2016 May;75(5):505–18. Available from: <http://doi.wiley.com/10.1111/aji.12496>
94. Ciucci A, Gabriele I, Percario ZA, Affabris E, Colizzi V, Mancino G. HMGB1 and cord blood: its role as immuno-adjuvant factor in innate immunity. *PLoS One* [Internet]. 2011;6(8):e23766. Available from: <http://www.ncbi.nlm.nih.gov/pubmed/21915243>
95. Tang D, Kang R, Zeh HJ, Lotze MT. High-mobility group box 1, oxidative stress, and disease. *Antioxid Redox Signal* [Internet]. 2011 Apr 1;14(7):1315–35. Available from: <http://www.liebertonline.com/doi/abs/10.1089/ars.2010.3356>
96. Andocs G, Meggyeshazi N, Balogh L, Spisak S, Maros ME, Balla P, Kiszner G, Teleki I, Kovago C, Krenacs T. Upregulation of heat shock proteins and the promotion of damage-associated molecular pattern signals in a colorectal cancer model by modulated electrohyperthermia. *Cell Stress Chaperones* [Internet]. 2015 Jan;20(1):37–46. Available from: <http://www.ncbi.nlm.nih.gov/pubmed/24973890>
97. Luong M, Zhang Y, Chamberlain T, Zhou T, Wright JF, Dower K, Hall JP. Stimulation of TLR4 by recombinant HSP70 requires structural integrity of the HSP70 protein itself. *J Inflamm (Lond)* [Internet]. 2012 Mar 26;9(1):11. Available from: <http://www.journal-inflammation.com/content/9/1/11>
98. Phimister EG, Phillippe M. Cell-free Fetal DNA — A Trigger for Parturition. *N Engl J Med* [Internet]. 2014;370(26):2534–6. Available from: <http://www.ncbi.nlm.nih.gov/pubmed/24963574>
99. Girard S, Heazell AEP, Derricott H, Allan SM, Sibley CP, Abrahams VM, Jones RL. Circulating cytokines and alarmins associated with placental inflammation in high-risk pregnancies. *Am J Reprod Immunol* [Internet]. 2014 Oct;72(4):422–34. Available from: <http://www.ncbi.nlm.nih.gov/pubmed/24867252>
100. Nadeau-Vallée M, Obari D, Palacios J, Brien M-È, Duval C, Chemtob S, Girard S. Sterile inflammation and pregnancy complications: a review. *Reproduction*

- [Internet]. 2016 Dec;152(6):R277–92. Available from:  
<http://www.ncbi.nlm.nih.gov/pubmed/27679863>
101. Mulla MJ, Myrtolli K, Potter J, Boeras C, Kavathas PB, Sfakianaki AK, Tadesse S, Norwitz ER, Guller S, Abrahams VM. Uric acid induces trophoblast IL-1 $\beta$  production via the inflammasome: implications for the pathogenesis of preeclampsia. *Am J Reprod Immunol* [Internet]. 2011 Jun;65(6):542–8. Available from: <http://doi.wiley.com/10.1111/j.1600-0897.2010.00960.x>
  102. Santoni G, Cardinali C, Morelli MB, Santoni M, Nabissi M, Amantini C. Danger- and pathogen-associated molecular patterns recognition by pattern-recognition receptors and ion channels of the transient receptor potential family triggers the inflammasome activation in immune cells and sensory neurons. *J Neuroinflammation* [Internet]. 2015 Feb 3;12:21. Available from: <http://www.pubmedcentral.nih.gov/articlerender.fcgi?artid=4322456&tool=pmcentrez&rendertype=abstract>
  103. Saïd-Sadier N, Ojcius DM. Alarmins, inflammasomes and immunity. *Biomed J* [Internet]. 2012;35(6):437–49. Available from: <http://www.ncbi.nlm.nih.gov/pubmed/23442356>
  104. Luo S-S, Ishibashi O, Ishikawa G, Ishikawa T, Katayama A, Mishima T, Takizawa T, Shigihara T, Goto T, Izumi A, Ohkuchi A, Matsubara S, Takeshita T, Takizawa T. Human Villous Trophoblasts Express and Secrete Placenta-Specific MicroRNAs into Maternal Circulation via Exosomes. *Biol Reprod* [Internet]. 2009;81(4):717–29. Available from: <http://www.biolreprod.org/cgi/doi/10.1095/biolreprod.108.075481>
  105. Lin J, Li J, Huang B, Liu J, Chen X, Chen X-M, Xu Y-M, Huang L-F, Wang X-Z. Exosomes: novel biomarkers for clinical diagnosis. *ScientificWorldJournal* [Internet]. 2015;2015:657086. Available from: [http://www.researchgate.net/publication/271515091\\_Review\\_Article\\_Exosomes\\_Novel\\_Biomarkers\\_for\\_Clinical\\_Diagnosis](http://www.researchgate.net/publication/271515091_Review_Article_Exosomes_Novel_Biomarkers_for_Clinical_Diagnosis)
  106. Frydrychowicz M, Kolecka-Bednarczyk a., Madejczyk M, Yasar S, Dworacki G. Exosomes - Structure, Biogenesis and Biological Role in Non-Small-Cell Lung Cancer. *Scand J Immunol* [Internet]. 2015;81(1):2–10. Available from: <http://doi.wiley.com/10.1111/sji.12247>
  107. Cai X, Janku F, Zhan Q, Fan J-B. Accessing Genetic Information with Liquid Biopsies. *Trends Genet* [Internet]. 2015;31(10):564–75. Available from: <http://linkinghub.elsevier.com/retrieve/pii/S0168952515001122>
  108. Rana S, Zöller M. Exosome target cell selection and the importance of exosomal tetraspanins: a hypothesis. *Biochem Soc Trans*. 2011;39(2):559–62.
  109. Raposo G, Stoorvogel W. Extracellular vesicles: exosomes, microvesicles, and friends. *J Cell Biol* [Internet]. 2013 Feb 18;200(4):373–83. Available from: <http://www.ncbi.nlm.nih.gov/pubmed/23420871>
  110. Stoorvogel W, Kleijmeer MJ, Geuze HJ, Raposo G. The biogenesis and functions of exosomes. *Traffic*. 2002;3(5):321–30.

111. Sabapatha A, Gercel-taylor C, Taylor DD. Specific isolation of placenta-derived exosomes from the circulation of pregnant women and their immunoregulatory consequences. *Am J Reprod Immunol*. 2006;56:345–55.
112. Salomon C, Torres MJ, Kobayashi M, Scholz-Romero K, Sobrevia L, Dobierzewska A, Illanes SE, Mitchell MD, Rice GE. A gestational profile of placental exosomes in maternal plasma and their effects on endothelial cell migration. *PLoS One* [Internet]. 2014;9(6):e98667. Available from: <http://www.pubmedcentral.nih.gov/articlerender.fcgi?artid=4048215&tool=pmcentrez&rendertype=abstract>
113. Salomon C, Yee S, Scholz-Romero K, Kobayashi M, Vaswani K, Kvaskoff D, Illanes SE, Mitchell MD, Rice GE. Extravillous trophoblast cells-derived exosomes promote vascular smooth muscle cell migration. *Front Pharmacol* [Internet]. 2014;5(August):175. Available from: <http://www.pubmedcentral.nih.gov/articlerender.fcgi?artid=4128075&tool=pmcentrez&rendertype=abstract>
114. Ouyang Y, Mouillet JF, Coyne CB, Sadovsky Y. Review: Placenta-specific microRNAs in exosomes - Good things come in nano-packages. *Placenta* [Internet]. 2014;35(SUPPL):S69–73. Available from: <http://dx.doi.org/10.1016/j.placenta.2013.11.002>
115. Donker RB, Mouillet JF, Chu T, Hubel CA, Stolz DB, Morelli AE, Sadovsky Y. The expression profile of C19MC microRNAs in primary human trophoblast cells and exosomes. *Mol Hum Reprod* [Internet]. 2012;18(8):417–24. Available from: <http://www.molehr.oxfordjournals.org/cgi/doi/10.1093/molehr/gas013>
116. Sadovsky Y, Mouillet J, Ouyang Y, Bayer A. The Function of TrophomiRs and Other MicroRNAs in the Human Placenta. 2015;
117. Salomon C, Kobayashi M, Ashman K, Sobrevia L, Mitchell MD, Rice GE. Hypoxia-induced changes in the bioactivity of cytotrophoblast-derived exosomes. *PLoS One* [Internet]. 2013;8(11):e79636. Available from: <http://www.pubmedcentral.nih.gov/articlerender.fcgi?artid=3823597&tool=pmcentrez&rendertype=abstract>
118. Poletti J, Silva MG, Kacerovsky M, Syed TA, Saade G, Menon R. Expression profiles of fetal membrane nicotinamide adenine dinucleotide phosphate oxidases (NOX) 2 and 3 differentiates spontaneous preterm birth and pPROM pathophysiology. *Placenta* [Internet]. 2014;35(3):188–94. Available from: <http://www.ncbi.nlm.nih.gov/pubmed/24439294>
119. Poletti J, Silva M, Syed T, Saade G, Menon R. 828: Screening of lysyl oxidase (LOX) and lysyl oxidase-like (LOXL) enzyme expression and activity in human fetal membranes. *Am J Obstet Gynecol* [Internet]. 2014;210(1):S402–3. Available from: <http://linkinghub.elsevier.com/retrieve/pii/S0002937813019261>
120. Noppe G, Dekker P, De Koning-Treurniet C, Blom J, Van Heemst D, Dirks RW, Tanke HJ, Westendorp RGJ, Maier AB. Rapid flow cytometric method for measuring senescence associated  $\beta$ -galactosidase activity in human fibroblasts. *Cytom Part A* [Internet]. 2009 Nov [cited 2015 Jun 4];75(11):910–6. Available

from: <http://www.ncbi.nlm.nih.gov/pubmed/19777541>

121. Cho S, Hwang ES. Fluorescence-Based Detection and Quantification of Features of Cellular Senescence. *Methods Cell Biol* [Internet]. 2011 Jan [cited 2015 Oct 25];103:149–88. Available from: <http://linkinghub.elsevier.com/retrieve/pii/B9780123854933000073>
122. Lässer C, Eldh M, Lötvall J. Isolation and characterization of RNA-containing exosomes. *J Vis Exp* [Internet]. 2012;(59):e3037. Available from: <http://www.pubmedcentral.nih.gov/articlerender.fcgi?artid=3369768&tool=pmcentrez&rendertype=abstract>
123. Bullerdiek J, Flor I. Exosome-delivered microRNAs of “chromosome 19 microRNA cluster” as immunomodulators in pregnancy and tumorigenesis. *Mol Cytogenet*. 2012;5:27.
124. Sheller-Miller S, Lei J, Saade G, Salomon C, Burd I, Menon R, Wong RJ. Feto-Maternal Trafficking of Exosomes in Murine Pregnancy Models. *Front Pharmacol* [Internet]. 2016 Nov 15;7(November):1–10. Available from: <http://journal.frontiersin.org/article/10.3389/fphar.2016.00432/full>
125. Sheller S, Papaconstantinou J, Urrabaz-Garza R, Richardson L, Saade G, Salomon C, Menon R. Amnion-Epithelial-Cell-Derived Exosomes Demonstrate Physiologic State of Cell under Oxidative Stress. *PLoS One* [Internet]. 2016;11(6):e0157614. Available from: <http://dx.plos.org/10.1371/journal.pone.0157614>
126. de Menezes-Neto A, Sáez MJF, Lozano-Ramos I, Segui-Barber J, Martin-Jaular L, Ullate JME, Fernandez-Becerra C, Borrás FE, Del Portillo HA. Size-exclusion chromatography as a stand-alone methodology identifies novel markers in mass spectrometry analyses of plasma-derived vesicles from healthy individuals. *J Extracell vesicles* [Internet]. 2015;4(4):27378. Available from: <http://www.pubmedcentral.nih.gov/articlerender.fcgi?artid=4495624&tool=pmcentrez&rendertype=abstract>
127. Bolger AM, Lohse M, Usadel B. Trimmomatic: a flexible trimmer for Illumina sequence data. *Bioinformatics* [Internet]. 2014 Aug 1;30(15):2114–20. Available from: <http://www.ncbi.nlm.nih.gov/pubmed/24695404>
128. Krzywinski M, Schein J, Birol I, Connors J, Gascoyne R, Horsman D, Jones SJ, Marra MA. Circos: an information aesthetic for comparative genomics. *Genome Res* [Internet]. 2009 Sep;19(9):1639–45. Available from: [http://circos.ca/intro/genomic\\_data/](http://circos.ca/intro/genomic_data/)
129. Debacq-Chainiaux F, Erusalimsky JD, Campisi J, Toussaint O. Protocols to detect senescence-associated beta-galactosidase (SA- $\beta$ gal) activity, a biomarker of senescent cells in culture and in vivo. *Nat Protoc* [Internet]. 2009;4(12):1798–806. Available from: <http://www.nature.com/doifinder/10.1038/nprot.2009.191>
130. Winther K, Thermofischer P. Direct Isolation of Exosomes from Cell Culture : Simplifying Methods for Exosome Enrichment and Analysis iMedPub Journals Direct Isolation of Exosomes from Cell Culture : Simplifying Methods for Exosome Enrichment and Analysis Abstract. 2015;(AUGUST).

131. Andreu Z, Yáñez-Mó M. Tetraspanins in Extracellular Vesicle Formation and Function. *Front Immunol* [Internet]. 2014;5(September):1–12. Available from: <http://journal.frontiersin.org/article/10.3389/fimmu.2014.00442/abstract>
132. Karrasch T, Steinbrecher KA, Allard B, Baldwin AS, Jobin C. Wound-induced p38MAPK-dependent histone H3 phosphorylation correlates with increased COX-2 expression in enterocytes. *J Cell Physiol* [Internet]. 2006 Jun;207(3):809–15. Available from: <http://doi.wiley.com/10.1002/jcp.20626>
133. Valbonesi P, Ricci L, Franzellitti S, Biondi C, Fabbri E. Effects of cadmium on MAPK signalling pathways and HSP70 expression in a human trophoblast cell line. *Placenta* [Internet]. 2008;29(8):725–33. Available from: <http://www.ncbi.nlm.nih.gov/pubmed/18571719>
134. Derynck R, Muthusamy BP, Saetern KY. Signaling pathway cooperation in TGF- $\beta$ -induced epithelial-mesenchymal transition. *Curr Opin Cell Biol* [Internet]. 2014 Dec;31:56–66. Available from: <http://www.ncbi.nlm.nih.gov/pubmed/25240174>
135. Papageorgis P. TGF $\beta$  Signaling in Tumor Initiation, Epithelial-to-Mesenchymal Transition, and Metastasis. *J Oncol* [Internet]. 2015;2015:587193. Available from: <http://www.ncbi.nlm.nih.gov/pubmed/25883652>
136. Fabregat I, Malfettone A, Soukupova J. New Insights into the Crossroads between EMT and Stemness in the Context of Cancer. *J Clin Med* [Internet]. 2016;5(3). Available from: <http://www.ncbi.nlm.nih.gov/pubmed/26985909>
137. Da C, Liu Y, Zhan Y, Liu K, Wang R. Nobiletin inhibits epithelial-mesenchymal transition of human non-small cell lung cancer cells by antagonizing the TGF- $\beta$ 1/Smad3 signaling pathway. *Oncol Rep* [Internet]. 2016 May;35(5):2767–74. Available from: <http://www.ncbi.nlm.nih.gov/pubmed/26986176>
138. Yeh Y-H, Wang S-W, Yeh Y-C, Hsiao H-F, Li T-K. Rhapontigenin inhibits TGF- $\beta$ -mediated epithelial-mesenchymal transition via the PI3K/AKT/mTOR pathway and is not associated with HIF-1 $\alpha$  degradation. *Oncol Rep* [Internet]. 2016 May 9;35(5):2887–95. Available from: <http://www.spandidos-publications.com/10.3892/or.2016.4664>
139. Romero R, Kusanovic JP, Gomez R, Lamont R, Bytautiene E, Garfield RE, Mittal P, Hassan SS, Yeo L. The clinical significance of eosinophils in the amniotic fluid in preterm labor. *J Matern Fetal Neonatal Med* [Internet]. 2010 Apr;23(4):320–9. Available from: <http://www.ncbi.nlm.nih.gov/pubmed/19900034>
140. Menon R, Fortunato SJ, Milne GL, Brou L, Carnevale C, Sanchez SC, Hubbard L, Drobek CO, Taylor RN. Amniotic fluid eicosanoids in preterm and term births: effects of risk factors for spontaneous preterm labor. *Obstet Gynecol*. 2011;118(1):121–34.
141. Harding C V., Heuser JE, Stahl PD. Exosomes: Looking back three decades and into the future. *J Cell Biol*. 2013;200(4):367–71.
142. Hornung D, Lebovic DI, Shifren JL, Vigne JL, Taylor RN. Vectorial secretion of vascular endothelial growth factor by polarized human endometrial epithelial cells. *FertilSteril*. 1998;69(5):909–15.

143. Mesiano S. Myometrial progesterone responsiveness. *Semin Reprod Med*. 2007;25(1):5–13.
144. Mesiano S, Wang Y, Norwitz ER. Progesterone receptors in the human pregnancy uterus: do they hold the key to birth timing? *Reprod Sci* [Internet]. 2011;18(1):6–19. Available from: <http://rsx.sagepub.com/content/18/1/6.abstract>
145. Dressing GE, Knutson TP, Schiewer MJ, Daniel AR, Hagan CR, Diep CH, Knudsen KE, Lange CA. Progesterone receptor-cyclin D1 complexes induce cell cycle-dependent transcriptional programs in breast cancer cells. *Mol Endocrinol* [Internet]. 2014;28(4):442–57. Available from: <http://www.ncbi.nlm.nih.gov/pubmed/24606123>
146. Beck C a., Zhang Y, Altmann M, Weigel NL, Edwards DP. Stoichiometry and Site-specific Phosphorylation of Human Progesterone Receptor in Native Target Cells and in the Baculovirus Expression System. *J Biol Chem* [Internet]. 1996;271(32):19546–55. Available from: <http://www.jbc.org/cgi/doi/10.1074/jbc.271.32.19546>
147. Beck CA, Zhang Y, Weigel NL, Edwards DP. Two Types of Anti-progestins Have Distinct Effects on Site-specific Phosphorylation of Human Progesterone Receptor. *J Biol Chem* [Internet]. 1996;271(2):1209–17. Available from: <http://www.jbc.org/content/271/2/1209.full>
148. Zhang Y, Beck CA, Poletti A, Edwards DP, Weigel NL. Identification of a group of Ser-Pro motif hormone-inducible phosphorylation sites in the human progesterone receptor [Internet]. Vol. 9, *Mol Endocrinol*. 1995. p. 1029–40. Available from: [http://www.ncbi.nlm.nih.gov/entrez/query.fcgi?cmd=Retrieve&db=PubMed&dopt=Citation&list\\_uids=7476977](http://www.ncbi.nlm.nih.gov/entrez/query.fcgi?cmd=Retrieve&db=PubMed&dopt=Citation&list_uids=7476977)
149. Delorme-Axford E, Bayer A, Sadovsky Y, Coyne CB. Autophagy as a mechanism of antiviral defense at the maternal-fetal interface. *Autophagy*. 2013;9(12):2173–4.
150. Li JYZ, Yong TY, Michael MZ, Gleadle JM. MicroRNAs: are they the missing link between hypoxia and pre-eclampsia? *Hypertens pregnancy* [Internet]. 2014;33(1):102–14. Available from: <http://www.ncbi.nlm.nih.gov/pubmed/24354525>
151. Vargas A, Zhou S, Ethier-Chiasson M, Flipo D, Lafond J, Gilbert C, Barbeau B. Syncytin proteins incorporated in placenta exosomes are important for cell uptake and show variation in abundance in serum exosomes from patients with preeclampsia. *FASEB J* [Internet]. 2014;28(8):3703–19. Available from: <http://www.fasebj.org/cgi/doi/10.1096/fj.13-239053>
152. Kambe S, Yoshitake H, Yuge K, Ishida Y, Ali MM, Takizawa T, Kuwata T, Ohkuchi A, Matsubara S, Suzuki M, Takeshita T, Saito S, Takizawa T. Human exosomal placenta-associated miR-517a-3p modulates the expression of PRKG1 mRNA in Jurkat cells. *Biol Reprod* [Internet]. 2014;91(5):129. Available from: <http://www.ncbi.nlm.nih.gov/pubmed/25273530>
153. Mincheva-Nilsson L, Baranov V. Placenta-Derived Exosomes and



- Syncytiotrophoblast Microparticles and their Role in Human Reproduction: Immune Modulation for Pregnancy Success. *Am J Reprod Immunol* [Internet]. 2014;72(5):440–57. Available from: <http://doi.wiley.com/10.1111/aji.12311>
154. Record M. Intercellular communication by exosomes in placenta: A possible role in cell fusion? *Placenta* [Internet]. 2014;35(5):297–302. Available from: <http://dx.doi.org/10.1016/j.placenta.2014.02.009>
  155. Kshirsagar SK, Alam SM, Jasti S, Hodes H, Nauser T, Gilliam M, Billstrand C, Hunt JS, Petroff MG. Immunomodulatory molecules are released from the first trimester and term placenta via exosomes. *Placenta* [Internet]. 2012;33(12):982–90. Available from: <http://www.pubmedcentral.nih.gov/articlerender.fcgi?artid=3534832&tool=pmcentrez&rendertype=abstract>
  156. Southcombe J, Tannetta D, Redman C, Sargent I. The immunomodulatory role of syncytiotrophoblast microvesicles. *PLoS One* [Internet]. 2011;6(5):e20245. Available from: <http://www.pubmedcentral.nih.gov/articlerender.fcgi?artid=3102084&tool=pmcentrez&rendertype=abstract>
  157. Atay S, Gercel-Taylor C, Suttles J, Mor G, Taylor DD. Trophoblast-derived exosomes mediate monocyte recruitment and differentiation. *Am J Reprod Immunol*. 2011;65:65–77.
  158. Atay S, Gercel-Taylor C, Taylor DD. Human trophoblast-derived exosomal fibronectin induces pro-inflammatory IL-1 $\beta$  production by macrophages. *Am J Reprod Immunol*. 2011;66(4):259–69.
  159. Redman CWG, Sargent IL. Circulating Microparticles in Normal Pregnancy and Pre-Eclampsia. *Placenta*. 2008;29(SUPPL.):73–7.
  160. Redman CWG, Tannetta DS, Dragovic R a., Gardiner C, Southcombe JH, Collett GP, Sargent IL. Review: Does size matter? Placental debris and the pathophysiology of pre-eclampsia. *Placenta* [Internet]. 2012;33(SUPPL.):S48–54. Available from: <http://dx.doi.org/10.1016/j.placenta.2011.12.006>
  161. Salomon C, Yee SW, Mitchell MD, Rice GE. The Possible Role of Extravillous Trophoblast-Derived Exosomes on the Uterine Spiral Arterial Remodeling under Both Normal and Pathological Conditions. *Biomed Res Int* [Internet]. 2014;2014:1–10. Available from: <http://www.hindawi.com/journals/bmri/2014/693157/>
  162. Kobayashi M, Salomon C, Tapia J, Illanes SE, Mitchell MD, Rice GE. Ovarian cancer cell invasiveness is associated with discordant exosomal sequestration of Let-7 miRNA and miR-200. *J Transl Med* [Internet]. 2014;12:4. Available from: <http://www.pubmedcentral.nih.gov/articlerender.fcgi?artid=3896684&tool=pmcentrez&rendertype=abstract>
  163. Migale R, Herbert BR, Lee YS, Sykes L, Waddington SN, Peebles D, Hagberg H, Johnson MR, Bennett PR, MacIntyre DA. Specific Lipopolysaccharide Serotypes Induce Differential Maternal and Neonatal Inflammatory Responses in a Murine

- Model of Preterm Labor. *Am J Pathol* [Internet]. 2015;185(9):2390–401. Available from: <http://dx.doi.org/10.1016/j.ajpath.2015.05.015>
164. Smith R. Alterations in the hypothalamic pituitary adrenal axis during pregnancy and the placental clock that determines the length of parturition. *J Reprod Immunol*. 1998;39(1–2):215–20.
  165. You X, Liu J, Xu C, Liu W, Zhu X, Li Y, Sun Q, Gu H, Ni X. Corticotropin-Releasing Hormone (CRH) promotes inflammation in human pregnant myometrium: The evidence of CRH initiating parturition? *J Clin Endocrinol Metab*. 2014;99(2):199–208.
  166. Golightly E, Jabbour HN, Norman JE. Endocrine immune interactions in human parturition. *Mol Cell Endocrinol* [Internet]. 2011;335(1):52–9. Available from: <http://dx.doi.org/10.1016/j.mce.2010.08.005>
  167. Dutta EH, Behnia F, Boldogh I, Saade GR, Taylor BD, Kacerovský M, Menon R. Oxidative stress damage-associated molecular signaling pathways differentiate spontaneous preterm birth and preterm premature rupture of the membranes. *Mol Hum Reprod*. 2015;22(2):143–57.
  168. Gomez-Lopez N, Romero R, Plazyo O, Schwenkel G, Garcia-Flores V, Unkel R, Xu Y, Leng Y, Hassan SS, Panaitescu B, Cha J, Dey SK. Preterm labor in the absence of acute histologic chorioamnionitis is characterized by cellular senescence of the chorioamniotic membranes. *Am J Obstet Gynecol* [Internet]. 2017;217(5):592.e1-592.e17. Available from: <https://doi.org/10.1016/j.ajog.2017.08.008>
  169. Friel LA, Romero R, Edwin S, Nien JK, Gomez R, Chaiworapongsa T, Kusanovic JP, Tolosa JE, Hassan SS, Espinoza J. The calcium binding protein, S100B, is increased in the amniotic fluid of women with intra-amniotic infection/inflammation and preterm labor with intact or ruptured membranes. *J Perinat Med* [Internet]. 2007;35(5):385–93. Available from: <http://www.ncbi.nlm.nih.gov/pubmed/17624933>
  170. T. C, O. E, J.P. K, E. V, S. M-T, F. G, N.G. T, P. M, Y.M. K, N. C, S. E, R. G, S.S. H, R. R, Chaiworapongsa T, Erez O, Kusanovic JP, Vaisbuch E, Mazaki-Tovi S, Gotsch F, Than NG, Mittal P, Kim YM, Camacho N, Edwin S, Gomez R, Hassan SS, Romero R. Amniotic fluid heat shock protein 70 concentration in histologic chorioamnionitis, term and preterm parturition. *J Matern Neonatal Med* [Internet]. 2008;21(7):449–61. Available from: <http://www.pubmedcentral.nih.gov/articlerender.fcgi?artid=2517420&tool=pmcentrez&rendertype=abstract%5Cnhttp://www.embase.com/search/results?subaction=viewrecord&from=export&id=L352000664%5Cnhttp://dx.doi.org/10.1080/14767050802054550%5Cnhttp://sfx.librar>
  171. Romero R, Chaiworapongsa T, Alpay Savasan Z, Xu Y, Hussein Y, Dong Z, Kusanovic JP, Kim CJ, Hassan SS. Damage-associated molecular patterns (DAMPs) in preterm labor with intact membranes and preterm PROM: a study of the alarmin HMGB1. *J Matern Fetal Neonatal Med* [Internet]. 2011 Dec;24(12):1444–55. Available from:

<http://www.ncbi.nlm.nih.gov/pubmed/21958433>

172. Plazyo O, Romero R, Unkel R, Balancio A, Mial TN, Xu Y, Dong Z, Hassan SS, Gomez-Lopez N. HMGB1 Induces an Inflammatory Response in the Chorioamniotic Membranes That Is Partially Mediated by the Inflammasome. *Biol Reprod* [Internet]. 2016;95(6):130–130. Available from: <https://academic.oup.com/biolreprod/article-lookup/doi/10.1095/biolreprod.116.144139>
173. Phillippe M. Cell-free fetal DNA, telomeres, and the spontaneous onset of parturition. *Reprod Sci*. 2015;22(10):1186–201.
174. Gomez-Lopez N, Romero R, Plazyo O, Panaitescu B, Furcron AE, Miller D, Roumayah T, Flom E, Hassan SS. Intra-Amniotic Administration of HMGB1 Induces Spontaneous Preterm Labor and Birth. *Am J Reprod Immunol* [Internet]. 2016 Jan;75(1):3–7. Available from: <http://doi.wiley.com/10.1111/aji.12443>
175. Eldh M, Ekström K, Valadi H, Sjöstrand M, Olsson B, Jernås M, Lötvall J. Exosomes Communicate Protective Messages during Oxidative Stress; Possible Role of Exosomal Shuttle RNA. *PLoS One*. 2010;5(12):1–8.
176. Verweij FJ, Middeldorp JM, Pegtel DM. Intracellular signaling controlled by the endosomal-exosomal pathway. *Commun Integr Biol* [Internet]. 2012 Jan 1;5(1):88–93. Available from: <http://www.ncbi.nlm.nih.gov/pubmed/22482020>
177. Krause M, Rak-Raszewska A, Naillat F, Saarela U, Schmidt C, Ronkainen V-P, Bart G, Ylä-Herttuala S, Vainio SJ. Exosomes as secondary inductive signals involved in kidney organogenesis. *J Extracell Vesicles* [Internet]. 2018;7(1):1422675. Available from: <https://www.tandfonline.com/doi/full/10.1080/20013078.2017.1422675>
178. Hayashi T, Hoffman MP. Exosomal microRNA communication between tissues during organogenesis. *RNA Biol*. 2017;14(12):1683–9.
179. Mallegol J, Van Niel G, Heyman M. Phenotypic and functional characterization of intestinal epithelial exosomes. *Blood Cells, Mol Dis*. 2005;35(1):11–6.
180. Lin XP, Almqvist N, Telemo E. Human small intestinal epithelial cells constitutively express the key elements for antigen processing and the production of exosomes. *Blood Cells, Mol Dis*. 2005;35(2):122–8.
181. Lakkaraju A, Rodriguez-Boulan E. Itinerant exosomes: emerging roles in cell and tissue polarity. *Trends Cell Biol* [Internet]. 2008 May;18(5):199–209. Available from: <http://www.ncbi.nlm.nih.gov/pubmed/18396047>
182. van Niel G, Heyman M. The epithelial cell cytoskeleton and intracellular trafficking. II. Intestinal epithelial cell exosomes: perspectives on their structure and function. *Am J Physiol Gastrointest Liver Physiol* [Internet]. 2002;283(2):G251-5. Available from: [http://www.ncbi.nlm.nih.gov/entrez/query.fcgi?cmd=Retrieve&db=PubMed&dopt=Citation&list\\_uids=12121870](http://www.ncbi.nlm.nih.gov/entrez/query.fcgi?cmd=Retrieve&db=PubMed&dopt=Citation&list_uids=12121870)
183. Rodriguez-Boulan E, Kreitzer G, Müsch A. Organization of vesicular trafficking

- in epithelia. *Nat Rev Mol Cell Biol.* 2005;6(3):233–47.
184. Condon J, Yin S, Mayhew B, Word RA, Wright WE, Shay JW, Rainey WE. Telomerase immortalization of human myometrial cells. *Biol Reprod* [Internet]. 2002;67(2):506–14. Available from: <http://www.ncbi.nlm.nih.gov/pubmed/12135889>
  185. Kudo Y, Boyd CAR, Kimura H, Cook PR, Redman CWG, Sargent IL. Quantifying the syncytialisation of human placental trophoblast BeWo cells grown in vitro. *Biochim Biophys Acta - Mol Cell Res.* 2003;1640(1):25–31.
  186. Gauster M, Huppertz B. The paradox of caspase 8 in human villous trophoblast fusion. *Placenta* [Internet]. 2010;31(2):82–8. Available from: <http://dx.doi.org/10.1016/j.placenta.2009.12.007>
  187. Hadley EE, Richardson LS, Torloni MR, Menon R. Gestational tissue inflammatory biomarkers at term labor: A systematic review of literature. *Am J Reprod Immunol.* 2017;(September):e12776.
  188. Myatt L, Sun K. Role of fetal membranes in signaling of fetal maturation and parturition. *Int J Dev Biol.* 2010;54(2–3):545–53.
  189. Norwitz ER, Bonney EA, Snegovskikh V V., Williams MA, Phillippe M, Park JS, Abrahams VM. Molecular regulation of parturition: The role of the decidual clock. *Cold Spring Harb Perspect Med.* 2015;5(11):1–20.
  190. El-Azzamy H, Balogh A, Romero R, Xu Y, LaJeunesse C, Plazyo O, Xu Z, Price TG, Dong Z, Tarca AL, Papp Z, Hassan SS, Chaiworapongsa T, Kim CJ, Gomez-Lopez N, Than NG. Characteristic Changes in Decidual Gene Expression Signature in Spontaneous Term Parturition. *J Pathol Transl Med* [Internet]. 2017;51(3):264–83. Available from: <http://www.ncbi.nlm.nih.gov/pubmed/28226203> <http://www.pubmedcentral.nih.gov/articlerender.fcgi?artid=PMC5445200> <http://jpatholm.org/journal/view.php?doi=10.4132/jptm.2016.12.20>
  191. Unal ER, Cierny JT, Roedner C, Newman R, Goetzl L. Maternal inflammation in spontaneous term labor. *Am J Obstet Gynecol* [Internet]. 2011;204(3):223.e1–223.e5. Available from: <http://dx.doi.org/10.1016/j.ajog.2011.01.002>
  192. Gomez-Lopez N, Romero R, Xu Y, Garcia-Flores V, Leng Y, Panaitescu B, Miller D, Abrahams VM, Hassan SS. Inflammasome assembly in the chorioamniotic membranes during spontaneous labor at term. *Am J Reprod Immunol.* 2017;77(5):1–10.
  193. Halstead JM, Lionnet T, Wilbertz JH, Wippich F, Ephrussi A, Singer RH, Chao JA. Translation. An RNA biosensor for imaging the first round of translation from single cells to living animals. *Science* [Internet]. 2015 Mar 20;347(6228):1367–671. Available from: <http://www.ncbi.nlm.nih.gov/pubmed/25792328>
  194. Iliodromiti Z, Antonakopoulos N, Sifakis S, Tsikouras P, Daniilidis A, Dafopoulos K, Botsis D, Vrachnis N. Endocrine, paracrine, and autocrine placental mediators in labor. *Hormones.* 2012;11(4):397–409.

195. Menon R. Human fetal membranes at term: Dead tissue or signalers of parturition? Vol. 44, Placenta. 2016. p. 1–5.
196. Fuxe J, Karlsson MCI. TGF- $\beta$ -induced epithelial-mesenchymal transition: A link between cancer and inflammation. *Semin Cancer Biol* [Internet]. 2012;22(5–6):455–61. Available from: <http://dx.doi.org/10.1016/j.semcancer.2012.05.004>
197. Epstein Shochet G, Tartakover-Matalon S, Drucker L, Pasmanik-Chor M, Pomeranz M, Fishman A, Lishner M. Placenta-breast cancer cell interactions promote cancer cell epithelial mesenchymal transition via TGF $\beta$ /JNK pathway. *Clin Exp Metastasis*. 2014;31(8):961–75.
198. Alcaraz A, Mrowiec A, Insausti CL, García-Vizcaíno EM, Ruiz-Canada C, López-Martínez MC, Moraleda JM, Nicolás FJ. Autocrine TGF- $\beta$  induces epithelial to mesenchymal transition in human amniotic epithelial cells. *Cell Transplant*. 2013;22(8):1351–67.
199. Kalluri R, Weinberg R a. Review series The basics of epithelial-mesenchymal transition. *J Clin Invest*. 2009;119(6):1420–8.
200. Janzen C, Sen S, Lei MYY, Gagliardi de Assumpcao M, Challis J, Chaudhuri G. The Role of Epithelial to Mesenchymal Transition in Human Amniotic Membrane Rupture. *J Clin Endocrinol Metab* [Internet]. 2016;102(April 2017):jc.2016-3150. Available from: <https://academic.oup.com/jcem/article-lookup/doi/10.1210/jc.2016-3150>
201. Khan JA, Amazit L, Bellance C, Guiochon-Mantel A, Lombès M, Loosfelt H. p38 and p42/44 MAPKs Differentially Regulate Progesterone Receptor A and B Isoform Stabilization. *Mol Endocrinol* [Internet]. 2011;25(10):1710–24. Available from: <https://academic.oup.com/mend/article-lookup/doi/10.1210/me.2011-1042>
202. Koh YQ, Chan HW, Nitert MD, Vaswani K, Mitchell MD, Rice GE. Differential response to lipopolysaccharide by JEG-3 and BeWo human choriocarcinoma cell lines. *Eur J Obstet Gynecol Reprod Biol* [Internet]. 2014;175(1):129–33. Available from: <http://dx.doi.org/10.1016/j.ejogrb.2013.12.032>
203. Purushothaman A, Bandari SK, Liu J, Mobley JA, Brown EE, Sanderson RD. Fibronectin on the Surface of Myeloma Cell-derived Exosomes Mediates Exosome-Cell Interactions. *J Biol Chem* [Internet]. 2016 Jan 22;291(4):1652–63. Available from: <http://www.jbc.org/lookup/doi/10.1074/jbc.M115.686295>
204. Christianson HC, Svensson KJ, van Kuppevelt TH, Li J-P, Belting M. Cancer cell exosomes depend on cell-surface heparan sulfate proteoglycans for their internalization and functional activity. *Proc Natl Acad Sci U S A* [Internet]. 2013;110(43):17380–5. Available from: <http://www.pubmedcentral.nih.gov/articlerender.fcgi?artid=3808637&tool=pmcentrez&rendertype=abstract>
205. Prada I, Meldolesi J. Binding and fusion of extracellular vesicles to the plasma membrane of their cell targets. *Int J Mol Sci*. 2016;17(8).
206. Mulcahy LA, Pink RC, Carter DRF. Routes and mechanisms of extracellular vesicle uptake. *J Extracell vesicles* [Internet]. 2014;3:1–14. Available from:

<http://www.pubmedcentral.nih.gov/articlerender.fcgi?artid=4122821&tool=pmcentrez&rendertype=abstract>

207. Zech D, Rana S, Büchler MW, Zöller M. Tumor-exosomes and leukocyte activation: An ambivalent crosstalk. *Cell Commun Signal*. 2012;10:1–17.
208. Morelli AE, Larregina AT, Shufesky WJ, Sullivan MLG, Stolz DB, Papworth GD, Zahorchak AF, Logar AJ, Wang Z, Watkins SC, Falo LD, Thomson AW. Endocytosis, intracellular sorting, and processing of exosomes by dendritic cells. *Blood*. 2004;104(10):3257–66.
209. Escrevente C, Keller S, Altevogt P, Costa J. Interaction and uptake of exosomes by ovarian cancer cells. *BMC Cancer* [Internet]. 2011;11(1):108. Available from: <http://www.biomedcentral.com/1471-2407/11/108>
210. Rodríguez M, Silva J, López-Alfonso A, López-Muñiz MB, Peña C, Domínguez G, García JM, López-González A, Méndez M, Provencio M, García V, Bonilla F. Different exosome cargo from plasma/bronchoalveolar lavage in non-small-cell lung cancer. *Genes, Chromosom Cancer* [Internet]. 2014 Apr 25 [cited 2015 Oct 7];53(9):n/a-n/a. Available from: <http://www.ncbi.nlm.nih.gov/pubmed/24764226>
211. Gomez-Lopez N, StLouis D, Lehr MA, Sanchez-Rodriguez EN, Arenas-Hernandez M. Immune cells in term and preterm labor. *Cell Mol Immunol* [Internet]. 2014;11(6):571–81. Available from: <http://www.pubmedcentral.nih.gov/articlerender.fcgi?artid=4220837&tool=pmcentrez&rendertype=abstract>
212. Srikhajon K, Shynlova O, Preechapornprasert A, Chanrachakul B, Lye S. A New Role for Monocytes in Modulating Myometrial Inflammation During Human Labor. *Biol Reprod* [Internet]. 2014;91(1):10–10. Available from: <http://www.biolreprod.org/cgi/doi/10.1095/biolreprod.113.114975>
213. Raimondo F, Morosi L, Chinello C, Magni F, Pitto M. Advances in membranous vesicle and exosome proteomics improving biological understanding and biomarker discovery. *Proteomics*. 2011;11(4):709–20.
214. Soo CY, Song Y, Zheng Y, Campbell EC, Riches AC, Gunn-Moore F, Powis SJ. Nanoparticle tracking analysis monitors microvesicle and exosome secretion from immune cells. *Immunology*. 2012;136(2):192–7.
215. Bátiz LF, Castro MA, Burgos P V, Velásquez ZD, Muñoz RI, Lafourcade CA, Troncoso-Escudero P, Wyneken U. Exosomes as Novel Regulators of Adult Neurogenic Niches. *Front Cell Neurosci* [Internet]. 2015;9(January):501. Available from: <http://journal.frontiersin.org/article/10.3389/fncel.2015.00501/abstract>
216. Willms E, Johansson HJ, Mäger I, Lee Y, Blomberg KEM, Sadik M, Alaarg A, Smith CIE, Lehtiö J, El Andaloussi S, Wood MJA, Vader P. Cells release subpopulations of exosomes with distinct molecular and biological properties. *Sci Rep* [Internet]. 2016;6(February):22519. Available from: <http://www.pubmedcentral.nih.gov/articlerender.fcgi?artid=4773763&tool=pmcentrez&rendertype=abstract>

217. Dudley DJ, Edwin SS, Mitchell MD. Macrophage inflammatory protein-I alpha regulates prostaglandin E2 and interleukin-6 production by human gestational tissues in vitro. *J Soc Gynecol Invest* [Internet]. 1996;3(1):12–6. Available from: <http://www.ncbi.nlm.nih.gov/pubmed/8796800>
218. Wood CE, Keller-Wood M. The critical importance of the fetal hypothalamus-pituitary-adrenal axis. *F1000Research* [Internet]. 2016;5(0):1–7. Available from: <http://f1000research.com/articles/5-115/v1>
219. Martin JA, Hamilton BE, Osterman MJKS. Births in the United States, 2016 Key findings Data from the National Vital Statistics System. 2016;(287):1–8. Available from: [https://www.cdc.gov/nchs/data/databriefs/db287\\_table.pdf#1](https://www.cdc.gov/nchs/data/databriefs/db287_table.pdf#1).
220. Shapiro-Mendoza CK, Barfield WD, Henderson Z, James A, Howse JL, Iskander J, Thorpe PG. CDC Grand Rounds: Public Health Strategies to Prevent Preterm Birth. *MMWR Morb Mortal Wkly Rep* [Internet]. 2016;65(32):826–30. Available from: <http://www.cdc.gov/mmwr/volumes/65/wr/mm6532a4.htm>
221. Hamilton BE, Martin JA, Osterman MJK, Curtin SC, Matthews TJ. Births: Final Data for 2014. *Natl Vital Stat Rep* [Internet]. 2015 Dec;64(12):1–64. Available from: <http://www.ncbi.nlm.nih.gov/pubmed/26727629>
222. Romero R, Miranda J, Chaiworapongsa T, Korzeniewski SJ, Chaemsaihong P, Gotsch F, Dong Z, Ahmed AI, Yoon BH, Hassan SS, Kim CJ, Yeo L. Prevalence and Clinical Significance of Sterile Intra-amniotic Inflammation in Patients with Preterm Labor and Intact Membranes. *Am J Reprod Immunol* [Internet]. 2014 Nov;72(5):458–74. Available from: <http://www.ncbi.nlm.nih.gov/pubmed/20402989>
223. Hirota Y, Daikoku T, Tranguch S, Xie H, Bradshaw HB, Dey SK. Uterine-specific p53 deficiency confers premature uterine senescence and promotes preterm birth in mice. *J Clin Invest*. 2010;120(3):803–15.
224. Deng W, Cha J, Yuan J, Haraguchi H, Bartos A, Leishman E, Viollet B, Bradshaw HB, Hirota Y, Dey SK. P53 coordinates decidual sestrin 2/AMPK/mTORC1 signaling to govern parturition timing. *J Clin Invest*. 2016;126(8):2941–54.
225. Kobayashi H. The entry of fetal and amniotic fluid components into the uterine vessel circulation leads to sterile inflammatory processes during parturition. *Front Immunol*. 2012;3(OCT):1–6.
226. Stephen GL, Lui S, Hamilton SA, Tower CL, Harris LK, Stevens A, Jones RL. Transcriptomic Profiling of Human Choriondecidua During Term Labor: Inflammation as a Key Driver of Labor. *Am J Reprod Immunol*. 2015;73(1):36–55.
227. Hessvik NP, Llorente A. Current knowledge on exosome biogenesis and release. *Cell Mol Life Sci*. 2018;75(2):193–208.
228. Pokharel D, Padula MP, Lu JF, Tacchi JL, Luk F, Djordjevic SP, Bebawy M. Proteome analysis of multidrug-resistant, breast cancer-derived microparticles. *J Extracell Vesicles* [Internet]. 2014 Jan 1;3(1):24384. Available from: <https://doi.org/10.3402/jev.v3.24384>

229. Murrow L, Debnath J. Atg12–Atg3 coordinates basal autophagy, endolysosomal trafficking and exosome release. *Mol Cell Oncol* [Internet]. 2015 May 26;0. Available from: <https://doi.org/10.1080/23723556.2015.1039191>
230. Yáñez-Mó M, Siljander PRM, Andreu Z, Zavec AB, Borràs FE, Buzas EI, Buzas K, Casal E, Cappello F, Carvalho J, Colás E, Cordeiro-Da Silva A, Fais S, Falcon-Perez JM, Ghobrial IM, Giebel B, Gimona M, Graner M, Gursel I, Gursel M, Heegaard NHH, Hendrix A, Kierulf P, Kokubun K, Kosanovic M, Kralj-Iglic V, Krämer-Albers EM, Laitinen S, Lässer C, Lener T, Ligeti E, Line A, Lipps G, Llorente A, Lötvall J, Manček-Keber M, Marcilla A, Mittelbrunn M, Nazarenko I, Nolte-’t Hoen ENM, Nyman TA, O’Driscoll L, Olivan M, Oliveira C, Pállinger É, Del Portillo HA, Reventós J, Rigau M, Rohde E, Sammar M, Sánchez-Madrid F, Santarém N, Schallmoser K, Ostenfeld MS, Stoorvogel W, Stukelj R, Van Der Grein SG, Helena Vasconcelos M, Wauben MHM, De Wever O. Biological properties of extracellular vesicles and their physiological functions. *J Extracell Vesicles*. 2015;4(2015):1–60.
231. Sheller-Miller S, Urrabaz-Garza R, Saade G, Menon R. Damage-Associated molecular pattern markers HMGB1 and cell-Free fetal telomere fragments in oxidative-Stressed amnion epithelial cell-Derived exosomes. *J Reprod Immunol* [Internet]. 2017 Aug [cited 2017 Aug 28];123(June):3–11. Available from: <http://dx.doi.org/10.1016/j.jri.2017.08.003>
232. Dixon CL, Richardson L, Sheller-Miller S, Saade G, Menon R. A distinct mechanism of senescence activation in amnion epithelial cells by infection, inflammation, and oxidative stress. *Am J Reprod Immunol*. 2017;(August):1–8.
233. Santangelo L, Giurato G, Cicchini C, Montaldo C, Mancone C, Tarallo R, Battistelli C, Alonzi T, Weisz A, Tripodi M. The RNA-Binding Protein SYNCRIP Is a Component of the Hepatocyte Exosomal Machinery Controlling MicroRNA Sorting. *Cell Rep* [Internet]. 2016;17(3):799–808. Available from: <http://dx.doi.org/10.1016/j.celrep.2016.09.031>
234. Keller A, Nesvizhskii AI, Kolker E, Aebersold R. Empirical statistical model to estimate the accuracy of peptide identifications made by MS/MS and database search. *Anal Chem*. 2002;74(20):5383–92.
235. Nesvizhskii AI, Keller A, Kolker E, Aebersold R. A statistical model for identifying proteins by tandem mass spectrometry. *Anal Chem*. 2003;75(17):4646–58.
236. Consortium TGO. Gene ontologie: Tool for the unification of biology. *Nat Genet*. 2000;25(1):25–9.
237. Vargis E, Brown N, Williams K, Al-Hendy A, Paria BC, Reese J, Mahadevan-Jansen A. Detecting Biochemical Changes in the Rodent Cervix During Pregnancy Using Raman Spectroscopy. *Ann Biomed Eng* [Internet]. 2012 Aug 13;40(8):1814–24. Available from: <http://link.springer.com/10.1007/s10439-012-0541-4>
238. Kirby MA, Heuerman AC, Custer M, Dobyns AE, Strilaeff R, Stutz KN, Cooperrider J, Elsisy JG, Yellon SM. Progesterone Receptor-Mediated Actions



- Regulate Remodeling of the Cervix in Preparation for Preterm Parturition. *Reprod Sci*. 2016;23(11):1473–83.
239. Faul F, Erdfelder E, Lang A-G, Buchner A. G\*Power: A flexible statistical power analysis program for the social, behavioral, and biomedical sciences. *Behav Res Methods [Internet]*. 2007;39(2):175–91. Available from: <http://www.gpower.hhu.de/>
  240. Dobyns AE, Goyal R, Carpenter LG, Freeman TC, Longo LD, Yellon SM. Macrophage gene expression associated with remodeling of the prepartum rat cervix: Microarray and pathway analyses. *PLoS One*. 2015;10(3).
  241. Hui C, Lili M, Libin C, Rui Z, Fang G, Ling G, Jianping Z. Changes in coagulation and hemodynamics during pregnancy: A prospective longitudinal study of 58 cases. *Arch Gynecol Obstet*. 2012;285(5):1231–6.
  242. Keren-Politansky A, Breizman T, Brenner B, Sarig G, Drugan A. The coagulation profile of preterm delivery. *Thromb Res*. 2014;133(4):585–9.
  243. Mogami H, Kishore AH, Word RA. Collagen Type 1 Accelerates Healing of Ruptured Fetal Membranes. *Sci Rep [Internet]*. 2018;8(1):696. Available from: <http://www.nature.com/articles/s41598-017-18787-9>
  244. Lappas M, Riley C, Lim R, Barker G, Rice GE, Menon R, Permezel M. MAPK and AP-1 proteins are increased in term pre-labour fetal membranes overlying the cervix: Regulation of enzymes involved in the degradation of fetal membranes. *Placenta [Internet]*. 2011;32(12):1016–25. Available from: <http://dx.doi.org/10.1016/j.placenta.2011.09.011>
  245. Burdet J, Paula A, Rubio D, Inés A, Laura M, Ibarra C, Rubio APD, Salazar AI, Ribeiro ML, Ibarra C, Franchi AM. Inflammation, infection and preterm birth. *Curr Pharm Des [Internet]*. 2014;20(29):4741–8. Available from: <http://www.ncbi.nlm.nih.gov/pubmed/24588830>
  246. Esplin MS, Romero R, Chaiworapongsa T, Kim YM, Edwin S, Gomez R, Mazor M, Adashi EY. Monocyte chemotactic protein-1 is increased in the amniotic fluid of women who deliver preterm in the presence or absence of intra-amniotic infection. *J Matern Fetal Neonatal Med*. 2005;17(6):365–73.
  247. Yellon SM. Contributions to the dynamics of cervix remodeling prior to term and preterm birth. *Biol Reprod [Internet]*. 2017;96(1):13–23. Available from: <https://academic.oup.com/biolreprod/article/96/1/13/2731920/Contributions-to-the-dynamics-of-cervix-remodeling>
  248. Kishore AH, Liang H, Kanchwala M, Xing C, Ganesh T, Akgul Y, Posner B, Ready JM, Markowitz SD, Word RA. Prostaglandin dehydrogenase is a target for successful induction of cervical ripening. *Proc Natl Acad Sci [Internet]*. 2017;114(31):E6427–36. Available from: <http://www.pnas.org/lookup/doi/10.1073/pnas.1704945114>
  249. Madsen G, Zakar T, Ku CY, Sanborn BM, Smith R, Mesiano S. Prostaglandins Differentially Modulate Progesterone Receptor-A and -B Expression in Human Myometrial Cells: Evidence for Prostaglandin-Induced Functional Progesterone

Withdrawal. *J Clin Endocrinol Metab*. 2004;89(2):1010–3.

250. Patel B, Peters GA, Skomorovska-Prokvolit Y, Yi L, Tan H, Yousef A, Wang J, Mesiano S. Control of Progesterone Receptor-A Transrepressive Activity in Myometrial Cells: Implications for the Control of Human Parturition. *Reprod Sci*. 2018;25(2):214–21.
251. Brubaker D, Barbaro A, R. Chance M, Mesiano S. A dynamical systems model of progesterone receptor interactions with inflammation in human parturition. *BMC Syst Biol* [Internet]. 2016;10(1):1–14. Available from: <http://dx.doi.org/10.1186/s12918-016-0320-1>
252. Yoshida K, Mahendroo M, Vink J, Wapner R, Myers K. Material properties of mouse cervical tissue in normal gestation. *Acta Biomater* [Internet]. 2016 May 1 [cited 2018 Mar 20];36:195–209. Available from: <https://www.sciencedirect.com/science/article/pii/S1742706116300897>
253. Mackler AM, Iezza G, Akin MR, McMillan P, Yellon SM. Macrophage trafficking in the uterus and cervix precedes parturition in the mouse. *Biol Reprod* [Internet]. 1999 Oct;61(4):879–83. Available from: <http://www.biolreprod.org/content/61/4/879.abstract>
254. Payne KJ, Clyde LA, Weldon AJ, Milford T-A, Yellon SM. Residency and activation of myeloid cells during remodeling of the prepartum murine cervix. *Biol Reprod* [Internet]. 2012 Nov;87(5):106. Available from: <https://academic.oup.com/biolreprod/article-lookup/doi/10.1095/biolreprod.112.101840>
255. Edey LF, Georgiou H, O’Dea KP, Mesiano S, Herbert BR, Lei K, Hua R, Markovic D, Waddington SN, MacIntyre D, Bennett P, Takata M, Johnson MR. Progesterone, the maternal immune system and the onset of parturition in the mouse. *Biol Reprod* [Internet]. 2017;(November). Available from: <http://academic.oup.com/biolreprod/article/doi/10.1093/biolre/iox146/4628035>
256. Singh N, Herbert B, Sooranna GR, Orsi NM, Edey L, Dasgupta T, Sooranna SR, Yellon SM, Johnson MR. Is myometrial inflammation a cause or a consequence of term human labour? *J Endocrinol*. 2017;235(1):69–83.
257. Sadowsky DW, Adams KM, Gravett MG, Witkin SS, Novy MJ. Preterm labor is induced by intraamniotic infusions of interleukin-1 $\beta$  and tumor necrosis factor- $\alpha$  but not by interleukin-6 or interleukin-8 in a nonhuman primate model. *Am J Obstet Gynecol*. 2006;195(6):1578–89.
258. Yoshimura K, Hirsch E. Effect of stimulation and antagonism of interleukin-1 signaling on preterm delivery in mice. *J Soc Gynecol Investig*. 2005;12(7):533–8.
259. Gomez-Lopez N, Romero R, Arenas-Hernandez M, Panaitescu B, Garcia-Flores V, Mial T, Sahi A, Hassan S. Intra-amniotic administration of lipopolysaccharide induces spontaneous preterm labor and birth. *J Matern Neonatal Med* [Internet]. 2017;23(0):1–8. Available from: <http://dx.doi.org/10.1080/14767058.2017.1287894>
260. Gorczynski RM, Erin N, Zhu F. Serum-derived exosomes from mice with highly

- metastatic breast cancer transfer increased metastatic capacity to a poorly metastatic tumor. Vol. 5, *Cancer Medicine*. 2016. p. 325–36.
261. Wong WY, Lee MML, Chan BD, Kam RKT, Zhang G, Lu AP, Tai WCS. Proteomic profiling of dextran sulfate sodium induced acute ulcerative colitis mice serum exosomes and their immunomodulatory impact on macrophages. *Proteomics*. 2016;16(7):1131–45.
  262. Liu H, Gao W, Yuan J, Wu C, Yao K, Zhang L, Ma L, Zhu J, Zou Y, Ge J. Exosomes derived from dendritic cells improve cardiac function via activation of CD4<sup>+</sup> T lymphocytes after myocardial infarction. *J Mol Cell Cardiol* [Internet]. 2016;91:123–33. Available from: <http://linkinghub.elsevier.com/retrieve/pii/S0022282815301668>
  263. Gupta A, Pulliam L. Exosomes as mediators of neuroinflammation. *J Neuroinflammation* [Internet]. 2014;11(1):68. Available from: <http://www.pubmedcentral.nih.gov/articlerender.fcgi?artid=3994210&tool=pmcentrez&rendertype=abstract>
  264. Chahar HS, Bao X, Casola A. Exosomes and Their Role in the Life Cycle and Pathogenesis of RNA Viruses. *Viruses* [Internet]. 2015 Jun;7(6):3204–25. Available from: [www.mdpi.com/journal/viruses](http://www.mdpi.com/journal/viruses)
  265. Zomer A, Vendrig T, Hopmans ES, van Eijndhoven M, Middeldorp JM, Pegtel DM. Exosomes: Fit to deliver small RNA. *Commun Integr Biol* [Internet]. 2010 Sep 28;3(5):447–50. Available from: <http://www.tandfonline.com/doi/abs/10.4161/cib.3.5.12339>
  266. Ramachandra L, Qu Y, Wang Y, Lewis CJ, Cobb BA, Takatsu K, Boom WH, Dubyak GR, Harding C V. Mycobacterium tuberculosis synergizes with ATP to induce release of microvesicles and exosomes containing major histocompatibility complex class II molecules capable of antigen presentation. *Infect Immun*. 2010;78(12):5116–25.
  267. Hashimoto K, Ochi H, Sunamura S, Kosaka N, Mabuchi Y, Fukuda T, Yao K, Kanda H, Ae K, Okawa A, Akazawa C, Ochiya T, Futakuchi M, Takeda S, Sato S. Cancer-secreted hsa-miR-940 induces an osteoblastic phenotype in the bone metastatic microenvironment via targeting ARHGAP1 and FAM134A. *Proc Natl Acad Sci* [Internet]. 2018;201717363. Available from: <http://www.pnas.org/lookup/doi/10.1073/pnas.1717363115>
  268. Mutschelknaus L, Azimzadeh O, Heider T, Winkler K, Vetter M, Kell R, Tapio S, Merl-Pham J, Huber SM, Edalat L, Radulović V, Anastasov N, Atkinson MJ, Moertl S. Radiation alters the cargo of exosomes released from squamous head and neck cancer cells to promote migration of recipient cells. Vol. 7, *Scientific Reports*. 2017.
  269. Sakha S, Muramatsu T, Ueda K, Inazawa J. Exosomal microRNA miR-1246 induces cell motility and invasion through the regulation of DENND2D in oral squamous cell carcinoma. *Sci Rep* [Internet]. 2016;6(December):1–11. Available from: <http://dx.doi.org/10.1038/srep38750>

270. Peinado H, Alečković M, Lavotshkin S, Matei I, Costa-Silva B, Moreno-Bueno G, Hergueta-Redondo M, Williams C, García-Santos G, Ghajar C, Nitadori-Hoshino A, Hoffman C, Badal K, Garcia B a, Callahan MK, Yuan J, Martins VR, Skog J, Kaplan RN, Brady MS, Wolchok JD, Chapman PB, Kang Y, Bromberg J, Lyden D. Melanoma exosomes educate bone marrow progenitor cells toward a pro-metastatic phenotype through MET. *Nat Med* [Internet]. 2012;18(6):883–91. Available from: <http://www.nature.com.sire.ub.edu/nm/journal/v18/n6/full/nm.2753.html>
271. Pillay P, Maharaj N, Moodley J, Mackraj I. Placental exosomes and pre-eclampsia: Maternal circulating levels in normal pregnancies and, early and late onset pre-eclamptic pregnancies. *Placenta* [Internet]. 2016;46:18–25. Available from: <http://dx.doi.org/10.1016/j.placenta.2016.08.078>
272. Liu W, Xu C, You X, Olson DM, Chemtob S, Gao L, Ni X. Hydrogen sulfide delays LPS-Induced preterm birth in mice via anti-inflammatory pathways. *PLoS One*. 2016;11(4):1–13.
273. Edey LF, O’Dea KP, Herbert BR, Hua R, Waddington SN, MacIntyre DA, Bennett PR, Takata M, Johnson MR. The Local and Systemic Immune Response to Intrauterine LPS in the Prepartum Mouse [Internet]. Vol. 95, *Biology of Reproduction*. 2016. p. 125–125. Available from: <https://academic.oup.com/biolreprod/article-lookup/doi/10.1095/biolreprod.116.143289>
274. Roizen JD, Asada M, Tong M, Tai HH, Muglia LJ. Preterm birth without progesterone withdrawal in 15-hydroxyprostaglandin dehydrogenase hypomorphic mice. *Mol Endocrinol* [Internet]. 2008;22(1):105–12. Available from: <http://www.ncbi.nlm.nih.gov/pubmed/17872381>
275. Sugimoto Y, Yamasaki A, Segi E, Tsuboi K, Aze Y, Nishimura T, Oida H, Yoshida N, Tanaka T, Katsuyama M, Hasumoto KY, Murata T, Hirata M, Ushikubi F, Negishi M, Ichikawa A, Narumiya S. Failure of parturition in mice lacking the prostaglandin F receptor. *Science* (80- ). 1997;277(5326):681–3.
276. Hirsch E, Muhle R. Intrauterine bacterial inoculation induces labor in the mouse by mechanisms other than progesterone withdrawal. *Biol Reprod*. 2002 Oct;67(4):1337–41.
277. Muzumdar MD, Tasic B, Miyamichi K, Li L, Luo L. A global double-fluorescent Cre reporter mouse. *Genesis* [Internet]. 2007 Sep;45(9):593–605. Available from: <http://www.ncbi.nlm.nih.gov/pubmed/17868096>
278. Asea A. Initiation of the Immune Response by Extracellular Hsp72: Chaperokine Activity of Hsp72. *Curr Immunol Rev* [Internet]. 2006 Aug 1;2(3):209–15. Available from: <http://www.pubmedcentral.nih.gov/articlerender.fcgi?artid=1868403&tool=pmcentrez&rendertype=abstract>
279. Rashed MH, Bayraktar E, Helal GK, Abd-Ellah MF, Amero P, Chavez-Reyes A, Rodriguez-Aguayo C. Exosomes: From garbage bins to promising therapeutic targets. *Int J Mol Sci*. 2017;18(3).

280. Snyder CS, Harrington AR, Kaushal S, Mose E, Lowy AM, Hoffman RM, Bouvet MM. A dual color, genetically engineered mouse model for multi-spectral imaging of the pancreatic microenvironment. *Pancreas*. 2013;42(6):952–8.
281. Yim N, Choi C. Extracellular vesicles as novel carriers for therapeutic molecules. *BMB Rep* [Internet]. 2016 Nov;49(11):585–6. Available from: <http://www.nature.com/doifinder/10.1038/nbt.1807>
282. Andersson S, Minjarez D, Yost NP, Word RA. Estrogen and progesterone metabolism in the cervix during pregnancy and parturition. *J Clin Endocrinol Metab*. 2008;93(6):2366–74.
283. Liu L, Oza S, Hogan D, Chu Y, Perin J, Zhu J, Lawn JE, Cousens S, Mathers C, Black RE. Global, regional, and national causes of under-5 mortality in 2000–15: an updated systematic analysis with implications for the Sustainable Development Goals. *Lancet* [Internet]. 2016;388(10063):3027–35. Available from: [http://dx.doi.org/10.1016/S0140-6736\(16\)31593-8](http://dx.doi.org/10.1016/S0140-6736(16)31593-8)
284. Nadeem L, Shynlova O, Mesiano S, Lye S. Progesterone via its type-a receptor promotes myometrial gap junction coupling. *Sci Rep* [Internet]. 2017;7(1):1–12. Available from: <http://dx.doi.org/10.1038/s41598-017-13488-9>
285. Sheller-Miller S, Urrabaz-Garza R, Saade G, Menon R. Damage-Associated Molecular Pattern Markers HMGB1 and Cell-Free Fetal Telomere Fragments in Oxidative-Stressed Amnion Epithelial Cell-Derived Exosomes. *J Reprod Immunol* [Internet]. 2017 Aug [cited 2017 Aug 28];123(June):3–11. Available from: <http://dx.doi.org/10.1016/j.jri.2017.08.003>
286. Pillay P, Moodley K, Moodley J, Mackraj I. Placenta-derived exosomes: Potential biomarkers of preeclampsia. *Int J Nanomedicine*. 2017;12:8009–23.
287. Samanta S, Rajasingh S, Drosos N, Zhou Z, Dawn B, Rajasingh J. Exosomes: new molecular targets of diseases. *Acta Pharmacol Sin* [Internet]. 2017;1–12. Available from: <http://www.ncbi.nlm.nih.gov/pubmed/29219950>  
<http://www.nature.com/doifinder/10.1038/aps.2017.162>
288. Wang H, Stjernholm YV. Plasma membrane receptor mediated MAPK signaling pathways are activated in human uterine cervix at parturition. *Reprod Biol Endocrinol*. 2007;5:3.
289. Xu C, Liu W, You X, Leimert K, Popowycz K, Fang X, Wood SL, Slater DM, Sun Q, Gu H, Olson DM, Ni X. PGF 2 $\alpha$  modulates the output of chemokines and pro-inflammatory cytokines in myometrial cells from term pregnant women through divergent signaling pathways. *Mol Hum Reprod* [Internet]. 2015 Jul;21(7):603–14. Available from: <http://www.ncbi.nlm.nih.gov/pubmed/25882540>

## Curriculum Vita

### PRESENT POSITION AND ADDRESS:

Graduate Assistant  
Laboratory of Ramkumar Menon, PhD, and George Saade, M.D.  
Biochemistry and Molecular Biology Graduate Program  
University of Texas Medical Branch  
11.154 Medical Research Building  
301 University Boulevard, Galveston, Texas 77555

### BIOGRAPHICAL:

Citizenship: United States  
Phone: 409-747-0497  
Email: sashelle@utmb.edu

### EDUCATION:

7/2014 – Present	PhD Candidate	Biochemistry and Molecular Biology University of Texas Medical Branch Galveston, TX
8/2004 – 5/2008	B.S.	Biochemistry Stonehill College Easton, MA

### CERTIFICATIONS:

11/2011 – 11/2015	National Institutes of Health (NIH) Protection Human Subject Research Participants Boston IVF Waltham, MA
11/2013 – 11/2014	DOT/IATA Shipping Dangerous Goods Beth Israel Deaconess Medical Center/Boston IVF Waltham, MA

### PROFESSIONAL WORK HISTORY AND TEACHING EXPERIENCE:

10/2011 – 7/2014	Laboratory Technician Supervisor: Denny Sakkas, PhD Boston IVF Waltham, MA
6/2013 – 6/2014	Research Associate Supervisor: Edna Tirado, MD/PhD

	Reprosource Diagnostics Woburn, MA
7/2011 – 9/2011	Research Associate (Contract Assignment) Predictive Biosciences Lexington, MA
11/2010 – 2/2011	Associate Scientist II (Contract Assignment) Biogen Idec Cambridge, MA
5/2010 – 11/2010	Research Associate (Contract Assignment) Xcellerex Marlborough, MA
2/2010 – 5/2010	Research Associate (Contract Assignment) Genzyme Corporation Framingham, MA
6/2008 – 10/2009	Scientist Supervisor: Hyun-Goo Choi, PhD Bioscale, Inc. Cambridge, MA
5/2006 – 8/2006	Center for Biophotonics Science and Technology Supervisor: Kit Lam, MD, PhD Sacramento, CA
8/2006 – 5/2008	Independent Chemical Research Supervisor: Valentino Tramontano, PhD Stonehill College Easton, MA
8/2006 – 5/2008	Laboratory/Teaching Assistant Stonehill College Easton, MA
5/2007 – 9/2007	Stonehill College Undergraduate Research Experience (SURE) Supervisor: Louis Liotta, PhD Easton, MA

## **RESEARCH ACTIVITIES:**

### **A. Areas of Research**

1. Mechanisms of preterm birth in murine models of pregnancy
2. Exosome signaling and inflammation

## B. Grant Support

1. NIEHS Predoctoral Fellow: NIEHS Training Grant (T32ES007254), 2017-present

## COMMITTEE RESPONSIBILITIES:

### International

2017 Preterm birth International Collaborative (PREBIC) Annual Meeting Organizing Committee (1/2017-05/2017)

### UTMB

Internal Advisory Committee  
Graduate Student Representative (9/2016 – Present)

Biochemistry Student Organization  
Co-chair (9/2016 – 8/2017)  
Treasurer (9/2015 – 9/2016)

BMB Recruitment Committee  
Member (9/2016 – Present)

BMB Curriculum Committee  
Member (9/2015 – 9/2016)

BMB Chalk Talk Committee  
Chair (9/2014 – Present)

### Other

Asian American Society  
Secretary (9/2007 – 6/2008)  
Stonehill College, Easton MA

## TEACHING RESPONSIBILITIES AT UTMB

### A. Teaching

Facilitator	2017-present Small Group Sessions Molecular Biology and Genetics Course Directors: Jose Barral, Ph.D. Donald Bouyer, Ph.D.
Lecturer	06/2017 Exosome Lab Practical (Present current techniques in exosome research and design hands-on experience for students) Cellular & Molecular Mechanisms in Health & Disease Course Director: Pomila Singh, PhD
Course Director	06/2016-08-2016 BBSC 6103



## Introduction to the Study of Biological Systems

### B. Students/Mentees/Advisees/Trainees

Katherine Haver	Ball High School Student 9/2017-Present UTMB Bench Mentor Program
Luis Monsivais, MD	Maternal Fetal Medicine Fellow Basic laboratory skills, exosomes, animal handling and surgery 1/2018-Present Mentor: Ramkumar Menon, PhD
Jin Jin, MD	Medical Fellow 1/2017-Present Basic laboratory skills, flow cytometry, exosomes Mentor: Ramkumar Menon, PhD
Lauren Richardson	Graduate Student 10/2015-Present Experimental design and troubleshooting, flow cytometry, exosomes Mentor: Ramkumar Menon, PhD
Laura Martin	Graduate Student 5/2017-9/2017 Experimental Design and troubleshooting, flow cytometry Mentor: Ramkumar Menon, PhD
Luke Dixon, MD	Maternal Fetal Medicine Fellow Basic laboratory skills, flow cytometry, exosomes 4/2016-11/2016 Mentor: Ramkumar Menon, PhD
Emily Hadley, MD	Maternal Fetal Medicine Fellow Basic laboratory skills, flow cytometry, exosomes 11/2015-4/2016 Mentor: Ramkumar Menon, PhD

### AWARDS & HONORS:

2018	Poster Presentation Award 65th Annual Meeting of the Society for Reproductive Investigation (SRI) San Diego, CA
2018	Travel Award 65th Annual Meeting of the Society for Reproductive Investigation (SRI) San Diego, CA
2017	Ann and John Hamilton Endowed Scholarship University of Texas Medical Branch

Galveston, TX

- 2017 Shirley Patricia Parker Scholarship Endowment  
University of Texas Medical Branch  
Galveston, TX
- 2017 Irma Mendoza Graduate Student Award  
University of Texas Medical Branch  
Galveston, TX
- 2017 Biological Chemistry Student Organization Award  
University of Texas Medical Branch  
Galveston, TX
- 2017 First Place, Outstanding Platform Presentation  
Texas Forum for Reproductive Sciences 23<sup>rd</sup> Annual Meeting  
Houston, TX
- 2017 Stobo Award Nominee  
University of Texas Medical Branch  
Galveston, TX
- 2016 Ann Anderson Scholarship  
University of Texas Medical Branch  
Galveston, TX
- 2016 Dr. John Gusdon Memorial New Investigator Award Finalist  
2016 American Society for Reproductive Immunology 36<sup>th</sup> Annual Meeting  
Baltimore, MD
- 2016 Travel Award  
2016 American Society for Reproductive Immunology 36<sup>th</sup> Annual Meeting  
Baltimore, MD
- 2016 2<sup>nd</sup> Place in Basic Research category  
2016 Center for Interdisciplinary Research in Women's Health Poster Session  
University of Texas Medical Branch  
Galveston, TX
- 2016 T1-T4 in 3 Competition Finalist  
2016 Clinical & Translational Research Forum  
University of Texas Medical Branch  
Galveston, TX
- 2015 Excellence in Student Research  
19<sup>th</sup> Annual Forum on Aging  
University of Texas Medical Branch  
Galveston, TX

2014	Bohdan Nechay Endowment University of Texas Medical Branch Galveston, TX
2004-2008	Presidential Scholarship Stonehill College Easton, MA
2004-2006	South Ukiah Rotary Scholarship South Ukiah Rotary Club Ukiah, CA

## MEMBERSHIP IN SCIENTIFIC SOCIETIES/PROFESSIONAL ORGANIZATIONS

1. Member, American Society for Reproductive Immunology, 2016-2017

## TRAINING/WORKSHOPS ATTENDED:

1. Survival Surgery in CD-1 Mice Training, Johns Hopkins University, Baltimore, MD January 16-30, 2016.

## MEDIA REPORTS ON MY RESEARCH:

1. "UTMB researchers show signals carried by exosomes trigger labor and delivery". *Exosome RNA Research and Industry News*, August 3, 2016.
2. "Researchers at Boston IVF Develop Saliva Test to Replace Blood Test". *New England Cable News*, March 24, 2014.

## PUBLICATIONS:

1. Laura Martin, Lauren Richardson, **Samantha Sheller-Miller**, Ramkumar Menon. Dexamethasone induces amnion cell senescence through p38MAPK independent but telomere - p21 dependent pathway. *Manuscript in preparation*.
2. **Samantha Sheller-Miller**, Steven M. Yellon, Ramkumar Menon. Gestational Profiling of Mouse Plasma Exosomes Reveals Inflammatory Biomarkers Increase Prior To Parturition and Promote Inflammatory Changes in Prepartum Cervix and Uterus. *Manuscript submitted to PNAS*.
3. Jin Jin; Lauren Richardson; **Samantha Sheller-Miller**; Nanbert Zhong; Ramkumar Menon. Oxidative stress induces p38MAPK-dependant senescence in the feto-maternal interface cells. *Manuscript submitted to Placenta*.
4. C Luke Dixon, **Samantha Sheller-Miller**, George R Saade, Stephen J Fortunato, Andrew Lai, Carlos Palma, Dominic Guazon, Carlos Salomon, Ramkumar Menon (2018). Amniotic Fluid Exosome Proteomic Profile Exhibits Unique Pathways of Term and Preterm Labor, *Endocrinology*, <https://doi.org/10.1210/en.2018-00073>

5. **Samantha Sheller-Miller**, Lauren Richardson, Laura Martin, Jin Jin, Ramkumar Menon. Systematic Review of p38 Mitogen Activated Kinase and its Functional Role in Reproductive Tissues. *Manuscript in preparation*.
6. Emily E Hadley, **Samantha Sheller-Miller**, Brandie D Taylor, George Saade, Carlos Salomon, Sam Mesiano, Robert Taylor, Ramkumar Menon. Effect of amnion derived exosomes on fetal and maternal gestational cells: novel signalers in the labor cascade. *Manuscript under review at American Journal of Obstetrics & Gynecology*.
7. C. Luke Dixon, Lauren Richardson, **Samantha Sheller-Miller**, George Saade, Ramkumar Menon (2017). Distinct mechanisms of senescence activation in amnion by infection, inflammation and oxidative stress. *Am. J. Reprod. Immunol.*
8. **Sheller-Miller, S.**, Urrabaz-Garza, R., Saade, G., Menon, R. (2017). Damage-Associated Molecular Pattern Markers HMGB1 and Cell-Free Fetal Telomere Fragments in Oxidative-Stressed Amnion Epithelial Cell-Derived Exosomes. *J. Reprod. Immunol.*
9. Richardson LS, Vargas G, Brown T, Ochoa L, **Sheller-Miller S**, Saade GR, Taylor RN, Menon R, Discovery and Characterization of Human Amniochorionic Membrane Microfractures, *The American Journal of Pathology* (2017).
10. **Sheller-Miller, S.**, Lei, J., Saade, G., Salomon, C., Burd, I., Menon, R. (2016). Feto-Maternal Trafficking of Exosomes in Murine Pregnancy Models. *Frontiers in Pharmacology*, 7(November), 1–10.
11. **Sheller, S.**, Papaconstantinou, J., Urrabaz-Garza, R., Richardson, L., Saade, G., Salomon, C., Menon, R. Amnion-Epithelial-Cell-Derived Exosomes Demonstrate Physiologic State of Cell under Oxidative Stress. *PLoS One*. 2016;11(6).
12. Behnia, F., **Sheller, S.**, Menon, R. Mechanistic Differences Leading to Infectious and Sterile Inflammation. *Am J Reprod Immunol*. 2016;75(5):505–18.

#### Thesis

**Sheller, S.** (2008). “Synthesis and Characterization of Novel Biodegradable Polyurethanes with Applications in Cartilage Tissue Engineering.” Undergraduate Thesis, Stonehill College.

#### **ORAL PRESENTATIONS AT NATIONAL AND INTERNATIONAL MEETINGS**

1. **Sheller-Miller, S.**, Menon, R. Gestational Profiling of Mouse Plasma Exosomes Reveals Inflammatory Biomarkers Increase Prior to Parturition. March 2018: Society for Reproductive Investigation 65<sup>th</sup> Annual Meeting: Oral Presentation.
2. **Sheller-Miller, S.**, Lei, J., Burd, I., Menon, R. Human amnion epithelial cell-derived exosomes: functional role on myometrial cells and trafficking in pregnant mice. April 2017: Texas Forum for Reproductive Sciences Annual Meeting: Oral Presentation.

3. Hadley, E.E., **Sheller, S.**, Urrabaz-Garza, R., Kechichian, T., Saade, G.R., Menon, R. Effect of amnion derived exosomes on feto-maternal gestational cells: new signalers in the labor cascade? March 2017: Society for Reproductive Investigation Annual Meeting: Oral Presentation.
4. **Sheller, S.**, Lei, J., Burd, I., Menon, R. Human amnion epithelial cell-derived fetal exosomes: functional role on uterine cells and trafficking in murine models of pregnancy. January 2017: American Society for Physician Scientists South Regional Meeting: Oral Presentation.
5. **Sheller, S.**, Lei, J., Burd, I., Menon, R. Functional role of human amnion epithelial cell-derived fetal exosomes on uterine cells and their trafficking in murine models of pregnancy. November 2016: American Society for Reproductive Immunology 36<sup>th</sup> Annual Meeting: Oral Presentation. *Travel award*
6. **Sheller, S.**, Saade, G., Taylor, B., Richardson, L., Mesiano, S. Taylor, R.N., Menon, R. Oxidative Stress Induced Amnion Cell Derived Exosomes Produce Inflammatory Changes in Myometrial Cells: Feto-Maternal Signaling in Human Parturition. March 2016: Society for Reproductive Investigation Annual Meeting: Oral Presentation.
7. Zimon, A., Lannon, B., **Sheller, S.**, Sakkas, D., Ulrich, M., Alper, M. Venopuncture-Free IVF: Measurement of Estrogen in Controlled Ovarian Stimulation IVF Cycles Using a “Patient-Friendly” Saliva-Based Estradiol Assay. October 2013: American Society for Reproductive Medicine Annual Meeting: oral presentation

#### POSTER PRESENTATIONS AT NATIONAL AND INTERNATIONAL MEETINGS

1. **Sheller-Miller, S.**, Choi, C., Menon, R. Development of a Cre-Reporter Mouse Model to Determine Maternal-Fetal Exosome Communication and Functional Effects During Pregnancy. March 2018: Society for Reproductive Investigation Annual Meeting: Poster Presentation.
2. **Sheller-Miller, S.**, Arita, Y., Menon, R., Peltier, M. Environmental Toxicant Induced Cellular Injury is Reflected in Placental Exosomes. March 2018: Society for Reproductive Investigation Annual Meeting: Poster Presentation – *Travel award and Poster Presentation Award*.
3. **Sheller-Miller, S.**, Yellon, S., Menon, R. Term Plasma Exosomes Promote Inflammatory Changes in Prepartum Murine Cervix and Uterus. March 2018: Society for Reproductive Investigation Annual Meeting: Poster Presentation.
4. **Sheller-Miller, S.**, Richardson, L., Martin, L., Jin, J., Torloni, MR, Menon, R. Systematic review of p38 MAPK in reproductive tissues. March 2018: Society for Reproductive Investigation Annual Meeting: Poster Presentation.

5. Jin, J., Luo, M., **Sheller-Miller, S.**, Zhong, N., Menon, R. Oxidative stress and senescence in human primary decidual cells. March 2018: Society for Reproductive Investigation Annual Meeting: Poster Presentation.
6. Martin, L., Richardson, L., **Sheller-Miller, S.**, Menon, R. Dexamethasone causes amnion cell senescence through a p38 MAPK independent but p21 dependent pathway. March 2018: Society for Reproductive Investigation Annual Meeting: Poster Presentation.
7. Hadley, E.E., **Sheller, S.**, Urrabaz-Garza, R., Kechichian, T., Saade, G.R., Menon, R., 2017. 742: Effect of amnion derived exosomes on feto-maternal gestational cells: new signalers in the labor cascade? Am. J. Obstet. Gynecol. 216, S431–S432.
8. Menon, R., **Sheller, S.**, Saade, G., Salomon, C. Oxidative stress induced amnion cell derived exosomes produce inflammatory changes in myometrial cells: A feto-maternal signaling in human parturition. Placenta. 2016;45:111–112.
9. **Sheller, S.**, Urrabaz-Garza, R., Kechichian, T., Saade, G., Menon, R. 2016. 801: Isolation and characterization of amnion epithelial cell-derived exosomes. Am. J. Obstet. Gynecol. 214, S417–S418.
10. **Sheller, S.**, Urrabaz-Garza, R., Saade, G., Menon, R. 2016. 802: Packaging of alarmin, HMGB1, in oxidative stress induced amnion cell exosomes: a signal from senescent fetal cells at term. Am. J. Obstet. Gynecol. 214, S418.
11. **Sheller, S.**, Urrabaz-Garza, R., Kechichian, T., Saade, G., Menon, R. 2016. 352: Contractile gene activation of myometrial cells treated with amnion epithelial cell-derived exosomes. Am J Obstet Gynecol. 214, S417–S418.
12. Koyfman, A., Appavu, R., **Sheller, S.**, Rudra, J. Self-Assembly of Heterochiral Peptides with Varied Sequence Patterns. Poster session presented at: Society for Biomaterials 39<sup>th</sup> Annual Meeting. 2015 April 15-18; Charlotte, North Carolina.
13. Pazdrak, K., Stafford, S., Maroto, M.R., **Sheller, S.**, Kurosky, A. Priming for Degranulation in Eosinophils Stimulated with Interleukin-5 (IL-5) Is Reversible. February 2015: American Academy of Allergy, Asthma & Immunology. Journal of Allergy and Clinical Immunology, Volume 135, Issue 2, AB221.
14. **Sheller, S.**, Liotta, L. “Conversion of D-Galactose and D-Mannose to Vinyl Pyrrolizidines”. Stonehill College Undergraduate Research Experience (SURE), 2007.

## COMMUNITY SERVICE

Ronald McDonald House

- Ice Cream Scooper

Austin Middle School Science Fair

- Volunteer Judge

Osler Society Halloween Carnival

- Volunteer

Stonehill College Asian American Society Annual Fashion Show

- Assistant Coordinator for the event

Relay for Life

- Volunteer

Interact Club

- Highway Cleanup Volunteer

Permanent address: 4925 Fort Crockett Blvd #114

Galveston, TX 77551

This dissertation was typed by Samantha Sheller-Miller